

https://dspace.org/

The active failure of embankments of cohesionless materials

Marais, G. v. R. (Gerrit van Rooyen)

1965
https://hdl.handle.net/10539/32937

Downloaded from a DSpace repository. https://dspace.org/

THE ACTIVE FAILURE OF EMBANKMENTS OF COHESIONLESS MATERIALS

A dissertation submitted in partial fulfilment of the requirements for the degree of Master of Science in Engineering of the University of the Witwatersrand.

Gerrit van Rooyen Marais

November, 1965.

DECLARATION BY CANDIDATE

I, Gerrit van Rooyen Marais, hereby declare that this thesis is my own work and that it has not been submitted for a degree of another university.

G vR Marais

November, 1965.

C O N T E N T S

The Active Failure of Embankments of Cohesionless Materials

ERRATA

Page	Should read
2.4	$A \frac{du}{dx} - F = 0$ 2.6
	In Section 2.7 the non characteristic boundary curve....
	Following the procedure set out in Section 2.5
2.17	The solution of the partial differential equation 2.17....
3.21	plastic zone is then described by hyperbolic partial....
3.27	Figure 3.6. let the density of the body to equal to ____....
4.7	and substituting equation 4.35 and 4.36 in equation 4.37....
	Noting that $\text{Cot}\ __ = \frac{\text{Cos}\ __}{\text{Sin}\ __}$, substituting in equation 4.38....
4.10	x_3 = ... 4.46
	y_3 = ... 4.47
	Using these values of $x_3 y_3$ in equation 5.44 and 5.45, ϕ and σ_3 can be obtained giving
	ϕ_3 = 4.48
	σ_3 = 4.49
4.15	The solution in region OCB is of Type 2(b)....
5.24	The fact that the solution is accurate for the value of
	S_o = 2/3 _____ is no guarantee....
5.29	Flattening of the slopes will influence the location....
5.9	5.4 The determination of the _____ stresses....
10.11	by Trollope's and Rendulic's methods (Figure 10.4) shows....

Note: Underlined words, symbols or numbers (except total underlining in 5.9) are the required corrections.

C O N T E N T S

Summary	
Scope of thesis	Section 1
The theory of hyperbolic partial differential equations	Section 2
The partial differential equations for plastic failure of soil media	Section 3
Cohesionless soil	Section 4
The active critical equilibrium of wedges of cohesionless materials	Section 5
Some experimental confirmation of the theory of active critical equilibrium of wedges	Section 6
Comparison between the rigorous and approximate methods of analysis of a wedge of cohesionless material in a state of active failure	Section 7
Description of the failure of Sache's Dam East	Section 8
Properties of the materials in Sache's Dam East wall and the foundation	Section 9
Stability analysis of Sache's Dam East	Section 10
References	
Numerical solution of the set of differential equations governing the critical stresses in symmetrical wedges of cohesionless materials under active failure conditions	Appendix 1
Solution for the active critical state in symmetrical wedges of cohesionless material for an angle of internal friction of 30°	Appendix 2
Acknowledgments	

SUMMARY

The theory of quasi-linear hyperbolic partial differential equations which forms the basis of the mathematical theory of plasticity for soil media, together with their solution by numerical methods, are set out. The assumptions made in the plastic theory regarding the properties of the soil media are briefly examined. Following the exposition of Sokolovski, the partial differential equations describing the failures of cohesive and cohesionless soil media are derived. The differential equations describing the active failure of wedges of cohesionless material are discussed in detail, and for an angle of internal friction equal to 30°, the complete solutions for symmetrical wedges with slopes 0, 5, 10, 15, 20, 25 and 30° determined. The theoretical predictions as to the forms of the failures of these wedges are tested experimentally by inducing sliding failure along the bases of model wedges of cohesionless material. The experimental results show good agreement with the theory; hence it is concluded that the mathematical theory gives an adequate description of the failures, and that the theory can be accepted as a criterion by which to judge approximate methods. The horizontal thrusts in wedges of cohesionless material failing by sliding along their bases as determined by the plastic theory are compared with the thrusts determined by the methods of Hummel-Finnan-Trollope and Rendulic. It is concluded that Rendulic's method gives values only <u>insignificantly</u> smaller, and Trollope's method values <u>significantly</u> smaller than those predicted by the

plastic theory. As the forms of the failures are also given approximately correctly by Rendulic's method, it is further concluded that Rendulic's method is the best approximate one available. The external forms of failures by sliding of two embankments of cohesionless material 260 ft and 600 ft high respectively, at Cullinan, South Africa, are described and appear to conform to the predictions from the plastic theory. Utilizing the experimentally determined strength and consolidation properties of the materials in the embankment and the sub-soils, and using Rendulic's approximate method, the stability of the 260 ft high embankment is determined. The analysis gives a reasonable account of the failure behaviour.

S E C T I O N 1

1. SCOPE OF THE THESIS

1.1 Introduction

There are two methods available for the calculation of the disturbing forces in the active failure by sliding of embankments of cohesionless material. The first is due to Hummel & Finnan (1921) and Trollope (1951) and the second is due to Rendulic (1938). Using these two methods in the stability analysis of a sliding failure of a 260 ft high earth dam at Cullinan, South Africa, showed that there was a significant difference in the horizontal thrusts as determined by the two methods. The conditions under which the failure took place were such that it was not possible to determine which method gave the more reliable estimate of the thrust. In order to judge which method is the more acceptable, the active failure of wedges of cohesionless material was investigated by means of the mathematical theory of plasticity for soil media.

The mathematical theory of plasticity for soil media has been developed to a remarkable degree by the Russian applied mathematician, Sokolovski (1960). It is based on certain postulations and idealizations as to the strength properties of soil media; in consequence, solutions obtained by the mathematical theory are not absolute criteria by which solutions obtained by approximate methods can be judged, but relative ones in the sense that approximate methods require a number of postulations in addition to those in the mathematical theory, and hence intuitively are expected to give correspondingly less reliable solutions.

Judgement on the mathematical theory will depend on the success with which it explains failure phenomena. With regard to the plastic failure of cohesionless wedges it is fortunately relatively simple to induce active failure by sliding along the base in model wedges of cohesionless materials, and certain predictions of the mathematical theory, particularly the forms of the failures, can be compared with the forms found in the experimental failures. Confidence in the theory as a criterion by which to judge approximate methods will depend on the degree of conformity of the experimental with the theoretical results.

The mathematical theory by which the plastic failure of soil media can be described is that of quasi-linear hyperbolic partial differential equations. These equations do not normally form a part of the instruction of civil engineers in South Africa - very few engineers even know of their existence. However, the whole structure of the plastic theory is so intimately bound up with these equations that a lack of understanding of them gives little hope of acquiring facility in this field of study. Sokolovski presumes this understanding and a person lacking it will find his exposition very difficult, if not incomprehensible. Although a number of expositions on the theory of hyperbolic partial differential equations have been written, most of them are concerned with their application to supersonic flow and shock waves, and expositions oriented towards their application in the plastic theory are difficult to find, and generally not very explicit. For these reasons the basic tenets of the theory, appropriately oriented, are prerequisite to the study of the failure of

soil media.

1.2 Scope

With these few introductory remarks, the scope of the thesis can be set out as follows:-

1. A short exposition of the theory of hyperbolic partial differential equations and the numerical methods of their solution, oriented towards their use in the analysis of the plastic failure of soil media.
2. A brief discussion of the basic assumptions in the plastic theory for soil media and, following Sokolovski, a derivation of the partial differential equations describing the plastic failure of soil media.
3. Derivation of the partial differential equations describing the plastic failure of cohesionless materials, with some solutions.
4. Derivation in detail of the ordinary differential equations describing the active failure of wedges of cohesionless material, and the complete solutions for symmetrical wedges having an angle of internal friction equal to 30° and slopes equal to 0, 5, 10, 15, 20, 25 and 30°.
5. Investigation of the validity of some of the theoretical predictions by the failure of experimental model wedges of cohesionless material.
6. Comparison of the solutions for the thrusts in wedges of cohesionless material in a state of active failure as obtained by the plastic theory, with the approximate solutions.
7. Description of failures by sliding of two embankments of cohesionless material, 260 ft and 600 ft high

respectively, and a comparison of these failures with the theoretical predictions from the plastic theory.

8. Description of the tests for the determination of the strength and consolidation characteristics of the materials in the 260 ft high dam wall and the sub-soils.

9. Performance of a stability analysis of the failure of the dam wall.

S E C T I O N 2

2. THE THEORY OF HYPERBOLIC PARTIAL DIFFERENTIAL EQUATIONS

2.1 Introduction

On the assumption of rigid-plastic behaviour and Mohr's criterion for plastic yield, the plastic failure of soil media can be described by a system of two first order quasi-linear partial differential equations of the hyperbolic type in two dependent variables (u,v) and two independent variables (x,y). Their derivation will be deferred until Section 3 so that the general properties and behaviour of this system of partial differential equations can first be discussed.

The concept of characteristic curves will be introduced. Essentially, they are curves in the XY plane along which the two partial differential equations degenerate to four ordinary differential equations, two giving the characteristic curves and two giving the values of u and v along these curves. This method of solution is called the Method of Characteristics. It is the most powerful method available for the solution of problems of plastic failure. The method is also particularly appropriate as the characteristic curves have a physical significance in that they correspond to the lines of slip in the failure zone of the soil media.

2.2 Linearity and quasi-linearity (Collatz 1960)

Consider the partial differential equation of order n in the dependent variable, u, and two independent variables x_1 and x_2:

$$A_0 u + A_1 \frac{\partial u}{\partial x_1} + B_1 \frac{\partial u}{\partial x_2} + A_2 \frac{\partial^2 u}{\partial x_1^2} + B_2 \frac{\partial^2 u}{\partial x_2^2} + \cdots A_n \frac{\partial^n u}{\partial x_1^n} + B_n \frac{\partial^n u}{\partial x_2^n} = 0$$

If the coefficients A,B are functions of x_1 and x_2 only the equation is said to be linear in

$$u, \frac{\partial u}{\partial x_1}, \frac{\partial u}{\partial x_2}, \frac{\partial^2 u}{\partial x_1^2}, \ldots\ldots, \frac{\partial^n u}{\partial x_1^n}, \frac{\partial^n u}{\partial x_2^n}.$$

and is termed a linear partial differential equation. If the coefficients A,B are functions of

$$x_1, x_2, u, \frac{\partial u}{\partial x_1}, \frac{\partial u}{\partial x_2}, \ldots \frac{\partial^{n-1} u}{\partial x_1^{n-1}}, \frac{\partial^{n-1} u}{\partial x_2^{n-2}}$$

the equation is said to be linear in $\frac{\partial^n u}{\partial x_1^n}, \frac{\partial^n u}{\partial x_2^n}$.

and is termed a quasi-linear partial differential equation. Hence, quasi-linearity in a partial differential equation implies linearity in the highest order partial derivatives. This definition can be extended to include more than one dependent variable.

2.3 Single quasi-linear first order partial differential equations (Hill 1960)

This equation has no application in the theory of plastic failure of soils but because of its simplicity it is very suitable for the illustration of the properties of characteristic curves.

Consider the quasi-linear first order differential equation

$$A \frac{\partial u}{\partial x} + B \frac{\partial u}{\partial x} = F \qquad 2.1$$

in the dependent variable, u, and the independent variables, x and y. Due to the quasi-linear restriction A, B, F are functions of u, x, y, but not of $\partial u/\partial x$ and $\partial u/\partial y$.

The solution of the equation 2.1 can be graphically illustrated in a set of right-angled Cartesian co-ordinates,

U X Y, as a curved surface, U(xy), over the XY plane, called the surface of solution. (See Figure 2.1)

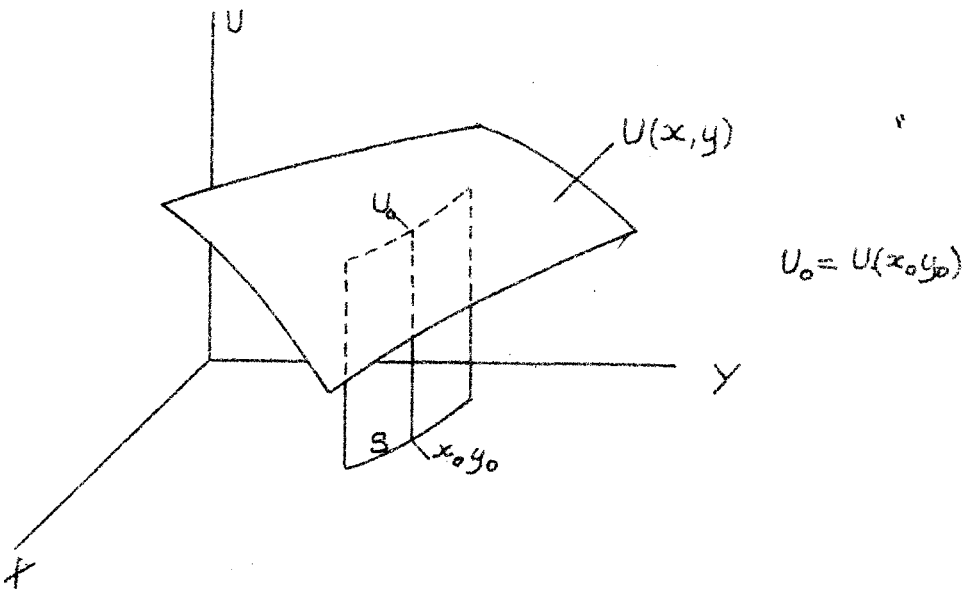

Fig. 2.1

The solution, $U(x_o,y_o)$ at point x_o,y_o is given by the vertical projection of point x_o,y_o, onto the solution surface. Similarly, the solution on curve S in the XY plane is given by the vertical projection of S onto the solution surface.

2.4 The determination of the solution along a characteristic curve (Hartree 1957)

At any point x,y on a smooth curve S, in the XY plane, the rate of change of u with respect to S is given by

$$\frac{du}{ds} = \frac{\partial u}{\partial x} \cdot \frac{dx}{ds} + \frac{\partial u}{\partial y} \cdot \frac{dy}{ds} \qquad 2.2$$

solving for $\partial u/\partial x$ gives

$$\frac{\partial u}{\partial x} = \left[\frac{du}{ds} - \frac{\partial u}{\partial y} \cdot \frac{dy}{ds}\right] \cdot \frac{ds}{dx} \qquad 2.3$$

Substituting equation 2.3 in equation 2.1 and grouping the terms containing $\partial u / \partial y$ gives

$$A \frac{du}{dx} - \frac{\partial u}{\partial y} \left[A \frac{dy}{dx} - B \right] = F$$

that is

$$\left[A \frac{du}{dx} - F \right] - \frac{\partial u}{\partial y} \left[A \frac{dy}{dx} - B \right] = 0 \qquad 2.4$$

Equation 2.4 is the partial differential equation for u along any curve S in the XY plane. The partial differential equation 2.1, valid over a region in the XY plane, has now been reduced to a partial differential equation valid along any curve in the XY plane. Due to the presence of the partial derivative, $\partial u / \partial y$, this differential equation is still awkward. If, however, the curve is chosen so that

$$A \frac{dy}{dx} - B = 0 \qquad 2.5$$

then, for all finite values of $\partial u / \partial y$ equation 2.4 reduces to

$$A \frac{du}{dx} - F = 0$$

Thus, along curves in the XY plane which satisfy equation 2.5 the partial differential equation 2.1 degenerates to two ordinary differential equations, the first defining the slope of a curve at any point x,y, in the XY plane and the second defining the rate of change of u at point x,y along this curve. Curves in the XY plane obtained from the solution of equation 2.5 are called <u>characteristic curves</u> or <u>characteristics</u>. Equations 2.5 and 2.6 constitute a set of <u>characteristic equations</u>.

In the solution of equations 2.5 and 2.6, if the coefficients A,B and F are functions of x and y only,

equation 2.5, defining the slope of the characteristic curve, can be solved independently of equation 2.6. If these coefficiencies are functions of x, y and u, the simultaneous solution of the two differential equations 2.5 and 2.6 is required. These characteristic equations have only been defined for finite values of the first partial derivatives of u with respect to x and y. In the case where one or more of the first partial derivatives become infinite a finite discontinuity occurs in u and v. This will be discussed later.

2.5 An alternative method for deriving the characteristic equations (Crandall 1956)

A more elegant method of deriving the characteristic equations is to use the theory of linear algebraic equations.

Equations 2.1 and 2.2 can be written as follows:

$$A\frac{\partial u}{\partial x} + B\frac{\partial u}{\partial y} = F \qquad 2.7$$

$$dx\frac{\partial u}{\partial x} + dy\frac{\partial u}{\partial y} = du \qquad 2.8$$

(Equation 2.8 is in the total differential form, whereas in equation 2.2 the derivative along S was used. The form used here is allowable provided dS/dx and dS/dy remain finite. It is always possible to ensure this by rotating the X and Y axis about the U axis.)

From the quasi-linear definition, A, B and F are independent of $\frac{\partial u}{\partial x}$, $\frac{\partial u}{\partial y}$. Hence, at any point x, y it is possible to consider equations 2.7 and 2.8 as two linear equations in the variables $\frac{\partial u}{\partial x}$ and $\frac{\partial u}{\partial y}$. Conveniently, these two equations can be written in matrix form, i.e.

$$\underset{(D)}{\begin{vmatrix} A & B \\ dx & dy \end{vmatrix}} \begin{vmatrix} \partial u/\partial x \\ \partial u/\partial y \end{vmatrix} = \begin{vmatrix} F \\ du \end{vmatrix} \qquad 2.9$$

Now the object is not to determine the values of $\partial u/\partial x$ and $\partial u/\partial y$ but to seek a relationship giving u independent of these derivatives. If the determinant, D, formed from the matrix of the coefficients on the left hand side of equation 2.9 is set equal to zero, the values of $\partial u/\partial x$ and $\partial u/\partial y$ become indeterminate and a linear relationship then exists between the coefficients on the left hand side of equations 2.7 and 2.8. This relationship can be found by expanding the determinant, D, and equating the expansion equal to zero, i.e.

$$D = \begin{vmatrix} A & B \\ dx & dy \end{vmatrix} = 0 \qquad 2.10$$

Expanding $A\,dy - B\,dx = 0$

giving $$\frac{dy}{dx} = \frac{B}{A} \qquad 2.11$$

which is idential to equation 2.5.

The right hand side of the matrix equation 2.9 must be compatible with the left hand side. This can be achieved in linear algebraic theory by replacing one of the columns of the coefficient matrix on the left hand side of the matrix equation by the column on the right hand side and equating the coefficient determinant equal to zero. Replacing the second column gives

$$\begin{vmatrix} A & F \\ dx & du \end{vmatrix} = 0$$

and expanding the determinant gives

$$\frac{du}{dx} = \frac{F}{A} \qquad 2.12$$

which is identical to equation 2.6.

A little consideration will show that the two derivatives for the characteristic equations are, in fact, equivalent, but that the second derivation, due to its association with the theory of linear algebra, can easily be generalized to systems consisting of more than one quasi-linear first order equation. The second derivation serves to emphasize the importance of quasi-linearity.

2.6 Numerical determination of the characteristic curves and the values of u on the characteristics (Crandall 1956, Hill 1960)

Before further discussion of the properties of these equations, it is instructive to study the numerical solution of the characteristic equations.

Let the initial values u_o, x_o, y_o be given. The solution is "marched out" from these initial conditions. The finite difference approximation to equation 2.11, which defines the slope of the characteristic curve, can be written in terms of the known poing x_o, y_o and an unknown point, x_1, y_1 on the characteristic near the known point.

$$\frac{y_1 - y_o}{x_1 - x_o} = \frac{B_o}{A_o} \qquad 2.13$$

where A_o and B_o are functions of u, x and y and can be evaluated from x_o, y_o, u_o. Hence

$$y_1 = y_o + \frac{B_o}{A_o}(x_1 - x_o) \qquad 2.14$$

As the selected step $(x_1 - x_o)$ is made smaller the value of y_1 in equation 2.14 approaches the true value, although it is not often possible to determine the accuracy of the result.

The value of u_1 can be determined from the finite difference form of equation 2.12, i.e.

$$\frac{U_1 - U_0}{x_1 - x_0} = \frac{F_0}{A_0} \qquad 2.15$$

where F_0, which is also a function of u,x and y and can be evaluated at point y_0, x_0, u_0. Hence

$$U_1 = U_0 + \frac{F_0}{A_0}(x_1 - x_0) \qquad 2.16$$

Knowing the values of u_1, x_1, y_1, the coefficients A_1, B_1, F_1, can be evaluated and serve as initial values for determining a further point x_2, y_2, u_2 on the characteristics. By this step by step procedure the solutions of the equations can be extended from the initial value along the characteristics as far as we please.

2.7 Surface of solution

Consider a curve, S, in the XY plane on which the value of u is known at every point. Assume that both the curve, S, and the values of u on S are smooth, i.e., the functions $y = S(x)$ and $u = U(xy)$ are continuous and differentiable. Assume, furthermore, that the curve, S, is nowhere coincident with the characteristic direction. (This assumption is necessary, because if S is coincident with a characteristic the solution can only extend outward along the trace of the characteristic).

From any point, x_0, y_0 on S, points on the characteristic curve through x_0y_0, and their associated values of u, can be calculated by the step by step procedure described in section 2.6. (See Figure 2.2)

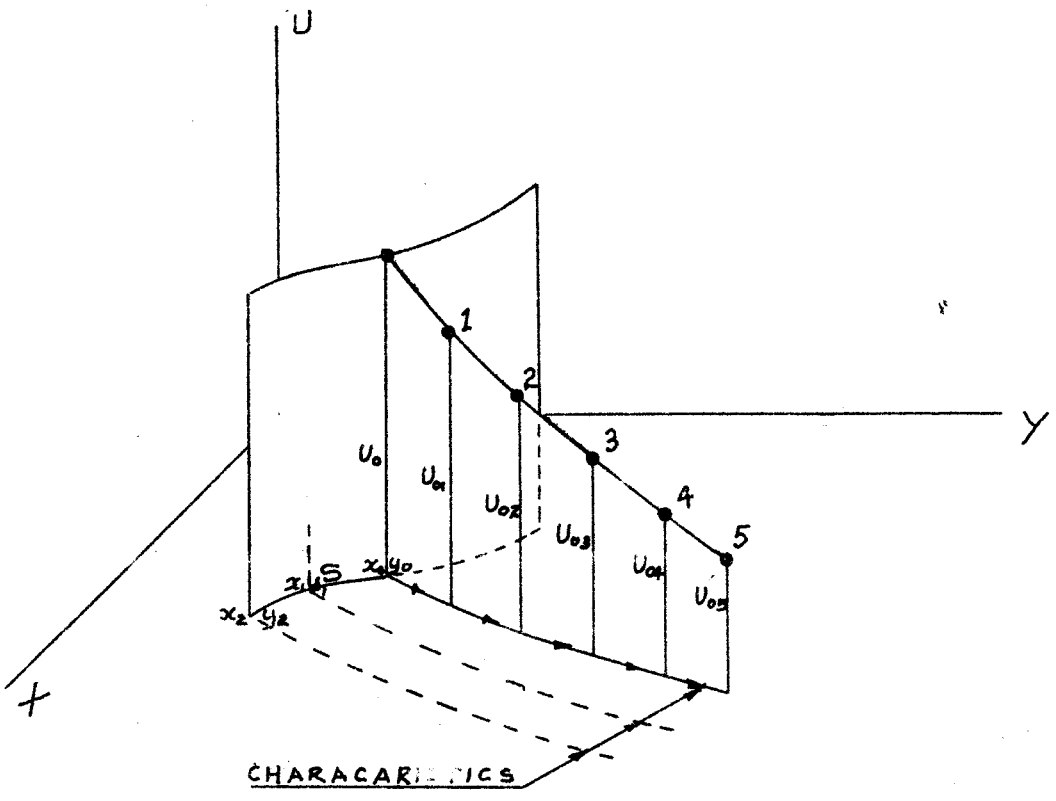

Fig. 2.2

If a number of points x_1y_1, x_2y_2, with their associated values, u_1, u_2, are selected on the curve S, the solutions on the characteristics through these points can be obtained. The values of u on these characteristics give points on the surface of solution, u(x,y).

The following observations can be noted:

1. The surface of solution extends in a transverse direction on either side away from the initial values on the "boundary" to infinity. Along S, the solution is bounded by the characteristics through the extremities of the curve S.

2. Once a value of u is specified on S, at point x,y, the value of u along the characteristic through x,y is uniquely determined because each point on the characteristic ultimately depends on the initial subscribed value. The curve, S, must therefore be such that it does not intercept the same characteristic more than once, since the value of u can only

be arbitrarily assigned at one point of the characteristic curve. In particular, a solution is not possible for arbitrary initial values on a closed boundary. When these conditions are satisfied it is said that the initial conditions are specified on an open boundary.

3. As the curve S and the values of u on S are continuous and differential, then, provided $\partial u/\partial x$ and $\partial u/\partial y$ remain finite, these derivatives will also be continuous and differentiable along the characteristics through S, giving a smooth surface of solution.

2.8 Discontinuities and regions of solution (Courant & Frederichs 1948)

In Section 2.5 the non-characteristic boundary curve, S, and the values of u on S were stipulated to be continuous and differentiable. However, boundary conditions may be encountered where the curve S and/or the value of u on S may be continuous but discontinuities occur in the first derivative dy/dx or du/ds. The occurrence of a discontinuity in du/ds is particularly instructive and will now be examined.

Assume that the non-characteristic boundary curve, S, in the XY plane is continuous and differential and that the value of u is continuous and differential except at point x_o, y_o on S where a finite discontinuity occurs in the first derivative du/ds (that is in $\partial u/\partial x$ or $\partial u/\partial y$ or both). There are two values for the partial derivatives at this point. (See Figure 2.3)

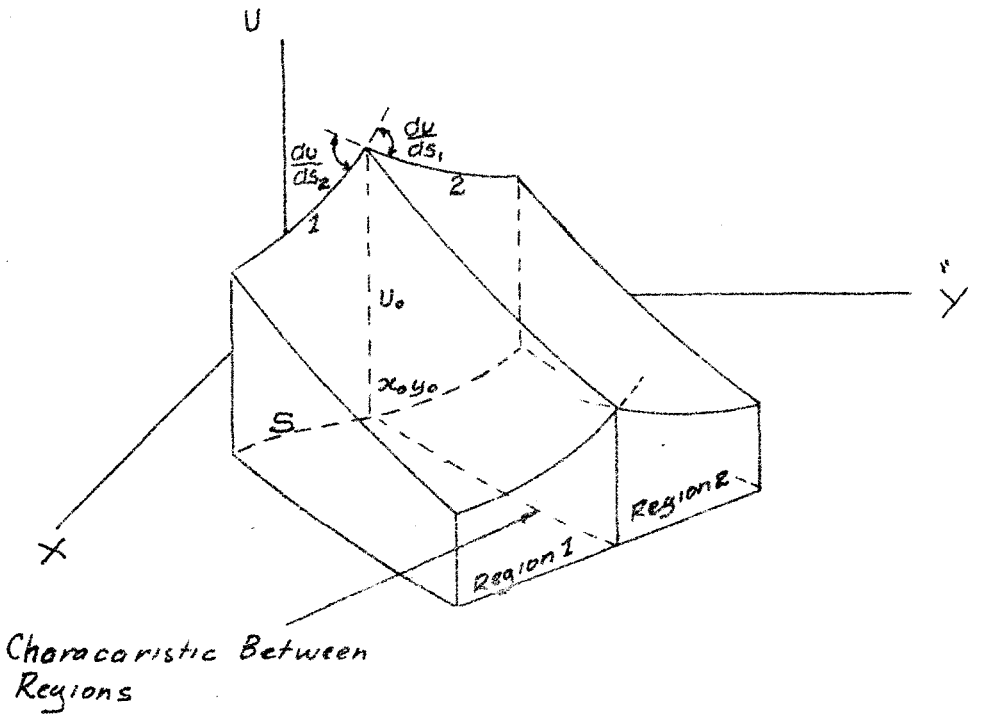

Fig. 2.3

The curve S can be divided into two sections, the point of division being x_o, y_o. The solution of u can be obtained by the method of characteristics for each of the sections. Because the characteristic equations due to the quasi-linear restriction depend only on u, x and y, the characteristic through point x_o, y_o must be common to both solutions as the value of u_o is common. The two solutions therefore join on the characteristic through x_o, y_o, thus dividing the solution into two domains or regions of solution. Here again the importance of quasi-linearity is evident.

In section 2.4 the derivation of the characteristic equations required only that $\frac{\partial u}{\partial x}, \frac{\partial u}{\partial y}$ remained finite. It is now evident that, provided this condition is fulfilled, the values of the derivation need not be the same on both sides of the characteristic. Within each region of solution, the first partial derivatives will be continuous but at the junction of two regions the partial derivatives may be discontinuous. Once a discontinuity in the first derivative

is specified in the initial values at a point on the boundary, this discontinuity is preserved along the characteristic through this point.

2.9 A system of two quasi-linear first order partial differential equations

The form of the two equations is

$$A_1\frac{\partial u}{\partial x} + B_1\frac{\partial u}{\partial y} + C_1\frac{\partial v}{\partial x} + D_1\frac{\partial v}{\partial y} = F_1$$

$$A_2\frac{\partial u}{\partial x} + B_2\frac{\partial u}{\partial y} + C_2\frac{\partial v}{\partial x} + D_2\frac{\partial v}{\partial y} = F_2 \qquad 2.17$$

Being quasi-linear, the coefficients A, B, C, D and F are functions of x, y, u and v only.

Consider any continuous and differentiable curve S in the XY plane and any point x,y on S. The total differentials at this point can be written

$$du = \frac{\partial u}{\partial x}dx + \frac{\partial u}{\partial y}dy$$

$$dv = \frac{\partial v}{\partial x}dx + \frac{\partial v}{\partial y}dy \qquad 2.18$$

Following the procedure for determining the characteristic equations set out in section 2.5, the matrix form for equations 2.17 and 2.18 can be written

$$\begin{vmatrix} A_1 & B_1 & C_1 & D_1 \\ A_2 & B_2 & C_2 & D_2 \\ dx & dy & 0 & 0 \\ 0 & 0 & dx & dy \end{vmatrix} \begin{vmatrix} \partial u/\partial x \\ \partial u/\partial y \\ \partial v/\partial x \\ \partial v/\partial y \end{vmatrix} = \begin{vmatrix} F_1 \\ F_2 \\ du \\ dv \end{vmatrix} \qquad 2.19$$

The equation(s) for the characteristic curve(s) in the XY plane is/are given by equating the determinant of the coefficient on the left hand side of equation 2.19 equal to zero. Expanding the determinant and dividing by $(dx)^2$ and collecting terms under $(dy/dx)^2$ and (dx/dx) gives

$$(A_1C_2 - A_2C_1)\left(\frac{dy}{dx}\right)^2 - \left[(A_1D_2 - A_2D_1) + (B_1C_2 - B_2C_1)\right]\frac{dy}{dx} + (B_1D_2 - B_2D_1) = 0 \qquad 2.20$$

Let $a = (A_1C_2 - A_2C_1)$

$b = -\left[(A_1D_2 - A_2D_1) + (B_1C_2 - B_2C_1)\right]$

$c = (B_1D_2 - B_2D_1)$

and equation 2.20 becomes

$$a\left(\frac{dy}{dx}\right)^2 + b\left(\frac{dy}{dx}\right) + c = 0 \qquad 2.21$$

This is a quadratic equation in the variable dy/dx and has two roots given by

$$\frac{dy}{dx} = \frac{-b \pm \sqrt{b^2 - 4ac}}{2a} \qquad 2.22$$

Hence, through point x,y there are two characteristic directions. These two directions may be real and different, real repeated, or imaginary, depending on whether the discriminant, $b^2 - 4ac$, is positive, zero, or negative respectively. The system of differential equations can be sub-divided into different types, namely, (1) hyperbolic, if there are two real directions, (2) parabolic, if there is one repeated real direction, and (3) elliptic, if the directions are imaginary. Of these three, the elliptic and hyperbolic equations only are of importance to this discussion.

The elliptic type is associated with <u>equilibrium</u> problems. Well known examples are problems involving Laplace's equation and the biharmonic equation in elasticity. The boundary conditions are specified on a closed contour and the value of the dependent variable at any internal point

is dependent on the conditions specified over the whole boundary. The numerical solution of the differential equation within the closed contour is obtained by drawing a grid across this region and replacing the governing differential equation by its finite difference approximation at every nodal point of the grid, and, obtaining the solution of the set of simultaneous equations thus formed. For this purpose the Liebmann or Southwell's relaxation method is particularly suitable.

The hyperbolic type is associated with propagation problems. Examples are the flow of gasses and the plastic failure of metals and soil media. The boundary conditions cannot be specified arbitrarily on a closed contour and it is said that the "initial values" are specified on an "open boundary". The value of the dependent variable at any point in the region of solution is dependent on the values over a portion of the open boundary only, called the domain of dependence of the point. The numerical solution is "marched" out from the boundary by a step by step procedure along the characteristic curves, and points outside the characteristic curves through the extremities of the open boundary do not affect the solution. It is this property that, with certain restrictions, makes it possible to obtain, in elastoplastic problems, the plastic state independent of the adjacent elastic state.

Equation 2.22 gives the differential equation for locating the two characteristic curves through point x,y. The next problem is to determine the value of u and v on these characteristic curves.

Following the procedure set out in Section 2.4 substitute the right hand side column of the matrix equation 2.19 in the fourth column of the coefficient matrix and equate the coefficient determinant equal to zero, i.e.

$$\begin{vmatrix} A_1 & B_1 & C_1 & F_1 \\ A_2 & B_2 & C_2 & F_2 \\ dx & dy & 0 & du \\ 0 & 0 & dx & dv \end{vmatrix} = 0 \qquad 2.23$$

Expanding the determinant and gathering terms gives

$$(A_1B_2 - A_2B_1)\,du + \left[(A_1C_2 - A_2C_1)\frac{dy}{dx} - (B_1C_2 - B_2C_1)\right]dv +$$

$$+\left[(F_1A_2 - F_2A_1)\frac{dy}{dx} - (F_1B_2 - F_2B_1)\right] \qquad 2.24$$

Let

$$j = (A_1B_2 - A_2B_1)$$

$$k = (A_1C_2 - A_2C_1)$$

$$\ell = -(B_1C_2 - B_2C_1)$$

$$m = (F_1A_2 - F_2A_1)$$

$$n = (F_1B_2 - F_2B_1)$$

Then equation 2.24 can be written

$$j\,du + \left(k\frac{dy}{dx} + \ell\right)dv + \left(m\frac{dy}{dx} - n\right)dx = 0$$

$$j\frac{du}{dx} + \left(k\frac{dy}{dx} + \ell\right)\frac{dv}{dx} + \left(m\frac{dy}{dx} - n\right) = 0 \qquad 2.25$$

Referring to equation 2.22 for simplicity the two differential equations defining the slopes of the characteristic curves through point x,y can be written as follows:

$$\left(\frac{dy}{dx}\right)_1 = \alpha \qquad 2.26$$

$$\left(\frac{dy}{dx}\right)_2 = \beta \qquad 2.27$$

where

$$\left.\begin{matrix}\alpha \\ \beta\end{matrix}\right\} = \frac{-b \pm \sqrt{b^2-4ac}}{2a}$$

These characteristic curves can be called the α and β characteristics respectively.

Substituting equation 2.26 in equation 2.25 we obtain the differential equation for the value of u and v on the α characteristic. Similarly, substituting equation 2.27 in equation 2.25 gives the differential equation for the value of u and v on the β characteristic. The equations can be grouped together as follows:

$$\frac{dy}{dx} = \alpha \qquad 2.28$$

$$j\frac{du}{dx} + (k\alpha + \ell)\frac{dv}{dx} + (m\alpha - n) = 0 \qquad 2.29$$

2.32

$$\frac{dy}{dx} = \beta \qquad 2.30$$

$$j\frac{du}{dx} + (k\beta + \ell)\frac{dv}{dx} + (m\beta - n) = 0 \qquad 2.31$$

which gives the four ordinary differential equations (characteristic equations) replacing the two partial differential equations.

The solution of the partial differential equations 2.18 and 2.19 can be presented in three dimensional cartesian co-ordinates as two curved surfaces u(x,y) and v(x,y) over the XY plane. Employing the characteristic equations 2.32 the solution of u and v can be obtained on the characteristic curves. As there are two characteristic directions through every point XY the integration of equations 2.28 and 2.30 gives two sets of characteristic curves. If the coefficients A,B,C,D,E,F are functions of x and y these characteristic curves can be found independent of equations 2.29 and 2.31, but if one or more of the coefficients are dependent on u and v the determination of the characteristic curves must proceed simultaneously with the solution of u and v.

2.10 Numerical solution of the characteristic equations

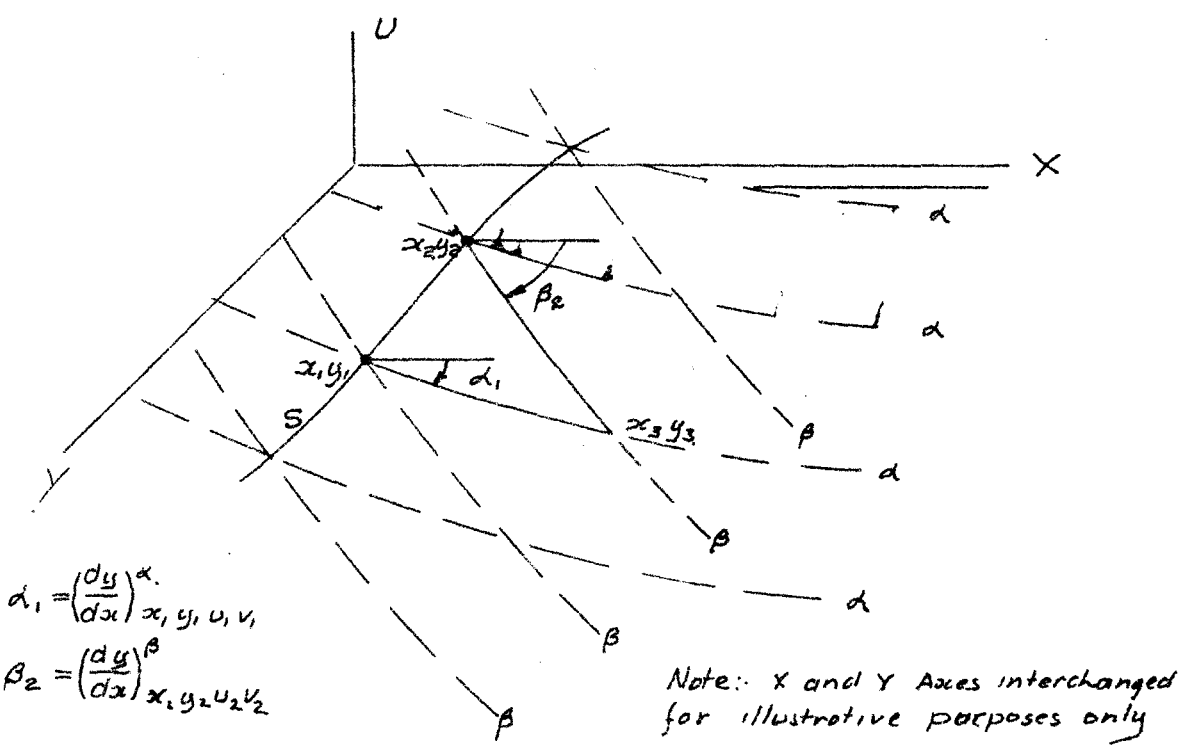

Fig. 2.4

The numerical solution of the characteristic curves and the values of u and v on these curves can be obtained by using the members of the two sets of characteristic curves as a finite difference curvilinear grid in the XY plane, as follows:

At the intersection of two characteristic curves, one from each set passing through the known points x_1, y_1, u_1, v_1 and x_2, y_2, u_2, v_2 respectively the value x_3, y_3, u_3 and v_3 is determined. Let the α characteristic through point x_1, y_1 and the β characteristic through point x_2, y_2 intersect at point x_3, y_3. (Figure 2.4)

The first order finite difference approximation to equation 2.28 is

$$\frac{y_3 - y_1}{x_3 - x_1} = \alpha_1 \qquad 2.33$$

where α_1 can be evaluated by substituting the known values of x_1, y_1, u_1, v_1 in the equation above.

Similarly for equation 2.30

$$\frac{y_3 - y_2}{x_3 - x_2} = \beta_2 \qquad 2.34$$

where β_2 can be evaluated by substituting the known values of x_2, y_2, u_2, v_2 in the equation above. The value x_3, y_3 can be obtained from the solution of these two simultaneous algebraic equations.

Having obtained the values of x_3, y_3 the values of u_3, v_3 can be found by evaluating j,k,l,m,n at point 1 and 2 respectively with the appropriate values of α_1 and β_2 in the finite difference form of equations 2.29 and 2.31

$$j\,\frac{u_3-u_1}{x_3-x_1}+(k_1\alpha_1+\ell_1)\frac{v_3-v_1}{x_3-x_1}+(m_1\alpha_1-n_1)=0 \qquad 2.35$$

$$j\,\frac{u_3-u_2}{x_3-x_2}+(k_2\beta_2+\ell_2)\frac{v_3-v_2}{x_3-x_2}+(m_2\beta_2-n_2)=0 \qquad 2.36$$

and solving these two equations simultaneously.

The finite difference form used here is crude and the values of u_3, v_3, x_3, y_3 serve as a first approximation only. In section 4 a procedure to improve on the values will be given.

2.11 Domains or regions of solution

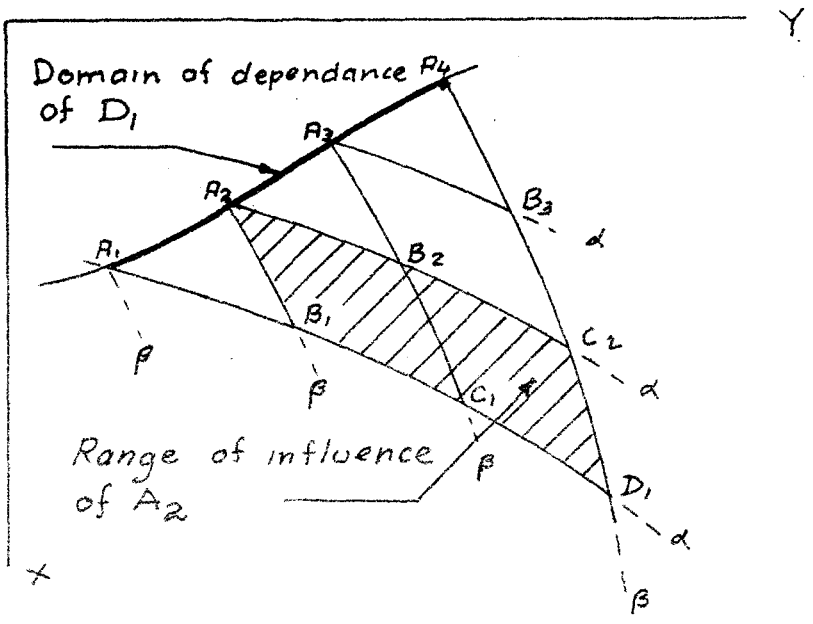

Fig. 2.5

Referring to Figure 2.5, if x, y, u and v are known at points A_1, A_2, A_3 and A_4 then by the numerical procedure described in section 2.10 the values B_1, B_2 and B_3 can be found and these serve as starting values to determine C_1 and C_2 from which D_1 can finally be determined. If the values

x,y, u and v are ascribed on a smooth non-characteristic curve A_1, A_4 and the numerical solution calculated by the step by step procedure until point D_1 is determined the area enclosed by A_1, A_4, D_1 is called the <u>domain or region of solution</u>.

2.12 <u>Domain of dependence</u>

It is clear that the calculated values of x, y, u and v at point D_1 depend on the initial values of u and v at A_1, A_2, A_3, A_4 on curve S(xy). (Figure 2.5) In general the value of the boundary values influencing the values of x, y, u and v at an internal point D_1 is given by the intersections of α and β characteristics through D_1 with the boundary (at points A_1, A_4). The <u>boundary A_1, A_4 is called the domain of dependence</u>.

2.13 <u>Range of Influence</u>

Assume that u and v are known on the smooth curve S and the region of solution A_1, A_4, D_1 has been determined. (Figure 2.5) Take any point, A_2, on curve S between A_1 and A_4. The α and β characteristic through this point intersects the characteristics A_1, D_1 and A_4, D_1 at B_1 and C_2 respectively. The area A_2, C_2, D_1, B_1 is called the <u>range of influence</u> of A_2 because any point internal to this area contains A_2 in its domain of dependence. The possession of a domain of dependence (and range of influence) is a distinguishing feature of hyperbolic differential equations. Whereas in solutions governed by elliptic differential equations every point on the boundary influences every internal point to the boundary, in hyperbolic differential equations any point internal to the boundary is only influenced by the boundary values within the domain of dependence of the internal point.

2.14 Discontinuities in the boundary conditions

If the boundary curve S and/or the values u and v on S contain finite discontinuities in the first derivatives then, as discussed in Section 2.8, these discontinuities are propagated along the characteristic curves passing through the point on the boundary where the discontinuity occurs. The solution is divided into regions which join on the characteristics along which the discontinuity is propagated.

Discontinuities in the initial values of u and v are often encountered in problems in the plastic theory and will be described in detail in the next section. For the present it is sufficient to state that the discontinuities in the value of u and v are not propagated internally along the characteristic curves, but lead to discontinuities in the first derivatives which are propagated along the characteristics through the point of discontinuity of u and v on S.

2.15 Boundary conditions and regions of solution

Depending on the specification of the boundary conditions certain types of solutions arise. One or more types may occur, the types fitting together along characteristic lines

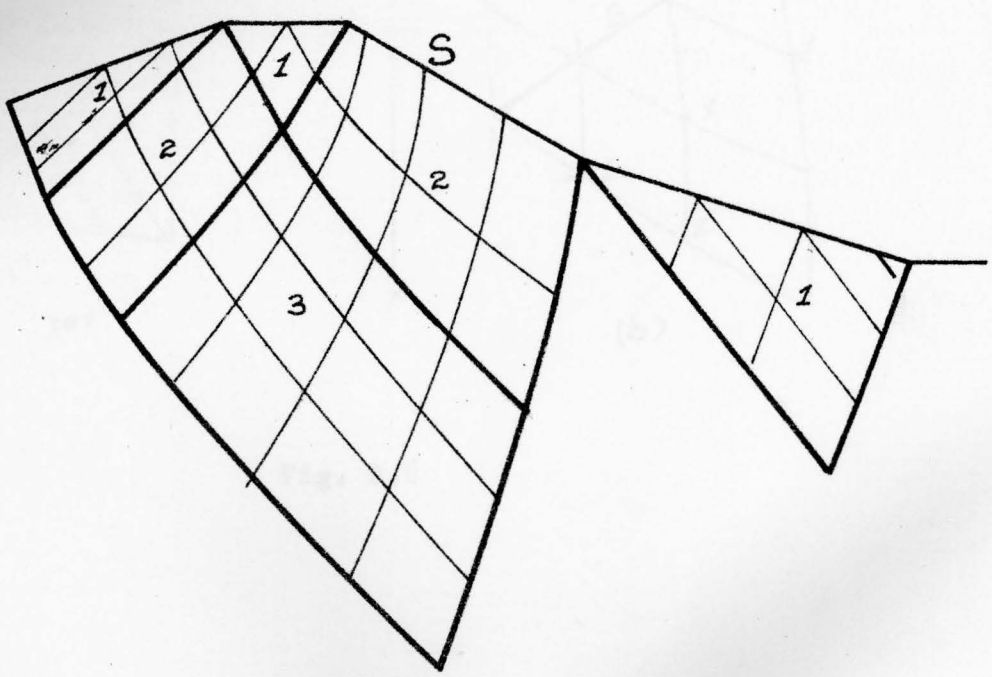

Type 1:

The curve, S, in the XY plane is continuous and differentiable and is nowhere coincident with a characteristic direction. On the curve S the values of u and v are prescribed, also continuous and differentiable. The solution is uniquely determined in the curvilinear triangle formed by the curve S and the α characteristic through the one extremity and the β through the other extremity of S. As there are two characteristics through each point two regions of solutions are defined, one on each side of the curve S. Normally only one region will have physical significance which will be evident from the requirements of the problem. For instance, the curve S may be the surface slope of an embankment and the required solution will be the region occupied by the embankment material. In Figure 2.6(a) the surfaces of solution for u and v are shown, and in Figure 2.6(b) the characteristic lines in the region of solution at some stage of the numerical solution is shown.

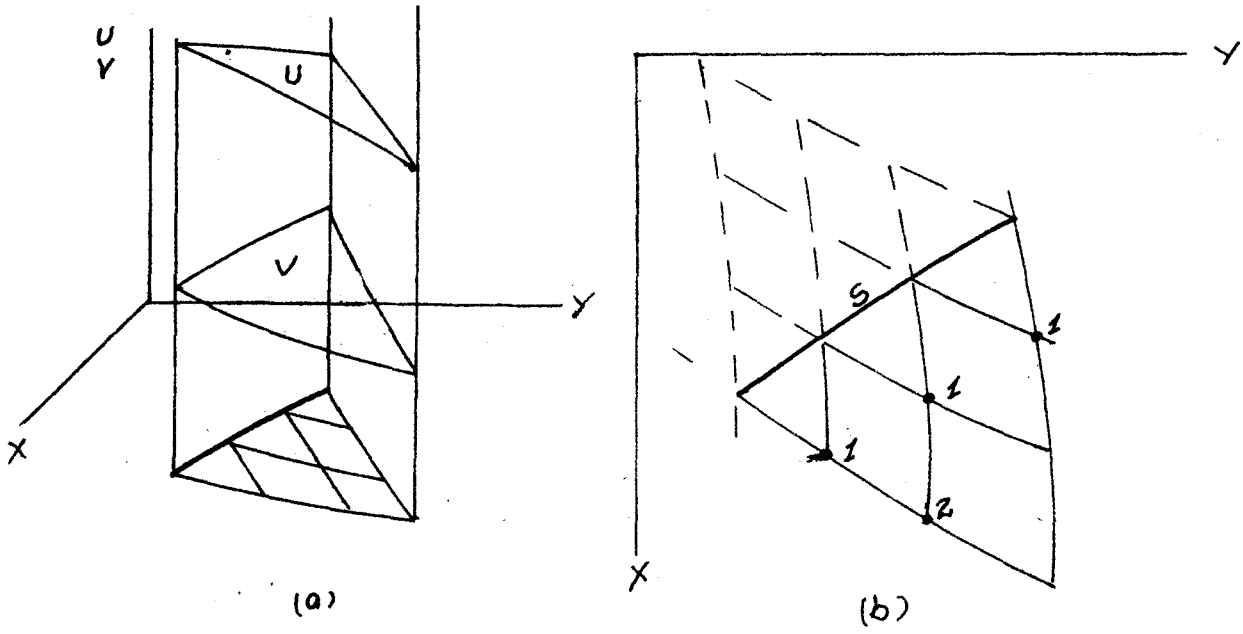

Fig. 2.6

Type 2:

Sub-type (a): The values of u or v are known along each of the two characteristic curves α and β through point P and u and v are known and single valued at point P. The values of u and v at point P must satisfy the differential equations for u and v along each of the characteristics. If for instance u and v are known at P and u along the α characteristic the value of v along this characteristic can be calculated from differential equation 2.29 or 2.31 which gives the relationship between u and v along the characteristic. Similarly both u and v can be calculated on the β characteristic. Once u and v are known along the α and β characteristic up to point A and C respectively the solution is uniquely determined in the curvilinear quadrangle PCBA formed by the characteristic PA and PC and the characteristics through A and C. The surface of solutions for u and v are shown in Figure 2.7(a), and in Figure 2.7(b) the characteristic lines at some stage of the numerical solution is shown, the order of calculation of the points being indicated.

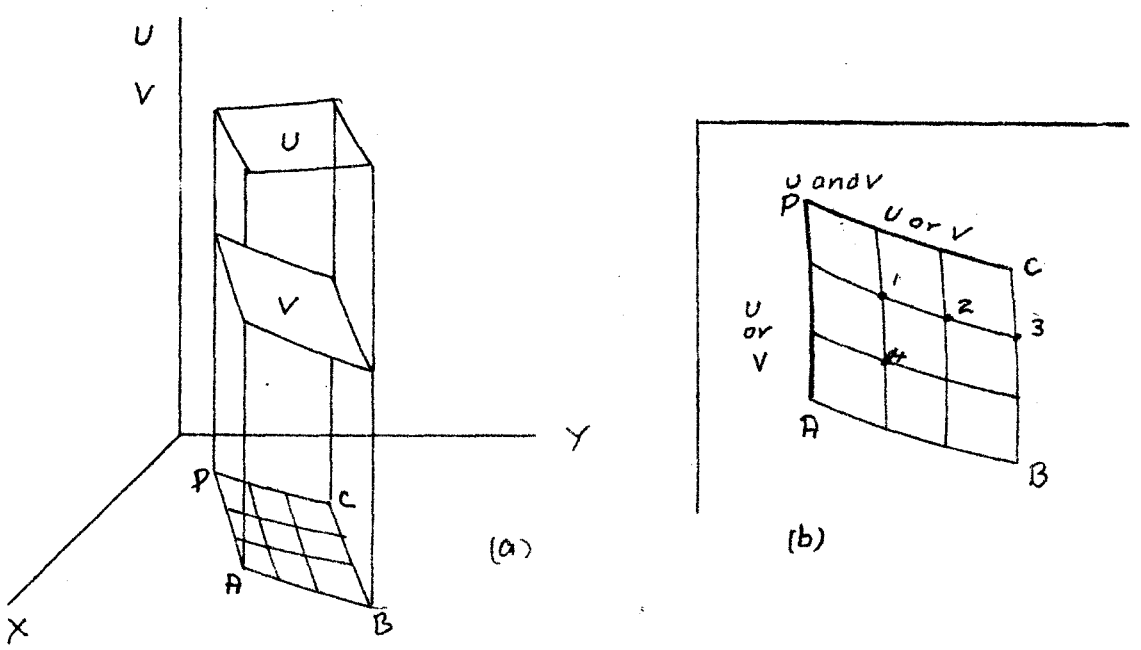

Fig. 2.7

Sub-type (b): Physical requirements of the problem may lead to two values for u and v at point P, that is a finite discontinuity occurs in the values of u and v. Continuously differential values of u or v are prescribed along the one characteristic through P, but at P two values of u and for v are given. The surface of solution for, say, the dependent variable u is shown diagramatically in Figure 2.8(a). The characteristic lines and region of solution are shown in Figure 2.8(b). At point P, because a change in values in u and v takes place with x and y constants, a relationship between u and v can be established from equations 2.29 and 2.31. These changes are considered to take place on one characteristic of infinitely short length. All the characteristics of the equation pass through this point of discontinuity and by choosing arbitrarily values for u or v within the limits of the discontinuity the corresponding values for v or u can be determined. The solution then proceeds as with Type 2(a). An example with detailed procedure as to the solution of u and v at the point of discontinuity is given in Section 4.

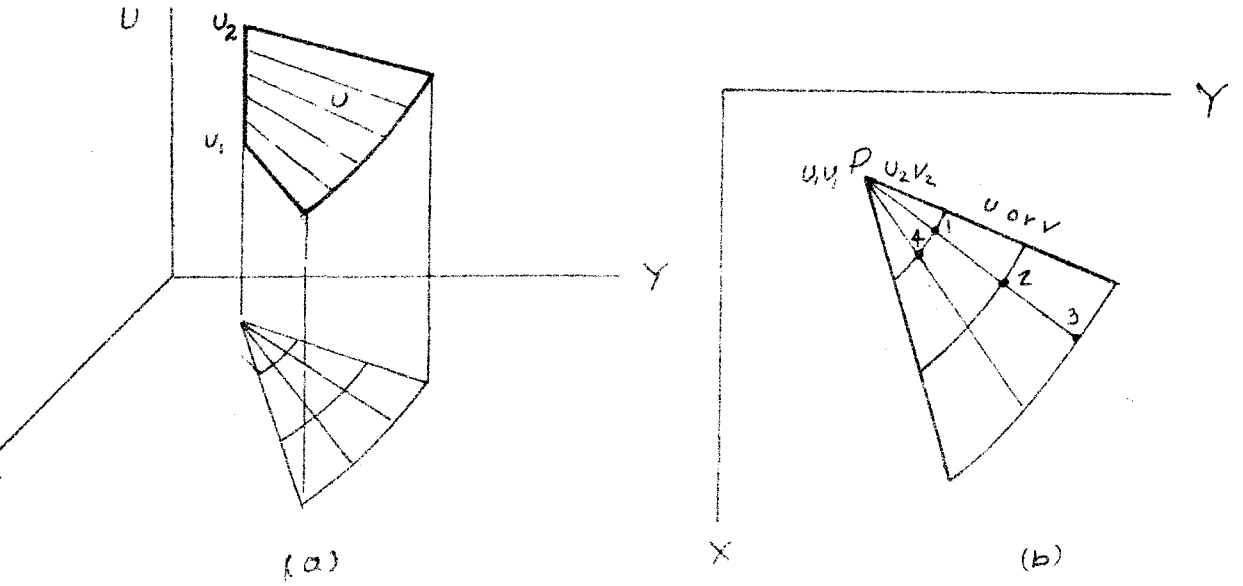

Fig. 2.8

S E C T I O N 3

3. THE PARTIAL DIFFERENTIAL EQUATIONS FOR PLASTIC FAILURE OF SOIL MEDIA

3.1 Introduction

The theory of plasticity has been defined as the mathematical study of stress and strain in plastically deformed bodies (Hill, 1961). This is a very wide definition embracing not only the immediate plastic deformation due to the applied loads, but also the effects of time, strain, hardening, repeated loading, etc. on the plastic deformation.

In order to construct a mathematical manageable theory some drastic simplifications must be made in respect of the properties of the plastic material. Every such simplification accepted within the framework of the theory lessens the agreement between the theoretically predicted plastic state and that found in reality. However, when considering the practical intent of the theory and bearing in mind the mathematical resources and experimental evidence available, the object cannot yet be an exact description of the phenomena as observed, but an adequate one for the purpose in mind. This requires the separation of the significant factors from the insignificant in so far as it affects the problem.

Even with the simplifications, the process of solution of plastic problems by the mathematical theory of plasticity can be very difficult and is not suited to routine application. As a result, approximate methods which require additional postulations as to the plastic behaviour of the body have been developed, and are widely used. These approximate solutions are approximate in a relative sense only - when compared with solutions obtained by the mathematical theory

of plasticity, within the framework of the postulated model of the properties of the material. The postulated model for the properties of soil media have evolved after much experimental work and throught, and within the limitations of our present knowledge the mathematical theory yields the most realistic solution. In consequence, such solutions are used as criteria to judge the accuracy of the solution obtained by approximate methods. In this context the mathematical theory has been invaluable and justifies the effort required to obtain "rigorous" solutions.

In many situations the comparison between the rigorous solution and the approximate one is difficult due to the different approaches employed in the two methods. The following example on the stability analysis of an embankment will serve as an illustration:-

In the approximate analysis the outline of the embankment is chosen and a failure plane surface assumed within the embankment (Figure 3.1(a)). Based on certain postulations as to the distribution of stresses on this failure surface, and assuming full mobilisation of the frictional and cohesive resisting forces on the surface, the "factor of safety" can be determined as follows:-

$$\text{Factor of safety} = \frac{\text{Resisting forces or moments}}{\text{Disturbing forces or moments}}$$

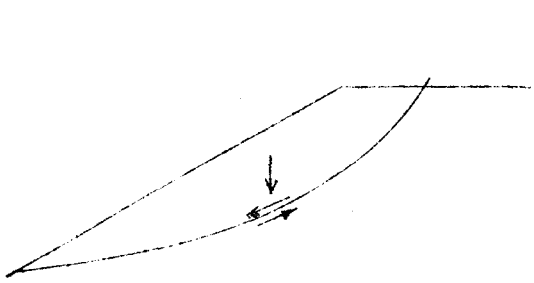

(a)

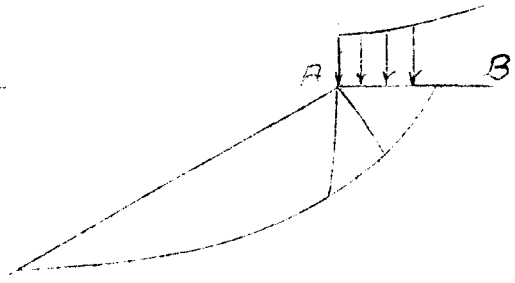

(b)

Figure 3.1

If the factor of safety is greater than one then the embankment is assumed to be in a state of complete or partial elastic equilibrium and the failure of the embankment is not considered likely, the degree of safety increasing as the factor of safety increases above one.

In the analysis of the embankment by the mathematical theory of plasticity a solution is not possible if the actual stresses in the embankment are in fact elastic or partially elastic and plastic. To induce a state of complete plasticity in the embankment additional forces must be applied somewhere on the contour of the embankment - in this case on the horizontal section AB (Figure 3.1(b)). With the superimposed distribution of forces (which are subject to certain restrictions) the contour of the slope at critical equilibrium can be determined by the plastic theory (Sokolovski, 1960). If, as in our example, the contour of the slope is fixed beforehand, solutions using various trial distributions of the forces on AB may be necessary before that distribution which gives the accepted contour is found. Assuming that this has been successfully achieved, then the only statement that can be made with respect to the safety of the embankment against plastic failure is that if the forces on AB are not applied the embankment will be in a state of partial or complete elastic equilibrium, that is, no statement as to the factor of safety, corresponding to that possible in the approximate analysis, can be made.

3.2 The theoretical model for soil media

In this Section very brief consideration will be given to the properties of real soil media and the modifications

necessary to develop the mathematical theory. It is not a discussion on the various theories relating to the plastic failure of soil media; the intention is to provide a background of the difficulties in the development of this theory. This is considered necessary firstly because the properties of this theoretical model are often not apparent from the theory, and secondly because a knowledge of the theoretical properties will bring about an awareness of the limitations of the theory.

3.2.1 Strength properties of soilmedia

A saturated soil medium is composed of two phases - solid and liquid. The solid phase is made up of two types of particles - clay and sand-like; the liquid phase is water. The two types of particles impart very different properties to the soil medium, in particular two components of shear resistance.

The clay particles are extremely small and, being disk-shaped, have an enormously large total surface area per unit weight. The surfaces are active and draw the liquid phase (i.e. the water) onto them, and also attract the adjacent particles. The thickness of the layers of "held" water around each particle influences the attraction between the particles, and in this way influences the bonding forces between the particles. These bonding forces are dependent upon the proximity of the particles to eachother, and hence are a function of the void ratio, the bonding forces increasing as the void ratio decreases. If the clay particles are randomly oriented, then in every direction the bonding forces should be the same. The resistance of the mass of particles is lower against tangential sliding than against normal

parting of planes. The maximum tangential sliding forces occur along the planes of maximum shear stress, which lie at 45° to the direction of the maximum principal stress, sliding being initiated when the shear stress exceeds the shear bonding strength of the material. A soil medium which has acquired shear strength due to these bonding forces is called cohesive, and the resistance against sliding is called the cohesive component of shear strength.

The discrete sandlike particles have surface areas per unit weight insignificant compared to clay particles, and the surfaces are relatively inert; consequently no bonding forces are present. A mass composed of these particles, when stressed, acquires strength due to the friction between, and the interlocking of, the particles - the shape, surface texture and packing of the particles being factors influencing these properties. On any plane through the mass the tangential shear resistance is dependent upon the intergranular normal stress acting on that plane. The potential resistance thus available is called the frictional resistance and the material is called cohesionless. Tangential sliding at a point in a stressed body develops along those planes where the ratio shear stress : normal stress exceeds a certain value called the coefficient of friction $\emptyset$. By normal and tangential resolution of the forces acting on various planes through a point in a stressed body of cohesionless material it can be shown that when the stress system is such that sliding failure occurs the angle, α, which the failure plane makes with the normal of the maximum principal stress is given by:-

$$\mu = \frac{1}{2}\left(\frac{\pi}{2} - \phi\right)^{\circ} = \left(45^{\circ} - \frac{\phi}{2}\right)^{\circ}$$

Generally a soil medium contains both clay and sand-like particles, thereby acquiring an intrinsic cohesive strength and the potential for the development of frictional strength. Because in a pure cohesive and a pure cohesionless material the failure planes lie at 45° and $(45 - \frac{\phi}{2})^{\circ}$ respectively to the direction of the maximum principal stress, in a mixture of clay and cohesionless materials the direction of failure lines must be intermediate between these two values, but to what degree the proportions of each material in the mass affect the direction of the failure lines is still a matter for conjecture.

The solid phase forms a skeleton of material, the interces of which are filled with the liquid phase. If a hydrostatic stress is applied to the body it is resisted by both the liquid and the soil skeleton, the division of stress between these two phases depending on their relative rigidities. The stress in the liquid is called the pore pressure; the nominal intergranular stress on any plane through the skeleton the effective stress; and the sum of these two the total stress. If a non-uniform stress is applied to a body, there is a division of stress between the liquid and the soil skeleton, but in this case the soil skeleton alone can resist the shear stresses. The shear resistance depends on the cohesive strength, which is constant for a constant void ratio, and the frictional strength which is dependent on the effective intergranular stress. It is therefore vitally important to know the pore pressure development in the mass in order to determine

the contribution to the shear strength due to friction.

The pore pressure in a sample under a non-uniform system of stress can be estimated from the triaxial test. In one such test, for example, the consolidated sheared undrained test with pore-pressure measurement, a cylindrical sample which is enclosed in an impermeable membrane is subjected to a hydrostatic pressure σ_3, and allowed to consolidate under this pressure, that is, allow the pore pressures to escape, with concomitant decrease in void ratio and increase in cohesive strength. An increasing deviator stress $(\sigma_1 - \sigma_3)$ is then applied along the axis of the cylindrical sample. As the stress is raised the strains lead to a rearrangement of the particles in the sample resulting in a change in void ratio which, if prevented, causes pore pressure to develop inside the sample.

By subtracting the pore pressure stresses from the total stresses (σ_1 and σ_3) the effective stresses (σ_1' and σ_3') can be determined, and either the effective deviator stress $(\sigma_1' - \sigma_3')$-strain or the total deviator stress $(\sigma_1 - \sigma_3)$-strain curves for the test sample can be determined.

The point on the stress-strain curve at which sliding failure is initiated, is called the yield point of the material. Whereas in plastic materials, for example mild steel, this point is well defined, in soils there is still considerable controversy as to when yield takes place in the soil. A number of theories on the initiation of yield has been advanced. For example, Jennings & Kirchmann (1961) from energy considerations deduced that the initial effective stress-strain curve for a normally consolidated soil, if the

stress is plotted against the log of the strain, should give a linear relationship. The yield point is defined as the stress at which the stress-strain curve deviates from this postulated linear relationship. From their experimental work they find that there are two linear sections in the initial part of the stress-strain curve. They conclude that the termination of the first linear section indicates the stress at which the cohesive component of shear strength, and termination of the second linear section the stress at which the frictional component of shear strength respectively are mobilised. This second point is considered to give the true yield value of the soil. However, this yield value is considerably below the maximum total deviator stress the soil could sustain, and conventionally the point on the stress-strain curve accepted as the yield point is the peak stress value on the total stress-strain curve.

A graphical representation of the stress system, total or effective, acting on the sample at any time during the loading period in the triaxial test can be given by the Mohr's circle of stress. If in a series of tests samples are consolidated under increasing pressures and then sheared with pore pressure measurements, the stress circles representing the stress systems at the defined yield points on the stress-strain curves can be drawn. A tangent curve to these circles represents an envelope of failure for the soil. Depending on the definition of the yield point and whether the total stresses or effective stresses are used, different envelopes can be drawn.

An interpretation of these envelopes is that for the drainage conditions of the test any circle of stress falling within the envelope represents a non-failure state, any circle touching the envelope a state of critical equilibrium, and any circle intersecting the envelope an inadmissable stress state.

A postulation is now made:- that the point of tangency of a critical circle to the envelope is related to the angle at which the failure line forms inside the sample. An uncritical acceptance of this postulation gives rise to a contradiction - if the total stress envelope is used, the angle of the failure lines with respect to the maximum principal stress differs from that using the effective stress envelope. This point is well appreciated, the error of accepting the total stress envelope as giving the angle of the failure lines being seldom made, but there is also reason to believe that the points of tangency of the critical circles to the effective stress envelope do not give the direction of the failure planes. This can best be illustrated by considering a pure cohesive material, i.e., a material with no co-efficient of friction. Under increasing consolidation pressures the reduction in void ratio would lead to an increase in the cohesion, hence a set of triaxial tests on such a material will lead to a set of critical stress circles increasing in diameter (Figure 3.2) depicting an effective strength envelope for a material apparently possessing a coefficient of friction; but in each test, because cohesion only is present, the failure lines will lie at 45° to the direction of the maximum principal stress. On the stress circles in Figure 3.2 these points are

designated by the letter B, and a curve through these points gives another strength envelope. One could conclude that the slope of the effective stress envelope for this pure cohesive material does not, firstly, indicate the true envelope although the difference from the true envelope and the tangential envelope may be quire small and, secondly, does not give the true angle at which the failure planes would lie.

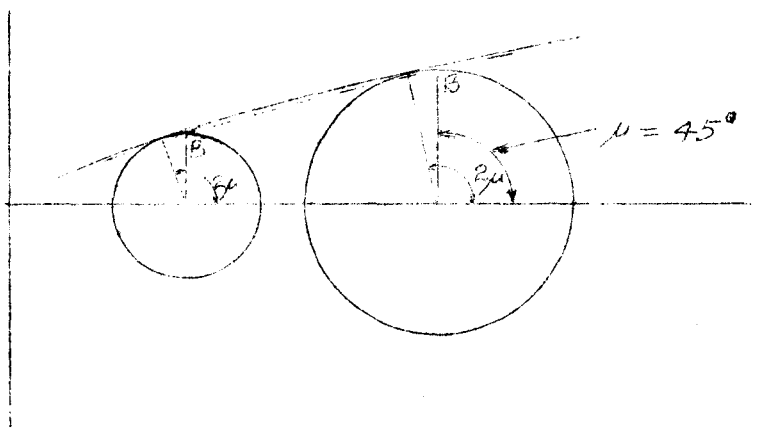

Figure 3.2

Similarly in a soil consisting of a mixture of cohesive and cohesionless material, the points of tangency of the critical circles do not coincide with the tangency points of the effective stress envelope. Although the difference between these two envelopes would be small, the angles which the failure planes form with the maximum principal stress would be significant (see Figure 3.2).

Effective strength envelopes obtained from using the peak point stress usually lead to linear envelopes. The intersection of the envelopes with the shear axis at zero normal stresses is taken as the "cohesion" and the slope of the envelope equal to the angle of internal friction. As it is known that the cohesive strength increases with

consolidation pressure, this presentation gives an erroneous picture of the relative components of strength, cohesive and frictional, in the body. However, in order to separate out the cohesive and the frictional components additional elaborate investigations are required, (Hvorslev, 1937), and their determination is not yet a practical proposition. Conventionally it is accepted that the values for the cohesion and the friction as given by the effective stress envelopes are the best practical estimates of these parameters available. The situation is, however, one of confusion for Jennings & Kirchmann (1961) found that the critical circles tangent to the envelope determined from their yield points did in fact give the correct angle for failure planes in the triaxial sample. For use in the mathematical theory, Jennings & Kirchmann's theory is however still not sufficiently verified.

In cohesionless soils only the friction component is present, hence the error in $\emptyset$ due to the cohesive element is absent, and the slope of the effective stress envelope gives a value for $\emptyset$ probably not far from the true value.

For the purpose of the mathematical theory of plasticity the situation regarding the strength envelope for soil media can be summed up as follows:-

In a pure cohesive material the critical circles will increase as the consolidation pressure increases, but as the strength in this material is the same in all directions the circle of stress tangent to this envelope will not, at its point of tangency, correctly indicate the location of the failure lines. In soil media in which both frictional and cohesive components are present, the same situation applies, with the slope of the envelope being greater than the true co-efficient of friction, and the cohesion a constant quantity. The best

estimates available for these parameters are the "constant" value for the cohesion, c, at zero effective stress, and ϕ, the angle of internal friction given by the slope of the effective stress envelope. In cohesionless materials the value for the co-efficient of friction is probably very nearly correctly given by the slope of the effective stress envelope.

3.2.2 The stressed body

3.2.2.1 Plane strain and plane stress

Most of the stability problems in soil mechanics occur in conditions approximating plane strain; strains occur in, say, the XY plane, the strain in the Z direction being equal to zero. If Poisson's ratio is greater than zero, two-dimensional strains always lead to three-dimensional stresses, and vice versa (Case, 1948).

3.2.2.2 Plane eequilibrium of bodies

Irrespective of whether plane strain or plane stress conditions prevail, the differential equations for equilibrium under plane conditions can be written as follows:-

Assuming the XY plane is being considered, and the body force acts in the X direction, then:

$$\frac{\partial \sigma_x}{\partial x} + \frac{\partial \tau_{xy}}{\partial y} = \gamma$$

$$\frac{\partial \tau_{xy}}{\partial x} + \frac{\partial \sigma_y}{\partial y} = 0$$

These are two differential equations of equilibrium in terms of the three stresses σ_z, σ_y and τ_{xy}, and hence no unique solution is possible. The third relationship is determined by the behaviour of the material under stress, that is, whether the elastic or plastic states are considered.

3.2.2.3 Elastic conditions

A third relationship can be derived if the body, in addition to being elastic, obeys Hook's law, i.e., stress must be proportional to strain. The equation of compatibility of strains can be derived, i.e.:

$$\left(\frac{\partial^2}{\partial x^2} + \frac{\partial^2}{\partial y^2}\right)(\sigma_x + \sigma_y) = 0$$

From the three equations it is possible to derive a fourth order partial differential equation (called the bi-harmonic equation) in the dependent variable, F, called the Airy's stress function (Terzaghi, 1959).

$$\frac{\partial^2 F}{\partial x^2} - \frac{\partial^2 F}{\partial y \partial x} + \frac{\partial^2 F}{\partial y^2} = \gamma y + C$$

It should be noted that this differential equation does not require any of the elastic constants such as Young's modulus, Poisson's ratio, etc., provided Hook's law is obeyed.

The bi-harmonic equation is analogous to the elliptic partial differential equations mentioned in Section 2 and its boundary conditions are also similar, in that provided external equilibrium of forces on the body is maintained, these forces may be distributed in an arbitrary manner around the boundary; infinitesimal changes of stress or strain on the boundary lead to changes of stress and strain at every point internal to the boundary.

In plane strain conditions, on the XY plane the stresses in the z direction can be determined from the following equations (Case, 1948):-

$$\sigma_x = \frac{mE}{(m-1)(m+1)}\left[(m-1)e_x + e_y\right]$$

$$\sigma_y = \frac{mE}{(m-1)(m+1)}\left[(m-1)e_y + e_x\right]$$

$$\sigma_z = \frac{mE}{(m-1)(m+1)}\left[e_x + e_y\right]$$

$$\tau_{xy} = \frac{mE}{2m+1}$$

where 1/m = Poisson's ratio, and e_x, e_y, e_z are strains in the x, y, z, directions respectively, from which it can be seen that:

$$\sigma_x + \sigma_y = m\,\sigma_z$$

If Poisson's ratio = 0.5 then

$$\sigma_z = \frac{1}{2}(\sigma_x + \sigma_y)$$

The use of this last equation in the development of the mathematical theory will become apparent later.

3.2.2.4 The rigid body

It has been stated that Airy's stress function is independent of the elastic constants of the material. Consequently, the stresses derived from the solution of this function will be valid if Young's modulus increases indefinitely. A body with an infinitely high Young's modulus is defined as a rigid body. Although the strains are equal to zero, the stresses are correctly given by the solution of the Airy's stress function.

3.2.2.5 Plastic conditions

The third relationship for the plastic state will now be considered. The discussion starts from the formulation for the yield criterion in plastic metals and this is extended to give the formulation for the yield in soil media. This extension may appear to be somewhat artificial and in fact is so (because of our ignorance as to the true yield in soils), but by deriving the required relationship in this fashion attention is directed towards certain difficulties, inherent in a formulation applicable to plane strain conditions, difficulties that will have to be faced with any yield criteria.

Mathematically the difference between the yield criteria for metals and for soil media can be stated as follows:-

In metals the yield point is independent of the mean normal stress; in soil media the yield point is dependent upon the mean normal stress.

Considering the plastic metals there are two widely accepted criteria by which the yield point can be estimated, those due to Tresca and Levy & von Mises.

In the Tresca hypothesis yield in a body under a state of complex stress takes place when the maximum shear stress equals or exceeds a certain value, i.e.:

$$\frac{1}{2}(\sigma_{max} - \sigma_{min}) \geqslant k$$

where σ_{min} = minimum principal stress

σ_{max} = maximum principal stress.

It should be noted that the intermediate principal stress does not enter into the criterion.

Under plane strain conditions in the XY plane provided Poisson's ratio is greater than zero, the σ_z principal stress will always be intermediate to the principal stresses in the XY plane and therefore does not enter into the criterion; consequently for critical equilibrium the criterion for yield can be written:-

$$\sqrt{\left[\frac{\sigma_x - \sigma_y}{2}\right]^2 + \tau_{xy}^2} = k$$

In the Levy & von Mises criterion yield takes place when the shear strain energy, that is the energy due to distortion, exceeds a certain value. Under plane strain conditions there is no distortion in the z direction, hence no energy is contributed from this source, and σ_z, τ_{xz}, and τ_{yz} do not enter into the criterion. In consequence, under plane strain conditions it is possible to write Levy & von Mises' criterion in the identical form as Tresca's:-

$$\sqrt{\left[\frac{\sigma_x - \sigma_y}{2}\right]^2 + \tau_{xy}^2} = k'$$

but the constant K' is not equal to K. From experimental investigations it has been found that the Levy & von Mises' criterion is superior, but under plane strain conditions the two criteria have the same mathematical form, so either can be used in the mathematical development of the theory.

If the hypothesis is put forward that the yield depends on the mean normal stress, Tresca's and Levy & von Mises' criteria can be extended to incorporate this. For the plane strain condition Tresca's criterion can then be written:-

$$\sqrt{\left[\frac{\sigma_x - \sigma_y}{2}\right]^2 + \tau_{xy}^2} = f(\sigma_x + \sigma_y + \sigma_z) = f(\text{mean stress})$$

where the term f (mean stress) is usually taken as a linear function. That is

$$LHS = K''\left(\frac{\sigma_x + \sigma_y + \sigma_z}{3}\right) + C$$

It can be noted that σ_z enters into the criterion of yield; similarly for von Mises' criterion. If Poisson's ratio is equal to 0.5, then

$$\sigma_z = (\sigma_x + \sigma_y)\frac{1}{2}$$

and the criterion can be written

$$LHS = \frac{1}{2}(\sigma_x + \sigma_y)A + B$$

and the σ_z does not enter into the criterion. The constants A and B are functions of the co-efficient of friction ϕ, and the cohesion. Incorporating ϕ into the constants gives

$$\sqrt{\left[\frac{\sigma_x - \sigma_y}{2}\right]^2 + \tau_{xy}^2} = \left[\frac{\sigma_x + \sigma_y}{2}\right]\sin\varphi + c\cos\varphi \quad (a)$$

where c is the cohesive shear strength of the soil. In this form equation (a) is known as Mohr's criterion for yield.

In the studies of the yield in plastic metals it has been found that under plane strain conditions if the plastic

strain exceeds 2 - 5 times the elastic strain, Poisson's ratio does in fact tend to 0.5 in the plastic region, and σ_z would therefore be neglected in the plastic region. How valid this is in soil media is still a matter for conjecture, but for the purpose of the mathematical theory in order to eliminate the σ_z from the criterion of yield it will be required that Poisson's ratio is taken equal to 0.5.

With regard to its application to soil media it must be remembered that equation (a) is approximately true only for the effective stresses, and has no validity for total stress envelopes, where its use is simply a means for stating a linear relationship for the envelope. Sokolovski developed the mathematical theory of plasticity for soil media using the cohesive parameter c and the friction parameter ϕ, without apparently considering the influence of pore pressure development during failure. This does not in any way invalidate his work, for it is theoretically possible to incorporate the pore pressures in a manner similar to the incorporation of the seepage pressures (Sokolovski 1960) without disturbing the theoretical structure of his theory. A difficulty in using the effective stress parameters in such a theory will be to estimate the pore pressure development during failure in a mass where the consolidation prehistory varies throughout. Relationships between the pore pressure development at failure and the consolidation pressure will be required. An example of such a relationship is shown in Figure 9.39 and would be of vital importance to the analysis of the plastic failure in such a material. No attempt by means of the mathematical theory of plasticity has yet been made to obtain solutions of the plastic failure

of soil masses in which the pore pressures generated during failure are taken into account.

Sokolovski's work on "cohesive" soils in which he assumes that the cohesive parameter is the only one present (the concept of $\phi = 0$, i.e., no frictional strength component in soils) seems to have arisen from the total stress envelopes obtained from the unconsolidated undrained shear tests on saturated soils. Within the normal ranges of stresses encountered in soil mechanics, effective stress envelopes in which $\phi' = 0$ are most unlikely.

The assumption of a linear strength envelope in Sokolovski's mathematical analysis is a simplification which is not an essential requirement for the development of the mathematical theory of plasticity (Sokolovski 1960). He has in fact presented the elements of a theory in which a general form of stress envelope is postulated, but it is evident that the gain in generality will be offset by the increase in complexity of the analysis. However, with the use of electronic computers solutions to problems using the complex analysis should not present insurmountable difficulties. Curved envelopes of failure such as those obtained by Jennings & Kirchmann could be treated by this analysis.

Later it will be shown that the partial differential equations of failure are quasi-linear hyperbolic. These equations are so flexible that should methods for determining the true cohesion and true friction become practical it will be possible to incorporate these conditions into the equations.

Finally it should be remembered that the values ϕ and c are determined in triaxial tests where the failures do not take place under plane strain conditions. The analysis of

plane failure using the parameters determined in the triaxial tests will therefore be in error to the degree that the $\emptyset'$ and c' values deviated from the true values in plane strain.

3.2.2.6 The elasto-plastic failure of a body

The complete solution of the stresses and strains in a body, a portion of which is in a state of plastic failure, is one of extreme difficulty, and very few solutions are known at present (Hill, 1960). Where solutions have been obtained, it has been principally due to simplifying conditions of symmetry in the shape and the applied stresses. An example of such a solution is the elasto-plastic state of thick spherical shells under internal pressures sufficient to cause plastic deformation spreading outwards from the internal diameter of the shell while the outer diameter is still in an elastic state. Here the plastic strain is of the same order as the elastic strain, and the neglect of the elastic component leads to gross errors in certain of the stress components. (In soil mechanics a similar situation will arise in investigations of the plastic failure of deep-seated, point-loaded piles).

Where the plastic strain is not constrained by the surrounding elastic material, the plastic deformation can take place freely. With the progress of plastic deformation, the influence of the elastic component of strain reduces to insignificance, and its effect on the stresses can be neglected. Large plastic shear strains are normal in the majority of plastic failure problems of soil masses, and the neglect of the elastic components of strain in the plastic region should not lead to significant errors. In any case, in the present state of the theory, this assumption is essential if any solution is to be obtained at all.

3.2.2.7 The rigid-plastic body

Neglecting the elastic component of strain in the plastic region implies that the plastic shear strain takes place without volume changes. For consistency, the strains in the elastic zone of the body should also be neglected. This can be accomplished by assuming rigid body conditions, that is assuming E to tend to infinity. It is then still possible to calculate the elastic stress distribution but the elastic strains remain at zero! Because the value of Poisson's ratio tends to 0.5 in the plastic zone, in order to eliminate discontinuities in the theoretical stresses at the junction of the plastic and elastic zones, it is assumed that the Poisson's ratio is also equal to 0.5 in the elastic zone. The theoretical body in which the elastic components of strain in both the plastic and elastic zones are neglected is called a rigid-plastic body.

The assumption of rigid plasticity does not imply that in a body subject to increasing intensity of loading the intermediate states of plasticity cannot be calculated. But, during the transition stage before the plastic zone has penetrated through the body, the elastic components of strain are of the same order as the plastic components and the assumption of rigid plasticity leads to certain errors in the stress distribution. Once the plastic zone has penetrated through the body, even though adjacent elastic zones still exist, the plastic failure movement is unrestricted and the errors due to the confining influence of the elastic zone decrease to insignificance.

In the mathematical theory of plasticity it is usual to determine only the final plastic state. Because

of the assumption of rigid plasticity, and because the plastic zone is described by hyperbolic partial differential equations which require only the stress distribution on the external boundaries of the plastic zones, it is possible to determine the plastic zones independently of the elastic zones.

3.2.2.8 Statically determinate and statically indeterminate plastic failures

The concept of statically determinate and statically indeterminate plastic failures appears to be due to Hill (1960).

In the plastic regions of failure there are two conditions to be filled. The first is that the critical equilibrium state of the stress must be satisfied, and the second is that the plastic shear strain rates (or velocity of shear strains) must be compatible with the stress state for the initial shear strain rates. Hill shows that if the plastic failure is governed solely by the stress applied externally to the body, the critical stress state and the shear strain rate state are compatible, and the solution of the critical stresses only is required. This type of failure is called statically determinate.

The statically indeterminate state arises in the following circumstances:

(1) The externally applied strain rates of the body are controlled. In soil mechanics this situation, for instance, occurs in the failure of rigid foundations and retaining walls. The problem can be clarified by considering a footing under statically determinate conditions. To obtain a solution, the distribution of load on the footing is specified, and is applied, as it were, on a thin rubber

membrane which can deform as the soil underneath deforms with failure. In the statically indeterminate footing the deformation of the soil underneath would lead to a re-distribution of stress different from that originally applied if the soil is to remain in contact with the footing. Hence the stresses are not independent of the relative strain rates. In order to solve this problem by means of the mathematical theory of plasticity, a stress distribution must be assumed and the critical state throughout the failure region determined. The strain rates throughout the failure area then require determination, using the specified initial rates. Their solution is similar to the solution for the stress state, also being governed by hyperbolic partial differential equations. If the characteristics of the stress and strain rates are coincident, the solution is the correct one; if not, a different stress distribution must be assumed until compatibility between the strain rates and the critical stress state is achieved.

In the failure of retaining walls the same situation applies for the movement of the soil during failure is controlled by the rigid movement of the wall. This problem is of concern in soil mechanics, and Terzaghi emphasises the importance of the movement of the retaining wall on the form of the failure. (We must, however, be careful to observe the difference between the control of the plastic shear strain rates for statically indeterminate retaining wall problems in the plastic theory and the elastic strain movement that Terzaghi considers prior to failure. For instance, in Figure 3.3(a), according to

our definition, a statically indeterminate failure is taking place, the failure zone lying against the rigid wall and controlled by the movement of the wall. In Figure 3.3(b) a statically determinate failure is taking place. In Terzaghi's analysis, because he considers only elastic strains, he does not differentiate between these two failures theoretically, although in this particular example the solution of the statically indeterminate problem will probably be very near or identical to that given by the statically determinate solution).

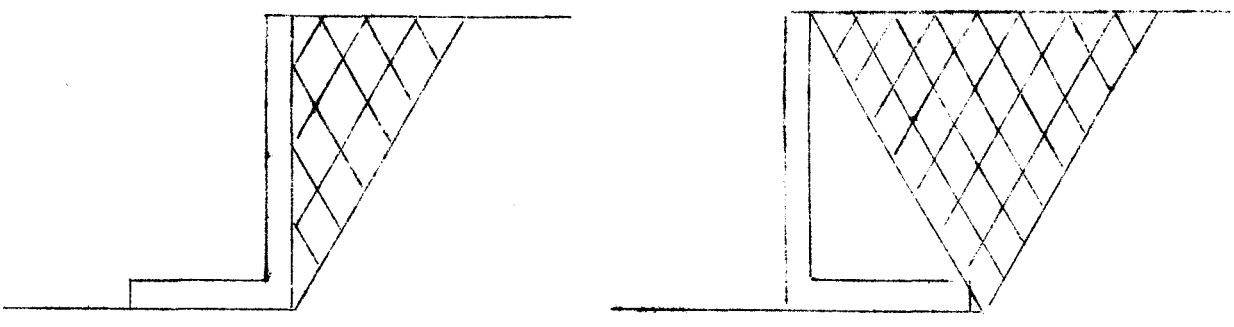

(a) (b)

Figure 3.3

Sokolovski provides a solution for the failure in Figure 3.3(a) by making certain assumptions as to the distribution of stress against the wall, but the uniqueness of his solution is only guaranteed if the strain rate solution coincides with the stress solution. He has not considered the shear strain rates which may require that at the wall the rates would not result in a linearly distributed total strain.

(2) A second statically indeterminate state arises when the

plastic zone develops internal to the body, i.e., the plastic state is surrounded by an elastic state. This condition can only be predicted if the elastic state in the body is determined at various stages under an increasing load, until the stress on the point internal to the body exceeds the yield point. A problem in which this situation occurs has been solved by Southwell & Allen, and here Hill criticises the solution in that the strain rates have not been considered. (Southwell & Allen, 1950).

The solutions of the plastic equations attempted in this thesis are all of the statically determinate type, and hence no consideration is given to the shear strain rates.

3.3 Derivation of the partial differential equations for plastic failure of soil media

The derivation of the quasi-linear partial differential equations describing the plastic failure of soil media will now be presented. The equations derived are those due to Sokolovski (1960). The transformations employed in the derivation are identical to his, but the procedures are different, following those set out in Section 2. It is hoped that by adopting this approach the unity of the equations of failure with the hyperbolic partial differential equations will become clear.

In order to preserve Sokolovski's notation, the angle of internal friction will be denoted by ρ and the cohesion by k instead of the conventional ϕ and c respectively. From the text the meaning attached to each symbol should be clear.

3.3.1 State of stress at a point in a body

The state of stress at a point in a body can be represented graphically by means of the Mohr's stress circle. The following conventions will be followed in constructing the stress circle:-

1. Compressive stresses are positive, plotted to the right.
2. Shear stress couples which act anti-clockwise are positive, and plotted vertically upwards.

In Figure 3.4(a) the stress on an elemental rectangle is shown. In Figure 3.4(b) the graphical representation of this stress condition by means of the Mohr stress circle is shown.

If the conventions set out above are followed, a rotation 2θ of a point on the stress circle conforms to a rotation, θ, in the same direction of the plane.

The stress state on the plane marked (I) is represented by the point marked (1) on the stress circle. The major

principal stress is indicated by point 2 on the stress circle. The plane on which this stress acts is found by noting that to reach point 2, point 1 must be rotated to 2θ clockwise from point 1. This means that the plane I in Figure 3.4(a) must be rotated clockwise an angle equal to θ to give the plane on which the major principal stress acts.

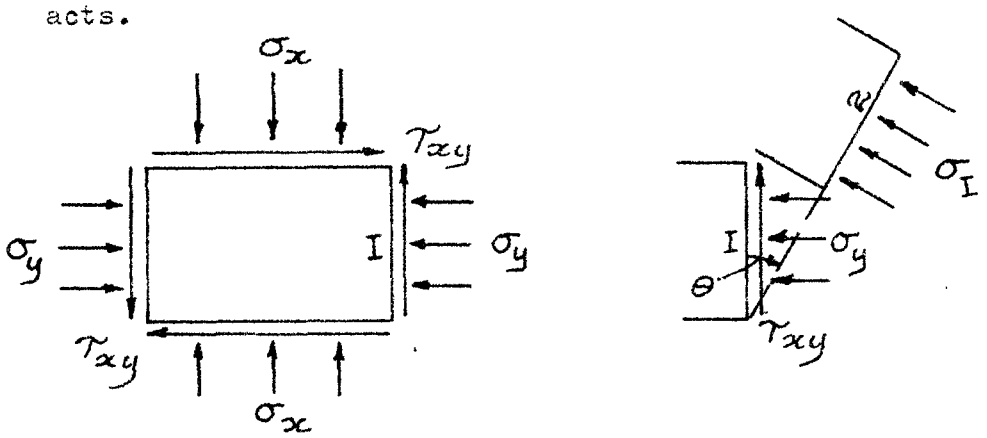

(a)

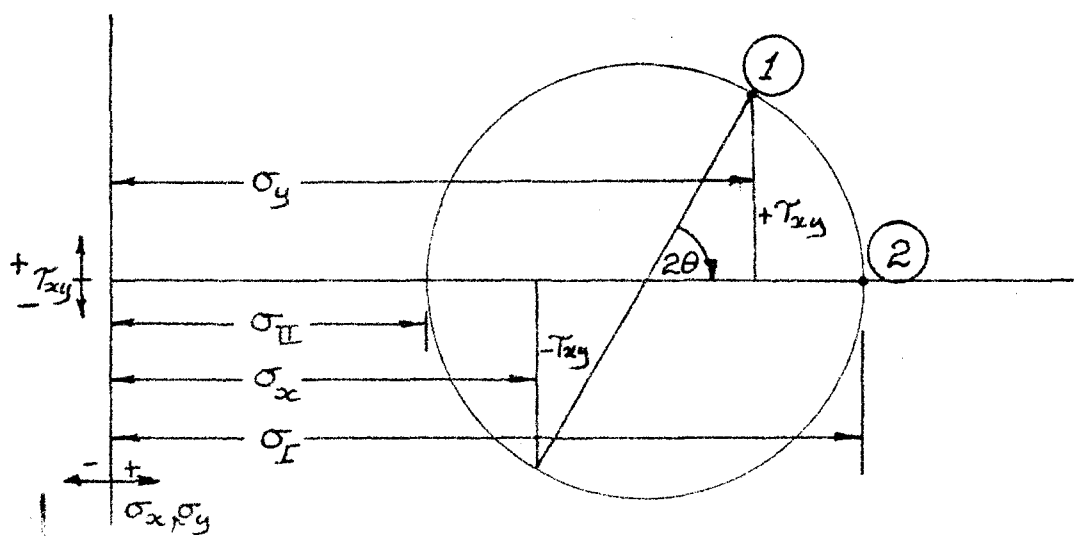

(b)

Figure 3.4

From Figure 3.4(b) it is a simple matter to write down the values of the major and minor principal stresses in terms of σ_x, σ_y, and τ_{xy}.

$$\left.\begin{matrix}\sigma_I \\ \sigma_{II}\end{matrix}\right\} = \frac{1}{2}(\sigma_x+\sigma_y) \pm \sqrt{\left[\tfrac{1}{2}(\sigma_x-\sigma_y)\right]^2+\tau_{xy}^2} \qquad 3.1$$

3.3.2 The co-ordinate system

Following Sokolovski, choose the positive direction of the X axis vertically downwards and the Y axis horizontally to the right. Measure all angles, unless indicated otherwise, from the X axis with anti-clockwise rotation as positive.

3.3.3 The stresses in an element in terms of the principal stresses

Let the direction of the normal of the maximum principal stress be equal to ϕ where this angle is measured in accordance with the convention laid down above. (See Figure 3.4). Let σ_I and σ_{II} be known. If the stresses σ_x, σ_y and τ_{xy} are required, these can be found by rotating the plane on which σ_I acts in a positive direction equal to θ. The corresponding stress circle diagram is shown in Figure 3.5(b) and the values of σ_x, σ_y and τ_{xy} can be determined from the geometry of the stress circle, giving

$$\sigma_x = \frac{1}{2}(\sigma_I + \sigma_{II}) + (\sigma_I - \sigma_{II})\cos 2\theta \qquad 3.2$$

$$\sigma_y = \frac{1}{2}(\sigma_I + \sigma_{II}) - (\sigma_I - \sigma_{II})\cos 2\theta \qquad 3.3$$

$$\tau_{xy} = (\sigma_I - \sigma_{II})\sin 2\theta \qquad 3.4$$

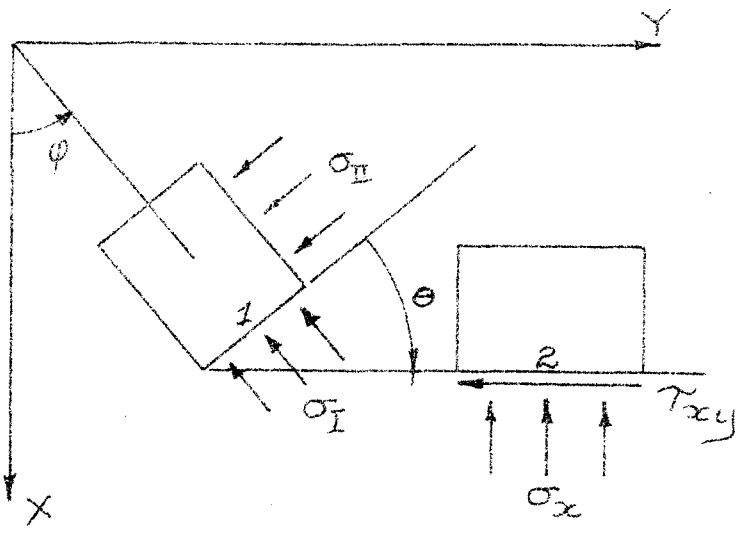

Figure 3.5(a)

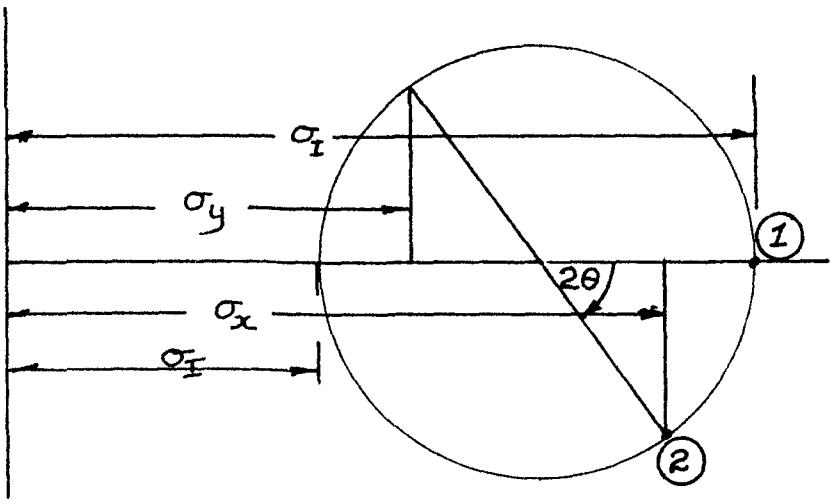

Figure 3.5(b)

3.3.4 Differential equations of equilibrium of an element in a body under stress

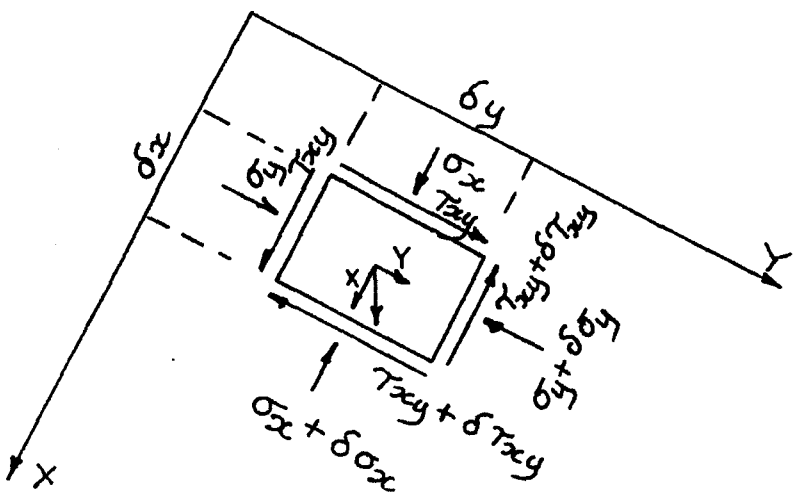

Figure 3.6

Consider an elemental rectangle in a body under non-uniform stress within the co-ordinate system shown in Figure 3.6. Let the density of the body be equal to and let the elemental weight of the body act vertically downwards. By taking moments about any point in the XY plane it can be shown that, for equilibrium, τ_{xy} is

equal to τ_{yx}. By resolving forces parallel with the X and Y axes, the following partial differential equations of equilibrium can be derived:

$$\frac{\partial \sigma_x}{\partial x} + \frac{\partial \tau_{xy}}{\partial y} = X \qquad 3.5$$

$$\frac{\partial \sigma_y}{\partial y} + \frac{\partial \tau_{xy}}{\partial x} = Y \qquad 3.6$$

These two equations are in terms of three unknown stresses σ_x, σ_y and τ_{xy} and hence the stress system is indeterminate. The third relationship is obtained by considering the critical plastic state of the element according to Mohr's hypothesis which states that, for a plastic state to exist, the following inequality must be satisfied:

$$\tau_n \geq k + \sigma_n \operatorname{Tan}\rho$$
$$\tau_n \geq (H + \sigma_n) \operatorname{Tan}\rho \qquad 3.7$$

where k, the cohesive strength of the soil = H Tan ρ, τ_n is the tangential shear stress on the plane on which the normal stress σ_n acts, and ρ is the angle of internal friction of the soil. Taking the equality sign which denotes a state of critical equilibrium, the stress circle graphically representing this state is illustrated in Figure 3.7(a).

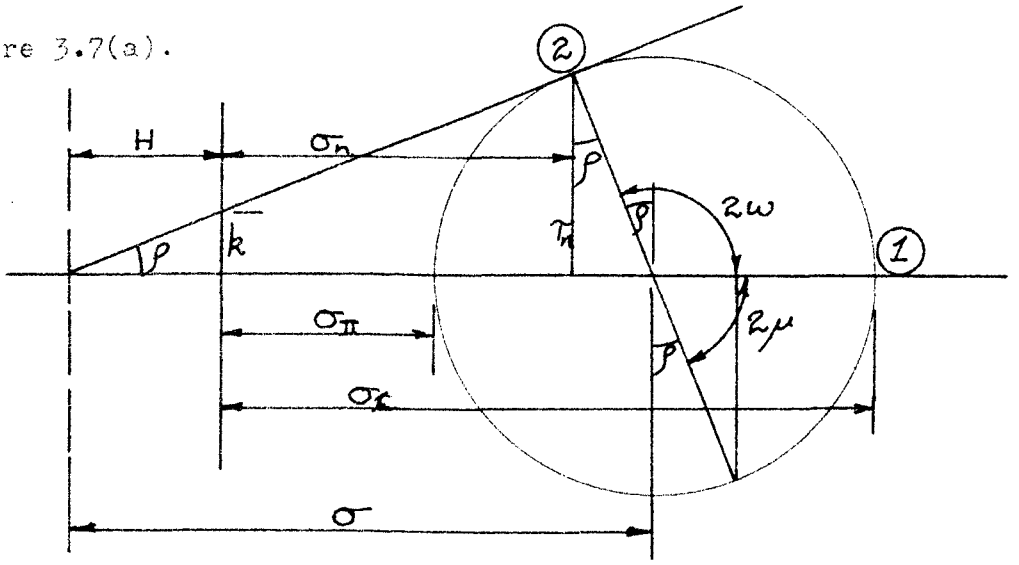

Figure 3.7(a)

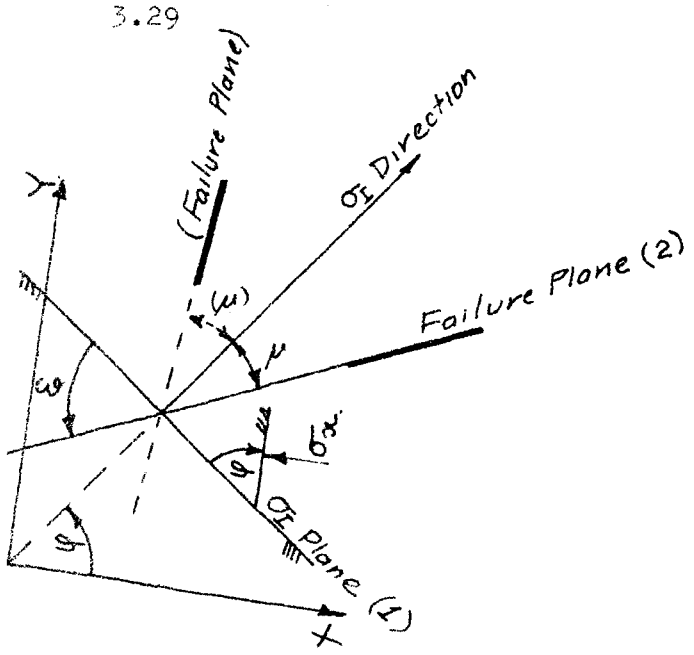

Figure 3.7(b)

From this diagram, it is clear that the plane (2) on which the critical stress condition is present can be found by rotating in an anti-clockwise direction equal to angle 2ω from the plane on which the major principal stress acts (1) (it is evident that $2\omega = 90 + \rho = \frac{\pi}{2} + \rho$). The angle of the critical plane with the normal on the plane on which the major principal stress acts, is given by:

$$2\mu = 90 - \rho = \frac{\pi}{2} - \rho \qquad \text{(see Figure 3.7(b).}$$

It is along these planes that the lines of slip or failure may appear in the plastic state.

With Mohr's criterion the three unknown stresses are now reduced to two and it is possible to transform equations 3.2, 3.3 and 3.4 in terms of two variables defined as follows:-

Let a pseudo mean stress be defined as follows:-

$$\sigma = H + \frac{\sigma_I + \sigma_{II}}{2} \qquad 3.8$$

and the angle of the normal on the plane of the maximum principal stress (i.e. the direction of the maximum principal stress) with the X axis be defined as $\emptyset$. (See Figure 3.7(b)).

Hence

$$\frac{\sigma_I + \sigma_{II}}{2} = \sigma - H \qquad 3.9$$

but from Figure 3.7(a)

$$\frac{\sigma_x + \sigma_y}{2} = \sigma \sin\rho \qquad 3.10$$

Again from Figure 3.7(a) and Figure 3.7(b)

$$\sigma_x = \sigma - H + \sigma \sin\rho \cos 2\varphi$$

$$= \sigma\left[1 + \sin\rho \cos 2\varphi\right] - H \qquad 3.11$$

$$\sigma_y = \sigma\left[1 - \sin\rho \cos 2\varphi\right] - H \qquad 3.12$$

$$\tau_{xy} = \sigma \sin\rho \sin 2\varphi \qquad 3.13$$

For purposes of simplification, a further transformation is required. Let

$$\sigma = \sigma_o e^{2\chi \tan\rho}$$

that is $$\log_e \sigma = \log_e \sigma_o + 2\chi \tan\rho \qquad 3.14$$

where $$\sigma_o = K$$

Substituting equations 3.11, 3.12, 3.13 and 3.14 in equations 3.5 and 3.6 gives:-

(the following partial differentials are required

$$\frac{\partial \sigma_x}{\partial x} = \frac{\partial \sigma_x}{\partial \sigma} \cdot \frac{\partial \sigma}{\partial \chi} \cdot \frac{\partial \chi}{\partial x} + \frac{\partial \sigma_x}{\partial \varphi} \cdot \frac{\partial \varphi}{\partial x} \qquad 3.15$$

$$\frac{\partial \sigma_y}{\partial y} = \frac{\partial \sigma_y}{\partial \sigma} \cdot \frac{\partial \sigma}{\partial \chi} \cdot \frac{\partial \chi}{\partial y} + \frac{\partial \sigma_y}{\partial \varphi} \cdot \frac{\partial \varphi}{\partial y} \qquad 3.16$$

$$\frac{\partial \tau_{xy}}{\partial x} = \frac{\partial \tau_{xy}}{\partial \sigma} \cdot \frac{\partial \sigma}{\partial \chi} \cdot \frac{\partial \chi}{\partial x} + \frac{\partial \tau_{xy}}{\partial \varphi} \cdot \frac{\partial \varphi}{\partial x} \qquad 3.17$$

$$\frac{\partial \tau_{xy}}{\partial y} = \frac{\partial \tau_{xy}}{\partial \sigma} \cdot \frac{\partial \sigma}{\partial \chi} \cdot \frac{\partial \chi}{\partial y} + \frac{\partial \tau_{xy}}{\partial \varphi} \cdot \frac{\partial \varphi}{\partial y} \qquad 3.18$$

This gives

$$\partial\sigma_x/\partial\sigma = 1 + \sin\rho \cos 2\varphi \;,\; \partial\sigma_y/\partial\sigma = 1 - \sin\rho \cos 2\varphi$$

$$\partial\tau_{xy}/\partial\sigma = \sin\rho \sin 2\varphi$$

$$\partial\sigma_x/\partial\varphi = -2\sigma \sin\rho \sin 2\varphi \;,\; \partial\sigma_y/\partial\varphi = 2\sigma \sin\rho \sin 2\varphi$$

$$\partial\tau_{xy}/\partial\varphi = 2\sigma \sin\rho \cos 2\varphi$$

Consider equation 3.14

$$\frac{\partial \sigma}{\partial \chi} \frac{1}{\sigma} = 2 \tan\rho$$

i.e.

$$\frac{\partial \sigma}{\partial \chi} = 2\sigma \tan\rho$$

Substituting in equation 3.5 gives:

$$[1+\sin\rho\cos 2\varphi][2\sigma\tan\rho]\frac{\partial\chi}{\partial x}-2\sigma\sin\rho\sin 2\varphi\frac{\partial\varphi}{\partial x}+$$
$$+[\sin\rho\sin 2\varphi][2\sigma\tan\rho]\frac{\partial\chi}{\partial y}+2\sigma\sin\rho\cos 2\varphi\frac{\partial\varphi}{\partial y}=\chi$$

Dividing by $2\sigma\tan\rho$

$$[1+\sin\rho\cos 2\varphi]\frac{\partial\chi}{\partial x}-\cos\rho\sin 2\varphi\frac{\partial\varphi}{\partial x}+\sin\rho\sin 2\varphi\frac{\partial\chi}{\partial y}$$
$$+\cos\rho\cos 2\varphi\frac{\partial\varphi}{\partial y}=\frac{\chi}{2\sigma\tan\rho} \qquad 3.19$$

Similarly, substituting in equation 3.6 and reducing gives

$$\sin\rho\sin 2\varphi\frac{\partial\chi}{\partial x}+[1-\sin\rho\cos 2\varphi]\frac{\partial\chi}{\partial y}+\cos\rho\cos 2\varphi\frac{\partial\varphi}{\partial x}+$$
$$+\cos\rho\sin 2\varphi\frac{\partial\varphi}{\partial y}=\frac{\gamma}{2\sigma\tan\rho} \qquad 3.20$$

Equations 3.19 and 3.20 are the basic differential equations, but suffer from the disadvantage that the dependent variables χ and φ occur simultaneously in each equation. It is however always possible to transform each equation to contain one dependent variable only. This is achieved by making the following substitution:

$$\xi=(\chi+\varphi)\tfrac{1}{2} \qquad \eta=(\chi-\varphi)\tfrac{1}{2} \qquad 3.21$$

i.e. $2\chi=\xi+\eta \qquad 2\varphi=\xi-\eta$

This substitution is equivalent to choosing a new axis, ξ and η, at 45° of the axes χ and φ.

$$\frac{\partial\chi}{\partial x}=\left[\frac{\partial\xi}{\partial x}+\frac{\partial\eta}{\partial x}\right]\frac{1}{2} \qquad \frac{\partial\varphi}{\partial x}=\left[\frac{\partial\xi}{\partial x}-\frac{\partial\eta}{\partial x}\right]\frac{1}{2} \qquad 3.22$$

$$\frac{\partial\chi}{\partial y}=\left[\frac{\partial\xi}{\partial y}+\frac{\partial\eta}{\partial y}\right]\frac{1}{2} \qquad \frac{\partial\varphi}{\partial y}=\left[\frac{\partial\xi}{\partial y}-\frac{\partial\eta}{\partial y}\right]\frac{1}{2}$$

Furthermore, for simplification the following substitution is convenient:

$$2\mu=\frac{\pi}{2}-\rho \qquad 3.23$$

(This relationship has been derived earlier, below equation 3.7).

Substituting equation 3.23 in equation 3.19

$$\left[1+\sin\left(\frac{\pi}{2}-2\mu\right)\cos 2\varphi\right]\frac{\partial\chi}{\partial x}+\sin\left(\frac{\pi}{2}-2\mu\right)\sin 2\varphi\,\frac{\partial\psi}{\partial y}$$
$$-\cos\left(\frac{\pi}{2}-2\mu\right)\sin 2\varphi+\cos\left(\frac{\pi}{2}-2\mu\right)\cos 2\varphi\,\frac{\partial\varphi}{\partial y}=\chi/2\sigma\tan\rho \quad 3.24$$

Now $\sin\left(\frac{\pi}{2}-2\mu\right)=\sin\frac{\pi}{2}\cos 2\mu-\cos\frac{\pi}{2}\sin 2\mu=\cos 2\mu$ 3.25

$$\cos\left(\frac{\pi}{2}-2\mu\right)=\cos\frac{\pi}{2}\cos 2\mu+\sin\frac{\pi}{2}\sin 2\mu=\sin 2\mu \quad 3.26$$

and substituting equations 3.25 and 3.26 in equation 3.24

$$\left[1+\cos 2\varphi\right]\frac{\partial\chi}{\partial x}+\sin 2\varphi\cos 2\mu\,\frac{\partial\chi}{\partial x}-\sin 2\varphi\sin 2\mu\,\frac{\partial\varphi}{\partial x}+$$
$$+\cos 2\varphi\sin 2\mu\,\frac{\partial\varphi}{\partial y}=\frac{\chi}{2\sigma\tan\rho}$$

Substituting χ and φ from equation 3.22 gives

$$\left[1+\cos 2\varphi\cos 2\mu\right]\left[\frac{\partial\xi}{\partial x}+\frac{\partial\eta}{\partial x}\right]+\left[\sin 2\varphi\cos 2\mu\right]\left[\frac{\partial\xi}{\partial y}+\frac{\partial\eta}{\partial y}\right]-$$
$$-\sin 2\varphi\sin 2\mu\left[\frac{\partial\xi}{\partial x}-\frac{\partial\eta}{\partial x}\right]+\cos 2\varphi\sin 2\mu\left[\frac{\partial\xi}{\partial y}-\frac{\partial\eta}{\partial y}\right]=\frac{\chi}{\sigma\tan\rho}$$

Multiplying out and gathering terms

$$\left[1+\cos 2\varphi\cos 2\mu-\sin 2\varphi\sin 2\mu\right]\frac{\partial\xi}{\partial x}+\left[1+\cos 2\varphi\cos 2\mu+\sin 2\mu\sin 2\varphi\right]\frac{\partial\eta}{\partial x}$$
$$+\left[\sin 2\varphi\cos 2\mu+\cos 2\varphi\sin 2\mu\right]\frac{\partial\xi}{\partial y}+\left[\sin 2\varphi\cos 2\mu-\cos 2\varphi\sin 2\mu\right]\frac{\partial\eta}{\partial y}=\text{RHS}.$$

which gives

$$\left[1+\cos 2(\varphi+\mu)\right]\frac{\partial\xi}{\partial x}+\left[1+\cos 2(\varphi-\mu)\right]\frac{\partial\eta}{\partial x}+$$
$$+\sin 2(\varphi+\mu)\cdot\frac{\partial\xi}{\partial y}+\sin(\varphi-\mu)\cdot\frac{\partial\eta}{\partial y}=\frac{\chi}{\sigma\tan\rho} \quad 3.27$$

Expanding the sum of angles and noting that $\sin^2\phi+\cos^2\theta=1$, equation 3.27 becomes

$$\left[(\sin^2(\varphi+\mu)+\cos^2(\varphi+\mu)+(\cos^2(\varphi+\mu)-\sin^2(\varphi+\mu)\right]\frac{\partial\xi}{\partial x}+2\sin(\varphi+\mu)\cos(\varphi+\mu)\frac{\partial\xi}{\partial y}+$$
$$\left[(\sin^2(\varphi-\mu)+\cos^2(\varphi-\mu)+(\cos^2(\varphi-\mu)-\sin^2(\varphi-\mu)\right]\frac{\partial\eta}{\partial x}+2\sin(\varphi-\mu)\cos(\varphi-\mu)\frac{\partial\eta}{\partial y}=\text{RHS}.$$

$$\therefore\quad 2\cos^2(\varphi+\mu)\frac{\partial\xi}{\partial x}+2\sin(\varphi+\mu)\cos(\varphi+\mu)\frac{\partial\xi}{\partial y}+$$
$$2\cos^2(\varphi-\mu)\frac{\partial\eta}{\partial y}+2\sin(\varphi-\mu)\cos(\varphi-\mu)\frac{\partial\eta}{\partial y}=\frac{\chi}{\sigma\tan\rho} \quad 3.28$$

Equation 3.20 can be similarly transformed to give:

$$2\sin(\varphi+\mu)\cos(\varphi+\mu)\frac{\partial\xi}{\partial x}+2\sin^2(\varphi+\mu)\frac{\partial\xi}{\partial y}+$$
$$+2\sin(\varphi-\mu)\cos(\varphi-\mu)\frac{\partial\eta}{\partial x}+2\sin^2(\varphi-\mu)\frac{\partial\eta}{\partial y}=\frac{\gamma}{\sigma\tan\rho} \quad 3.29$$

Multiplying equation 3.28 by Sin($\varphi + \mu$) and 3.29 by Cos($\varphi + \mu$), subtracting 3.29 from 3.28 gives

$$\left[2\cos^2(\varphi-\mu)\sin(\varphi+\mu) - 2\sin(\varphi-\mu)\cos(\varphi-\mu)\cos(\varphi+\mu)\right]\frac{\partial \eta}{\partial x} +$$

$$+\left[2\sin(\varphi-\mu)\cos(\varphi-\mu)\sin(\varphi+\mu) - 2\sin^2(\varphi-\mu)\cos(\varphi+\mu)\right]\frac{\partial \eta}{\partial y} =$$

$$= \frac{X\sin(\varphi+\mu) - Y\cos(\varphi-\mu)}{\sigma \tan\rho} \qquad 3.30$$

The co-efficient of $\frac{\partial \eta}{\partial x}$ can be written

$$2\cos(\varphi-\mu)\left[\sin(\varphi+\mu)\cos(\varphi-\mu) - \cos(\varphi+\mu)\sin(\varphi-\mu)\right]$$

i.e. $2\cos(\varphi-\mu)\left[\sin(\varphi+\mu-\varphi-\mu)\right]$

i.e. $2\cos(\varphi-\mu)\sin 2\mu.$

Similarly, the co-efficient of $\frac{\partial \eta}{\partial y}$ can be written

$$2\sin(\varphi-\mu)\sin 2\mu.$$

Substituting these values in equation 3.30 gives

$$2\cos(\varphi-\mu)\sin 2\mu\frac{\partial \eta}{\partial x} + 2\sin(\varphi-\mu)\sin 2\mu\frac{\partial \eta}{\partial y} = \frac{X\sin(\varphi+\mu) - Y\cos(\varphi+\mu)}{\sigma\tan\rho}$$

Dividing by 2Cos($\varphi - \mu$)Sin2μ gives

$$\frac{\partial \eta}{\partial x} + \tan(\varphi-\mu)\frac{\partial \eta}{\partial y} = \frac{X\sin(\varphi+\mu) - Y\cos(\varphi+\mu)}{2\cos(\varphi-\mu)\sin 2\mu\,\sigma\tan\rho}$$

By definition

$$\sin 2\mu = \sin(\pi/2 - \rho) = \sin\pi/2\cos\rho - \cos\pi/2\sin\rho$$

$$= \cos\rho$$

and by noting that $\cos\rho\tan\rho = \sin\rho$ equation 3.30 reduces to

$$\frac{\partial \eta}{\partial x} + \tan(\varphi-\mu)\frac{\partial \eta}{\partial y} = \frac{X\sin(\varphi+\mu) - Y\cos(\varphi+\mu)}{2\sigma\sin\rho\cos(\varphi-\mu)} \qquad 3.31$$

Multiplying equation 3.28 by Sin($\varphi - \mu$) and equation 3.29 by Cos($\varphi - \mu$), and subtracting 3.29 from 3.28, and treating the resultant equation in a manner similar to that above gives:

$$\frac{\partial \xi}{\partial x} + \tan(\varphi+\mu)\frac{\partial \xi}{\partial y} = -\frac{X\sin(\varphi-\mu) - Y\cos(\varphi-\mu)}{2\sigma\sin\rho\cos(\varphi+\mu)} \qquad 3.32$$

3.3.5 Determination of the characteristic equations

Consider any smooth curve S in the XY plane, the partial derivatives along S are given by

$$\frac{\partial \xi}{\partial x}\,dx + \frac{\partial \xi}{\partial y}\,dy = d\xi \qquad 3.33$$

$$\frac{\partial \eta}{\partial x}\,dx + \frac{\partial \eta}{\partial y}\,dy = d\eta \qquad 3.34$$

Following the method for determining the characteristic equations as set out in Section 2.5 the four differential equations 3.31, 3.32, 3.33 and 3.34 can be written

$$\begin{aligned} \frac{\partial \eta}{\partial x} + \frac{\partial \eta}{\partial y}\,\mathrm{Tan}(\varphi-\mu) &= a \\ \frac{\partial x}{\partial x}dx + \frac{\partial \eta}{\partial y}\,dy &= d\eta \\ \frac{\partial \xi}{\partial x} + \frac{\partial \xi}{\partial y}\,\mathrm{Tan}(\varphi+\mu) &= b \\ \frac{\partial \xi}{\partial x}dx + \frac{\partial \xi}{\partial y}\,dy &= d\xi \end{aligned} \qquad 3.35$$

where a and b are equal to the righthand side of equations 3.31 and 3.32 respectively.

In matrix form these equations can be written:

$$\begin{vmatrix} 1 & \mathrm{Tan}(\phi-\mu) & 0 & 0 \\ dx & dy & 0 & 0 \\ 0 & 0 & 1 & \mathrm{Tan}(\phi+\mu) \\ 0 & 0 & dx & dy \end{vmatrix} \begin{vmatrix} \partial\eta/\partial x \\ \partial\eta/\partial y \\ \partial\xi/\partial x \\ \partial\xi/\partial y \end{vmatrix} = \begin{vmatrix} a \\ d\eta \\ b \\ d\xi \end{vmatrix} \qquad 3.36$$

Equating the determinant formed from the square matrix of coefficients on the lefthand side of the matrix equation equal to zero, and expanding this determinant, gives the differential equations for locating the characteristics, i.e.

$$\left(\frac{dy}{dx}\right)^2 - \left[\mathrm{Tan}(\varphi+\mu) + \mathrm{Tan}(\varphi-\mu)\right]\frac{dy}{dx} - \mathrm{Tan}(\varphi-\mu)\,\mathrm{Tan}(\varphi+\mu) = 0$$

$$\therefore \frac{dy}{dx} = \frac{1}{2}\left[\mathrm{Tan}(\varphi+\mu) + \mathrm{Tan}(\varphi-\mu)\right] \pm \sqrt{\left[\mathrm{Tan}(\varphi+\mu) + \mathrm{Tan}(\varphi-\mu)\right]^2 - 4\,\mathrm{Tan}(\varphi-\mu)\,\mathrm{Tan}(\varphi+\mu)} \qquad 3.37$$

The expression in the square root reduces to

$$\left[\mathrm{Tan}(\varphi+\mu) - \mathrm{Tan}(\varphi-\mu)\right]^2.$$

Hence

$$\frac{dy}{dx} = Tan(\phi+\mu) \qquad 3.38$$

or $$\frac{dy}{dx} = Tan(\phi-\mu) \qquad 3.39$$

Equations 3.38 and 3.39 define the slopes of the two characteristics through any point x,y.

It can now be shown that the partial differential equations 3.31 and 3.32 are hyperbolic:-
Referring to Section 2.9 it was shown that if $b^2 - 4ac$ is greater than zero, the partial differential equations are hyperbolic. Now, $b^2 - 4ac = [Tan(\phi + \mu) - Tan(\phi - \mu)]^2$. The function inside the square brackets is different from zero for all values of ϕ and hence the square of this expression must always be greater than zero; hence the equations are hyperbolic.

The differential equations for determining the value of η and ξ along the characteristic curves is given by substituting the matrix column on the righthand side of equation 3.36 in the second column of the determinant of co-efficients on the lefthand side of this equation. Expanding the determinant of co-efficients and equating to zero gives:

$$d\eta\,dy - d\eta\,dx\,Tan(\phi+\mu) - a\,dx\,dy + a(dx)^2 Tan(\phi+\mu) = 0$$

and reducing gives

$$[dy - dx\,Tan(\phi+\mu)][d\eta - dx.a] = 0$$

Dividing by dx gives:

$$\left[\frac{dy}{dx} - Tan(\phi+\mu)\right]\left[\frac{d\eta}{dx} - a\right] = 0 \qquad 3.40$$

Now, substituting the equations for the characteristics, either $\frac{dy}{dx} = Tan(\phi + \mu)$ or $\frac{dy}{dx} = Tan(\phi - \mu)$. Substituting the first in equation 3.40 makes the lefthand side equal

to zero and hence there is an infinity of solutions.

Substituting the second gives:

$$[Tan(\varphi-\mu) - Tan(\varphi+\mu)]\left[\frac{d\eta}{dx} - a\right] = 0$$

Now, $[Tan(\phi - \mu) - Tan(\phi + \mu)]$ can never be equal to zero.

Hence

$$\frac{d\eta}{dx} - a = 0$$

for $\frac{dy}{dx} = Tan(\varphi - \mu)$.

Similarly, substituting the righthand column of the matrix equation in the 4th column of the matrix of co-efficients and reducing gives:

$$\frac{d\xi}{dx} - b = 0$$

for

$$\frac{dy}{dx} = Tan(\varphi+\mu)$$

Hence the characteristic equations are:

$$\left.\begin{aligned} \frac{dy}{dx} &= Tan(\varphi-\mu) && 3.41 \\ \frac{d\eta}{dx} &= a && 3.42 \end{aligned}\right\} \text{1st characteristic}$$

$$\left.\begin{aligned} \frac{dy}{dx} &= Tan(\varphi+\mu) && 3.43 \\ \frac{d\xi}{dx} &= b && 3.44 \end{aligned}\right\} \text{2nd characteristic}$$

3.3.6 Cannonical equations

Instead of referring the equations to the X and Y axes the equations can be referred to as the curvilinear grid of characteristics. Let the characteristic curves be plotted to a rectangular grid and the two co-ordinates be named α and β. The characteristic equations as referred to these characteristics then take the form:-

$$\frac{\partial y}{\partial \alpha} = Tan(\varphi-\mu)\frac{\partial x}{\partial \alpha}$$

$$\frac{\partial y}{\partial \beta} = Tan(\varphi+\mu)\frac{\partial x}{\partial \beta}$$

$$\frac{\partial \eta}{\partial \alpha} = a \frac{\partial x}{\partial \beta}$$

$$\frac{\partial \xi}{\partial \alpha} = b \frac{\partial x}{\partial \alpha}.$$

This set of equations are called cannonical equations. They are not of direct use in the numerical solution, but are used by Sokolovski and appear to simplify the statements for the initial conditions for the numerical solution. The properties of the cannonical equations are discussed by Forsythe & Wolfgang (1960).

Discussion

The complexity of the derivations of the partial differential equations describing the failure of soil media is due to the occurrence of both cohesive and frictional components of shear resistance in the soil. The analyses for pure cohesionless and pure cohesive materials are significantly simpler. The former will be considered more intensively in the following Section; the latter falls outside the scope of the thesis, but possesses an extensive literature on the analysis of the plastic failure of metals (Hill, 1960).

In approximate analyses, because equilibrium of the failure mass is considered, efforts are sometimes made to apply the elliptic type of differential equations. It has been shown that the equations of failure are in fact hyperbolic and therefore of the propagation type - even though a pseudo-equilibrium condition is considered by taking the equality sign in Mohr's criterion. Efforts to base approximate analyses on the elliptic type of equation are therefore fundamentally in error.

S E C T I O N 4

4. COHESIONLESS SOILS

4.1 Characteristic equations for cohesionless material

It is possible to derive the characteristic equations for cohesionless materials in terms of σ and φ instead of σ and ξ . They can conveniently be deduced from the characteristic equations for the cohesive material.

The dependent variables η and ξ were defined as follows:

$$\xi = \chi + \varphi \ , \ \eta = \chi - \varphi \quad \text{where } \chi = \frac{\cot\rho}{2} \log_e \frac{\sigma}{\sigma_o}$$

$$\xi = \frac{\cot\rho}{2} \log_e(\sigma/\sigma_o) + \varphi$$

$$\eta = \frac{\cot\rho}{2} \log_e(\sigma/\sigma_o) - \varphi$$

Now $d\xi = (\partial\xi/\partial\sigma)d\sigma + (\partial\xi/\partial\varphi)d\varphi$

$$d\eta = (\partial\eta/\partial\sigma)d\sigma + (\partial\eta/\partial\varphi)d\varphi$$

Hence $$d\xi = \frac{\cot\rho}{2} \cdot \frac{d\sigma}{\sigma} + d\varphi \qquad 4.1$$

$$d\eta = \frac{\cot\rho}{2} \cdot \frac{d\sigma}{\sigma} - d\varphi \qquad 4.2$$

The characteristic equations for a cohesive soil are:

$$\left.\begin{aligned} \frac{dy}{dx} &= \tan(\varphi - \mu) && 4.3 \\ \frac{d\eta}{dx} &= a && 4.4 \end{aligned}\right\} \text{1st characteristic set}$$

$$\left.\begin{aligned} \frac{dy}{dx} &= \tan(\varphi + \mu) && 4.5 \\ \frac{d\xi}{dx} &= b && 4.6 \end{aligned}\right\} \text{2nd characteristic set}$$

Substituting for $d\xi$ and $d\eta$ from equations 1 and 2 in 4 and

6 gives:

$$\frac{\cot\rho}{2}\cdot\frac{d\sigma}{\sigma} - d\varphi = a\,dx$$

$$\frac{\cot\rho}{2}\cdot\frac{d\sigma}{\sigma} + d\varphi = b\,dx$$

$$\therefore \quad d\sigma - 2\sigma\,\mathrm{Tan}\rho\,d\varphi_c = 2a\sigma\,\mathrm{Tan}\rho\,dx \qquad 4.7$$

$$\frac{dy}{dx} = \mathrm{Tan}(\varphi-\mu) \qquad 4.8$$

$$d\sigma + 2\sigma\,\mathrm{Tan}\rho\,d\varphi = 2b\sigma\,\mathrm{Tan}\rho\,dx \qquad 4.9$$

$$\frac{dy}{dx} = \mathrm{Tan}(\varphi+\mu) \qquad 4.10$$

where

$$a = \frac{X\,\mathrm{Sin}(\varphi+\mu)}{2\sigma\,\mathrm{Sin}\rho\,\mathrm{Cos}(\varphi-\mu)}\,, \quad (Y=0)$$

$$b = -\frac{X\,\mathrm{Sin}(\varphi-\mu)}{2\sigma\,\mathrm{Sin}\rho\,\mathrm{Cos}(\varphi+\mu)}$$

which gives the characteristic equations for a cohesionless soil.

4.2 Some solutions for critical equilibrium problems in cohesionless soils

4.2.1 Critical state in a semi-infinite body with a horizontal upper boundary under an infinite load P per unit length

Under these conditions the partial differential equations of equilibrium degenerate to ordinary equations, viz.:

$$\frac{d\sigma_x}{dx} = \gamma \qquad 4.11$$

$$\frac{d\tau_{xy}}{dx} = 0 \qquad 4.12$$

Integrating equations 4.11 and 4.12 gives:

$$\sigma_x = \gamma x + C \qquad 4.13$$

$$\tau_{xy} = C' \qquad 4.14$$

at $x = 0$, $\sigma_x = P$ 4.15

Hence C = P and equation 4.14 becomes

$$\sigma_x = \gamma x + P \qquad 4.16$$

$$\tau_{xy} = 0 \qquad 4.17$$

Now at critical equilibrium, from Mohr's circle, relationships for the stresses

$$\sigma_x = \sigma + \sigma \sin\rho \cos 2\varphi \qquad 4.18$$

$$\sigma_y = \sigma - \sigma \sin\rho \cos 2\varphi \qquad 4.19$$

$$\tau_{xy} = \sigma \sin\rho \sin 2\varphi \qquad 4.20$$

can easily be determined.

Substituting equation 4.16 in 4.19 gives

$$\gamma x + P = \sigma(1 + \sin\rho \cos 2\varphi)$$

$$\sigma = \frac{\gamma x + P}{1 + \sin\rho \cos 2\varphi} \qquad 4.21$$

and substituting equation 4.17 in equation 4.20 gives

$$\sigma \sin\rho \sin 2\varphi = 0 \qquad 4.22$$

For a solution to be possible $\sigma > 0$ in which case

$\sin 2\varphi = 0$ for $2\varphi = 0, \pi, 2\pi$

Taking the first two values for 2φ we can write

$2\varphi = (K - 1)\frac{\pi}{2}$, $K = \pm 1$ taking $K = 1$, i.e. $\varphi = 0$

and substituting this value in equation 4.21 gives

$$\sigma = \frac{\gamma x + P}{1 + \sin\rho} \qquad 4.23$$

This corresponds to the case of active failure. Taking K = -1, i.e., $\varphi = -\frac{\pi}{2}$ and substituting this value in equation 4.21 gives

$$\sigma = \frac{\gamma x + P}{1 - \sin\rho} \qquad 4.24$$

This corresponds to the case of passive failure. At the boundary x = 0, hence

$$\sigma = \frac{P}{1 + \sin\rho} \qquad \text{for } \varphi = 0 \qquad 4.25$$

$$\sigma = \frac{P}{1 - \sin\rho} \qquad \text{for } \varphi = -\frac{\pi}{2} \qquad 4.26$$

which give the boundary values of σ and φ for active and passive failure conditions respectively.

4.2.2 <u>Determination of the direction of the principal stress at a point on the surface of a cohesionless body free of applied external stress having a slope ξ at the point</u>.

For the medium to be in equilibrium the angle of inclination to the horizontal of the boundary curve ξ must not be greater than the angle of the internal friction ρ. As the boundary is free of applied stresses $\sigma = 0$ at the boundary. There being no cohesion, it is possible to write the equations of equilibrium in terms of σ and φ instead of ξ and η.

$$\chi = \frac{\cot\rho}{2} \log_e \sigma \qquad 2\mu = \frac{\pi}{2} - \rho \qquad 4.27$$

$$\xi = \chi + \varphi \quad , \quad \eta = \chi - \varphi$$

$$\therefore \xi = \frac{\cot\rho}{2}\log_e\sigma + \varphi \quad , \quad \eta = \frac{\cot\rho}{2}\log_e\sigma - \varphi \qquad 4.28$$

Consider the first equation of equilibrium:

$$\frac{\partial\eta}{\partial x} + \tan(\varphi-\mu)\frac{\partial\eta}{\partial y} = \frac{\chi \sin(\varphi+\mu)}{2\sigma\sin\rho\cos(\varphi-\mu)} = R \qquad 4.29$$

Partially differentiating η in equation 4.28 with respect to x and y and substituting for $\frac{\partial\eta}{\partial y}$ and $\frac{\partial\eta}{\partial x}$ in equation 4.20 gives

$$\left[\cot\rho \cdot \frac{1}{2\sigma}\cdot\frac{\partial\sigma}{\partial x} - \frac{\partial\varphi}{\partial x}\right] + \tan(\varphi-\mu)\left[\cot\rho\cdot\frac{1}{2\sigma}\frac{\partial\sigma}{\partial y} - \frac{\partial\varphi}{\partial y}\right] = R$$

i.e. $$\frac{\cot\rho}{2\sigma}\left[\frac{\partial\sigma}{\partial x} + \frac{\partial\sigma}{\partial y}\tan(\varphi-\mu)\right] - \left[\frac{\partial\varphi}{\partial x} + \frac{\partial\varphi}{\partial y}\tan(\varphi-\mu)\right] = R \qquad 4.30$$

Multiplying equation 4.30 by σ and noting that $\sigma = 0$ in the boundary, equation 4.29 reduces to

$$\cot\rho\left[\frac{\partial\sigma}{\partial x} + \frac{\partial\sigma}{\partial y}\tan(\varphi-\mu)\right] = \frac{\chi\sin(\varphi+\mu)}{\sin\rho\cos(\varphi-\mu)} \qquad 4.31$$

Multiplying equation 4.31 by $\sin\rho\cos(\varphi-\mu)$ and noting that $\sin\rho\cot\rho = \cos\rho$ and $\cos(\varphi-\mu)\tan(\varphi-\mu) = \sin(\varphi-\mu)$ gives

$$\cos(\varphi-\mu)\frac{\partial\sigma}{\partial x} + \sin(\varphi-\mu)\frac{\partial\sigma}{\partial y} = \gamma\sin(\varphi+\mu)/\cos\rho \qquad 4.32$$

where $\gamma = \chi$ = density of the material.

Similarly, considering the second equation of equilibrium it can be shown that

$$\mathrm{Cos}(\varphi+\mu)\frac{\partial\sigma}{\partial x} + \mathrm{Sin}(\varphi+\mu)\frac{\partial\sigma}{\partial y} = -\gamma\,\mathrm{Sin}(\varphi-\mu)/\mathrm{Cos}\rho \qquad 4.33$$

Equations 4.32 and 4.33 are two equations in two unknowns $\frac{\partial\sigma}{\partial x}$ and $\frac{\partial\sigma}{\partial y}$. To solve for $\frac{\partial\sigma}{\partial x}$ and $\frac{\partial\sigma}{\partial y}$ multiply equation 4.32 by $\mathrm{Cos}(\varphi+\mu)$, equation 4.33 by $\mathrm{Cos}(\varphi-\mu)$, subtracting equation 4.33 from 4.32 gives

$$\frac{\partial\sigma}{\partial y}\left[\mathrm{Sin}(\varphi-\mu)\mathrm{Cos}(\varphi+\mu) - \mathrm{Sin}(\varphi+\mu)\,\mathrm{Cos}(\varphi-\mu)\right] =$$

$$\frac{\gamma}{\mathrm{Cos}\rho}\left[\mathrm{Sin}(\varphi+\mu)\,\mathrm{Cos}(\varphi+\mu) + \mathrm{Sin}(\varphi-\mu)\,\mathrm{Cos}(\varphi-\mu)\right] \qquad 4.34$$

Consider the lefthand side of equation 4.34, from the multiple angle trigonometrical formulae

$$\mathrm{Sin}\left(\overline{\varphi-\mu} - \overline{\varphi+\mu}\right) = \mathrm{Sin}(-2\mu) = -\mathrm{Sin}\left(\tfrac{\pi}{2}-\rho\right)$$
$$= -\left(\mathrm{Sin}\tfrac{\pi}{2}\mathrm{Cos}\rho - \mathrm{Cos}\tfrac{\pi}{2}\mathrm{Sin}\rho\right) = -\mathrm{Cos}\rho$$

The righthand side of equation 4.34 in brackets gives

$$\tfrac{1}{2}\mathrm{Sin}\,2(\varphi+\mu) + \tfrac{1}{2}\mathrm{Sin}\,2(\varphi-\mu)$$

which reduces to

$$\text{RHS} = \tfrac{1}{2}\left[2\,\mathrm{Sin}\tfrac{4\varphi}{2}\,\mathrm{Cos}\tfrac{4\mu}{2}\right]\frac{\gamma}{\mathrm{Cos}\rho}$$
$$= \left[\mathrm{Sin}\,2\varphi\,\mathrm{Cos}\,2\mu\right]\frac{\gamma}{\mathrm{Cos}\rho}$$

and $\mathrm{Cos}\,2\mu = \mathrm{Cos}\left(\tfrac{\pi}{2}-\rho\right) = \mathrm{Cos}\tfrac{\pi}{2}\mathrm{Cos}\rho + \mathrm{Cos}\tfrac{\pi}{2}\mathrm{Sin}\rho = \mathrm{Sin}\rho$

i.e. $\text{RHS} = \left[\mathrm{Sin}\,2\varphi\,\mathrm{Sin}\rho\right]\frac{\gamma}{\mathrm{Cos}\rho}$

Equation 4.34 becomes

$$\frac{\partial \sigma}{\partial y} = -\frac{\gamma}{\cos^2\varphi}\left(\sin\rho \sin 2\varphi\right) \qquad 4.35$$

Similarly, solving for $\partial\sigma/\partial x$ gives

$$\frac{\partial \sigma}{\partial x} = \frac{\gamma}{\cos^2\varphi}\left[1 - \sin\rho \cos 2\varphi\right] \qquad 4.36$$

Along the boundary $\sigma = 0$. Hence the rate of change of σ along the boundary is equal to zero. That is,

$$\frac{d\sigma}{ds} = \frac{\partial \sigma}{\partial x}\cdot\frac{dx}{ds} + \frac{\partial \sigma}{\partial y}\cdot\frac{dy}{ds} = 0$$

$$\therefore \quad \frac{\partial \sigma}{\partial x}\,dx + \frac{\partial \sigma}{\partial y}dy = 0$$

i.e.

$$\frac{dy}{dy} = -\frac{\partial\sigma/\partial x}{\partial\sigma/\partial y}$$

But at the boundary

$$\frac{dy}{dx} = -\cot\xi$$

i.e.

$$\cot\xi = -\frac{\partial \sigma}{\partial x}\cdot\frac{1}{\frac{\partial \sigma}{\partial y}} \qquad 4.37$$

and substituting equations 4.35 and 4.34 in equation 4.36 gives

$$\cot\xi = -\frac{1 - \sin\rho \cos 2\varphi}{\sin\rho \sin 2\varphi} \qquad 4.38$$

Noting that $\cot\xi = \frac{\sin\xi}{\cos\xi}$, substituting in equation 4.37, crossmultiplying and reducing gives

$$\sin\xi + \sin\rho \sin(2\varphi - \xi) = 0$$

hence $$\sin(2\varphi - \xi) = \sin\xi / \sin\rho$$

and $$2\varphi - \xi = -K\sin^{-1}\left[\sin\xi/\sin\rho\right] + \left[K-1\right]\cdot\frac{\pi}{2}$$

$$\therefore \quad 2\varphi = \xi + \left[K-1\right]\frac{\pi}{2} - K\sin^{-1}\left[\sin\xi/\sin\rho\right] \qquad 4.39$$

where $K = \begin{cases} +1 & \text{for active failure} \\ -1 & \text{for passive failure} \end{cases}$

Equation 4.38 gives the direction of the maximum principal stress at the surface of a cohesionless embankment, without external stress and a slope of ξ at the point. The quantities derived above are depicted in Figure 4.1.

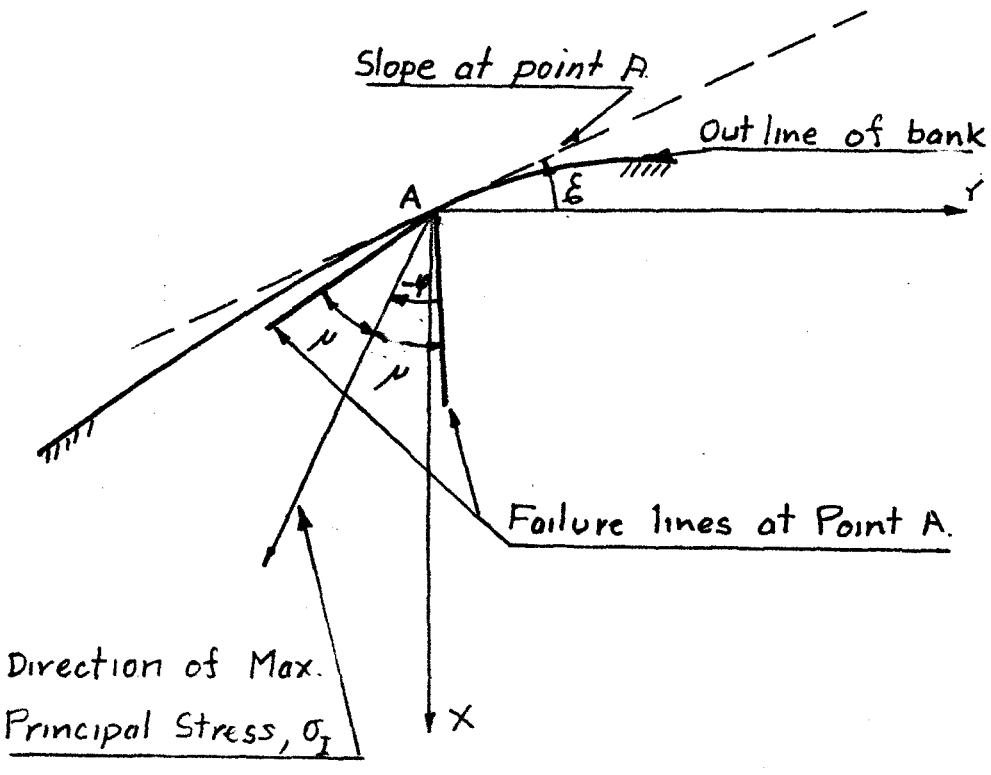

Fig. 4.1

4.3.1 Numerical solution of the differential equations

Given equations 4.7 to 4.10 and the values x_1, y_1, σ_1, ϕ_1 and x_2, y_2, σ_2, ϕ_2, (the points x_1y_1 and x_2y_2 in the XY plane being near to eachother), to determine x_3, y_3, σ_3, ϕ_3 by the method of characteristics. The problem is graphically illustrated in Figure 4.2

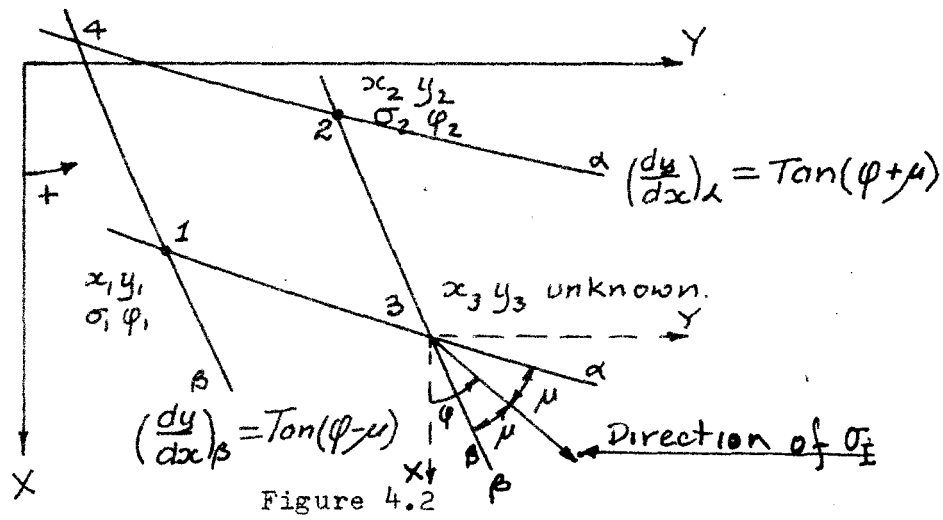

Figure 4.2

Through every point in the XY plane within the region of solution there pass two characteristics, α and β. The directions of these characteristics are given by:

$$\left(\frac{dy}{dx}\right)_\alpha = Tan(\varphi+\mu) \qquad 4.40$$

$$\left(\frac{dy}{dx}\right)_\beta = Tan(\varphi-\mu) \qquad 4.41$$

ϕ being the direction of the maximum principal stress.

As the value of ϕ is known at points 1 and 2, and the slopes $(\frac{dy}{dx})_{\alpha 1}$ and $(\frac{dy}{dx})_{\beta 2}$ of the α and β characteristic through points 1 and 2 respectively are known, the point x_3y_3 can be obtained approximately by graphically plotting points 1 and 2 in the XY plane and drawing the slopes of $(\frac{dy}{dx})_{\alpha 1}$ and $(\frac{dy}{dx})_{\beta 2}$ through points 1 and 2 respectively to intersect at x_3y_3. (It should be noted that if the characteristics α_2 and β_1 were chosen, point x_4y_4 would have been found - which characteristics of the family to use will depend on the region of solution required.)

The first order finite difference approximation to equations 4.7 to 4.10 can be written:

$$(y_3-y_2) = Tan\left(\underline{\varphi_2} - \mu\right)\cdot(x_3-x_2) \qquad 4.42$$

(β characteristic through point x_2y_2)

$$(y_3 - y_1) = Tan(\underline{\varphi_1 + \mu})(x_3 - x_1) \qquad 4.43$$

(α characteristic through $x_1 y_1$)

$$(\sigma_3 - \sigma_2) - 2\underline{\sigma_2} Tan\rho \cdot (\varphi_3 - \varphi_2) = \underbrace{\left[\frac{-\gamma Sin(\underline{\varphi_2} - \mu)}{Cos\rho\, Cos(\underline{\varphi_2} + \mu)}(x_3 - x_2)\right]}_{\epsilon} 4.44$$

$$(\sigma_3 - \sigma_1) + 2\underline{\sigma_1} Tan\rho \cdot (\varphi_3 - \varphi_1) = \underbrace{\left[\frac{\gamma Sin(\underline{\varphi_1} + \mu)}{Cos\rho\, Cos(\underline{\varphi_1} - \mu)}(x_3 - x_1)\right]}_{\delta} 4.45$$

The co-ordinates $x_3 y_3$ can be obtained by solving equations 4.42 and 4.43 giving:

$$x_3 = \frac{[x_1 Tan(\varphi_1 + \mu) - y_1] - [x_2 Tan(\varphi_2 - \mu) - y_2]}{Tan(\varphi_1 + \mu) - Tan(\varphi_2 - \mu)}$$

$$y_3 = \frac{[y_1 Cot(\varphi_1 + \mu) - x_1] - [y_2 Cot(\varphi_2 - \mu) - x_2]}{Cot(\varphi_1 + \mu) - Cot(\varphi_2 - \mu)}$$

Using these values of $x_3 y_3$ in equations 5.44 and 4.45, φ_3 and $_3$ can be obtained, giving

$$\varphi_3 = \frac{\epsilon - \delta - \sigma_1 + \sigma_2 - 2\sigma_1(\sigma_1 \varphi_1 + \varphi_2 \sigma_2) Tan\rho}{(\sigma_1 + \sigma_2) 2 Tan\rho}$$

$$\sigma_3 = \frac{2\sigma_1 \sigma_2 [1 - (\varphi_1 - \varphi_2) Tan\rho] + \epsilon\sigma_2 + \delta\sigma_1}{\sigma_1 + \sigma_2}$$

4.3.2 Improvement of estimates

The estimates x_3, y_3, φ_3, σ_3 are crude as the finite difference approximation requires the slopes of the curves at points 1 and 2, excluding the curvature between these points and point 3. An increase in accuracy is obtained by determining the average slopes between these points and

point 3. This is obtained by successive approximation procedure as follows:

Replace ϕ and σ by ϕ' and σ' as follows:

$$\sigma_1' = \frac{1}{2}(\sigma_1 + \sigma_3)$$
$$\varphi_1' = \frac{1}{2}(\varphi_1 + \varphi_3)$$
$$\sigma_2' = \frac{1}{2}(\sigma_2 + \sigma_3)$$
$$\varphi_2' = \frac{1}{2}(\varphi_2 + \varphi_3)$$

Using the values ϕ'_1 and ϕ'_2 in equations 4.42 and 4.43 (underlined values), improved values for x_3y_3 are obtained, and using ϕ'_1, ϕ'_2, σ'_1, σ'_2 in equations 4.44 and 4.45 (underlined values) and the improved values for x_3y_3, new values for σ_3 ϕ_3 are obtained. This process is repeated until the improved values become stationary.

4.4 Outline of the solution for the critical stress under a foundation on cohesionless material

4.4.1 Loading conditions

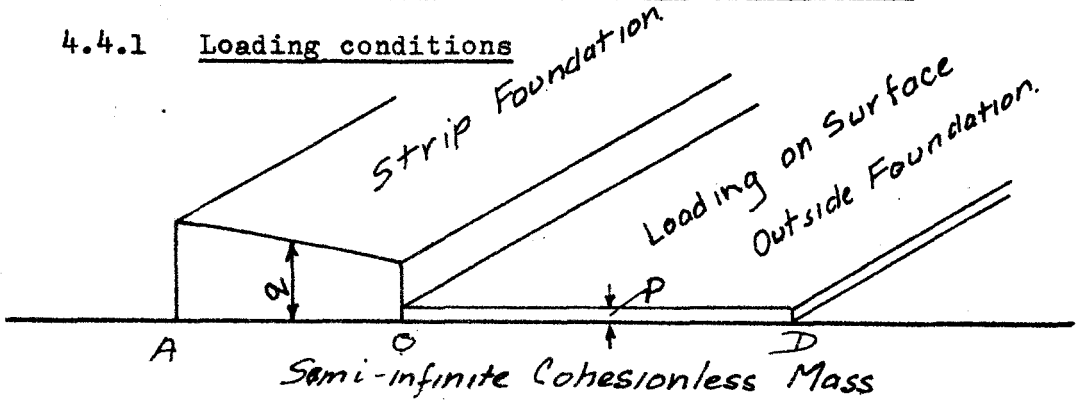

Figure 4.3

Assume that an infinitely long strip foundation rests on a semi-infinite horizontal surface (Figure 4.3). It will be shown that for a cohesionless semi-infinite mass unless there are other forces applied on the surface for a certain horizontal distance away from the foundation, no solution is possible. Assume therefore that a uniform load, p, is applied to the surface as shown in Figure 4.3. The problem

is to determine the critical distribution of forces below the foundation leading to a condition of critical equilibrium in the soil mass. Alternatively, the stresses, q, under the strip foundation may be specified (uniform, non-uniform, or skew). The solution will give a stress distribution, p, outside the foundation, which will vary according to the specified distribution, q.

In normal foundation conditions, if the structure is fairly rigid, the stresses in the foundation are <u>not</u> independent of the strains. Presented in this form the problem becomes statically indeterminate and requires in addition to the solution of the critical stresses the solution of the strain rates for initial values of the strain rates. If these two solutions are compatible, then the solution is the correct one. However, each solution for the specified stresses only is a valid one, but the strain rate conditions compatible with the stress conditions remain unknown; that is, if the stresses are applied without limitation of the strains the solution is correct. But if the strains are specified, a boundary stress system must be guessed and tested to see if it is compatible with the strain rates.

4.4.2 <u>Boundary conditions</u>

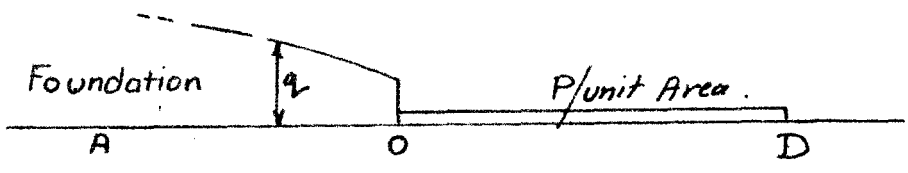

Figure 4.4

In Figure 4.4 the forces acting at the boundary of the semi-infinite body are shown. Assume the density of the material under the foundation is equal to γ and that the soil has a constant angle of internal friction, ϕ. Section OD is in a state of passive critical equilibrium.

Hence from Section 4.2 at the surface:

$$\sigma = p/(1-\sin\varphi)$$
$$\varphi = \pi/2$$

(Ø can have either the value $\frac{\pi}{2}$ or $-\frac{\pi}{2}$, but if Ø is taken equal to $-\frac{\pi}{2}$ the foundation stress on OA would fall to the right of point O and the passive failure region OD to the left.)

To the left of O a variable normal stress, q, is applied, as yet unknown. (If p is not normal to OD, the stress q will correspondingly not be normal to OA).

Section OA is in a state of active critical equilibrium. The force at the surface is vertical, hence:

$$\sigma = q/(1+\sin\varphi)$$
$$\varphi = 0$$

On OA the direction of the maximum principal stress is vertically downwards (see Figure 4.5)

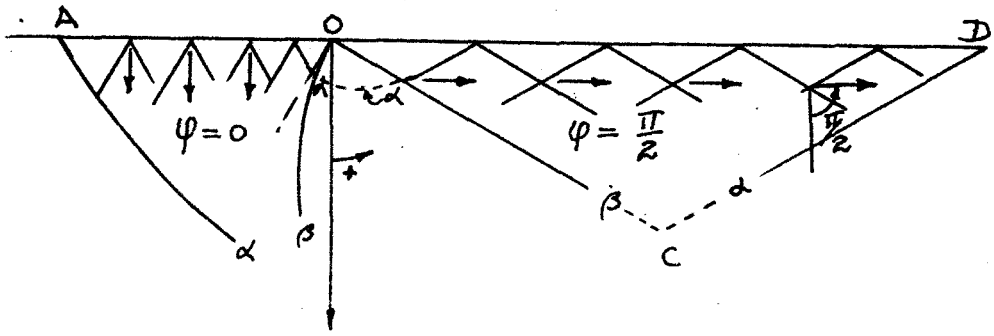

Figure 4.5

At point O there is a discontinuity in the value of the forces applied at the surface. The value of p_o is known, but the value of q_o is still unknown. However, the value of q_o depends only on the value of p_o; the α characteristic is defined by the slope $\left(\frac{dy}{dx}\right)_\alpha = \tan(\varphi+\mu)$ and the β characteristic by $\left(\frac{dy}{dx}\right)_\beta = \tan(\varphi-\mu)$. At point O the α characteristic has a curvature infinitely small, and x and y are constant. Hence dx = 0. From equation 4.9 valid on the α

characteristic, neglecting the term dx gives:

$$d\sigma + 2\sigma \tan\rho \, d\varphi = 0$$

which gives the relationship between σ and φ on the characteristic at point, O, re-written as follows:

$$\frac{1}{2\tan\rho}\frac{d\sigma}{\sigma} + d\varphi = 0 \qquad 4.50$$

It is known that just to the right of O, $\varphi_o = \frac{\pi}{2}$ and $\sigma_o = \frac{p_o}{1 - \sin\rho}$. To the left of O, $\varphi_o = 0$, and $\sigma_o = \frac{q_o}{1 + \sin\rho}$. The relationship between p_o and q_o can be determined by integrating equation 4.50 as follows:

$$\frac{1}{2\tan\rho}\int_{p_o/(1-\sin\rho)}^{q_o/(1+\tan\rho)} \frac{d\sigma}{\sigma} = -\int_{\pi/2}^{0} d\varphi \qquad 4.51$$

which gives

$$\frac{1}{2}\cdot\frac{1}{\tan\rho}\left[\log_e\left(\frac{q_o}{1+\sin\rho}\right) - \log_e\left(\frac{p_o}{1-\sin\rho}\right)\right] = \frac{\pi}{2}$$

i.e.

$$q_o = p_o\left[\frac{1+\sin\rho}{1-\sin\rho}\right] e^{\pi\tan\rho} \qquad 4.52$$

For various values of φ between the limits 0 and $\frac{\pi}{2}$, the value of q can be determined by integrating equation 4.51 between $\frac{\pi}{2}$ and the chosen value of φ:

$$\frac{1}{2\tan\rho}\int_{p_o/[1-\sin\rho)}^{q_{(\varphi)}/(1+\sin\rho)} \frac{d\sigma}{\sigma} = -\int_{\pi/2}^{\varphi} d\varphi$$

giving

$$q_{(\varphi)} = \left[\frac{1+\sin\rho}{1-\sin\rho}\right] p_o \, e^{2\tan\rho\cdot(\pi/2-\varphi)}$$

which gives the relationship between σ and φ as follows:

$$\sigma_{(\varphi)} = \sigma_r \, e^{2\tan\rho\cdot(\pi/2-\varphi)} \qquad 4.53$$

where σ_r is the value of σ just to the right of O.

4.5 The internal solution of the equations

In region OCD the initial conditions along OD have been

given by:

$$\varphi = \pi/2$$
$$\sigma = p_o/(1-\sin\rho)$$

The solution internal to OCD is a Type 1 solution, but because ϕ and σ are constant on OD, and the upper surface is horizontal, the internal values of σ and ϕ have already been given in Section 4.2, i.e.

$$\varphi = \pi/2$$
$$\sigma = (p+\alpha x)/(1-\sin\rho)$$

and the direction of the characteristics by:

$$(dy/dx)_{\alpha\beta} = \tan(\pi/2 \pm \mu)$$
$$\therefore \quad y_{\alpha\beta} = \tan(\pi/2 \pm \mu)\cdot x$$

Along OC, x, y, ϕ and σ are now known.

The solution in region OCB is of the Type 3(a). The values of σ and ϕ are known along the β characteristic OC, and along the infinitely short α characteristic O. At O, ϕ changes from $\frac{\pi}{2}$ to zero, and σ from $\frac{p_o}{1-\sin\rho}$ to $\frac{q_o}{1+\sin\rho}$.

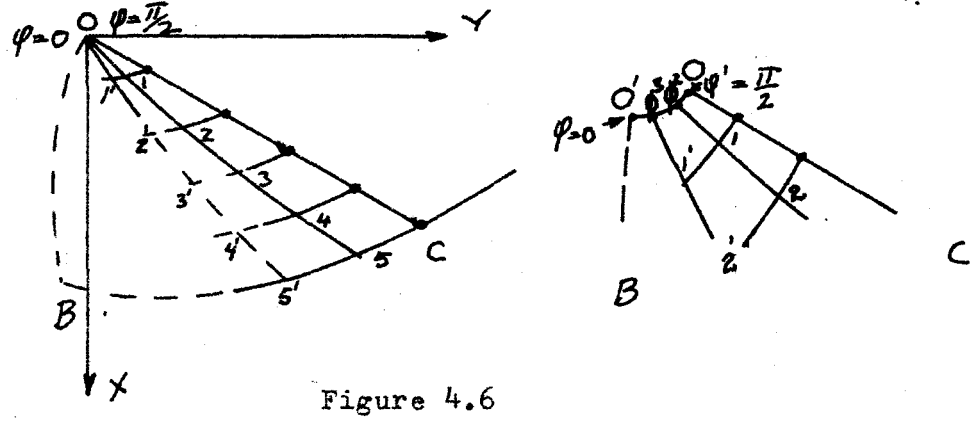

Figure 4.6

The solution proceeds as follows:

For point O divide ϕ into equal parts between $\frac{\pi}{2}$ and zero, and calculate from equation 4.53 the corresponding values of σ. For clarity, assume OO' is the α characteristic at O (see Figure 4.6). Then the values ϕ^1, ϕ^2, ϕ^3,

etc., and the corresponding values σ^1, σ^2, σ^3, etc. can be ascribed on this short characteristic. Values of σ and ϕ can then be determined at points 1, 2, 3, 4 successively by the normal numerical method, and then at 1', 2', 3', etc. until finally the characteristic with initial values $\sigma = \frac{q_o}{1 + \sin}$ and $\phi = 0$ is calculated. Finally thus the values of ϕ and σ are known along the characteristic OB, providing the initial values for solution in region AOB.

For the solution in region AOB, the values ϕ, σ, x and y are known along OB, and ϕ and x known along OA ($\phi = 0$, $x = 0$). The solution proceeds as follows:-

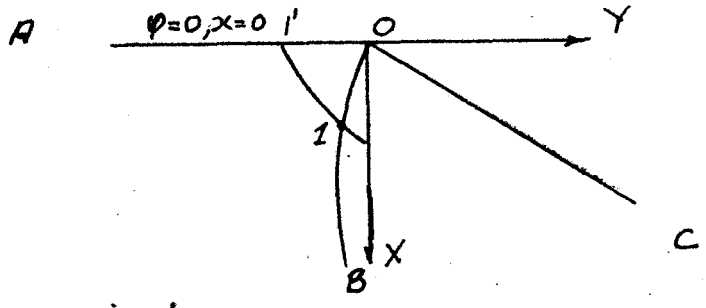

The finite difference approximation for the α characteristic with point 1 as starting point gives:

$$(y'_1 - y_1) = \text{Tan}\,(\phi_1 + \mu)(x_1 - x'_1) \qquad 4.54.$$

Now $x'_1 = 0$ and ϕ_1 and y_1 are known. Hence y'_1 is found by substituting in equation 4.54 above. From the two finite difference equations 4.48 and 4.49, substituting the values x_1, x'_1, y_1, y'_1, ϕ_1 and σ_1 in the equations, ϕ'_1 and σ'_1 at point 1' can be determined.

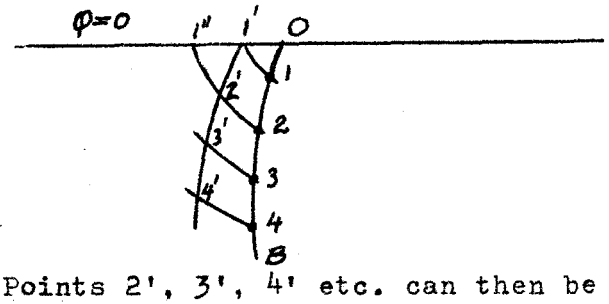

Points 2', 3', 4' etc. can then be determined by the

straightforward application of the four finite difference equations.

The whole procedure is repeated to determine firstly point 1" and then points 2", 3", etc.

In Figure 4.7 sketches of the characteristics and of the surfaces of solution for ϕ and σ are shown.

4.6 Discussion

It is evident that the solution of the plastic failures of the statically determinate type presents two problems:

(i) the specification of the open boundary conditions,

(ii) the numerical solution of the characteristic equations in the failure region.

The first problem is considerably more complicated than the second, and requires an intimate understanding of the characteristics of the failure. The second problem is relatively simple, and should present little difficulty. The numerical solutions are, however, tedious in the extreme and not suited to manual calculation, but with the aid of electronic computors the tedium of solution has virtually fallen away.

The setting up of the example and its method of solution discussed above is of the simplest nature, but if the mode of solution is understood, more complicated problems can be attempted with confidence.

Referring to equation 4.52 (page 4.14) the relationship between q_o and p_o is such that if $p_o = 0$ then $q_o = 0$, i.e., it is not possible to found on the surface of a cohesionless mass. The depth of founding can be determined from this equation by equating $p = \gamma h$, where h = depth below the

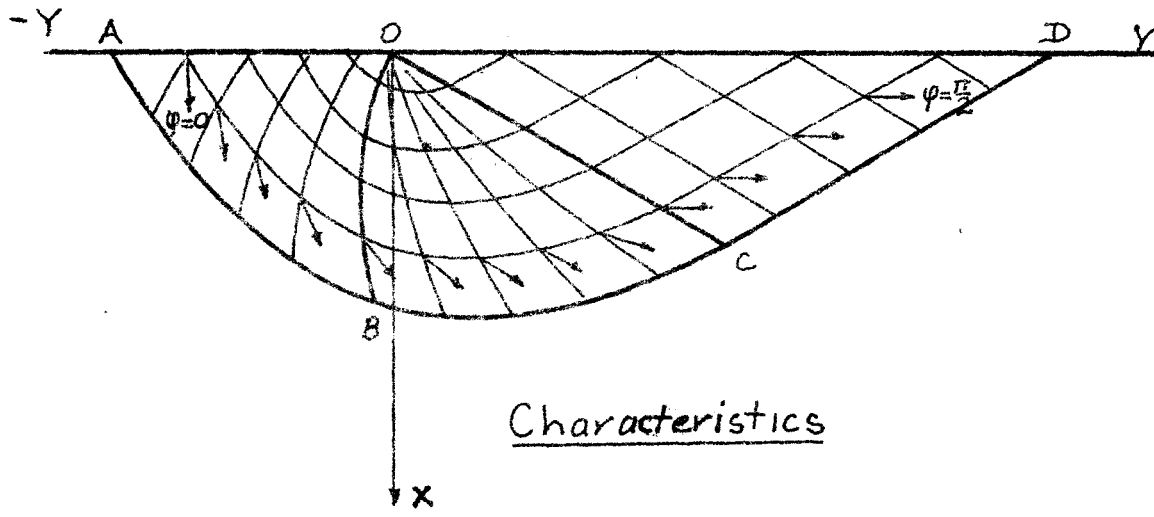

Characteristics

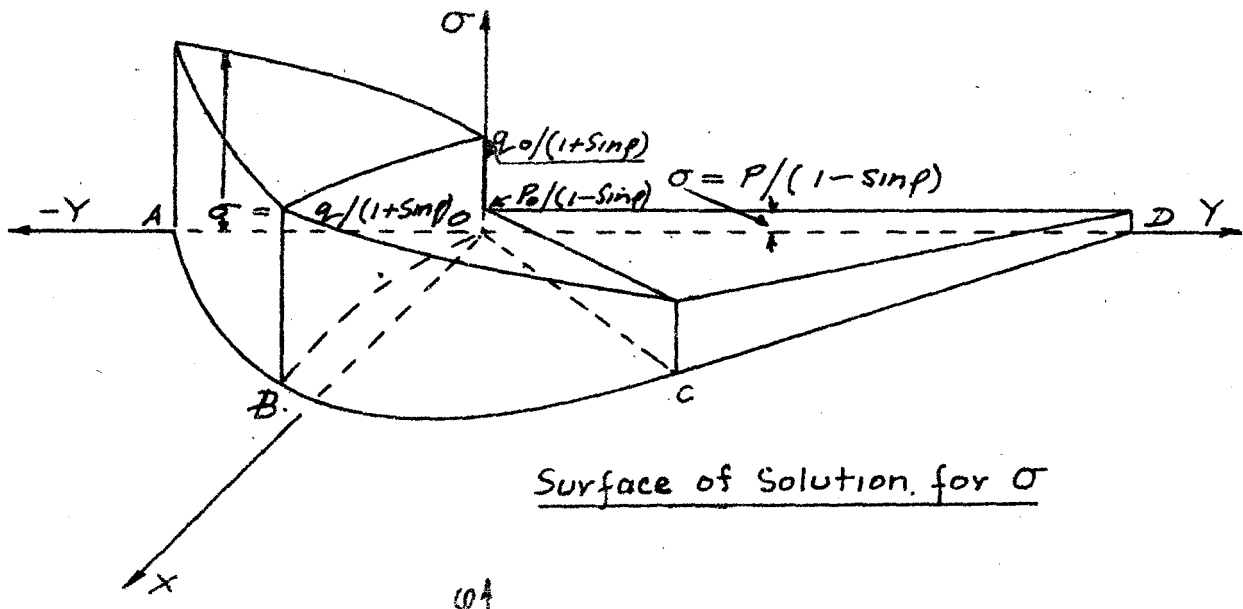

Surface of Solution for σ

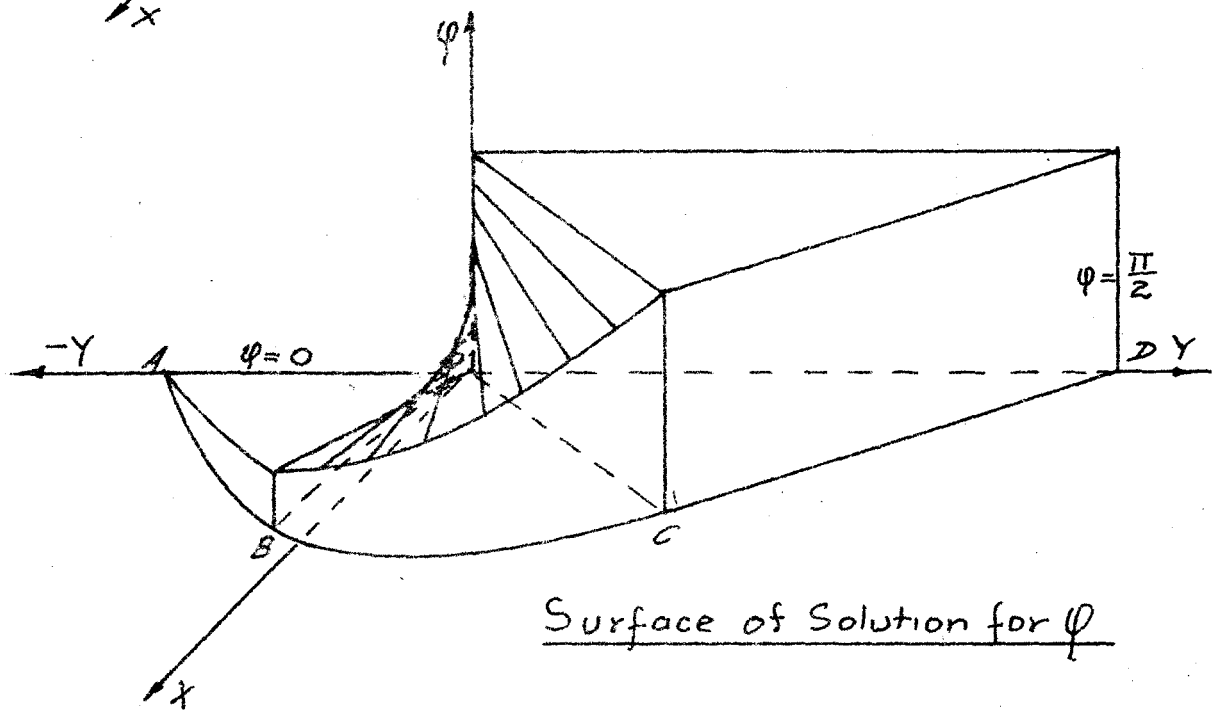

Surface of Solution for φ

Figure 4.7

surface, and solving for h.

$$\text{i.e.} \quad h = \frac{q_o}{\gamma}\left(\frac{1 - \sin\phi}{1 + \sin\phi}\right) e^{-\pi \tan\phi}$$

for $\phi = 30^\circ$ gives

$$h = 0.0543 \frac{q_o}{\gamma}$$

Compare this value for h with that given by the standard equation:

$$h = \frac{q_o}{\gamma}\left(\frac{1 - \sin\phi}{1 + \sin\phi}\right)^2$$

for $\phi = 30^\circ$ gives

$$h = 0.111 \frac{q_o}{\gamma}$$

that is, according to Sokolovski, the minimum founding depth is approximately half that given by the standard equation.

SECTION 5

5. THE ACTIVE CRITICAL EQUILIBRIUM OF WEDGES OF COHESIONLESS MATERIALS

5.1 Introduction

In this section consideration will be given to the critical equilibrium of wedges of cohesionless materials in a state of active failure due solely to their own weight. The theory has been summarised by Sokolovski in his book "Statics of Soil Media" (Sokolovski, 1960), but the derivations of many of the formulae and the range of their validity are not always clear. Hence it was decided to discuss the theory in detail before considering its applications.

In the general theory of hyperbolic equations as set out in Section 2, it was stated that, if discontinuities occurred in the first derivatives of the dependent variables along the open boundary curve, or discontinuities occurred in the slope of the boundary curve itself, these discontinuities were propagated along the characteristic curves. Up to now only smooth boundary curves have been considered. The wedge condition arises when a discontinuity occurs in the slope of the boundary curve.

If certain restrictive conditions are imposed on the wedge and the materials in the wedge, it is possible to obtain the solution of the active critical state of the wedge in a more simple fashion than by the application of the general method of characteristics. Unfortunately, the procedures of this special method are not as graphic to the mind as the method of characteristics, although the end results are the same. In the following sections, it should be remembered

that all the properties and characteristics of the general solution are inherent in the solution obtained by the special method.

The following restrictions apply to the wedge:-

1. The apex of the wedge points upwards.
2. The slopes of the sides of the wedge are constant but not necessarily equal.
3. The interior angle of the apex is smaller than or equal to 180°.
4. No external loads are applies to any section of the wedge; the wedge is stressed only by its own weight.
5. The angle of internal friction ρ , remains constant. This limits the maximum slope, ε , of the sides of the wedge (assuming (4) to apply) and the following inequality must be satisfied:-

$$\varepsilon \leq \rho$$

Outlines of wedges that satisfy these restrictions are shown in Figure 5.1

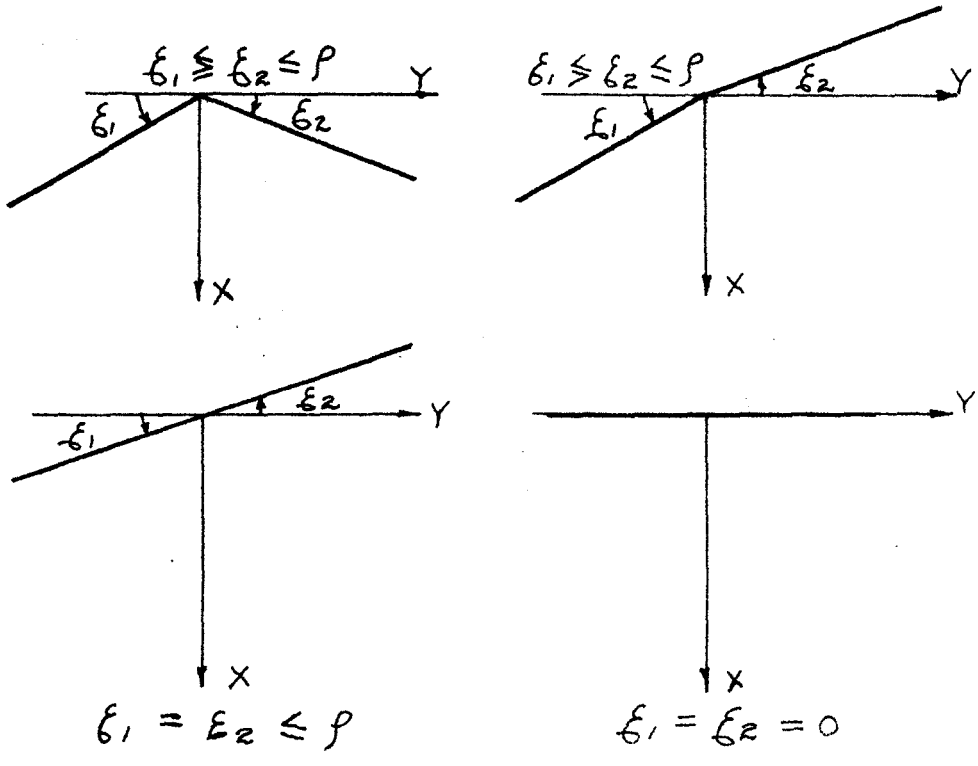

Fig. 5.1

The stresses and the characteristic lines which define the active critical state can be determined on the assumption that this state is attained at every poind in the interior of the wedge at the same instant. This does not have the effect of limiting the generality of the solutions obtained. On the contrary, the totality of all possible failures are found.

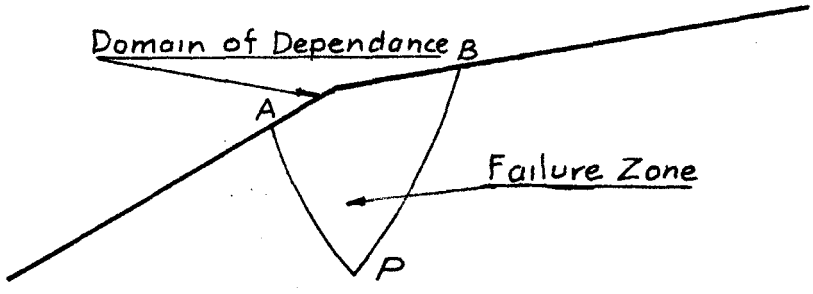

Fig. 5.2

In Figure 5.2, if an active failure state exists at point P, the state is governed by the conditions on the boundary along the length AB defined by the intersections of the two characteristics through P - the domain of dependence of P. In general, the zone of failure is fixed by the domain of dependence, the state of stress outside the characteristics through P not affecting the state at P. Once the general state of active failure of the wedge is known, then in any particular investigation the problem is reduced to the selection of the appropriate failure zone from the totality of zones given by the general failure state. The selection of the appropriate zone of failure will depend upon the conditions in the foundations and will be discussed at a later stage.

From Restriction (2), the following simplifying condition on the distribution of the critical stresses can be made:

> Along any selected radius arm, r, which has its origin at the apex of the wedge, the critical stresses are proportional to the length of the radius arm.

This condition allows the critical stresses to be determined independently ofthe characteristic curves. The four characteristic equations are reduced to two ordinary differential equations, from the solution of which the stresses and the characteristic curves can be determined.

5.2 Co-ordinate system

The analysis is most conveniently performed in polar co-ordinates θ and r. By referring to Figure 5.3 the definitions of some of the variables given below are graphically illustrated.

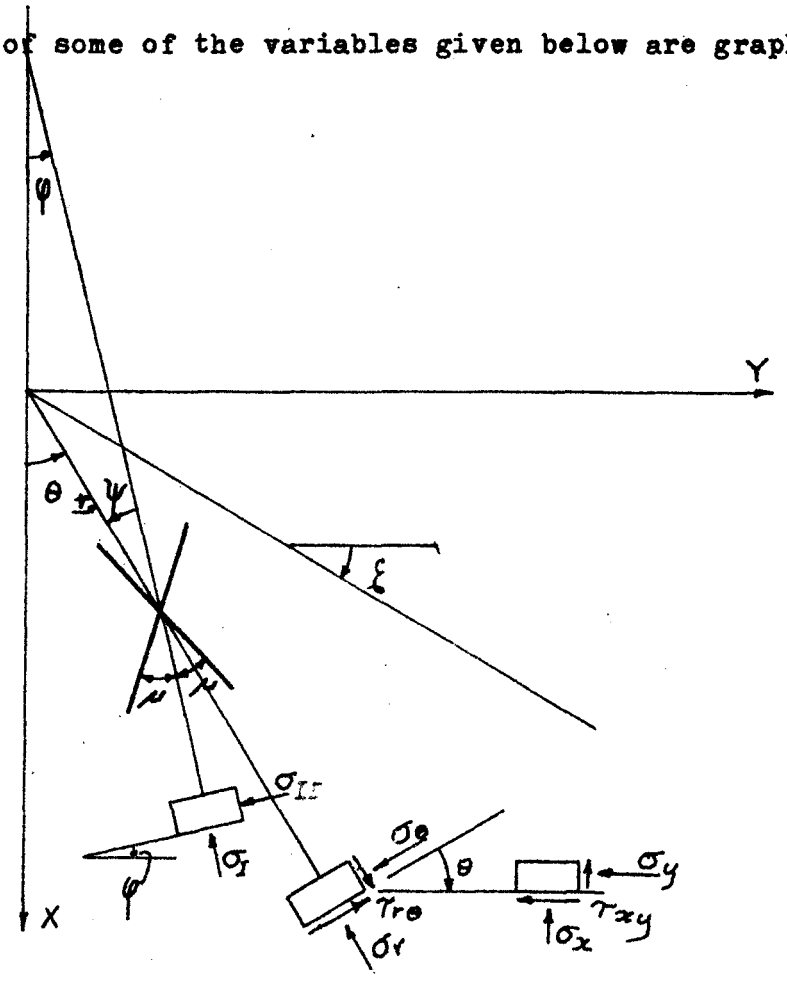

Fig. 5.3

Except where indicated otherwise, all angles are measured from the X axis with anti-clockwise rotation taken as positive.

Let

φ = angle of inclination of the direction of the maximum principal stress σ_I.

θ = angle of the radius arm, r.

$\psi = \varphi - \theta$ = angle between the direction of the maximum principal stress, σ_I, and the radius arm r.

5.3 Differential equations for critical equilibrium

Considering only the self weight of the soil acting vertically downwards, the partial differential equations of equilibrium (equations 3.5 and 3.8) can be written in polar co-ordinates:-

$$\frac{\partial \sigma_r}{\partial r} + \frac{1}{r}\frac{\partial \tau_{r\theta}}{\partial \theta} + \frac{\sigma_r - \sigma_\theta}{r} = \gamma \cos\theta \qquad 5.1$$

$$\frac{\partial \tau_{r\theta}}{\partial r} + \frac{1}{r}\frac{\partial \sigma_\theta}{\partial \theta} + 2\frac{\tau_{r\theta}}{r} = -\gamma \sin\theta \qquad 5.2$$

Mohr's condition for plastic yield becomes:-

$$\frac{1}{4}(\sigma_r - \sigma_\theta)^2 + \tau_{r\theta}^2 = \frac{1}{4}\sin^2\rho\,(\sigma_r + \sigma_\theta)^2 \qquad 5.3$$

Under critical equilibrium conditions, equation 5.3 applies and the critical stresses, σ_r, σ_θ, and $\tau_{r\theta}$ can be specified in terms of two variables, σ and ψ where

σ = mean normal stress $= \frac{1}{2}(\sigma_I + \sigma_{II}) = \frac{1}{2}(\sigma_x + \sigma_y)$

$= \frac{1}{2}(\sigma_r + \sigma_\theta)$ 5.4

ψ = angle between the direction of the maximum principal stress, σ_I, and the radius arm, r (See Figure 5.3).

The transformation of the stresses, σ_r, σ_θ, and $\tau_{r\theta}$ to σ and ψ is preferably performed by using Mohr's diagram for the state of the stresses at critical equilibrium. See Figure 5.4.

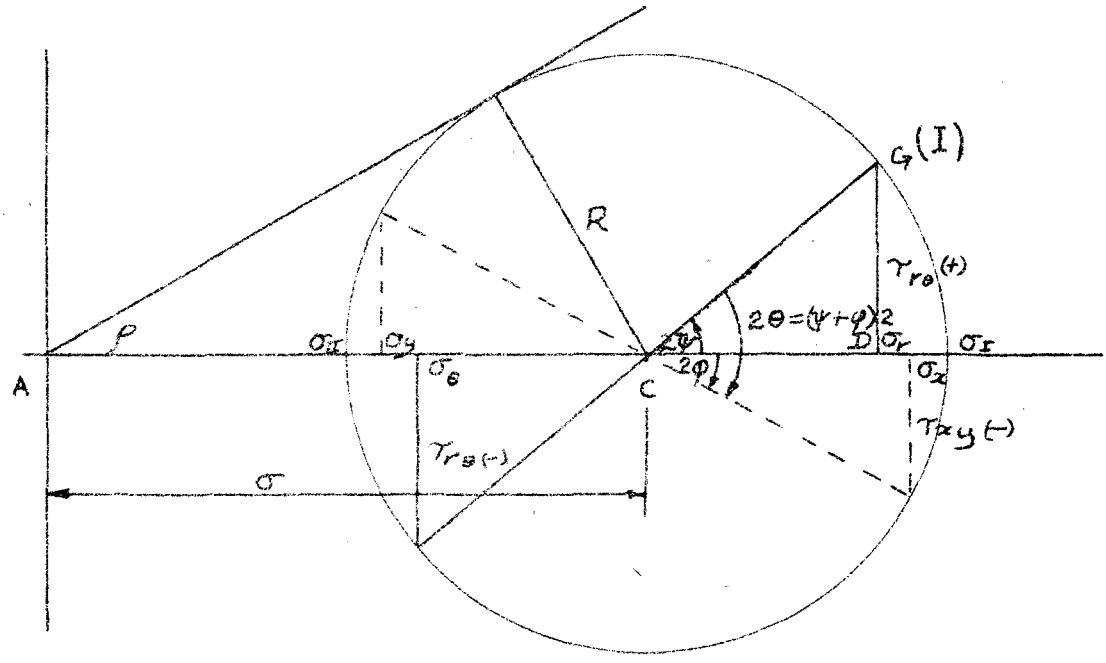

Fig. 5.4

$$\sigma = AC$$

$$R = AC \sin\rho = \sigma \sin\rho$$

$$CD = R\cos 2\psi = \sigma \sin\rho \cos 2\psi$$

$$\sigma_r = AC + CD = \sigma + \sigma \sin\rho \cos 2\psi$$

$$\therefore \quad \sigma_r = \sigma\left[1 + \sin\rho \cos 2\psi\right] \qquad 5.5$$

Similarly

$$\sigma_\theta = \sigma\left[1 - \sin\rho \cos 2\psi\right] \qquad 5.6$$

$$\tau_{r\theta} = GD = r \sin 2\psi = \sigma \sin\rho \sin 2\psi \qquad 5.7$$

From condition 2, Section 5.1, σ_r, σ_θ and $\tau_{r\theta}$ are proportional to the length of the radius arm, r, which from equation 5.4 implies that σ is proportional to r. From equations 5.5, 5.6 and 5.7 the critical stresses are functions of ψ, hence so is σ. But ψ is a function of θ only.

This is evident from noting that along a selected radius arm (θ = constant) the stresses are proportional to r and hence the angle, φ , must remain constant. From $\psi = \varphi - \theta$ the value of ψ must remain constant. As the radius arm rotates, θ varies and φ will vary correspondingly. This implies that ψ is a function of θ only. Therefore, it can be stated that σ is proportional to r and a function of θ . Hence the following relationship can be written:-

$$\sigma = \gamma r f(\theta)$$

(The "constant" of proportionality between σ and r is constant only along any selected radius arm and must be incorporated in $f(\theta)$ as it varies with θ . The constant, γ , is incorporated into the equation for convenience only.)

In order to conform to Sokolovski's notation, write

$$s = f(\theta)$$

$$\text{i.e.} \quad \sigma = \gamma r s \qquad 5.8$$

Substituting equation 5.8 in equations 5.5, 5.6 and 5.7 gives:-

$$\left.\begin{aligned} \sigma_r &= \gamma r s (1 + \sin\rho \cos 2\psi) \\ \sigma_\theta &= \gamma r s (1 - \sin\rho \cos 2\psi) \\ \tau_{r\theta} &= \gamma r s (\sin\rho \cos 2\psi) \end{aligned}\right\} \qquad 5.9$$

Partially differentiating equation 5.9 with respect to r and θ as follows:-

$$\frac{\partial \sigma_r}{\partial r} = \gamma s \left[1 + \sin\rho \cos 2\psi\right]$$

$$\frac{\partial \tau_{r\theta}}{\partial \theta} = \gamma r \frac{ds}{d\theta} \sin\rho \sin 2\psi + 2\gamma r s \sin\rho \cos 2\psi \frac{d\psi}{d\theta}$$

(dS/dθ and dψ/dθ are <u>ordinary</u> derivatives as S and ψ are functions of θ only).

$$\frac{\partial \tau_{r\theta}}{\partial r} = \gamma S \sin\rho \sin 2\psi$$

Substituting these derivatives in equation 5.1 gives:-

$$\gamma S\left[1+\sin\rho\cos 2\psi\right] + \frac{1}{r}\left[\gamma r \frac{dS}{d\theta}\sin\rho\sin 2\psi + 2\gamma r S \sin\rho\cos 2\psi \frac{d\psi}{d\theta}\right] +$$
$$+\frac{1}{r}\left[2\gamma r S \sin\rho\cos 2\psi\right] = \gamma\cos\theta$$

Multiplying out, cancelling and collecting terms, gives:-

$$\sin\rho\sin 2\psi\frac{dS}{d\theta} + \left[\frac{d\psi}{d\theta}+1\right]2S\sin\rho\cos 2\psi + S +$$
$$+ S\sin\rho\cos 2\psi = \cos\theta \qquad 5.10$$

Similarly, equation 5.2 reduces to:-

$$\left[1-\sin\rho\cos 2\psi\right]\frac{dS}{d\theta} + \left[\frac{d\psi}{d\theta}+1\right]2S\sin\rho\sin 2\psi + S\sin\rho\sin 2\psi =$$
$$= -\sin\theta \qquad 5.11$$

Solving for $\left[\frac{d\psi}{d\theta}+1\right]$ by multiplying equation 5.10 by $\left[1-\sin\rho\cos 2\psi\right]$ and equation 5.11 by $\left[\sin\rho\sin 2\psi\right]$ and subtracting equation 5.11 from equation 5.10 gives:-

$$LHS = 2S\left[\sin\rho\cos 2\psi - \sin^2\rho\right]\left[\frac{d\psi}{d\theta}+1\right] + S\left[1-\sin^2\rho\right]$$
$$RHS = \cos\theta\left[1-\sin\rho\cos 2\psi\right] + \sin\theta\sin\rho\sin 2\psi$$

Hence

$$\left[\frac{d\psi}{d\theta}+1\right] = \frac{\cos\theta - \sin\rho\cos(2\psi+\theta) - S\cos^2\rho}{2S\sin\rho(\cos 2\psi - \sin\rho)} \qquad 5.12$$

and, similarly, solving for $\frac{dS}{d\theta}$ gives:-

$$\frac{dS}{d\theta} = \frac{-\sin(2\psi+\theta) + S\sin 2\psi}{\cos 2\psi - \sin\rho} \qquad 5.13$$

With the appropriate boundary conditions, the solution of S and ψ on θ can be obtained from the integrals of these two differential equations.

5.4 The determination of the principal stresses in the soil from the solution of the differential equations of critical equilibrium

Once the values of S and ψ are known, the values of σ_r, σ_θ and $\tau_{r\theta}$ can be determined by substituting the values of S and ψ in equations 5.9. The values of σ_x, σ_y and τ_{xy} can be determined by noting in Figure 5.3 that the direction of the stress σ_x is at an angle $\varphi = \psi + \theta$ clockwise from the direction of the maximum principal stress. In Figure 5.4, rotating point 1 clockwise by an angle $2(\psi + \theta)$ the value of σ_x is given by:-

$$\sigma_x = \gamma r S \left[1 + \sin\rho \cos 2(\psi+\theta) \right]$$

Assume the height of the apex of the wedge above a horizontal plane is equal to a, then $r = a/\cos\theta$. Hence the vertical stress, σ_x and the other stresses are given by:-

$$\sigma_x = \frac{\gamma S a}{\cos\theta} \left[1 + \sin\rho \cos 2(\psi+\theta) \right] \qquad 5.14$$

$$\sigma_y = \frac{\gamma S a}{\cos\theta} \left[1 - \sin\rho \cos 2(\psi+\theta) \right] \qquad 5.15$$

$$\tau_{xy} = \frac{\gamma S a}{\cos\theta} \left[\sin\rho \sin 2(\psi+\theta) \right] \qquad 5.16$$

5.5 The determination of the characteristic curves

From the general theory, it is known that the two characteristic directions are given by:-

$$\left(\frac{dy}{dx}\right)_\alpha = \tan(\varphi+\mu)$$

$$\left(\frac{dy}{dx}\right)_\beta = \tan(\varphi-\mu)$$

Considering the first equation and converting to polar co-ordinates gives:-

$$r\frac{d\theta}{dr} = Tan(\psi+\mu)$$

Now ψ is a function of θ only. Hence, the variables can be separated as follows:-

$$\frac{dr}{r} = \frac{d\theta}{Tan(\psi+\mu)} \qquad 5.17$$

when $\theta = 0$, let $r = r_o$ and, integrating 5.17

$$\int_{r_o}^{r}\frac{dr}{r} = \int_{0}^{\theta}\frac{d\theta}{Tan(\psi+\mu)}$$

$$Log_e\left(\frac{r}{r_o}\right) = \int_{0}^{\theta}\frac{d\theta}{Tan(\psi+\mu)}$$

i.e.

$$r_\alpha = r_o\, e^{\int_0^{\theta}\frac{d\theta}{Tan(\psi+\mu)}} \qquad 5.18$$

As ψ is known for every value of θ (from the solutions of equations 5.12 and 5.13), the progressive sum of $Cot(\psi+\mu)d\theta$ gives the progressive values of r as θ increases. The radius arm, r, traces out the first characteristic.

Similarly, the second characteristic curve can be obtained by substituting $-\mu$ for $+\mu$ in equation 5.18. A diagrammatic trace of the two characteristics is shown in Figure 5.5.

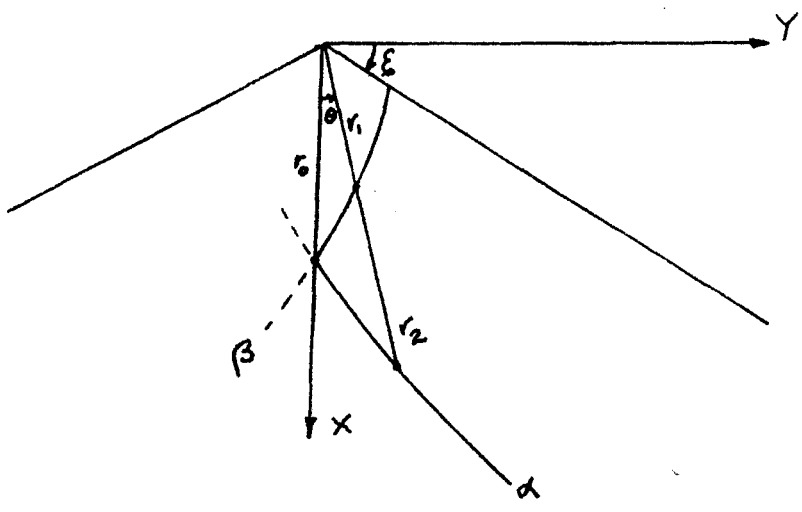

Fig. 5.5

5.6 State of active critical equilibrium in a slope of infinite extent

Case 1 Slope = $90 + \xi$ (see Figure 5.6)

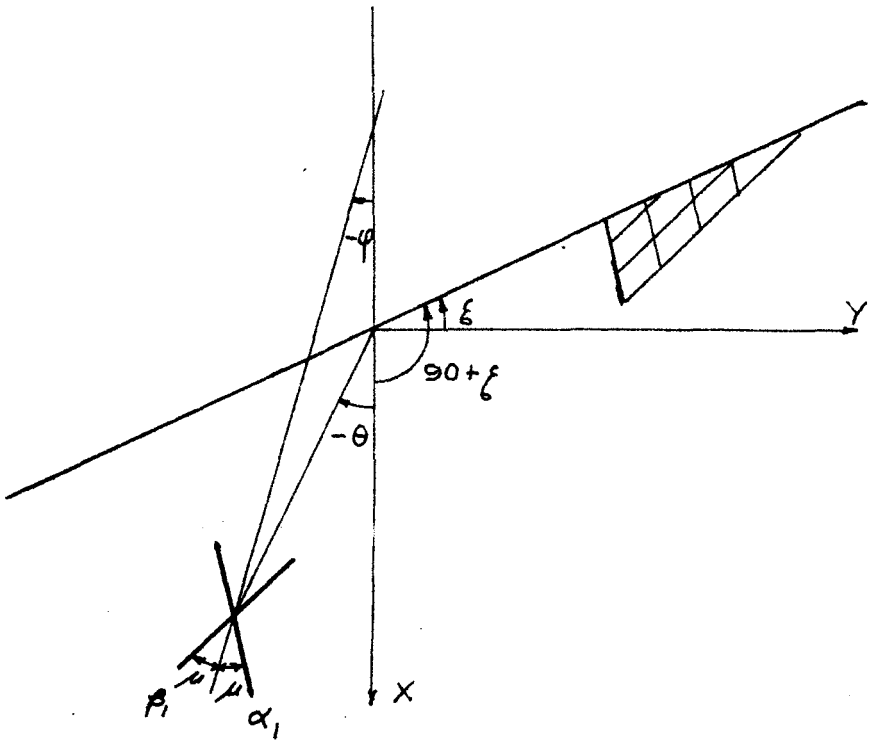

Fig. 5.6

The solution of this case is required as part of the solution of wedges in which the interior angle is smaller than 180°.

It is evident from the postulation of a slope of infinite extent that φ, the direction of the maximum principal stress, must remain constant and independent of θ. This being so, the characteristic curves must be straight lines.

The direction of φ

As φ is constant, the rate of change of ψ with respect to θ in

$$\psi = \varphi - \theta \qquad 5.19$$

gives

$$\frac{d\psi}{d\theta} = -1$$

Substituting this value for the derivative in equation 5.12 gives

$$0 = \frac{\cos\theta - \sin\rho\cos(2\psi+\theta) - S\cos^2\rho}{2S\sin\rho(\cos 2\psi - \sin\rho)}$$

that is $\cos\theta - \sin\rho\cos(2\psi+\theta) - S\cos^2\rho = 0$

and $$S = \frac{\cos\theta - \sin\rho\cos(2\psi+\theta)}{\cos^2\rho} \qquad 5.20$$

From equation 5.19, substituting for ψ in equation 5.20 gives

$$S = \frac{\cos\theta - \sin\rho\cos(2\varphi-\theta)}{\cos^2\rho} \qquad 5.21$$

At the boundary, $\sigma = 0$ which implies from equation 5.8, that the value of S must also be zero along the boundary. At the boundary, $\theta = \xi + 90$. Substituting these values in equation 5.21 gives

$$\cos(90+\xi) - \sin\rho\cos(2\varphi-90-\xi) = 0$$

Expanding the double angles and reducing gives

$$\sin\xi - \sin\rho\sin(2\varphi-\xi) = 0$$

Solving for φ,

$$2\varphi = (K-1)\frac{\pi}{2} + \xi - K\sin^{-1}\left(\frac{\sin\xi}{\sin\rho}\right) \qquad 5.22$$

where K =+1 denotes active failure.

From equation 5.22, the value of φ can be determined for any slope, ξ. From equation 5.21, the value of S can

be determined using the derived value of φ . Now, $\psi = \varphi - \theta$. Hence, if the stress vertically below a point on the surface is required, $\psi = \varphi$ and substituting in equation 5.9 gives the stress.

Equation 5.22 gives the direction of the maximum principal stress. The directions of characteristic lines are given by

$$\alpha_1 = \varphi + \mu$$

$$\beta_1 = \varphi - \mu$$

Considering only active failure

$$2\beta_1 = -2\mu + \xi - \sin^{-1}\left(\frac{\sin\xi}{\sin\rho}\right) \qquad 5.23$$

$$2\alpha_1 = +2\mu + \xi - \sin^{-1}\left(\frac{\sin\xi}{\sin\rho}\right) \qquad 5.24$$

Case 2 Slope = $90 - \xi$ (see Figure 5.7)

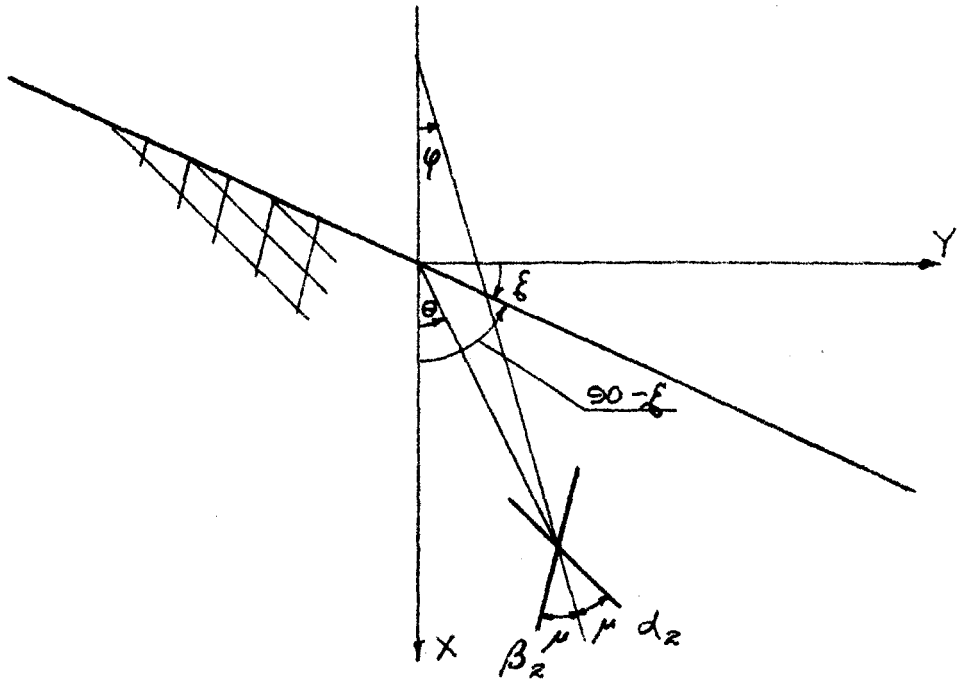

Fig. 5.7

If the slope is equal to $90 - \xi$ the directions of the α_2 and β_2 characteristic lines are given by

$$2\alpha_2 = 2\mu - \xi + \sin^{-1}\left(\frac{\sin\xi}{\sin\rho}\right) \qquad 5.25$$

$$2\beta_2 = -2\mu - \xi + \sin^{-1}\left(\frac{\sin\xi}{\sin\rho}\right) \qquad 5.26$$

From equation 5.25 the value of ξ can be conveniently determined as follows:

$$\sin^{-1}\left(\frac{\sin\xi}{\sin\rho}\right) = 2\alpha_2 - \frac{\pi}{2} + \rho + \xi$$

i.e.

$$\frac{\sin\xi}{\sin\rho} = \sin\left(\overline{2\alpha+\rho} + \overline{\xi - \frac{\pi}{2}}\right)$$

Expanding the righthand side and multiplying out gives

$$\text{RHS} = \sin(2\alpha_2+\rho).\sin\xi - \cos(2\alpha_2+\rho).\cos\xi$$

Dividing by $\sin\xi$ and solving for $\tan\xi$ gives

$$\tan\xi = \frac{\sin\rho.\cos(2\alpha_2+\rho)}{\sin\rho.\sin(2\alpha_2+\rho) - 1} \qquad 5.27$$

Comparing equation 5.27 with the corresponding equation in Sokolovski's book "Statistics of Soil Media", page 149, there appears to be a type-set error in his formula.

5.7 Domains of dependence in an infinite slope

The following information can be obtained from the characteristics of an infinite slope in a state of critical equilibrium. In Figure 5.8 three infinite slopes are shown.

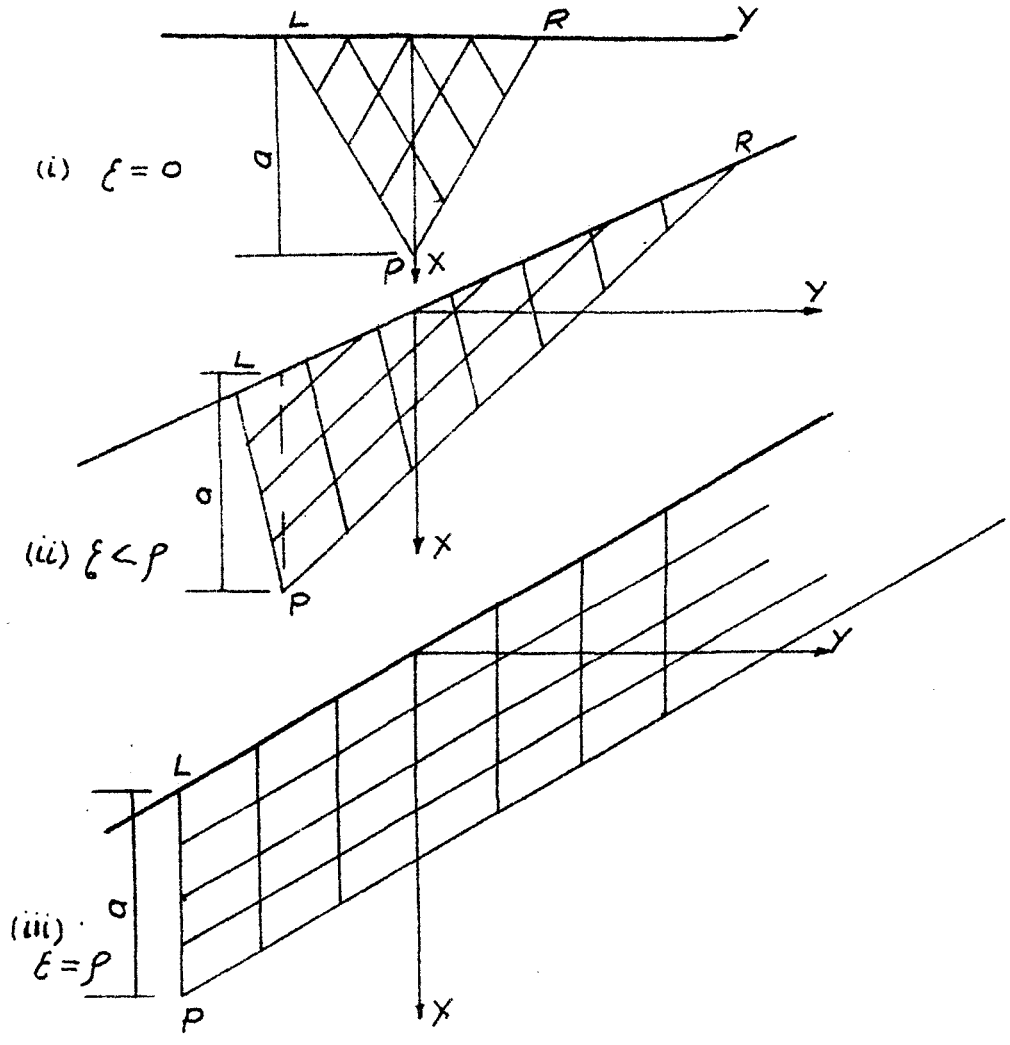

Fig. 5.8

The slopes of the characteristic lines are determined from equations 5.23 and 5.24. The domains of dependence of point P are given by LR, the intersection of the characteristics through point P with the surface of the slopes.

It is immediately evident that, in slopes (i) and (ii), for a finite value of the distance, a, the domains of dependence are finite, the domains increasing as the slope ε approaches ρ. When $\varepsilon = \rho$ the domain of dependence becomes infinite as shown in slope (iii). The surface of the slope is now itself

a characteristic line, the other characteristic line being vertical.

Where the slopes are not infinite in extent, in (i) and (ii) the critical state, as for an infinite slope, may yet exist over a finite length provided the domain of dependence of the point P is on the finite slope. In (iii), this critical condition cannot exist in any finite slope for any finite values of a. The critical region shrinks to a line at the surface, that is the region exists only for values of a = 0.

These observations can be applied to solutions of certain regions of wedges. In Figure 5.9 two wedges are shown. In wedge (i) the two slopes of ξ_1 and ξ_2 are both smaller than ρ. In wedge (ii) the two slopes ξ_1 and $\xi_2 = \rho$.

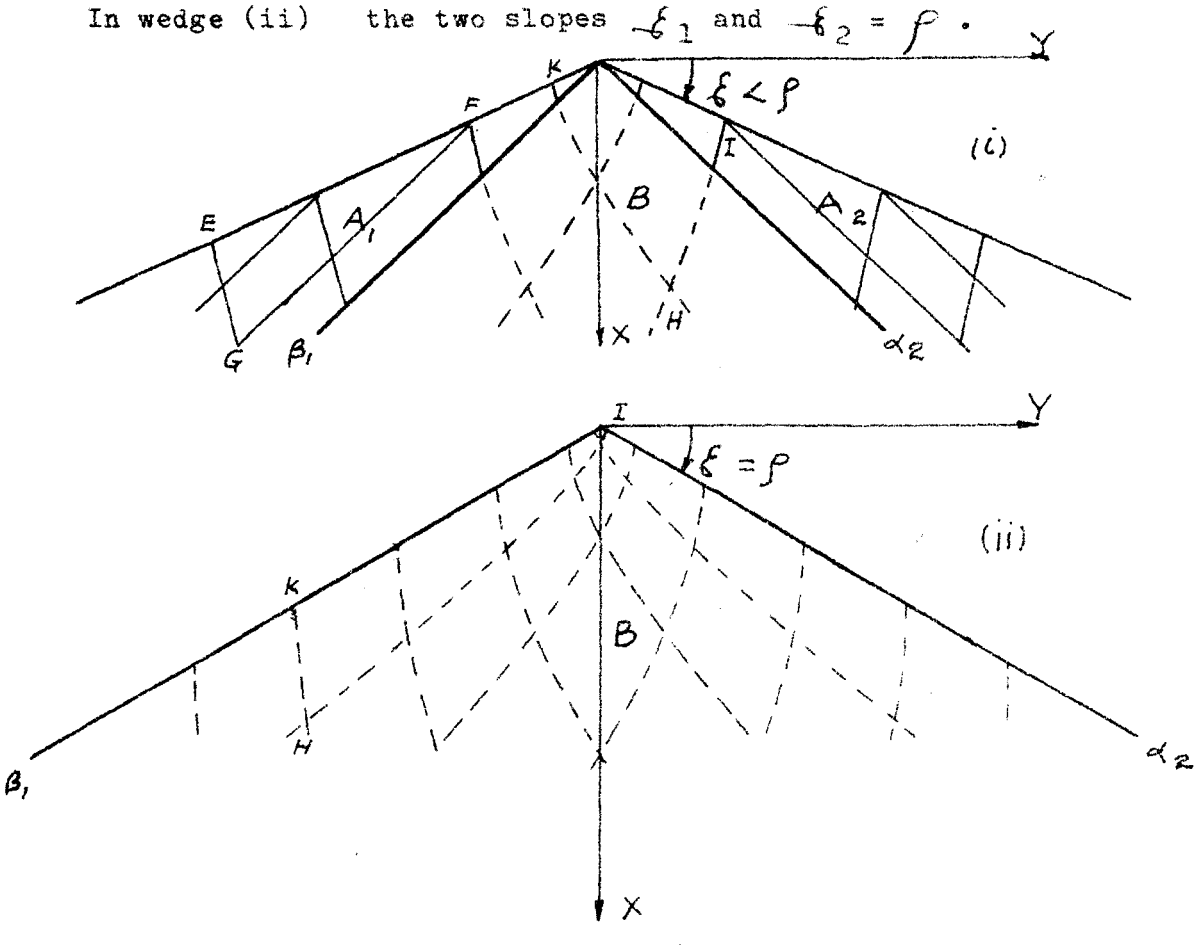

Fig. 5.9

In wedge (i) two regions exist marked A_1 and A_2 in which the critical stresses conform to the infinite slope condition. The limits of these regions are given by the β_1 and α_2 characteristics through the apex of the wedge and the surface slopes of the wedge respectively. The slopes of these characteristics are determined from equations 5.23 and 5.25 respectively. To the left of the β_1 characteristic and the right of the α_2 characteristic plastic failure such as indicated by EFG, completely confined to each flank of the wedge, can take place. Between the characteristic β_1 and α_2 (Region B) failure such as IHK can only take place by including portions of both flanks of the wedge.

In wedge (ii), because $\xi = \rho$, the infinite slope solution is only valid at the surface of the two flanks and Region B applies throughout the wedge. Failure can only take place by including portions of both flanks of the wedge. To summarise: whereas in wedge (i), with $\xi < \rho$, the failure of the wedge in certain regions is confined to one of the flanks, in wedge (ii), with $\xi = \rho$, failure must <u>always</u> include portions of both flanks.

The exact form of the failure lines in Region B are yet to be determined by the numerical solution of equations 5.12 and 5.13.

5.8 <u>A relationship along characteristics β_1 and α_2</u>

Along the characteristics β_1 and α_2 certain relationships exist which are of value in checking the numerical solution of the critical state in Region B. Consider the β_1 characteristic in Figure 5.10. When θ is equal to the angle at which the β_1 characteristic lies then

$$-\theta = -\varphi - \mu$$

but by definition $\psi = \varphi - \theta$

hence $\psi = -\mu$ 5.28

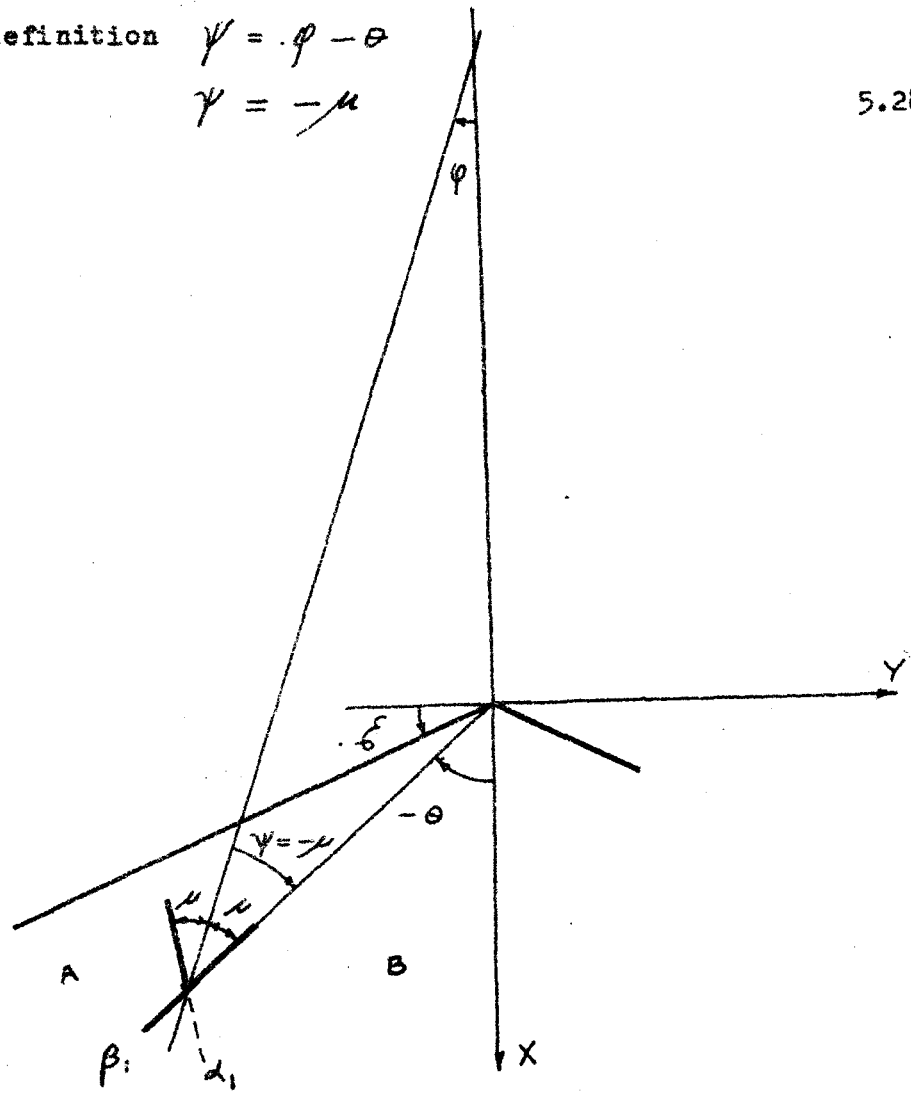

Fig. 5.10

Designating angle θ, at which the β_1 characteristic lies, by β_1 then

$$\theta = -\beta_1$$

and substituting this value for θ in equation 5.20 gives

$$S\,Cos^2\rho = Cos(-\beta) - Sin\rho\, Cos(\rho - \tfrac{\pi}{2} - \beta_1)$$

and as $|\beta|$ is smaller than $\frac{\pi}{2}$

$$S\,Cos^2\beta_1 = Cos\beta_1 - Sin\rho\, Cos(\rho - \beta_1 - \tfrac{\pi}{2})$$

$$= Cos\beta_1 - Sin\rho\, Sin(\rho - \beta_1)$$

$$= Cos\beta_1 - Sin\rho\, Sin\rho\, Cos\beta_1 + Sin\rho\, Cos\rho\, Sin\beta_1$$

$$= \cos\beta_1 (1 - \sin^2\rho) + \sin\rho \cos\rho \sin\beta_1$$

$$\therefore \quad S\cos\rho = \cos\beta_1 \cos\rho + \sin\beta_1 \sin\rho$$

$$= \cos(\beta_1 - \rho)$$

then
$$S = \frac{\cos(\beta_1 - \rho)}{\cos\rho} \qquad 5.29$$

Similarly it can be shown that for the α_2 characteristic

$$\psi = -\mu. \qquad 5.31$$

and

$$S = \frac{\cos(\alpha_2 + \rho)}{\cos\rho} \qquad 5.32$$

5.9 Solution of the plastic state in the wedge

5.9.1 Solution in Region A

Region A (Figure 5.9) conforms to the infinite plane conditions considered in Section 5.6 where the formulae for the critical stresses have been given.

5.9.2 Solution in Region B

In Region B the solution of the critical stress state must be obtained by the numerical integration of the differential equations 5.12 and 5.13.

5.9.2.1 Initial conditions

For any selected wedge with slopes ε_1 and ε_2 the slopes of the characteristics α_2 and β_1 which form the boundaries to Region B can be found from equations 5.25 and 5.23. On these characteristics from equations 5.28, 5.31, 5.32 and 5.29 the values of ψ and S are known and form a set of boundary conditions for the solution in B. However, attempts to solve the differential equations by using these initial values were not successful due to the following reasons:-

The first derivatives $d\psi/d\theta$ and $dS/d\theta$ tend to infinity at $\theta = \alpha_2$ and $\theta = \beta_1$. The approach to infinity is extremely rapid and it appears that a discontinuity in the first derivatives exist at these values of θ. (See Figures 5.15 and 5.16). As it is not possible to calculate the values of the first derivatives immediately inside Region B (that is θ just smaller than α_2 and θ just bigger than β_1) even by such methods requiring only the initial values of θ, ψ, and S, the solution cannot be advanced from these values.

The only method of solution is to choose the initial values of θ, ψ and S (to avoid confusion these initial values will henceforth be designated θ_o, ψ_o and S_o) in the Region B and to advance the solution by numerical integration of equations 5.12 and 5.13 in positive and negative directions of θ until in each of these directions the value $\psi = -\mu$ is attained. At this value for ψ the solution terminates and the concomittant values of θ and S can be found. The two values of θ correspond to the slopes of the α_2 and β_1 characteristics and hence from equations 5.25 (or equation 5.27) and 5.23 the values of the two slopes of the wedge ε_2 and ε_1 can be determined respectively.

The relationships between the slopes ξ_1 and ξ_2 and the chosen values of θ_o, ψ_o and S_o are as yet unknown, so the values of ξ_1 and ξ_2 determined in any particular numerical solution may be far removed from those required. In order to find the solution for any two specified slopes it is therefore necessary to make a series of solutions with different values for θ_o, ψ_o and S_o and then to determine the values of these parameters for the specified ξ_1 and ξ_2 by interpolation. The method of solution for specified slopes is therefore an indirect one.

A convenient initial value for θ_o is the semi-X axis. Here $\theta_o = 0$. As set out previously, by choosing different values for ψ_o and S_o different slopes ξ_1 and ξ_2 can then be calculated.

In the symmetrical wedge at $\theta_o = 0$ the direction of the maximum principal stress, φ, is in the direction of the X axis, i.e. $\varphi_o = 0$ and as

$$\psi_o = \varphi_o - \theta_o$$

the value of $\psi_o = 0$.

Within the limits the value of S_o can be selected arbitrarily. The upper limit of S_o is associated with a wedge with slopes $\xi_1 = \xi_2 = 0$, i.e., a horizontal infinite plane. Its value can be found from equation 5.20

$$S_o = \frac{\cos\theta - \sin\rho \cos(2\varphi - \theta)}{\cos^2\rho}$$

with $\theta_o = 0$, $\varphi_o = 0$ and if the angle of internal friction, ρ, is equal to 30° the value of S_o is correspondingly

$$S_o = \frac{1 - \frac{1}{2} \cdot 1}{\left(\frac{\sqrt{3}}{2}\right)^2} = \frac{1}{2} \cdot \frac{4}{3} = \frac{2}{3}$$

The lower limit of S_o, which for the symmetrical wedge occurs when the slopes are attheir natural angle of repose, can be found by solving differential equations 5.12 and 5.13 for a series of values of S_o (and finding the concomittant values of ξ) ranging from $S_o = \frac{2}{3}$ down to S_o corresponding to a value of ξ equal to the natural angle of repose.

5.9.2.2 Termination of the solution

The integration of equations 5.12 and 5.13 is performed by numerical step by step methods. It is known that if $\theta = \alpha_2$ or β_1, the value of $\psi = -\mu$. The solution is therefore terminated when ψ attains this value. The differential equations are, however, in terms of the independent variable θ . Hence, with the step by step method of solution it is virtually impossible to select the final step $\delta\theta$ so that ψ would attain the value of $-\mu$ at the end of that step. It is therefore necessary to transform the two differential equations, making ψ the independent variable and performing the numerical calculation in terms of this independent variable. Alternatively, the solution may be advanced in terms of θ and at some step before ψ attain the value of $-\mu$ to transform the differential equations to ψ as independent variable and advance the solution further in terms of the independent variable ψ .

In this investigation the second procedure was followed as the step length $\delta\theta$ could be chosen as a fraction of a degree such that the values of ψ and S could be listed in terms of whole degrees of θ . Only the last few values, when θ is determined from ψ , will θ not be in whole numbers.

5.9.2.3 Checks on the accuracy of the solutions

One of the problems in the solution of differential equations by numerical methods is the estimation of the degree of accuracy of the solution. Fortunately, in the solution of the equations governing the plastic state of the wedge there are two checks, one of which provides a powerful control on the accuracy:

1. The solution for the slopes $\xi_1 = \xi_2 = 0$, i.e. an infinite horizontal plane, is known in closed form and can be used as a check on the accuracy of the numerical solution. From the closed functional relationships, for $\rho = 30^\circ$, the value of $\sigma_x = 1.0\,\gamma h$, $\sigma_y = 0.33\,\gamma h$ and $\tau_{xy} = 0$. Furthermore, the radius of the α_2 characteristic for $\rho = 30^\circ$ lies at $\theta = \alpha_2 = 30^\circ$ and has the value

$$r = \frac{r_o}{2\cos\alpha_2}$$

Hence for $r_o = 1$ the value of $r = 0.57735$ (See Figure 5.11)

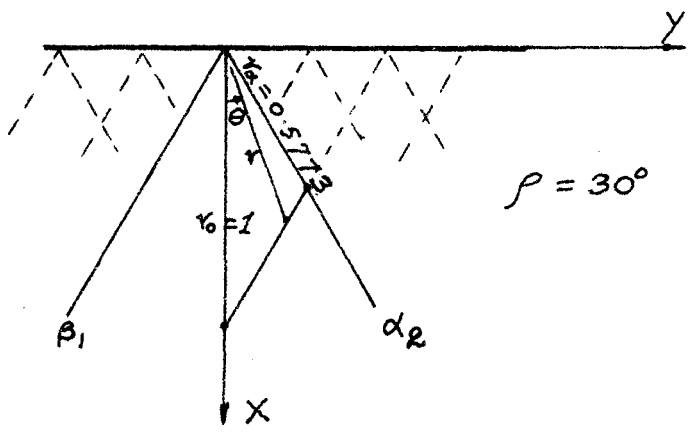

Fig. 5.11

Comparing the values listed above with those obtained from the numerical solution as given for $\xi = 0$ in Appendix 2 the values show agreement to the 6th decimal place. The numerical method of integration (to be considered later) appears therefore to provide solutions of sufficient accuracy for this slope configuration. (In passing, it is of interest to note in the last line of the list of values for $dS/d\theta$ and $d\psi/d\theta$ for $\xi = 0$ (Appendix 2) the occurrence of the discontinuity in these derivatives in the last step length of $\delta\theta = 0.005^{\circ}$.)

The fact that the solution is accurate for the values of $S_o = 2/3 = 0$ is no guarantee that it will be accurate for $S_o \approx 0.53$, which gives $\xi \approx 30^{\circ}$. All that this check ensures is that the procedure of the solution is correct (and accurate for this value of $S_o = 2/3$), but it does not ensure accuracy at lower values of S_o. For this purpose the second check is required.

2. The second check is provided by equation 5.32 which gives the relationship between S and θ at $\theta = \alpha_2$.

i.e. $$S = \cos(\alpha_2 + \rho)/\cos\rho$$

and $$\psi = -\mu.$$

The procedure of the check is as follows:

By solving equations 5.12 and 5.13 numerically, the solution of S and ψ is obtained up to the point where $\psi = -\mu$.. The check on the value of S is determined from equation 5.32 by substituting the value of α_2 corresponding to the value of $\psi = -\mu$. This value of S is compared with that obtained by means of the numerical integration method. If these two values are identical it is virtually guaranteed that the solution is correct.

5.9.2.4 Numerical integration procedures

To integrate the differential equations 5.12 and 5.13 the Rung-Kutta-Gill step by step method was used and programmed for

solution on an electronic computer according to the procedure set out by Romanelli (Ralston and Wilf, 1962).

It was found that as S_o decreased, instability and inaccuracy of the solution increased. As $S_o = 0.527$ is nearer the lower limit of S_o the step lengths were determined which would yield a stable solution for this value of S_o, and in which the check value of S (equation 5.32) on the α_2 characteristic agreed with the value obtained by the numerical method to five decimal places. The initial step length finally accepted was $d\theta = 0.5^o$. This value was decreased to the equivalent of 0.05^o when the equation was transformed with ψ as independent variable. Near the termination of the solution ($\psi \approx -\mu$) it was found that the derivatives changed very rapidly and required a further reduction of the step length to $^1/5$th its former value.

By halving all the step lengths no appreciable increase in accuracy was found. On the contrary in some instances a loss of accuracy was evident, apparently due to the accumulation of rounding off errors. Once the programme was found to be satisfactory for $S_o = 0.527$ the same step lengths were employed for the solutions for other values of S_o.

5.9.2.5 Value of σ_x, σ_y and τ_{xy}

From the numerical solution, once the values of S and ψ for θ were known the stresses in the plastic region could be determined as follows:

Assuming it is required to calculate the stresses along the horizontal base of the wedge a distance, a, below the apex (Figure 5.12).

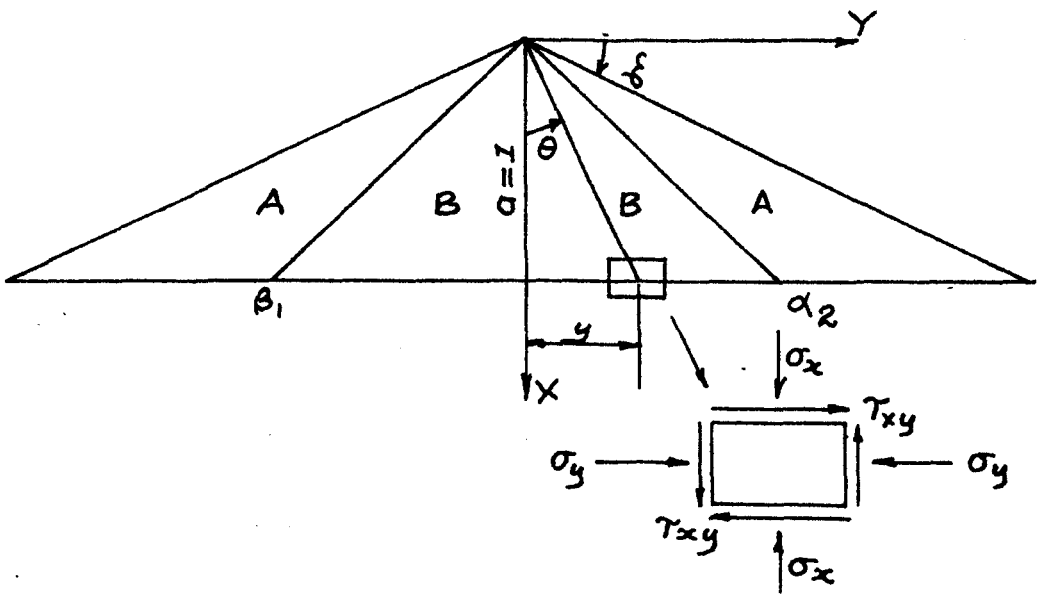

Fig. 5.12

At angle θ the value y is given by

$$y = a\,\mathrm{Tan}\,\theta$$

The stresses, σ_x, σ_y, τ_{xy}, are found from equations 5.14, 5.15 and 5.16. If γ and a are taken to equal one, the solutions are given for a wedge of unit height and unit density and the values of the stresses can be found for any height and any density by multiplying the solutions by a and γ.

5.9.2.6 The slope ξ

Assuming that the solution has been completed up to $\psi = -\mu$ then the value of θ is known at this point. The value of θ here corresponds to the angle α_2, in equation 5.27. The slope of the wedge corresponding to this angle α_2 can then be found from this equation.

5.9.2.7 The characteristic or failure lines in the wedge

As $\delta\theta$ advanced step by step to $\theta = \alpha_2$ the integrals

as given in Section 5.5, can be progressively evaluated numerically, the values of r_1 and r_2 sweeping out the failure lines. If r_o is chosen as unity on the X-axis the failure lines for any other value of r_o can be found by multiplying the numerically calculated values by this value of r_o (See Figure 5.13).

5.9.2.8 Numerical solution

The computer programme to determine $d\psi/d\theta$, $dS/d\theta$, θ, S, ψ, σ_x, σ_y, τ_{xy}, r_1 and r_2 for $\rho = 30^\circ$ and chosen initial values for S_o, ψ_o and θ_o is given in Appendix 1. This programme is designed to obtain solutions for symmetric wedges only. Solutions were obtained for theright-hand sides of the symmetric wedges only. The initial values for θ_o and ψ_o were fixed at zero and solutions for the initial values of $S_o = 0.66666667$, then $S_o = 0.66$, thereafter decreasing by increments of 0.01 down to 0.53, thereafter decreasing by increments of 0.001 down to 0.527 were calculated.

Lists of the values of the slopes of the α_2 characteristics corresponding to these values of S_o are given in Table 5.1. In this table the check values of S on the α_2 characteristic are also listed. It can be noted that the two values of S agree to at least the fourth decimal place and provide a picture of the accuracy of the solutions. The relationship between ξ and S_o is shown in Figure 5.14.

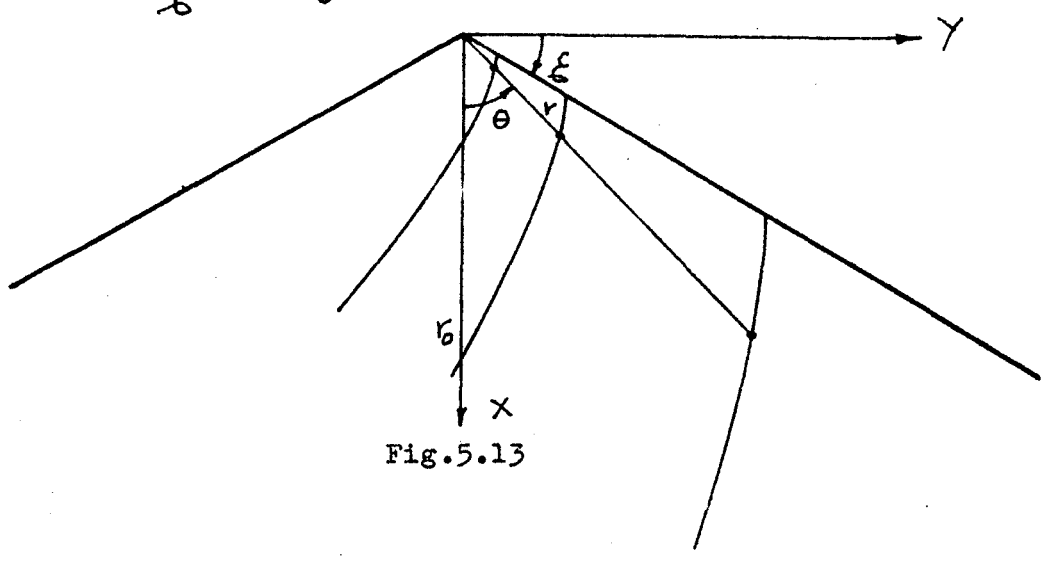

Fig.5.13

TABLE 5.1

S_0	α_2	S		Difference
		Numerical Solution	$\frac{\cos(\alpha_2+\rho)}{\cos\rho}$	
0.6666	0.52359926	0.577350	0.577350	< 0.000001
0.66	0.53241261	0.568513	0.568514	- 0.000001
0.65	0.54628014	0.554523	0.554522	+ 0.000001
0.64	0.56098931	0.539545	0.539565	- 0.000020
0.63	0.57671388	0.523433	0.523446	- 0.000013
0.62	0.59359289	0.505980	0.505999	- 0.000019
0.61	0.61186296	0.486935	0.486953	- 0.000018
0.60	0.63181645	0.465953	0.465966	- 0.000013
0.59	0.65385694	0.442567	0.442569	- 0.000002
0.58	0.67854300	0.416100	0.416109	- 0.000009
0.57	0.70677053	0.385528	0.385543	- 0.000015
0.56	0.74001865	0.349148	0.349148	< 0.000001
0.55	0.78095479	0.303810	0.303811	- 0.000001
0.54	0.83584676	0.242226	0.242234	- 0.000008
0.53	0.92938952	0.135718	0.135719	- 0.000001
0.529	0.94536602	0.117381	0.117382	- 0.000001
0.528	0.96517272	0.094606	0.094608	- 0.000002
0.527	0.99328027	0.062227	0.062228	- 0.000001

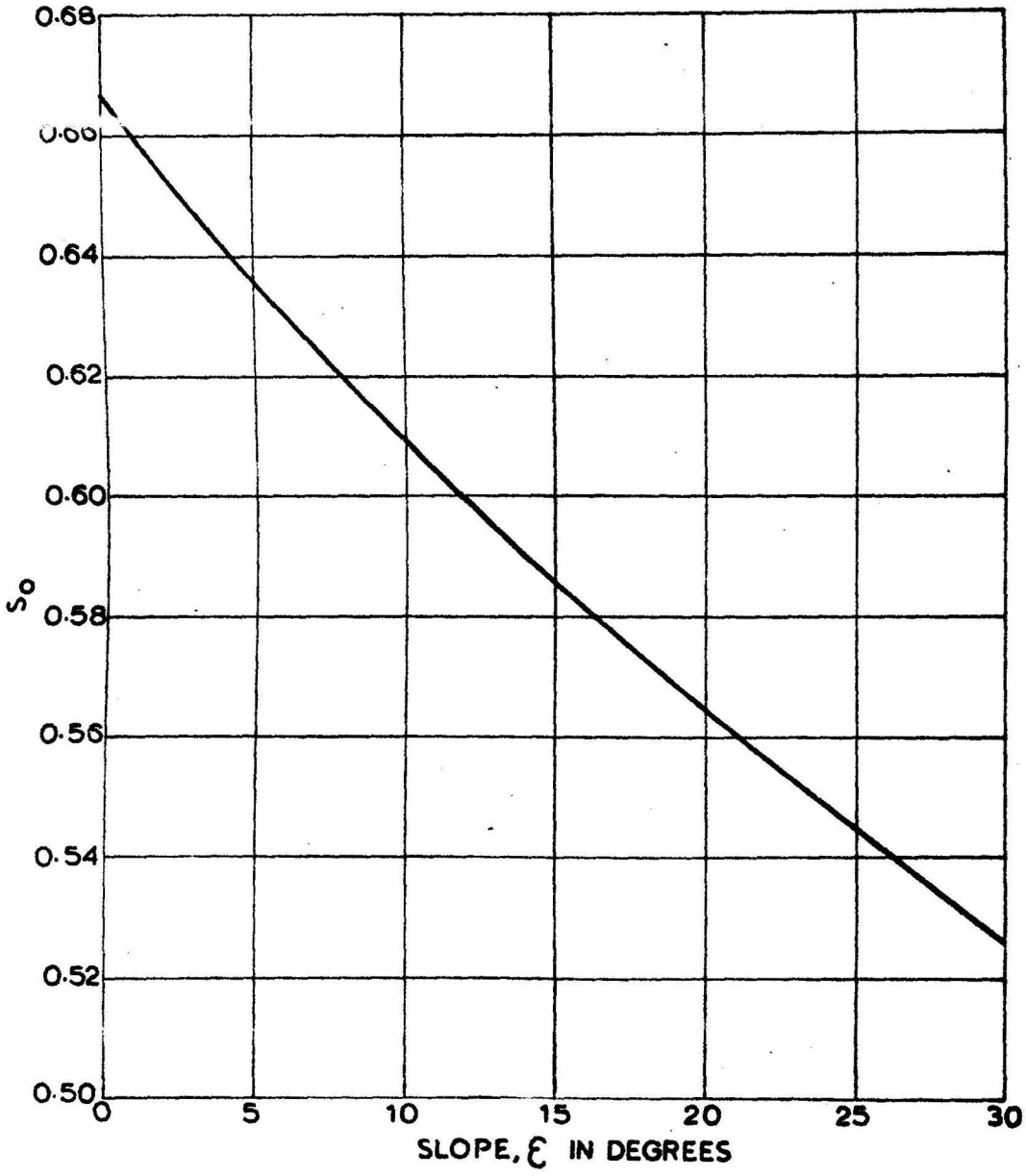

RELATIONSHIP BETWEEN THE INITIAL VALUES OF S ON THE SEMI X-AXIS AND THE SLOPE, ε.

FIG. 5.14

The values of S_o between 0.66 and 0.53 were differenced and it was found that random variation occurs in the 5th differences. In consequence a 4th order Lagrangian interpolation was used to determine the values of S_o corresponding to the slopes ξ = 0, 5, 10, 15, 20, 25, 30°. These interpolated values of S_o were then used as initial values to determine the plastic states for wedges with the corresponding slopes. The lists of the completed solutions are given in Appendix 2.

From the lists in Appendix 2 the various parameters of interest in numerical solutions of the critical state are plotted in the following diagrams:

1. $dS/d\theta$ versus θ - Figure 5.15
2. $d\psi/d\theta$ versus θ - Figure 5.16
3. S versus θ - Figure 5.17
4. ψ versus θ - Figure 5.18
5. α_2 versus ξ - Figure 5.19
6. Stresses along the base of the wedges - Figure 5.20
7. The failure lines in wedges with 30° and 25° slopes - Figures 5.21 and 5.22 respectively.

5.9.3 Discussion of the Solutions of the active critical state in wedges

From Figures 5.15, 5.16 and 5.19 it is apparent that S, ψ, and α_2 become sensitive to the value of the slope, ξ, as it approaches the natural angle of repose. For instance, a change of slope from 30° to 29° causes a shift in the angle of the α_2 characteristic from 60° to 55° approximately. (Figure 5.19). The stresses, which are dependent on S and ψ, will reflect this sensitivity, and the locations of the failure lines tend to be indeterminate.

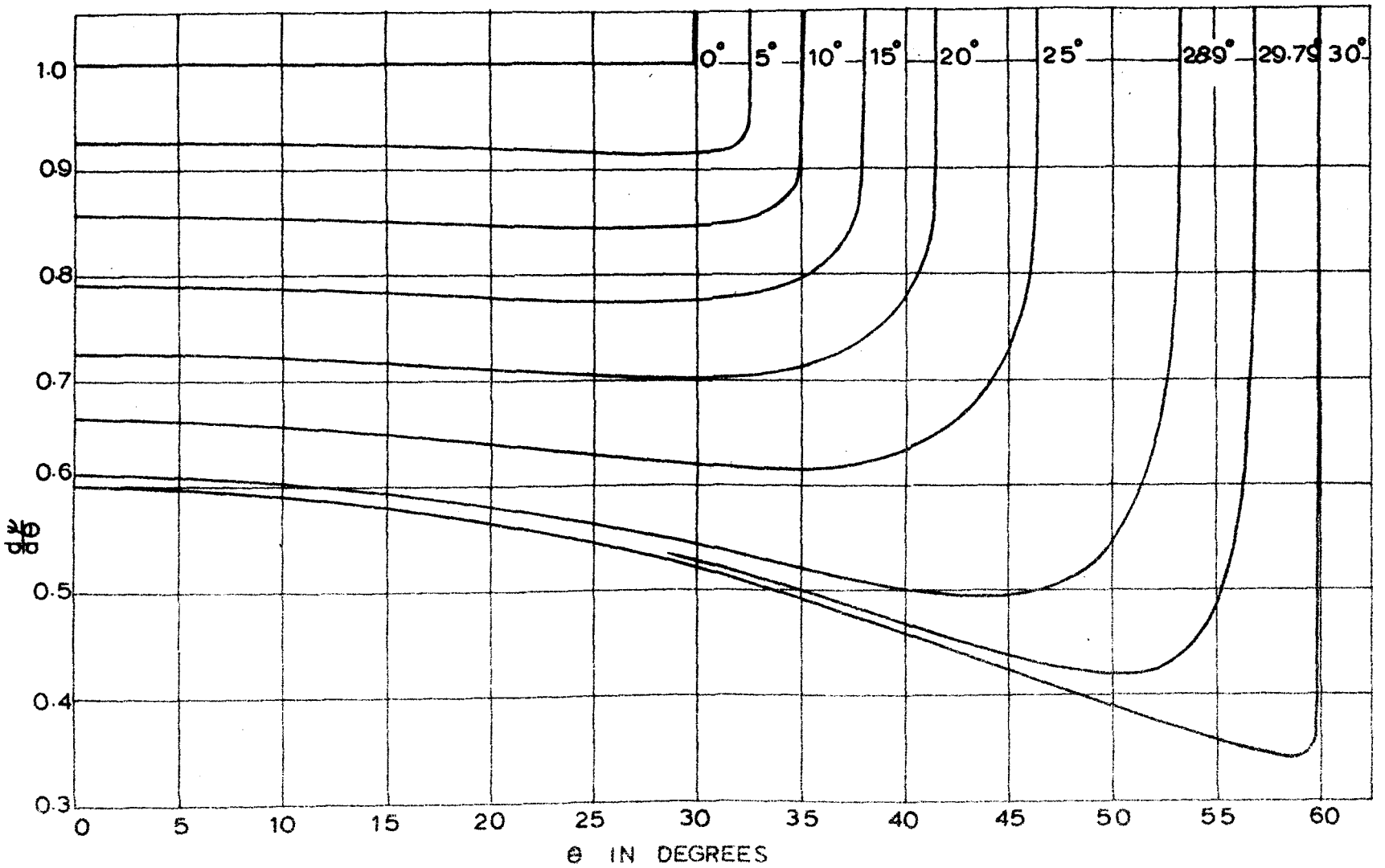

RELATIONSHIP BETWEEN $\frac{d\psi}{d\theta}$ & θ FOR SYMMETRICAL WEDGES OF COHESIONLESS MATERIAL FOR VARIOUS SLOPES

FIG.5.15

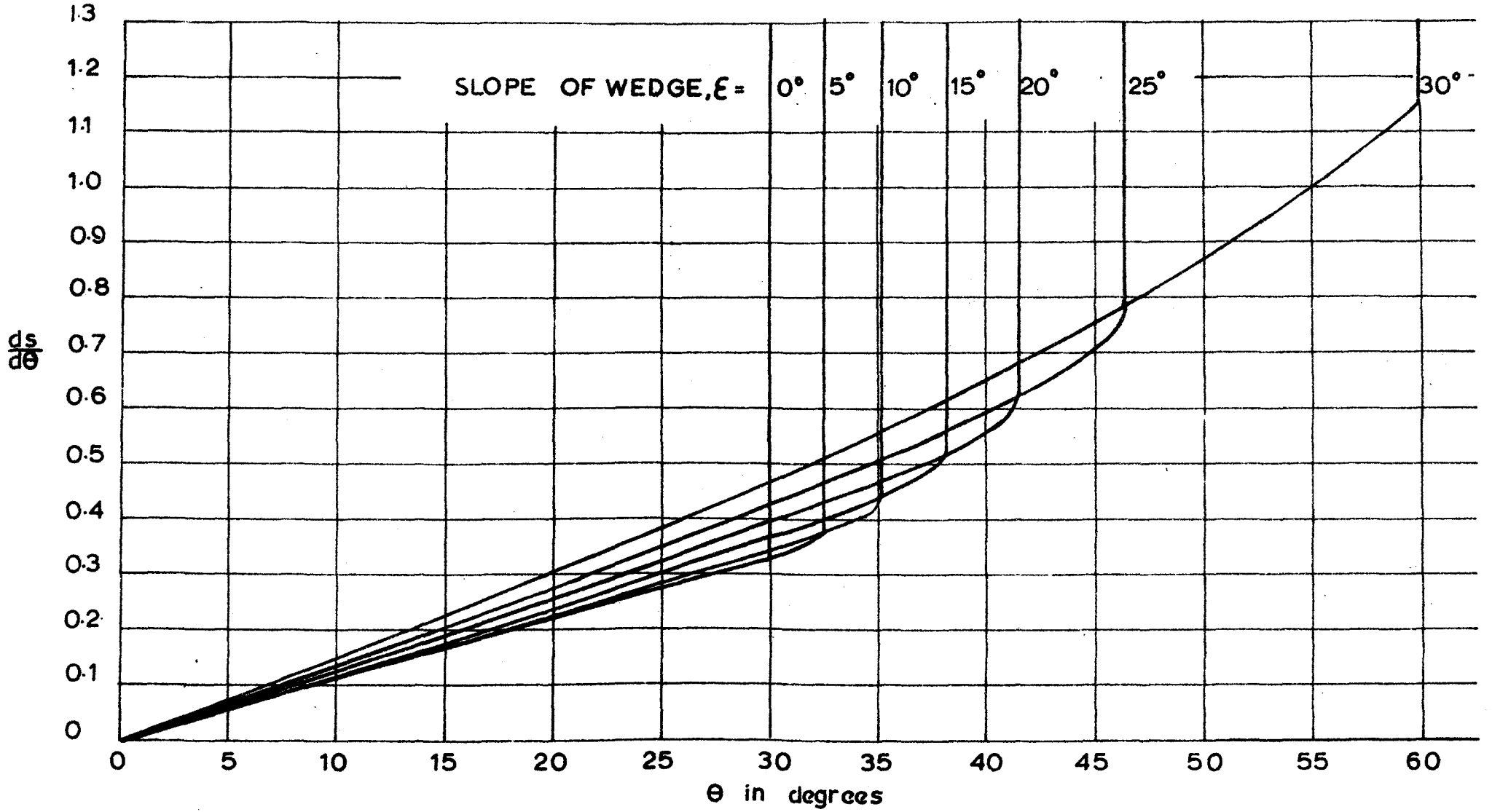

CHANGE OF $\frac{ds}{d\theta}$ WITH θ FOR SYMMETRICAL WEDGES

FIG. 5.16

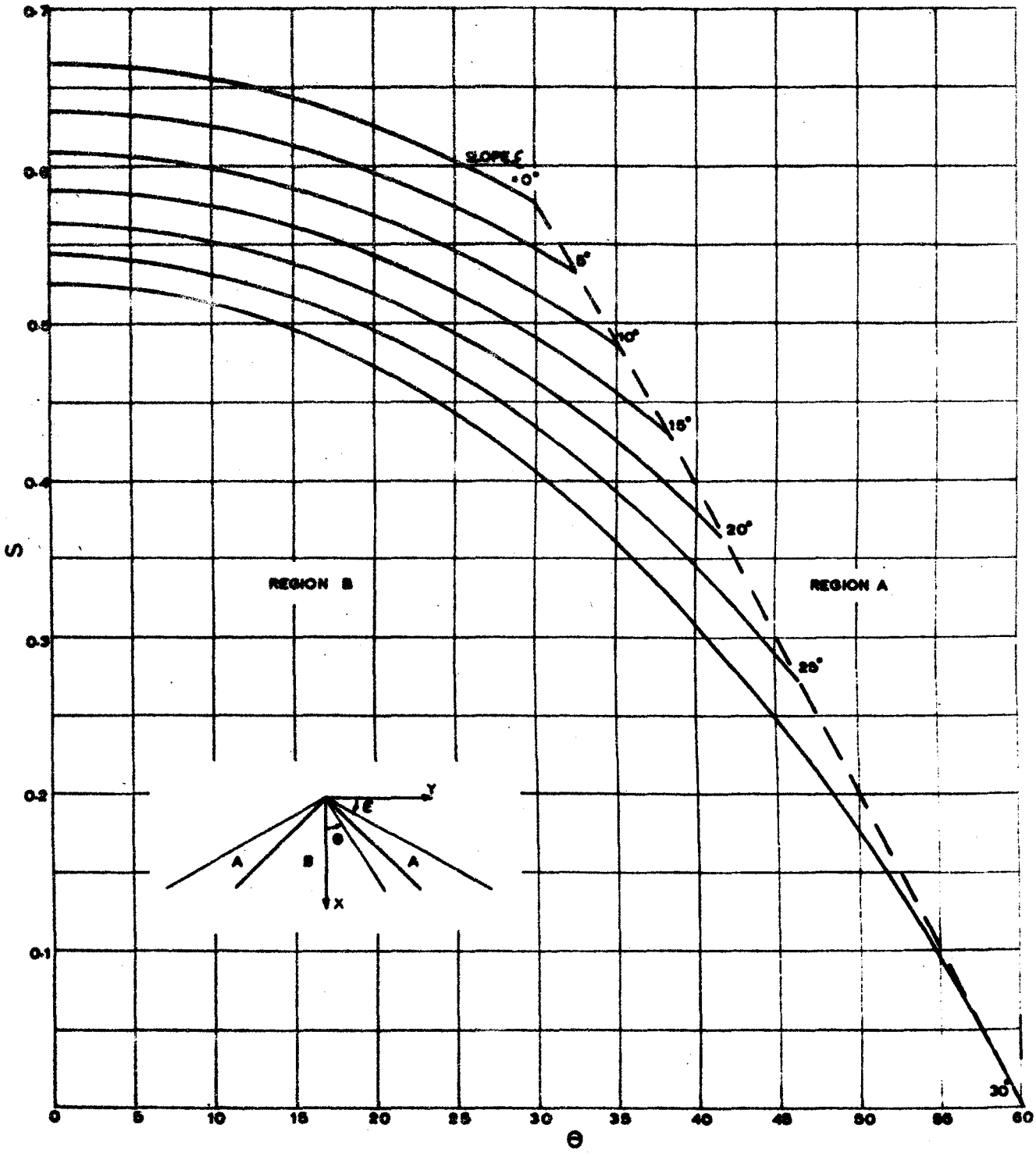

RELATIONSHIP BETWEEN S & θ FOR SYMMETRICAL WEDGES OF COHESIONLESS MATERIAL FOR VARIOUS VALUES OF ε.

FIG. 5.17

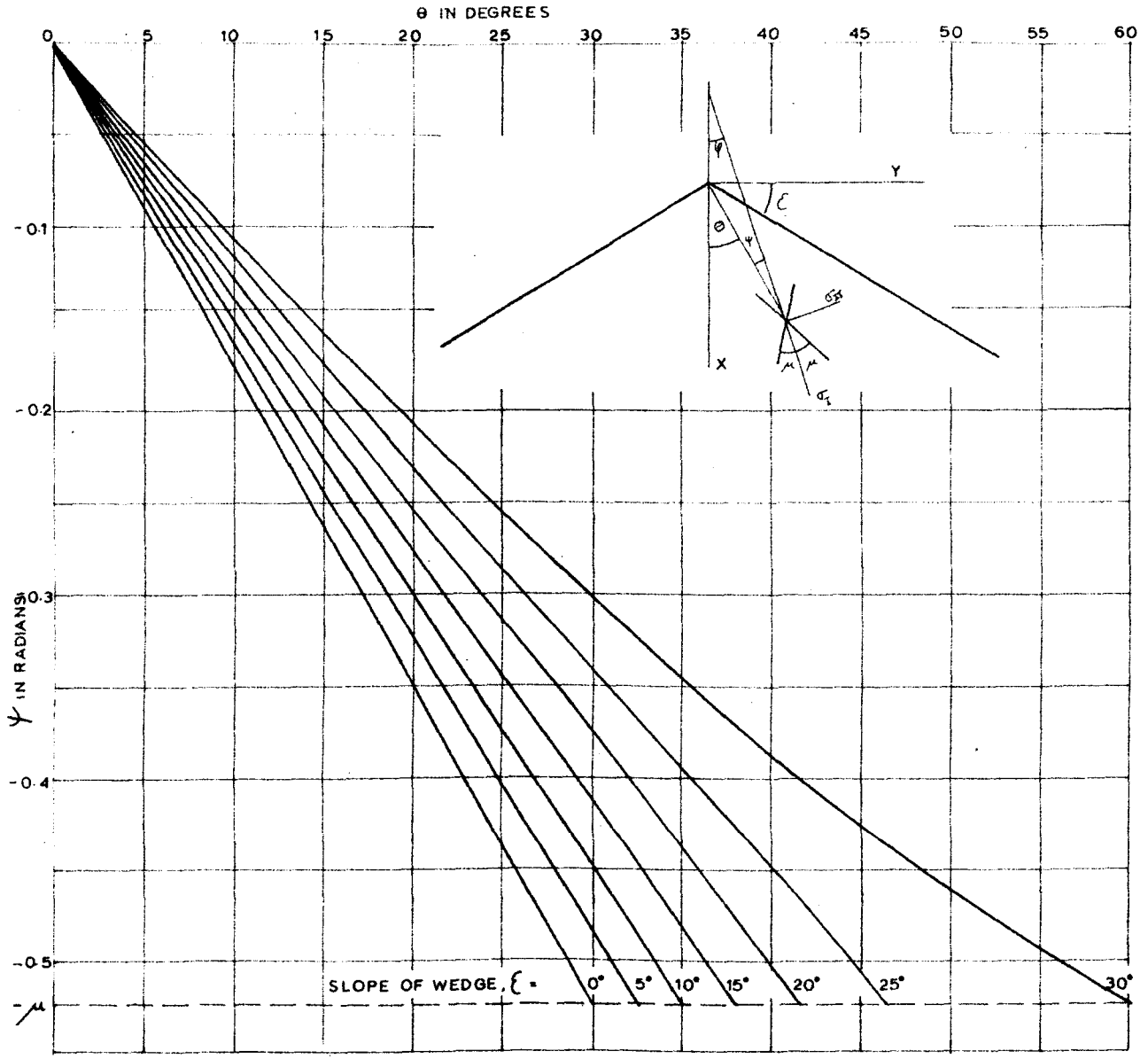

RELATIONSHIP BETWEEN ψ AND θ FOR SYMMETRICAL WEDGES

FIG. 5.18

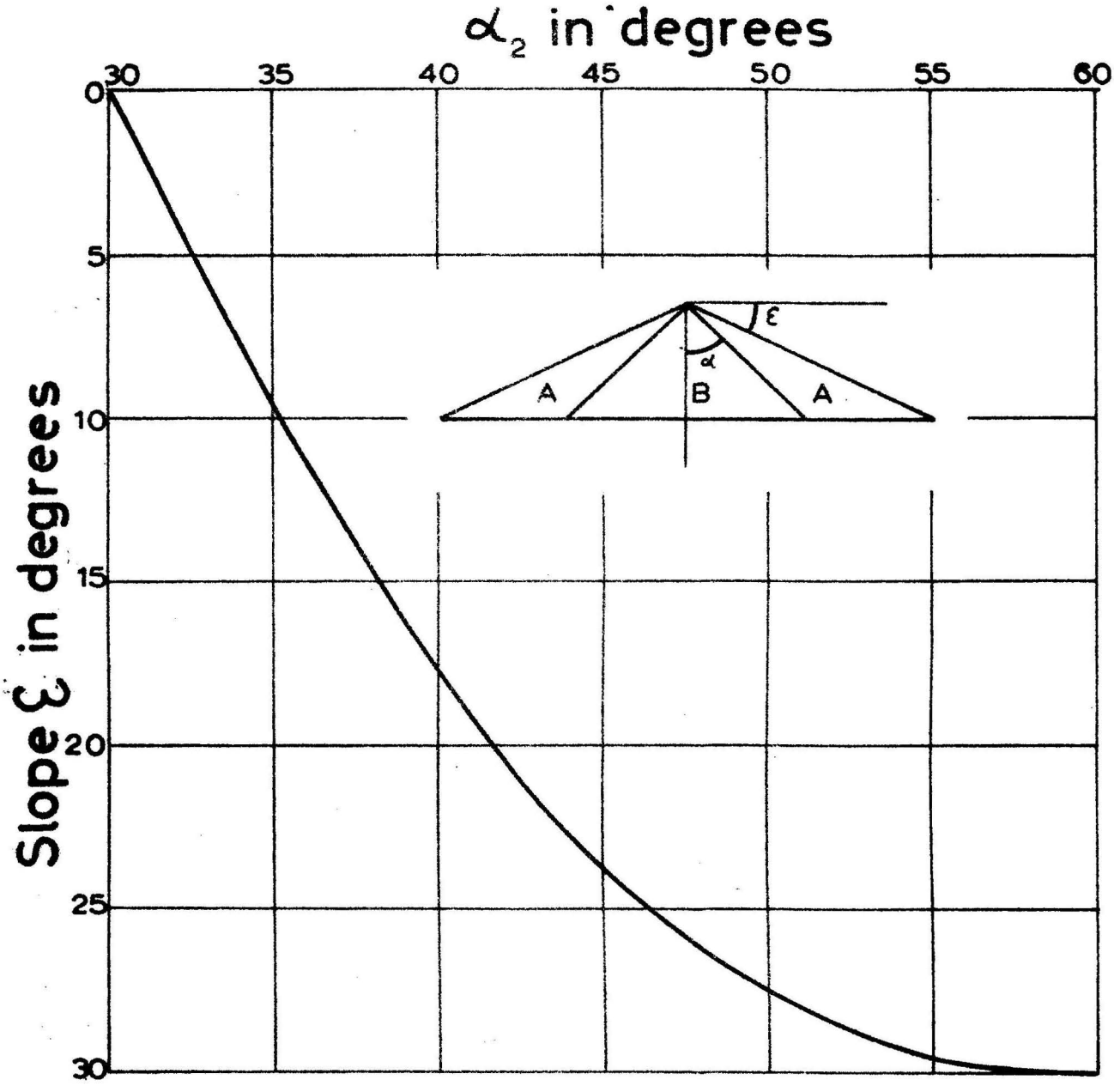

VALUE OF SLOPE vs. α_2

FIG. 5.19

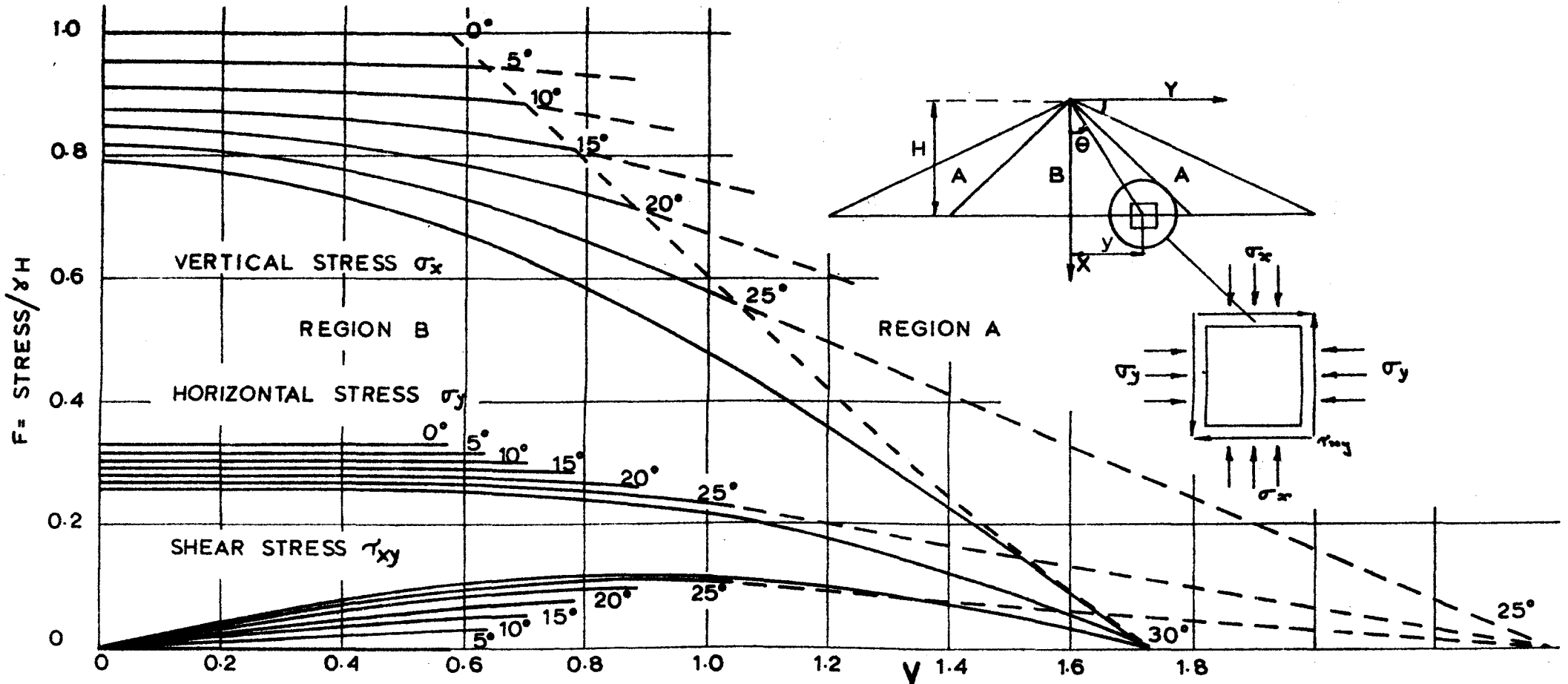

STRESSES IN REGION B FOR SYMMETRICAL WEDGES OF COHESIONLESS MATERIAL IN A STATE OF ACTIVE CRITICAL EQUILIBRIUM FOR VARYING SLOPES, $\rho = 30°$

FIG. 5.20

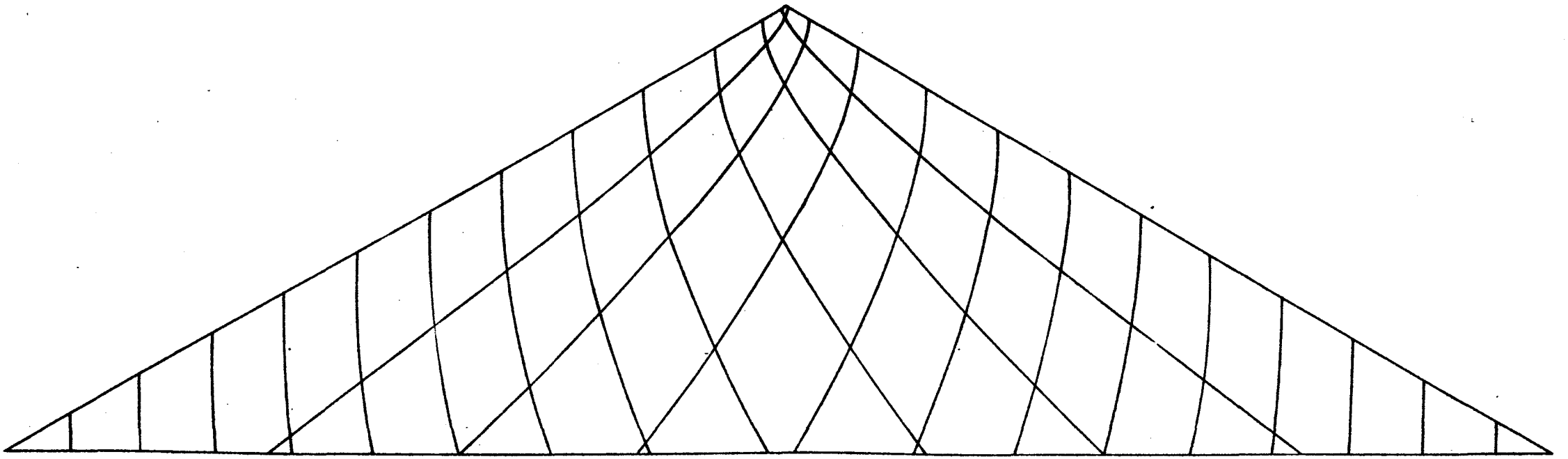

FAILURE LINES IN A 30° SYMMETRICAL WEDGE OF COHESIONLESS MATERIAL. INTERNAL ANGLE OF FRICTION = 30°

FIG. 5.21

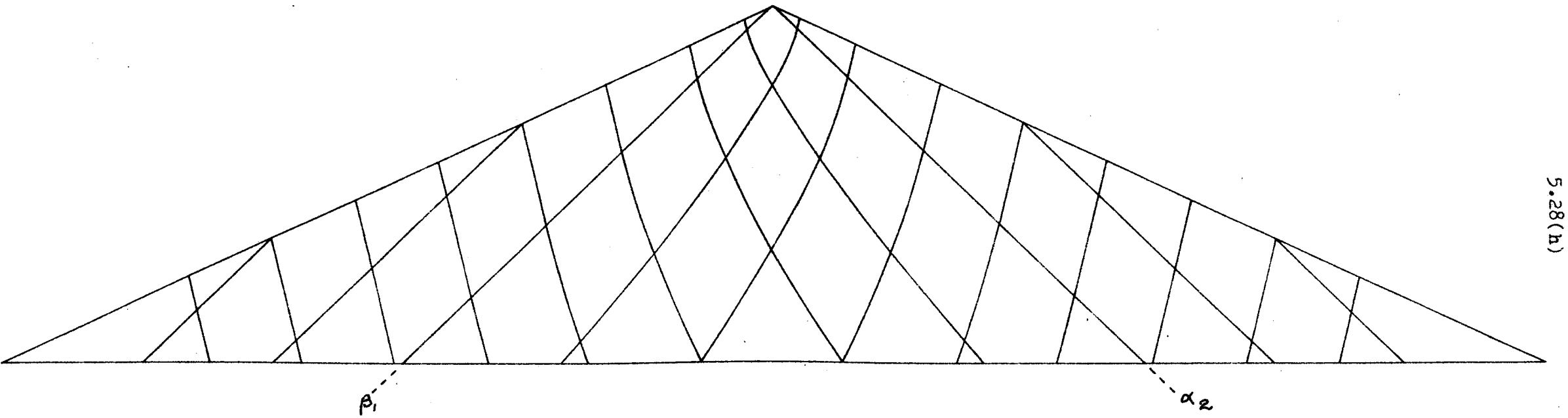

FAILURE LINES IN A 25° SYMMETRICAL WEDGE OF COHESIONLESS MATERIAL. ANGLE OF INTERNAL FRICTION = 30°

FIG 5.22

If large strains precede rupture failure the resultant plotting of the slopes will influence the location of the failure lines, this being determined by the slope at the moment of failure. This will be particularly noticeable in a wedge with slopes at the natural angle of repose. Under the rigid plastic state postulated for the wedge, the deeper legs of all failure lines penetrate beyond the apex point of the wedge. In practice, with the slight flattening of the slope, due to pre-rupture strains, it is possible that, in a toe failure, the deeper failure legs intersect the surface of the wedge before the apex of the wedge.

SECTION 6

6. SOME EXPERIMENTAL CONFIRMATION OF THE THEORY OF ACTIVE CRITICAL EQUILIBRIUM OF WEDGES

6.1 Introduction

In order to investigate the validity of the theoretical predictions of the critical active state of wedges, series of experiments in which model wedges were failed under active critical conditions were undertaken. As it was not possible to measure the stresses in the wedges during failure, emphasis was placed on investigation of the forms of the failures.

Active failure in wedges can be induced by causing the wedge to fail by sliding out on the base. This was the method employed in all experiments.

6.2 First series of experiments

This series was of an exploratory nature.

A model wedge of sand was formed on a table, part of the base extending over a sheet of paper, as shown diagramatically in Figure 6.1(a). The paper was gradually pulled outwards from the bank for a short distance. Two points of failure developed, as shown by points A and B. The zone between A and B sank and the area between B and C moved outwards as a body. Figure 6.1(b) shows a photograph of this test.

A further model was formed on a number of sheets of paper, each extending different lengths along the base, as shown diagramatically in Figure 6.2(a). These sheets were then pulled outwards consecutively, starting with the sheet ending nearest the centre of the model. A series of parallel failure ridges appeared on the surface of the

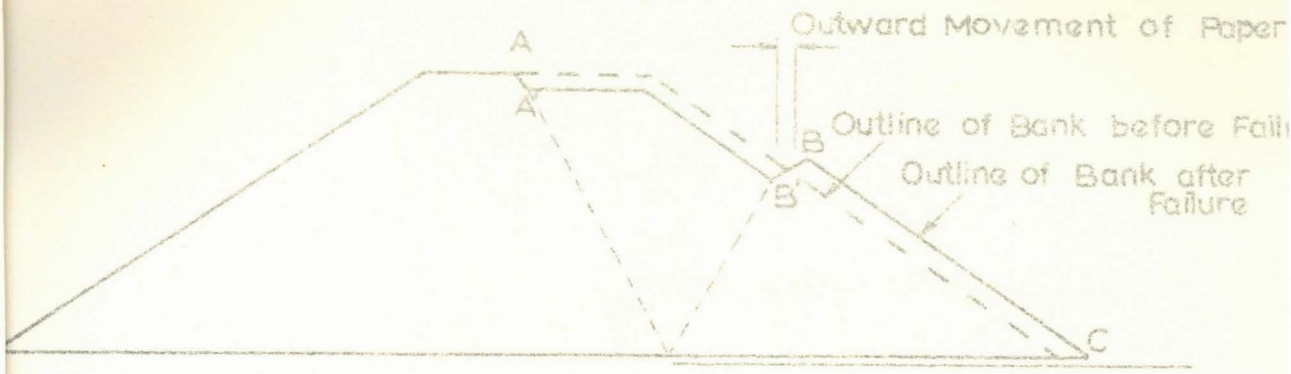

DIAGRAMATIC SKETCH OF OUTLINE OF MODEL BANK AFTER FAILURE

FIG 6.1(a)



FAILURE OF MODEL BANK

FIG 6.1(b)

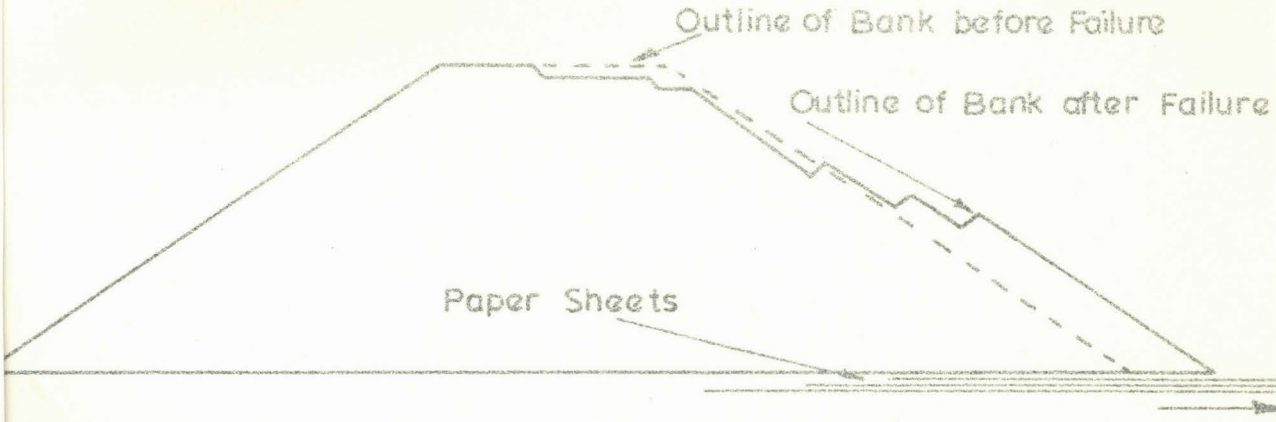

DIAGRAMATIC SKETCH OF OUTLINE OF MODEL BANK AFTER FAILURE.

FIG 6.2(a)



FAILURE OF MODEL BANK

FIG 6.2(b)

wedge, as shown diagramatically in Figure 6.2(a). A photograph of the test is shown in Figure 6.2(b).

Yet another model wedge composed of two sands of contrasting colours in layers, was formed and multiple failure induced. The model was soaked with a commercial gell and allowed to set. The failure was exposed by cutting the model at right angles to the apex ridge of the wedge. This showed the failure planes very clearly. (See Figure 6.3).

6.3 Second series

The first series of experiments was artificial in that the point on the base of the wedge at which failure develops was pre-selected. Furthermore, outside the failure zones it is not possible for the wedge material to deform. It was therefore decided to undertake a series of experiments in which the model wedges were to be constructed on very stiff tar and failure induced by reducing the shear resistance of the tar by heating. Wedges failed in this fashion would be free to deform elastically and plastically in accordance with the natural laws governing these types of strains.

Two experiments were performed, in the first a wedge with sides at the natural angle of repose was failed, without any pressure applied to the flanks. In the second, the influence on the failure pattern of water pressure against the one flank of the wedge was investigated.

6.3.1 Apparatus

Model table

A diagramatic sketch of the apparatus is shown in Figure 6.4. The table plate 1 on which the model wedge

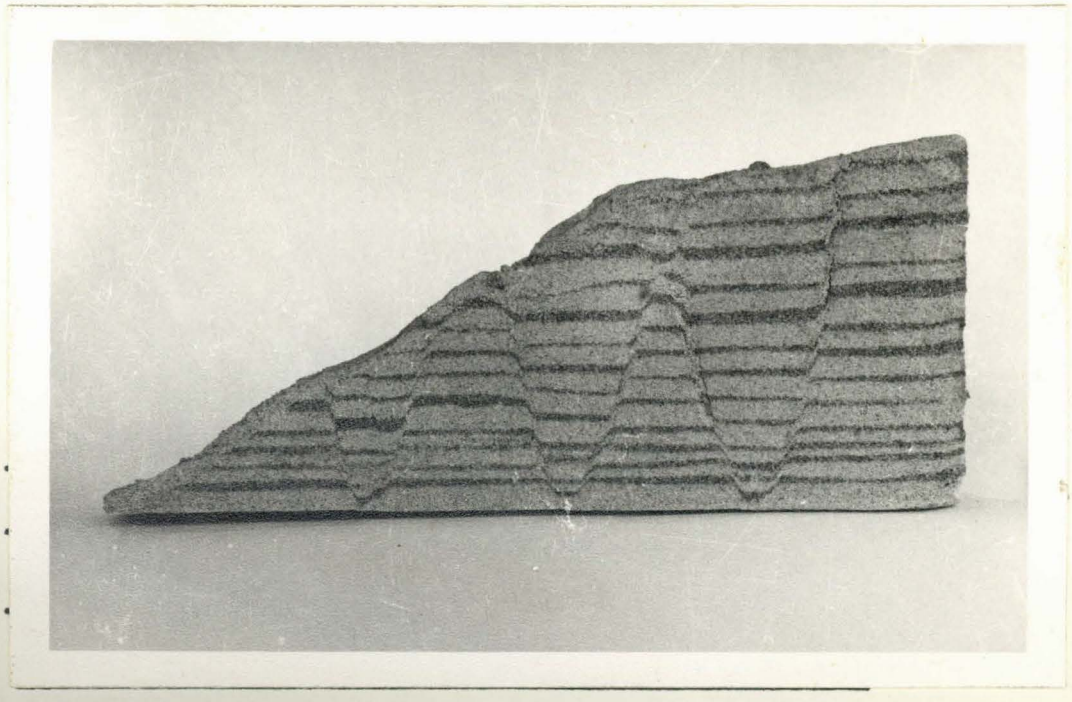

Figure 6.3 Failure lines in model wedge.

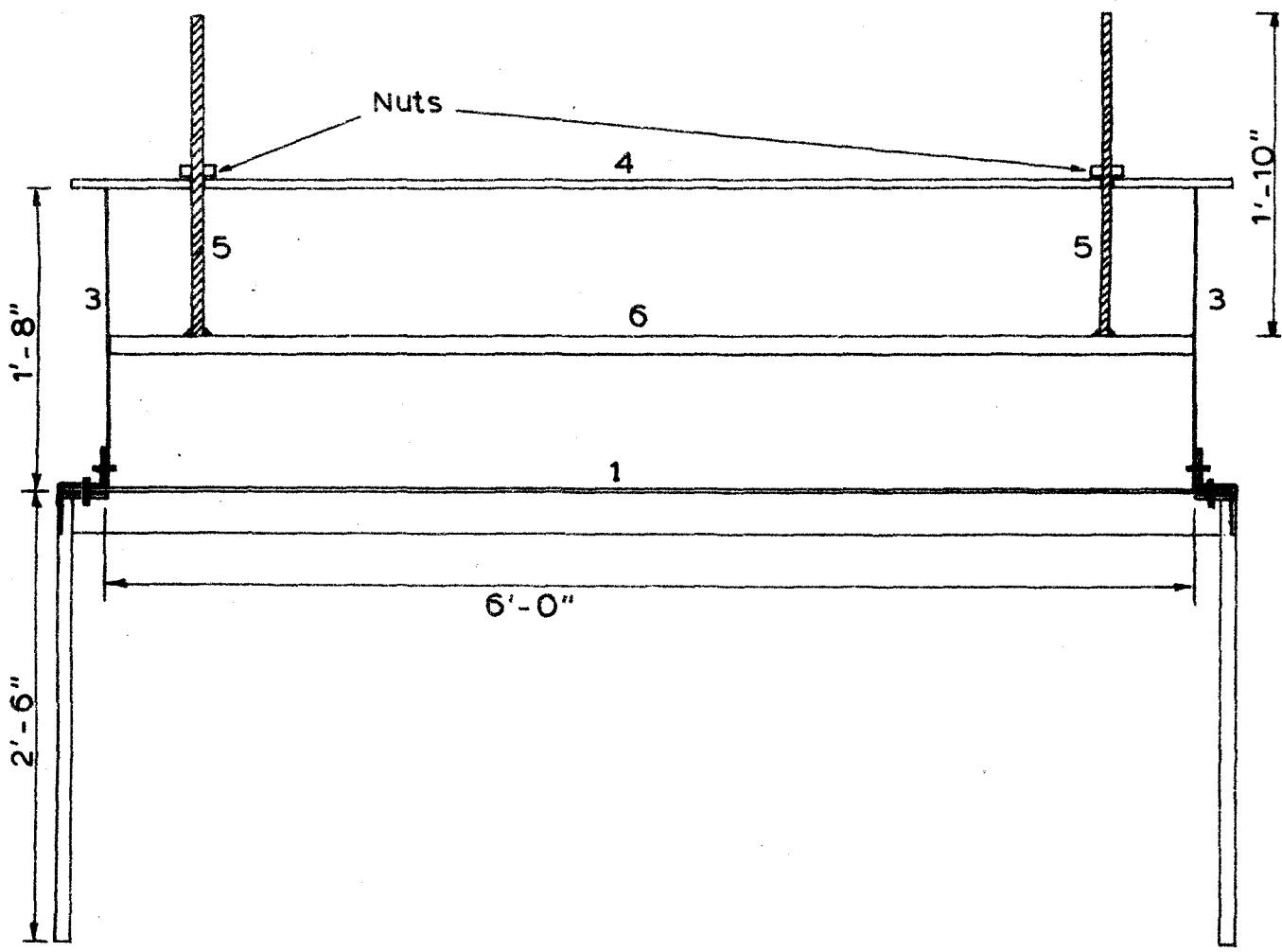

DIAGRAMATIC SKETCH OF MODEL TABLE

FIG 6.4

was to be formed was a single sheet of steel plate ¼" thick, measuring 15' x 6'. The plate was supported level on a frame 2'6" above the ground. The slide plates 3, each 20" high, were bolted along the edges on the longer sides of the table plate, the top of the side plates being filed straight and smooth, and set parallel to the table plate. The forming blade, by means of which the wedge was to be constructed, consisted of a bar 4 which rested on the side plates and through which passed two bolts 5, each 22" long, screwed over the whole length and welded to a straight edge 6. The straight edge could be set by adjusting the two nuts supporting the straight edge on the bar.

Sand

Two sands of contrasting colours were used. The one sand was derived from the tailings and was of a grey-blue colour, the other was river sand of a yellowship-white colour. Each sand was well washed and dried in an oven at low heat - at 100°F, (to ensure that the tailings sand did not shatter on drying) and then sieved to isolate + 100 - 14 Tyler fraction.

Tar

The tar which simulated the clay layer under the wedge was of the kind used in cable junctions, being very stiff at room temperature.

6.3.2 Forming of the model wedge

The tar was melted by means of a blow torch and spread evenly to 1/16" over the table plate. A very thin layer of fine sand was sieved over the tar in order to prevent, on heating, the penetration of the tar in the model's sand. The outline of the model wedge was drawn on the side plates, together with a number of vertical

lines. (Figure 6.5(a). The limits of the base of the wedge were marked on the tar covering the table plate. These lines were to serve as guides in forming the wedge. (Figure 6.5(a).

The forming blade was set level at a distance of about 1½" above the table plate. One of the sands was poured onto the table plate in the base area marked out and levelled by means of the forming blade. (Figures 6.5(b) and 6.5(c)). The edges of each layer were formed by setting the blade parallel to the longitudinal section of the wedge and gently pushing the sand under the blade until the flank was correctly formed at its angle of repose (Figures 6.5(d) and 6.5(e)). The level of the forming blade was then set higher and a different colour sand poured. It was found that the slopes of the wedge could be formed so accurately, that the guide lines on the side plate were unnecessary. The process of forming the wedge was repeated layer upon layer until the wedge was completed to a height of about 19". (Figure 6.5(f)). Fine white sand was then gently sieved over the wedge. This was done for the purpose of distinguishing the failed areas from the unfailed. (Figure 6.5(g)).

6.3.3 Failure of the wedge

The failure of the wedge was achieved as follows:- Hessian sacking was threaded with steel wire, dipped in paraffin and arranged evenly over the floor beneath the table plate, and fired. As soon as the tar had softened sufficiently for the wedge to show signs of failing, the burning hessian was withdrawn from under the table by means of the steel wire and the underside of the table plate hosed with cold water. This effectively stopped the failure



Figure 6.5(a) Model table with tar spread over base and base and side lines chalked.

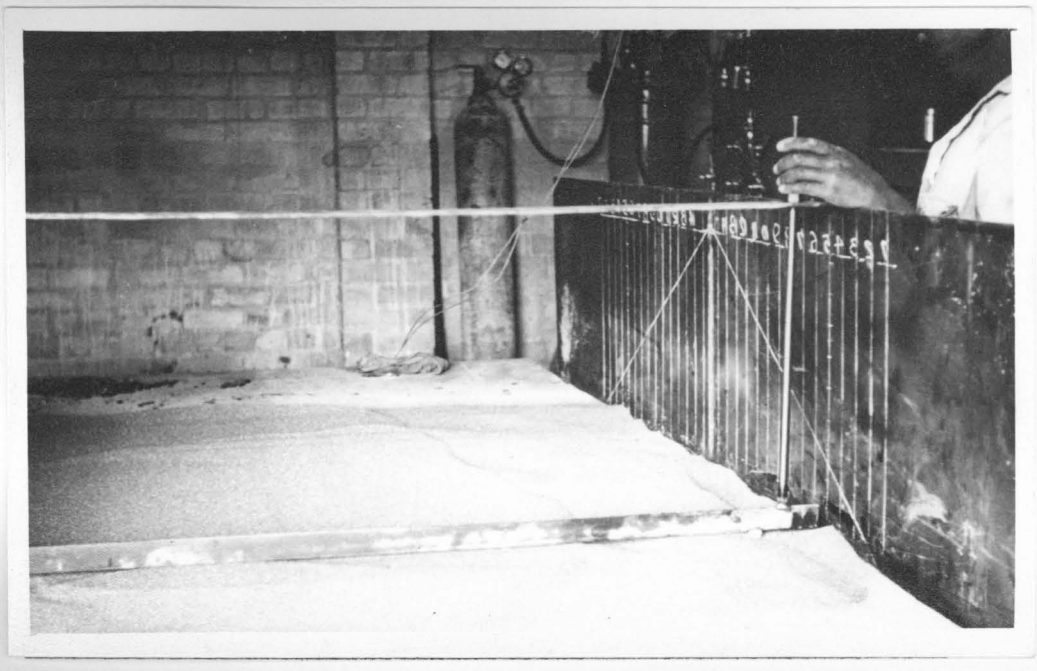

Figure 6.5(b) Sand poured on to base and levelled by means of forming blade.

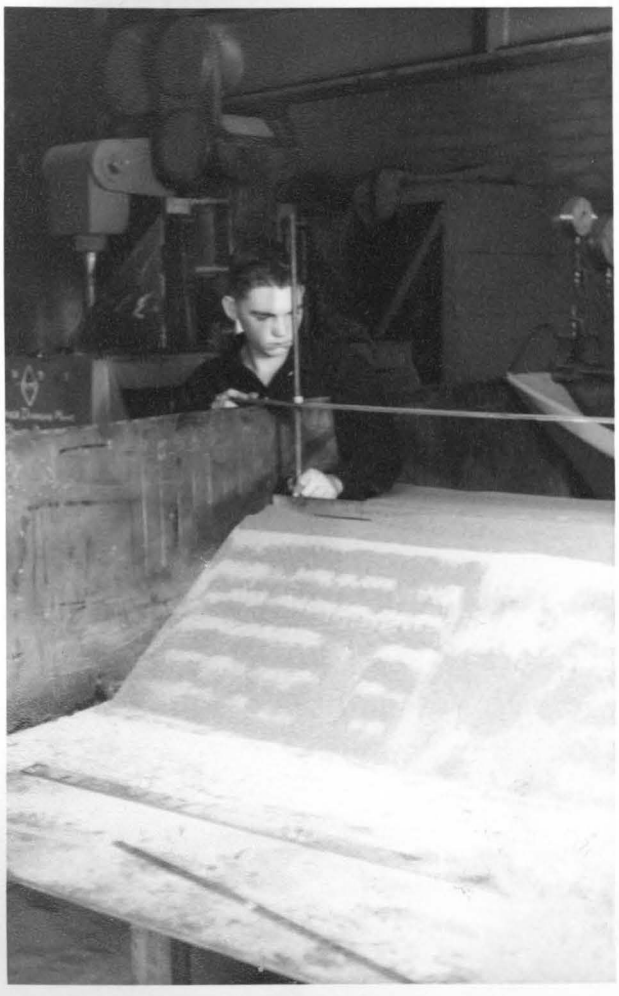

Figure 6.5(c) Photograph shows a layer of sand, by which the model is progressively built up, being levelled.

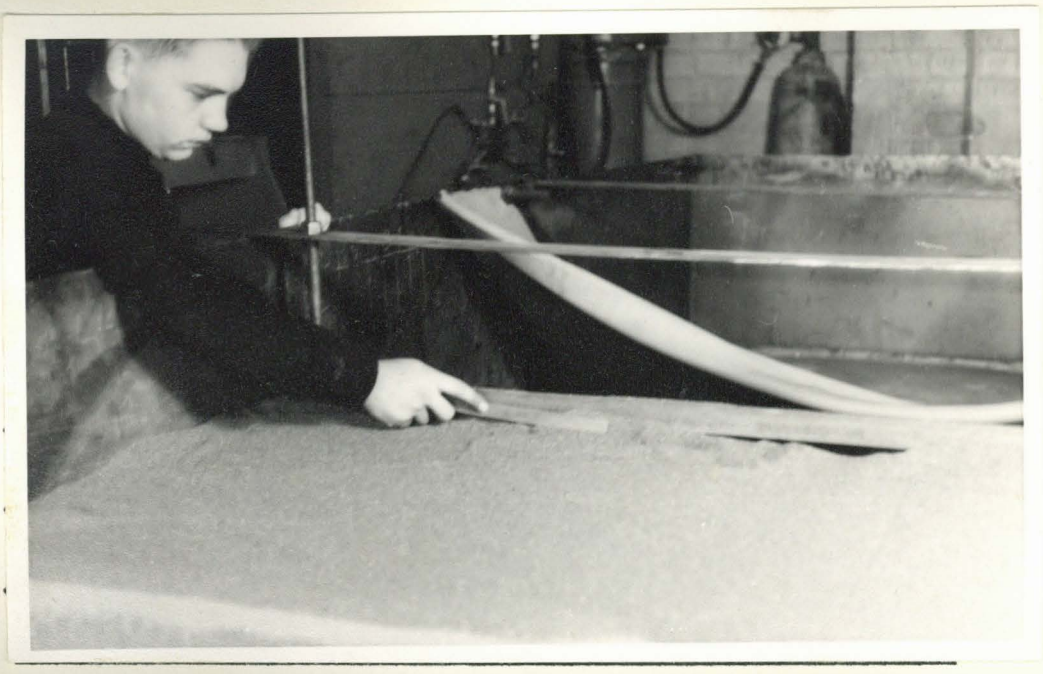

Figure 6.5(d)



Figure 6.5(e) Photograph shows method employed to form the edges of the layer to the angle of repose. The blade is set at the edge and sand carefully pushed below the blade till the angle is correctly formed.



Figure 6.5(f) Wedge completely formed.

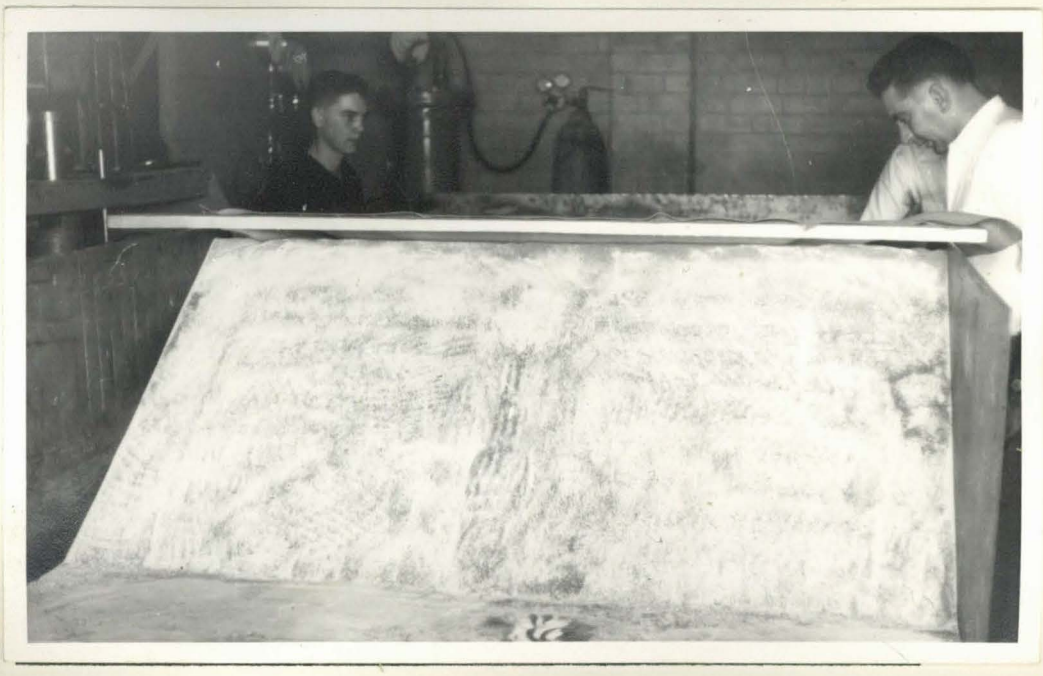

Figure 6.5(g) Side of wedge sifted with fine white sand.

movement. The progress of the failure was recorded photographically and is shown in Figures 6.6(a), 6.6(b) and 6.6(c).

To preserve and distinguish the numerous ridges of failure, a fine white sand was carefully sieved about ½" thick over the whole model, and on top of this, sand was packed to a depth of 4". A commercial gell was pumped into the model. (See Figure 6.6(d)). The model was left for 24 hours to allow the gell to set.

To expose the failure cross section, the side plates were removed and slices parallel to the side plates at 1 - 2" spacings made across the face. The following photographs of the significant cross sections are shown:

(i) The failed cross section at the side plates (Figure 6.7(a)).

(ii) Near the side of the failure (Figures 6.7(b) and 6.7(c)).

(iii) Near the centre of the failure (Figures 6.7(d) and 6.7(e)).

(iv) At the centre (Figure 6.7(f)).

The deformations in the tar due to the failure are shown in Figure 6.7(g).

In the second experiment after the wedge was formed (Figure 6.8) water pressure was applied to one side of the wedge (Figure 6.9). The wedge was then failed by heating the tar base. The time sequence of the failure is shown in Figures 6.10(a), 6.10(b) and 6.10(c). Cross sections of the wedge after failure are shown at the following positions:

(i) At the side plate (Figure 6.11(a)).



Figure 6.6(a)

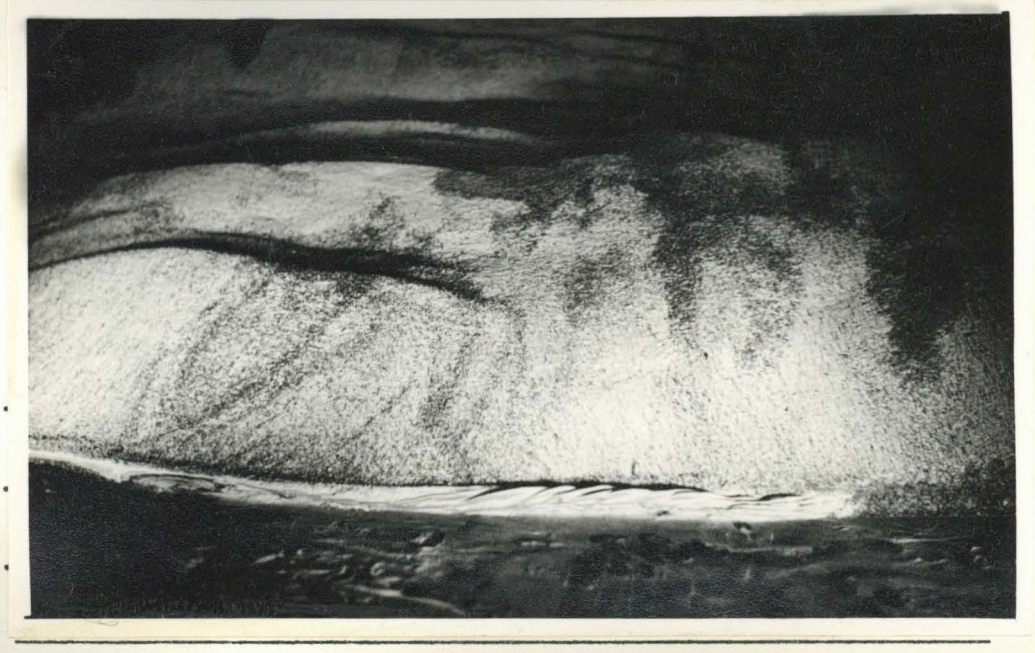

Figure 6.6(b) Time sequence of failure of model wedge. Note in the upper photograph the first failure ridge and a few minutes later the formation of the second failure ridge in the lower photograph.



Figure 6.6(c) Final external form of failure of model wedge. There is little external appearance of regularity in the failure.

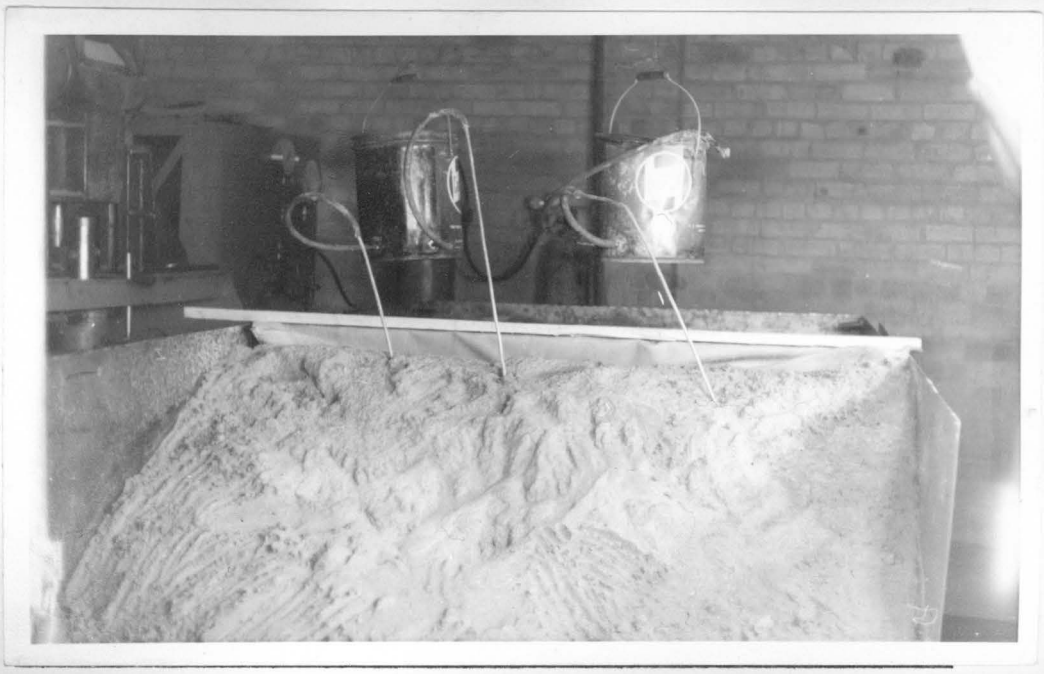

Figure 6.6(d) Failed wedge is covered with a layer of fine and rough sand, and gell pumped into the model. The layer of fine sands contains the gell inside the model.

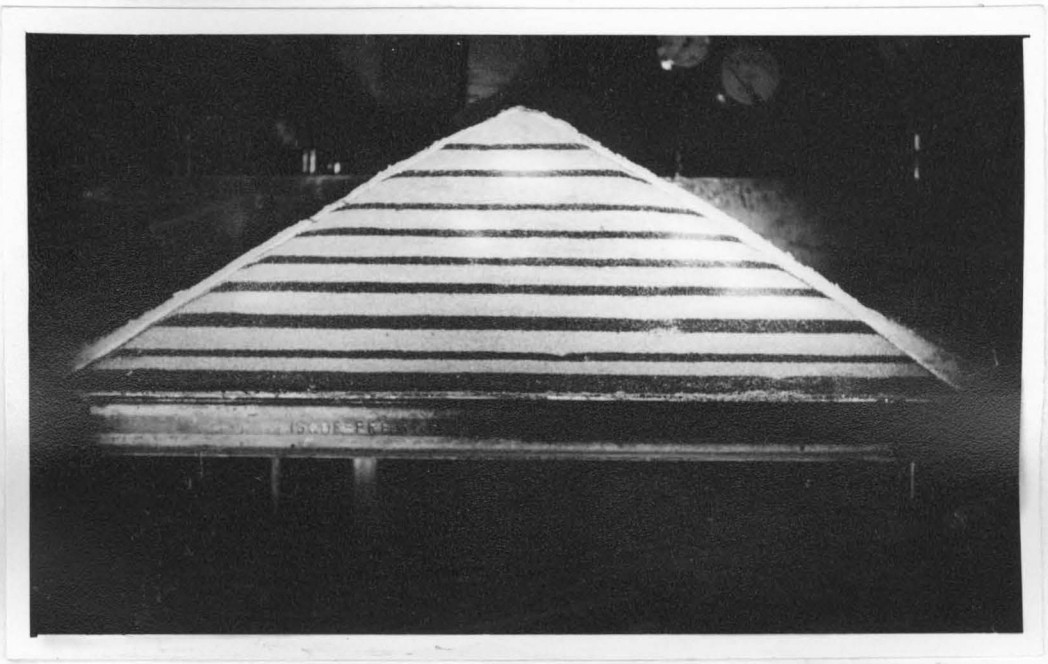

Figure 6.7(a) Cross section of model at the side plates. Deformation has taken place but no failure. Note the slight flattening of the upper sections of the flanks relative to the lower sections.

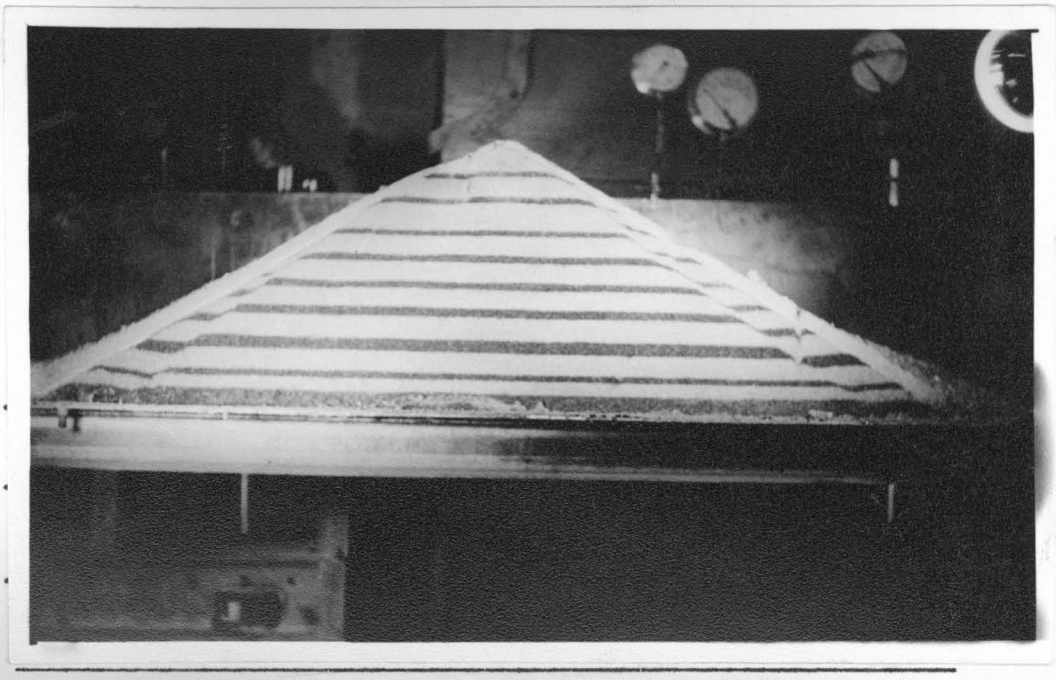

Figure 6.7(b)

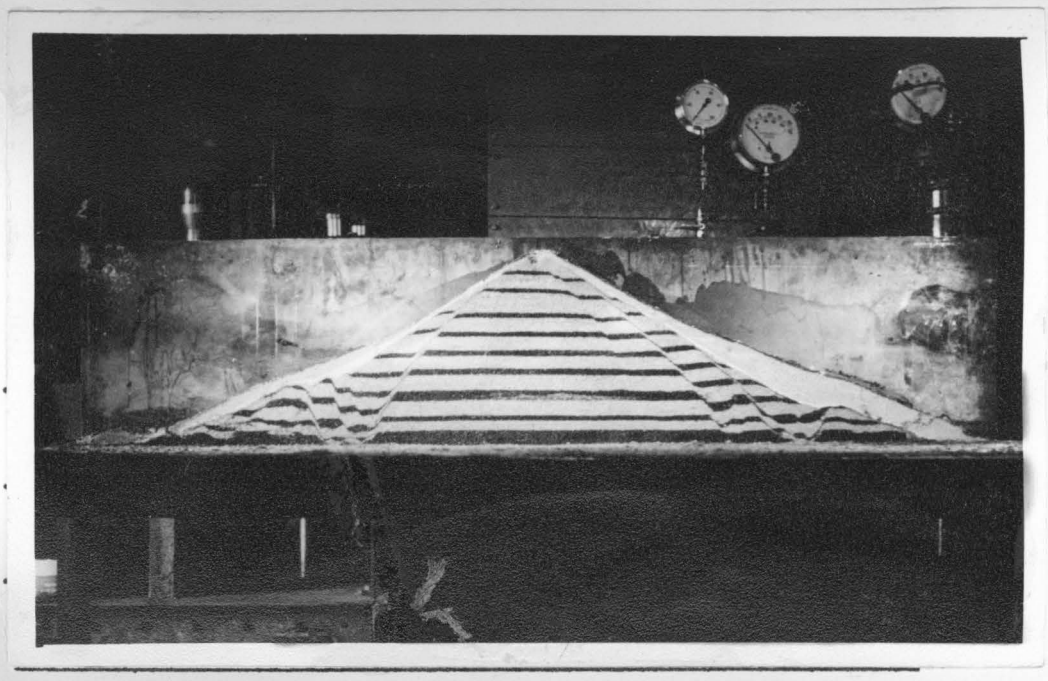

Figure 6.7(c) Cross section near sides of failure. Note that the bottom apex of the failure is near the flanks and that the inner leg of the failure is nearly parallel to the flanks. Note also in the lower photograph a failure line developing, but not yet completed.

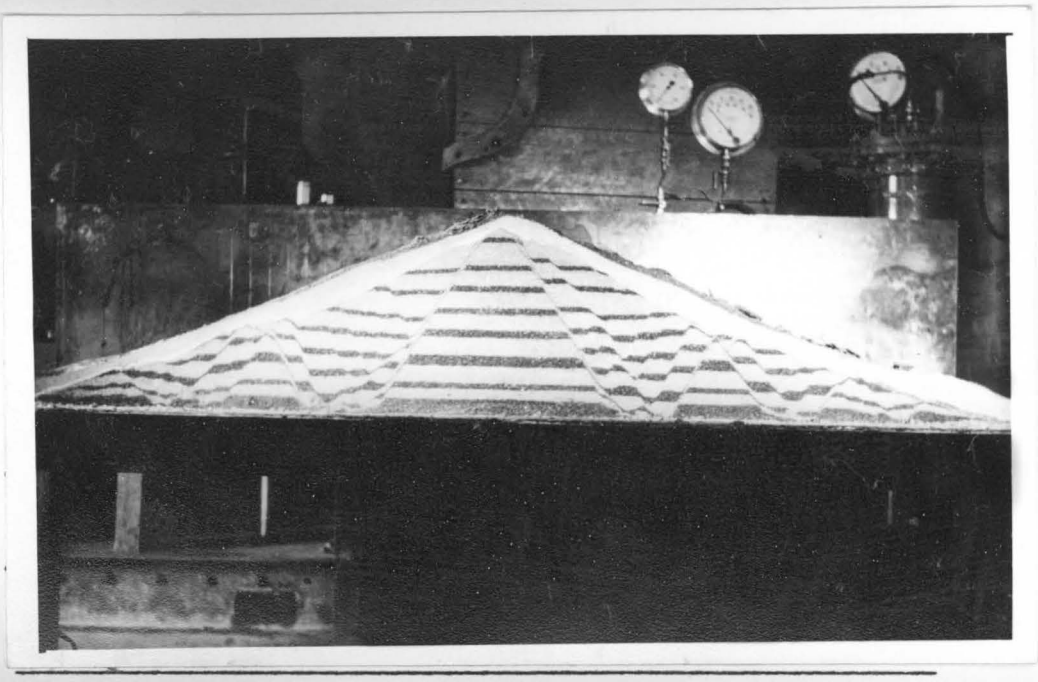

Figure 6.7(d)

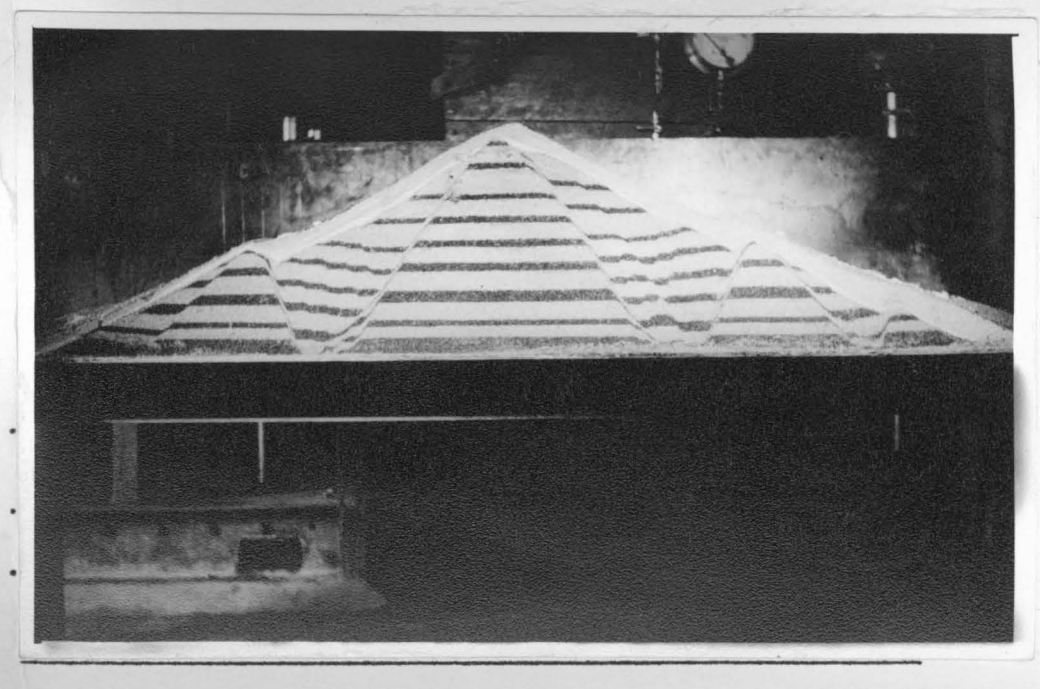

Figure 6.7(e) Cross section near the centre of the failure zone. Note the inner leg of the failure is a much steeper slope than the flanks of the wedge. Also, failure lines internal to the main failure lines have developed.

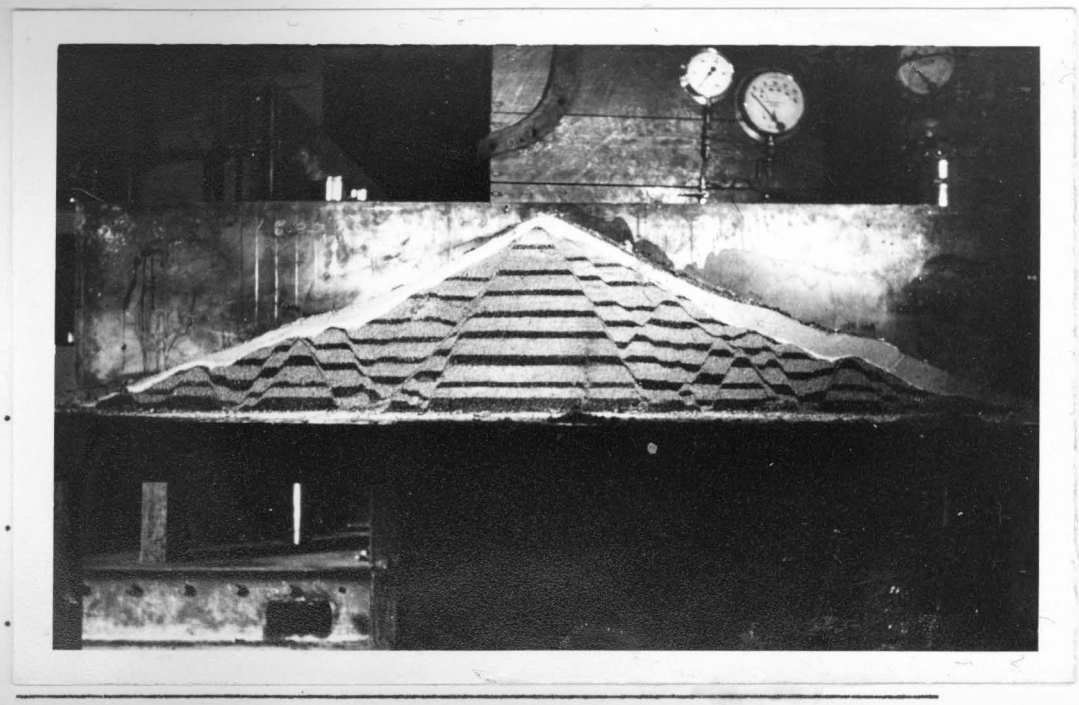

Figure 6.7(f) Cross section at centre of failure. Failure is extensive with a sequence of 3 main failures recognisable. Note the unfailed wedges.

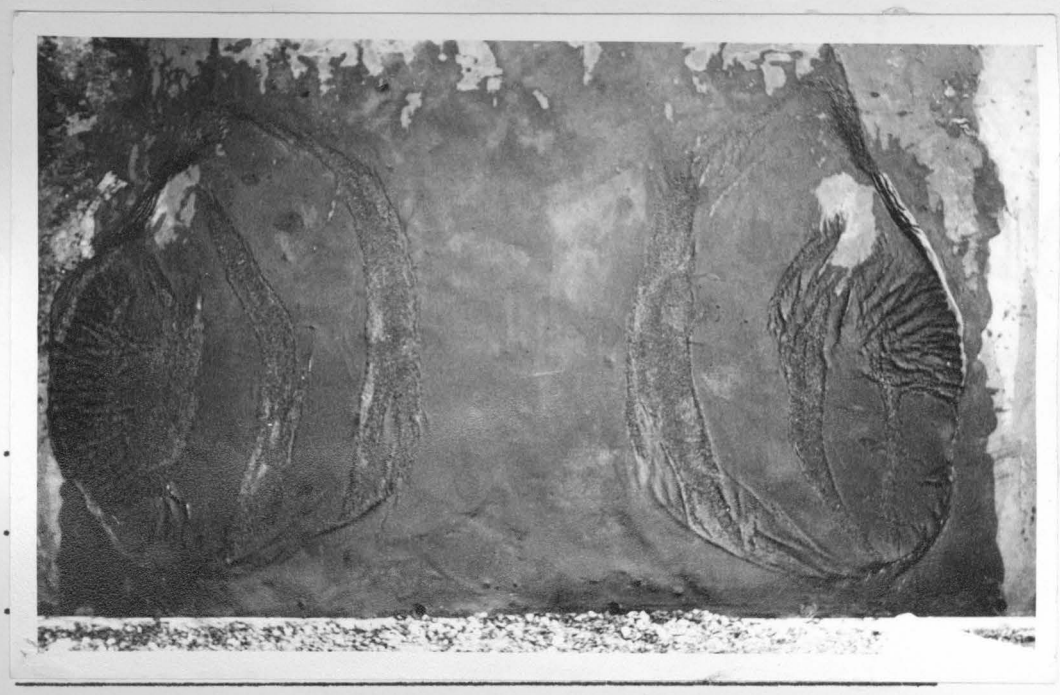

Figure 6.7(g) Tar deformation due to failure of model wedge. Note the transverse failures at the toe region of the failure.

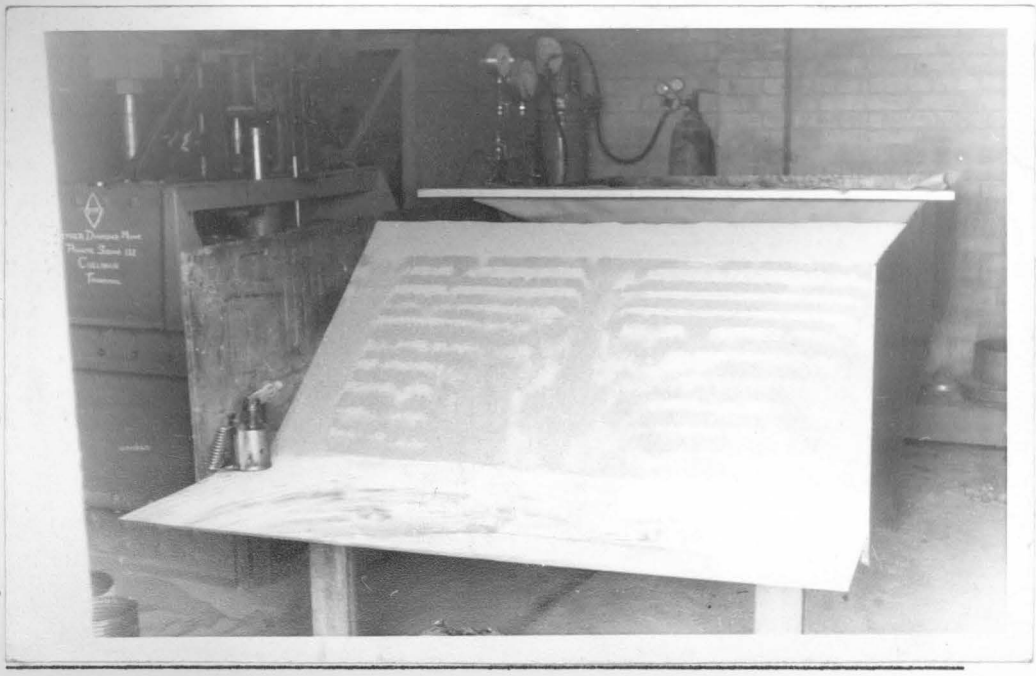

Figure 6.8 Completed wedge with thin rubber membrane of tank in background.



Figure 6.9 Tank being filled to supply water pressure against wedge.



Figure 6.10(a) Stress free slope of model wedge lightly covered with fine white sand. Photograph taken obliquely above slope.



Figure 6.10(b) Main failure developing in model wedge.



Figure 6.10(c) Secondary failure developing in unfailed wedge pushed out before main failure.

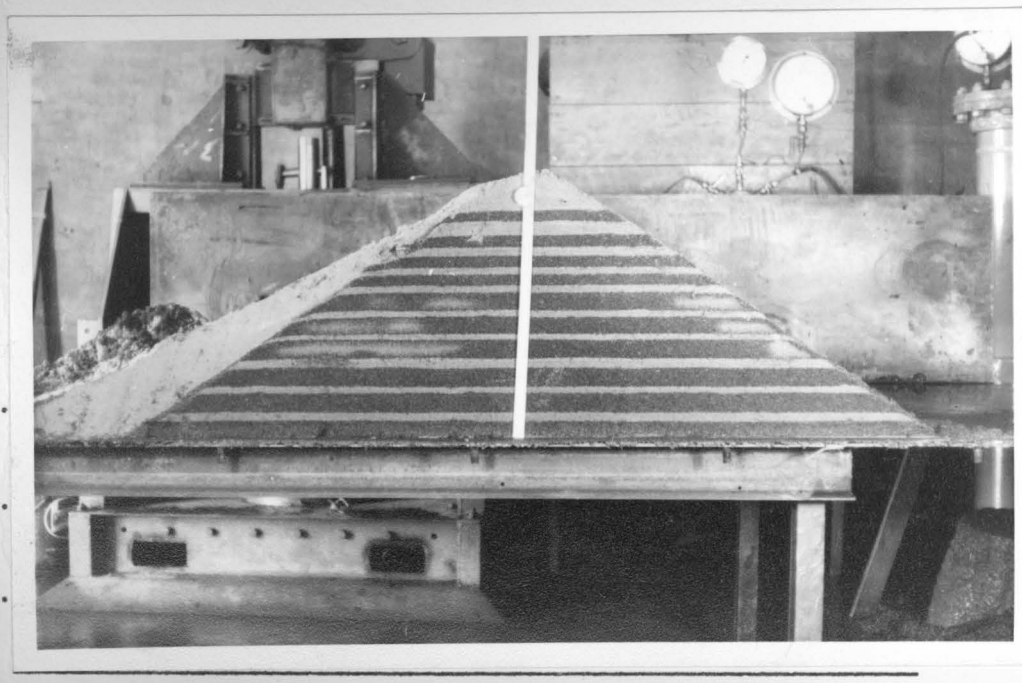

Figure 6.11(a) Cross section of wedge at side plates of the failure.

(ii) At the side of the failure (Figure 6.11(b)).

(iii) At the centre of the failure (Figure 6.11(c)).

The deformations of the tar base are shown in Figure 6.12.

6.4 Discussion

6.4.1 Location of main failure

It has been shown in Section 3 that the failure of a soil mass is governed by two partial differential equations of the hyperbolic type. The form of the active failure zone is in consequence governed by the boundary stresses at the top of the surface of the wedge and the contour of the wedge, and the extent of the failure zone is governed by the domain of dependence of the bottom apex point of the failure. The boundary conditions outside the domain of dependence does not affect the failure zone. Hence it is immaterial whether these regions are in an elastic or plastic state. By inducing sliding at the base of the wedge the bottom apex of the failure will be centred at the base (which also is the point giving the domain of dependence). This point, then, governs the extent of the failure at the surface. Referring to the photographs in Figures 6.7(d) and 6.11(c) it is clear that the apex of the failure is at the base, and that the form of the failure conforms approximately to that predicted theoretically. (Compare Figure 6.7(c) with Figure 5.21).

Theoretically, the position of the failure in a wedge on a base of tar can be predicted as follows:
Referring to Figure 6.13 the shear stresses along the base of a wedge with 30° slopes were accumulated from the toe to the centre of the wedge to give the total disturbing

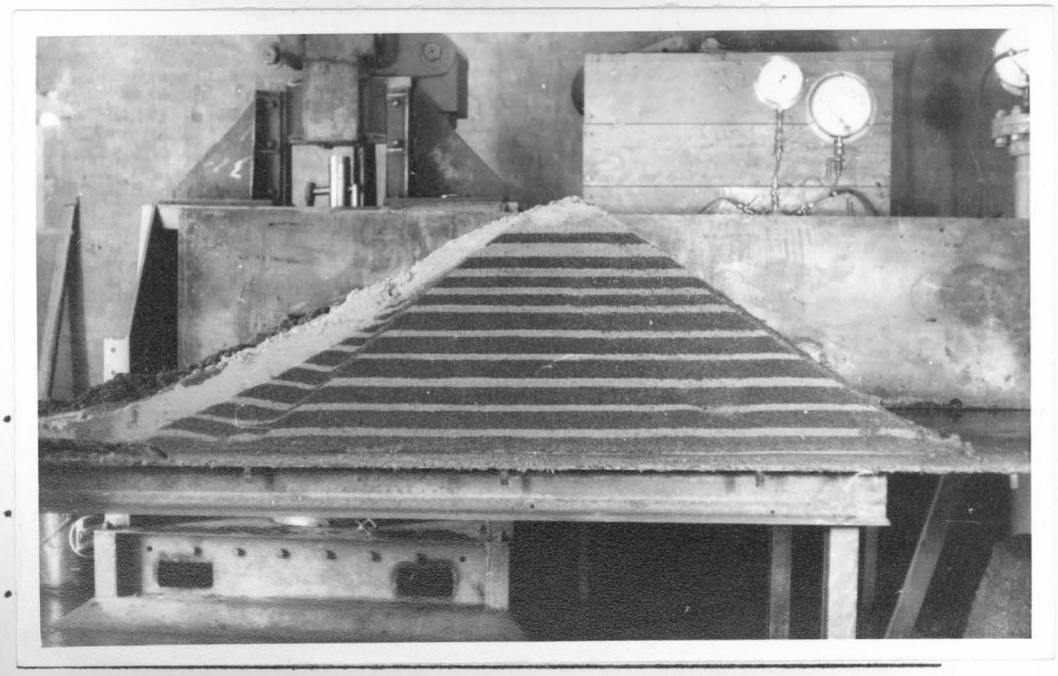

Figure 6.11(b) Cross section of wedge after failure near side of failure zone.



Figure 6.11(c) Cross section of wedge at centre of failure zone. Note primary and secondary failure wedges.



Figure 6.12 Deformation of the tar on base plate due to failure. Note beginnings of a transverse failure in the tertiary failure zone.

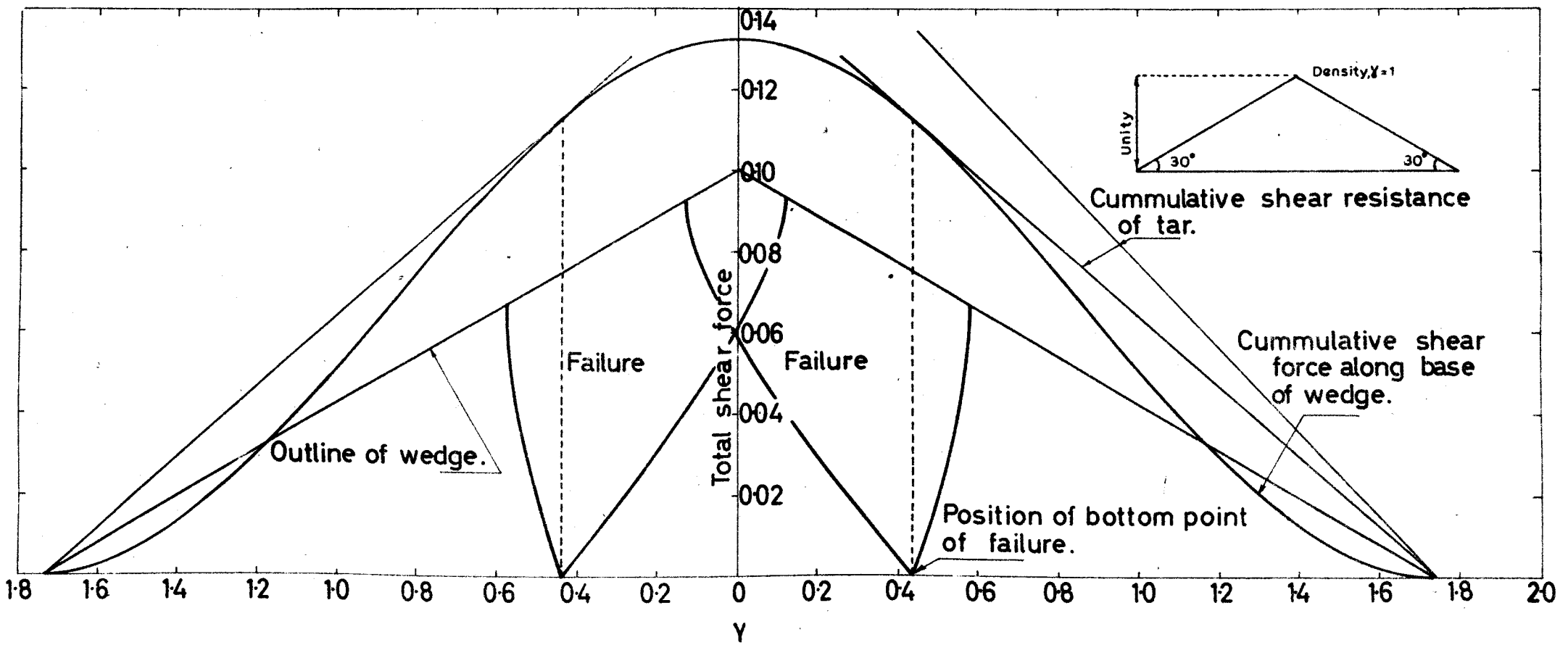

THEORETICAL EXPECTATION OF FAILURE IN A SYMMETRICAL WEDGE OF 30° SLOPES ON A BASE LAYER OF TAR. $\varrho = 30°$. FIG.

FIG 6.13

6.6(a)

shear force (or horizontal thrust) at any point along the base of the wedge. The shear resistance of the tar layer on which the base of the wedge rests is a function of the temperature and if this temperature is uniform the shear resistance per unit length will be constant along the base. The cumulative shear resistance from the toe to the centre line of the wedge will be a straight line, having its maximum value at the centre line of the wedge. As the temperature of the tar increases the shear resistance per unit area decreases, causing a decrease in the slope of the total resistance line. When this slope is reduced sufficiently so that the total shear resistance line touches the disturbing shear force curve, the point of tangency would indicate the position of the failure at the base of the wedge. In Figure 6.13 this point of tangency and the associated theoretical failure zones are shown.

6.4.2 Time sequence of the failure

In Figures 6.6(a) and 6.6(b), and 6.10(b) and 6.10(c), the movement of the failure with time is shown. The first, or main, failure occurred, pushing a wedge of material still in a state of elastic equilibrium ahead of it. The main failure is located approximately as discussed in Section 6.4.1. After this failure had occurred, with additional heating, the shear resistance of the tar decreased further and allowed a secondary failure to develop in the elastic wedge pushed ahead of the main failure. In a similar manner a tertiary failure developed. If the tar temperature had been slowly raised sufficient for the main failure to occur, and thereafter kept constant,

the secondary failures could not have developed.

After the failures had penetrated beyond the confining influence of the unfailed section of the wedge, transverse secondary failures developed near the toe of the failure zone. These are not externally apparent but are indicated by the ridges formed in the tar base. (Figures 6.7(g) and 6.12).

6.4.3 Strains preceding failure

The slopes of the wedges immediately after they were formed gave values ranging from 34° to 34.7°, a mean of 34.3°. It is of interest to note that this mean slope is virtually identical to that measured on the embankment of tailings at Cullinan, i.e., 34.5°.

Failures of the wedges occurred midway between the side plates (see Figures 6.10(b) and 6.7(g)), the confining influence of the side plates apparently having a stabilising effect on the slopes there. At the side plates after the failure had taken place the apex of the wedge dropped approximately ½ inch from the original height of 19 inches and the base width of the wedge increased by about 1½ inches. The outlines of the wedge at the side plates before and after failure are shown in Figure 6.14. It is apparent that the slopes near the apex of the wedge flatten to approximately 30° and near the toe to approximately 33°. These changes in shape indicate that considerable strains have taken place before rupture failure commenced, and consequently stress redistribution had taken place within the wedge.

The flattening of the slopes of the wedge at the time of failure would theoretically influence the form of the

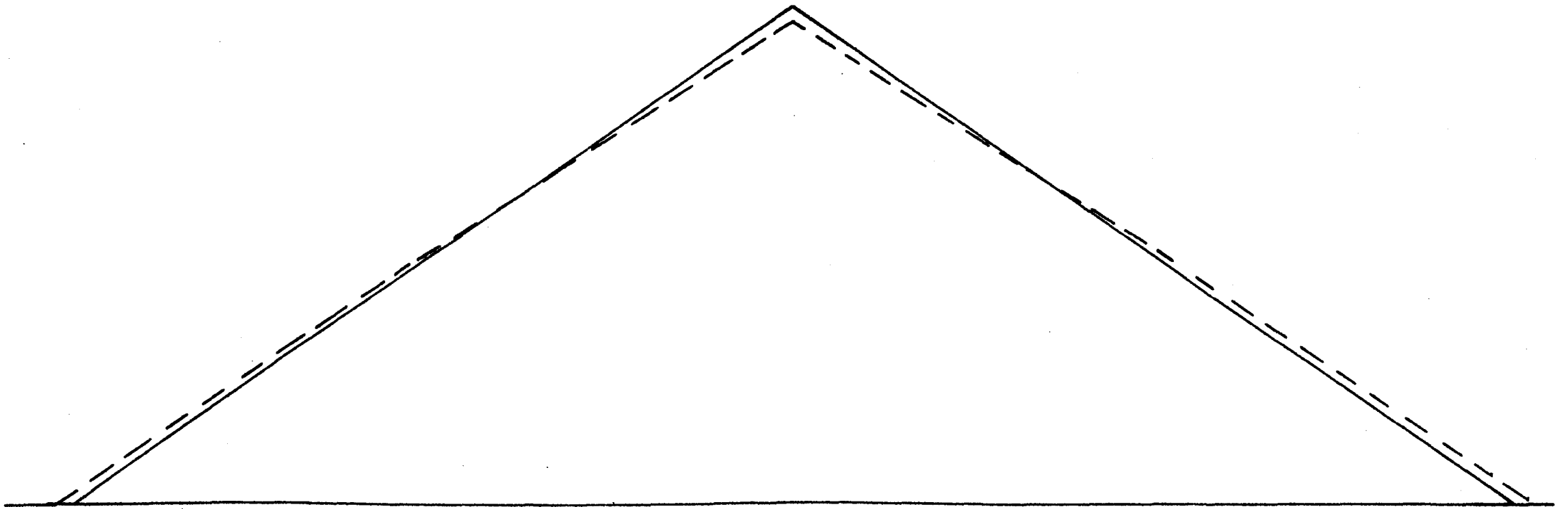

OUTLINE OF WEDGE AT SIDE PLATE AFTER FAILURE MOVEMENT
FIG 6.14

failure lines that develop; it was mentionned previously that if the slope of the wedge is near the natural angle of repose, slight changes in the slope have large effects on the α_2 and β_1 characteristic lines, and it is possible that where the failures are centred on the base, near the toe of the wedge the failure apex may be located in the region A (Section 5. 7) and both legs of the failure intersect one side of the wedge.

A study of Figures 6.7(g) and 6.12 shows that the bottom apeces of the failure were located approximately on the arc of a circle. However, this does not mean that the failure was not plane, for a study of the striations in the tar in the zone of failure (not apparent in the photographs) indicates that the movement was parallel and normal to the apex ridge of the wedge. Thus, although the form of the failure is approximately circular, the failure took place under conditions of plane strain.

Referring to Figures 6.7(b) and 6.7(c), which show cross sections of the failure with the apeces near the toe of the wedge, it can be noted that the deeper legs of the failure are almost parallel to the slope of the wedge. This conforms to theoretical prediction (Section 5.7 and Figure 5.21). As the bottom apeces of the failure penetrate into the body of the wedge, the deeper legs lie at steeper angles (Figures 6.7(d), 6.7(e) and 6.7(f)), again as predicted by the theory.

In the central region of the failure, the movement was extensive, and numerous failure lines developed. The intersecting angles of these failure lines give a mean value of approximately 58°, which conforms to the value

predicted for an angle of internal friction of 34°. In order to show the failure pattern more clearly, enlarged traces of the failures in Figures 6.7(b), 6.7(e) and 6.7(f) are shown in Figures 6.15, 6.16 and 6.17.

A direct comparison of the theoretical and experimental failure forms is not possible, as the theoretical solutions assumed an angle of internal friction of 30°, whereas experimentally this angle appears to be 34° approximately. Furthermore, even if a theoretical solution for $\varphi = 34^{\circ}$ was available, the form of the main failure would be given approximately by the solution for 30° slopes, due to the flattening of the slopes before failure.

6.4.3 The influence of water pressure on the failure

It is clear from Figure 6.11(e) that the water pressure on a flank of a dam has a stabilising influence on that flank. The stress-free flank is insignificantly affected by the water pressure, the influence of the water pressure being only of significance for the failure zone between the apex of the wedge and the point of intersection of the deeper leg of the failure and upstream flank.

6.5 Conclusion

If the change in shape of the wedge due to pre-failure stress is taken into account, the experimental failures are in good agreement with the theoretical failures.

Change in shape due to pre-failure stress cannot be predicted theoretically, as the theory assumes a rigid plastic behaviour of the soil. If rigid plastic behaviour is to be approximated it seems that the method by which failure was induced in the first series of experiments should be employed, for here no significant elastic strains in the unfailed region due to movement of the base underneath are possible. For an exact solution of the failure of the wedge,

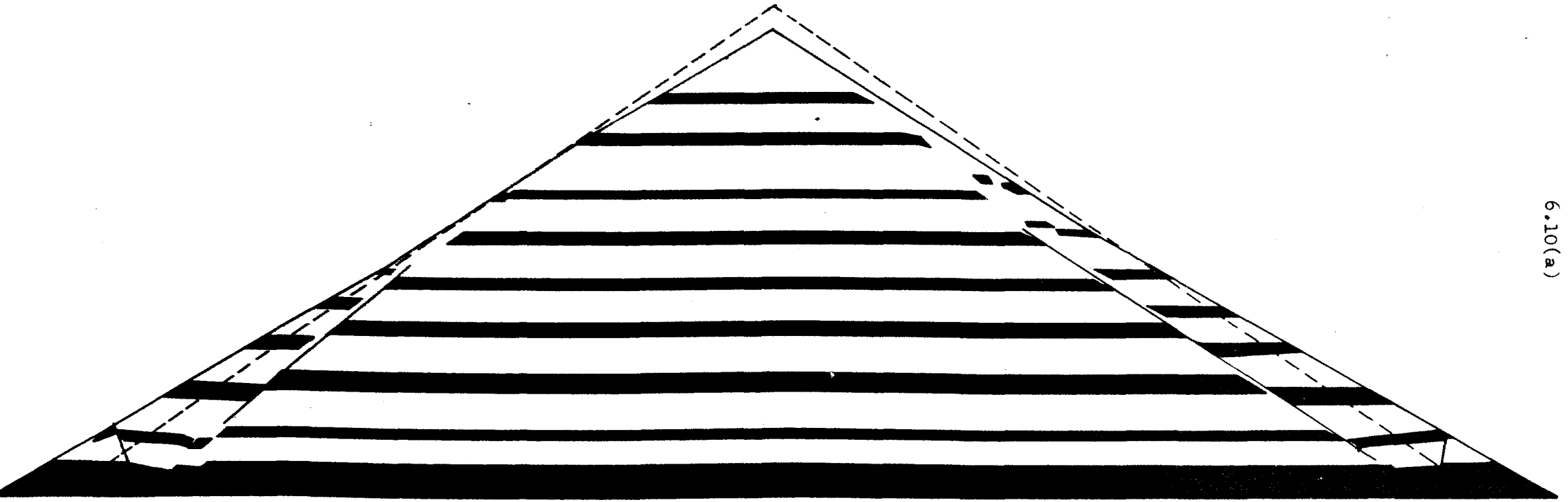

CROSSECTION AT SIDE OF FAILURE OF MODEL WEDGE

FIG 6.15

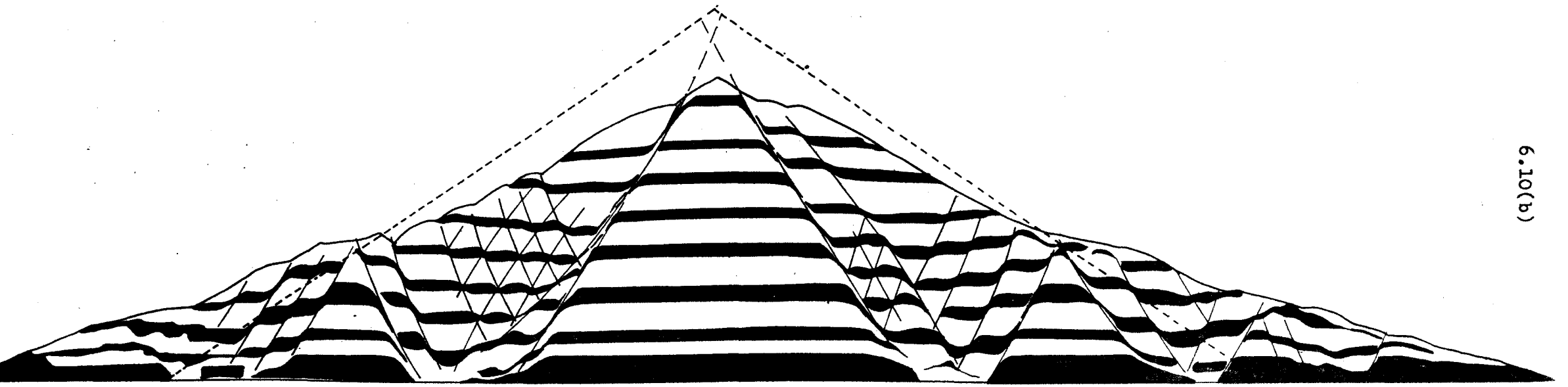

CROSSECTION NEAR CENTRE OF FAILURE OF MODEL WEDGE

FIG 6.16

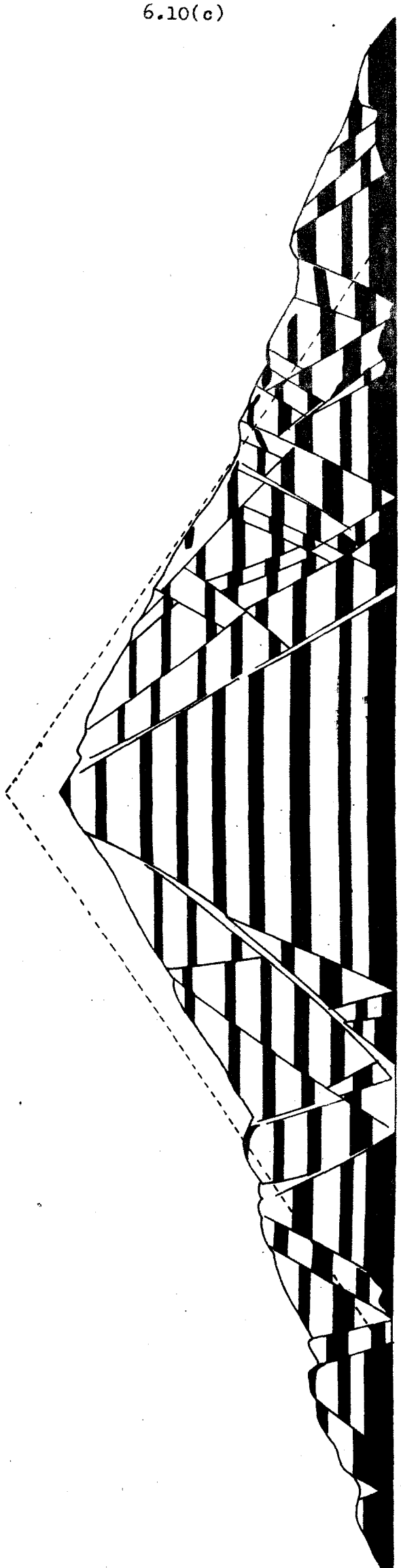

CROSSECTION AT CENTRE OF FAILURE OF MODEL WEDGE

FIG 6.17

taking pre-failure strains into account, the analysis will have to be performed on the shape just prior to failure. Such an analysis would have to be made in terms of the general theory as the flanks of the wedges will no longer be straight - a requirement that must be satisfied in the special wedge theory.

SECTION 7

7. COMPARISON BETWEEN THE RIGOROUS AND APPROXIMATE METHODS OF ANALYSIS OF A WEDGE OF COHESIONLESS MATERIAL IN A STATE OF ACTIVE FAILURE

7.1 Introduction

In Section 5, by means of the mathematical theory of plasticity, the differential equations governing the active critical state in wedges of cohesionless material were derived. By numerically integrating these differential equations the solutions of the critical state for a series of symmetrical wedges with slopes ranging from 0° to 30° and an angle of internal friction of 30° were obtained. In this section it is the intention to compare the pertinent results obtained from the rigorous solutions with those obtained by approximate methods, and select the best approximate method. For design application and the analysis of stability failures such a selection is a necessity for the following reasons:

In practice the embankments of cohesionless material may have angles of internal friction different from 30°, the embankment may be flat-topped and the slopes not symmetrical. As each of these variables affects the critical stress distribution in the embankment, it would be impractical to attempt rigorous solutions for each case, particularly as these solutions cannot be obtained directly for the specified outline of the embankment. Even if a large selection of such solutions were available, the data may not always be readily available to a designer. Simplified procedures which give the solutions of sufficient accuracy for design purposes are therefore required.

7.2 Hummel & Finnan's theory

Hummel & Finnan (1921) presented a theory whereby the stresses in an embankment of cohesionless materials could be determined. They postulated that under plane strain conditions the weight of any particle in the cross-section is transmitted to the adjacent particles in two directions making equal angles with the vertical. From this postulation it was deduced that the stresses at any point in a cohesionless mass could be determined from the pressures due to two columns of material extending from the point to the surface at angles $\beta = \frac{90 + \rho}{2}$ to the horizontal. (See Figure 7.1). This gives rise to a system of conjugate stresses at this point and hence the vertical, horizontal and shear stresses can be found:

$$\sigma_y = \gamma \frac{h_1 + h_2}{2}$$

$$\sigma_x = \gamma \frac{h_1 + h_2}{2} \cot^2\beta$$

$$\tau_{xy} = \gamma \frac{h_1 - h_2}{2} \cot\beta$$

where h_1 and h_2 are the vertical distances from the point under consideration to the points of intersection of the two columns with the surface.

Using model embankments they measured the vertical stresses, σ_y, along the base of the embankments and found good agreement with the theoretically predicted values. No measurements of the horizontal and shear stresses were undertaken.

7.3 Trollope's theory

Trollope (1957) postulated a theoretical model to represent the particles in an embankment of cohesionless material. For plane strain conditions the particles were idealized as smooth rigid mono-sized disks assuming the configuration shown in Figure 7.2. As the disks are smooth no tangential forces can

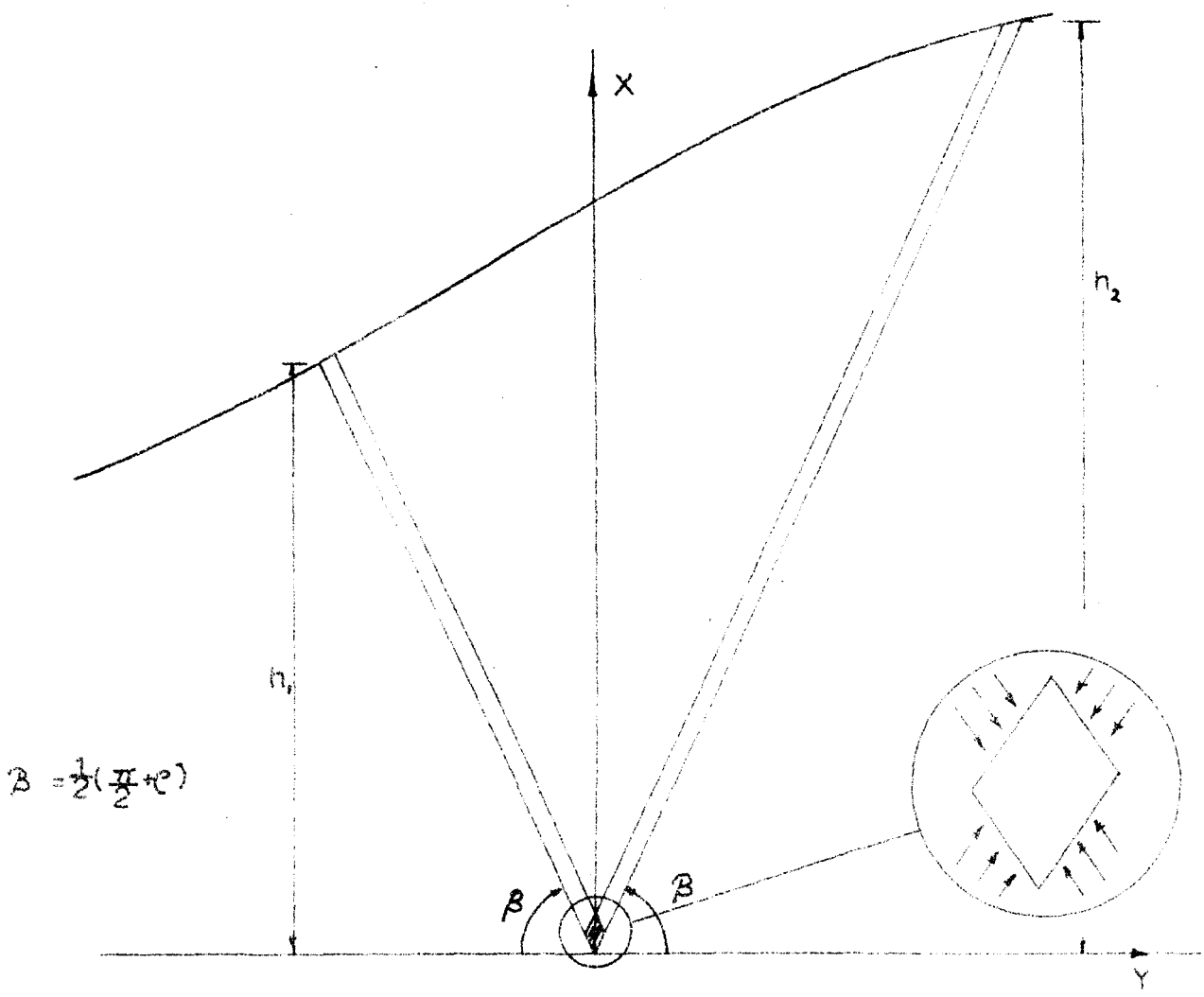

FIG·7.1

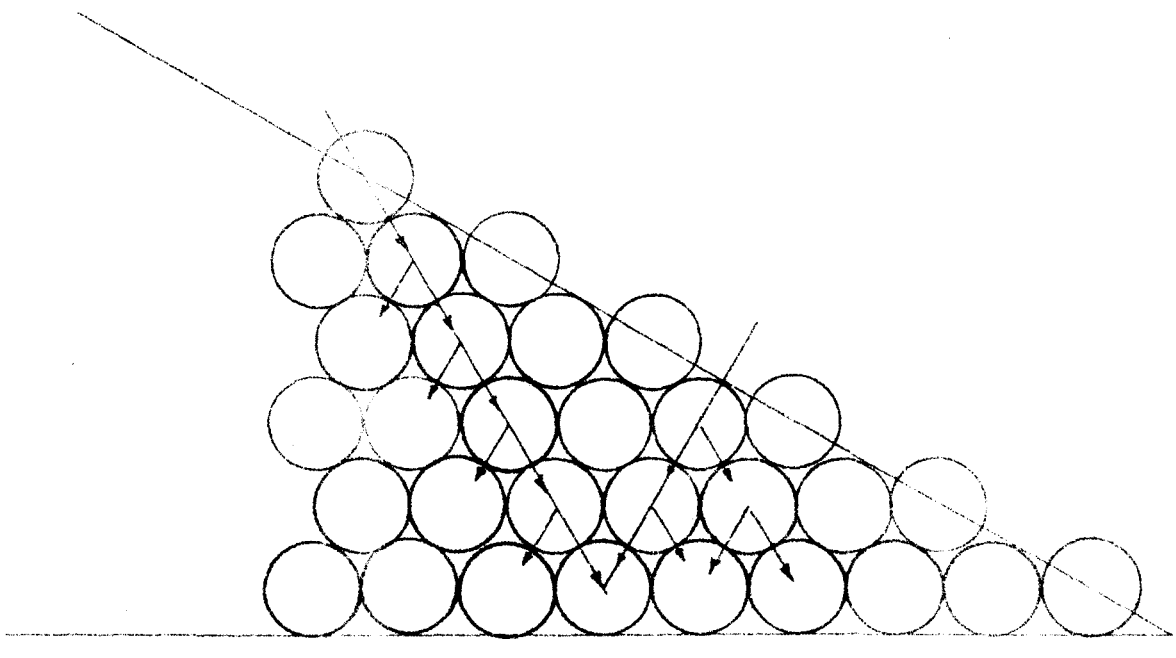

FIG·7.2

be transmitted at the point of contact between the disks. Being discrete the disks cannot transmit tensile forces.

Trollope considered two cases, the first in which no vertical deformation of the base occurred, and the second in which deformation of the base, similar to consolidation under an embankment, occurred. These two cases he termed the "no arching" and "arching" cases respectively.

Considering the no arching case, Trollope's method for determining the stresses in an embankment is in essence equivalent to that due to Hummel and Finnan, (that is each disk transmitted its weight equally to the two disks below it. See Figure 7.2), except that due to the physical properties of Trollope's model the "coefficient of friction", ρ, in terms of Hummel and Finnan's analysis becomes fixed at 30°.

Trollope tested this hypothesis by measuring the vertical stresses only under model embankments and it was found that the theoretical and experimental stresses showed good agreement.

7.4 A critical examination of Hummel & Finnan's and Trollope's theories

Hummel and Finnan postulated that each particle transmitted its weight along two lines at equal angles to the vertical, whereas this was a natural consequence in Trollope's physical model for the no arching case. The latter's approach is in this context more fundamental and will be taken as the basis for the critical review.

In Figure 7.3 the stresses along the base of a symmetrical wedge, with slopes of 30° and $\rho = 30^{\circ}$ determined according to Trollope and Sokolovski's theories, are given. Because in Sokolovski's analysis ρ is taken as equal to 30°, the two stress distributions are directly comparable. The similarity of the two stress distributions can be noted.

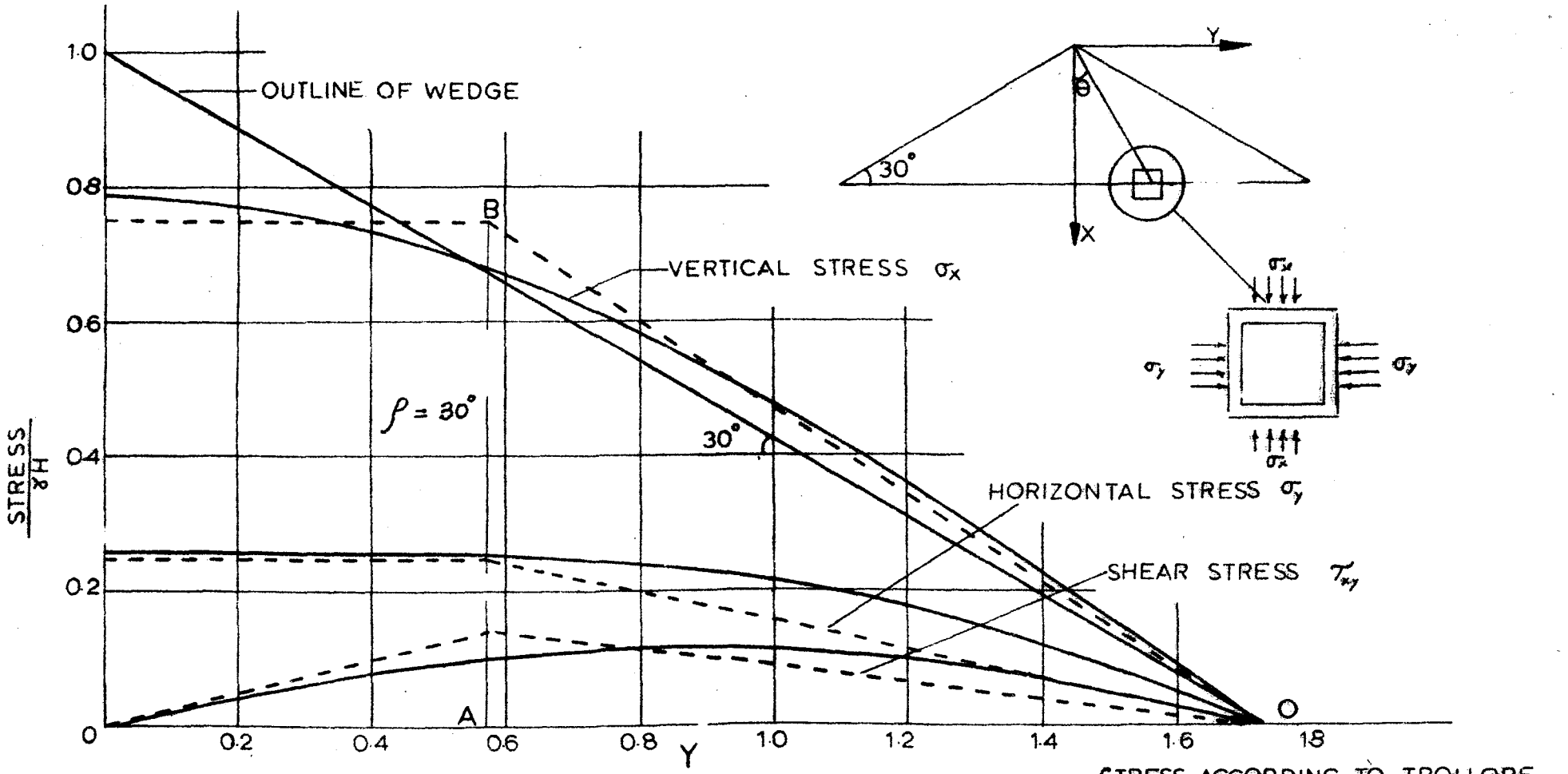

STRESSES ALONG BASE OF 30° WEDGE OF COHESIONLESS MATERIAL IN A STATE OF ACTIVE CRITICAL EQUILIBRIUM

FIG. 7.3

FIG. 7.3(a)

In Figure 7.4(d) the stress circle for the stresses, according to Trollope's analysis, at point A for the wedge in Figure 7.3 (or 7.4(b)) is drawn. It is apparent that the stress system is inadmissable under Mohr's criterion for yield. From point A to the toe of the wedge the ratios of stresses remain constant, hence the stress system throughout this section is inadmissable. From point A to the centre line of the wedge the σ_x and σ_y stresses remain constant. At the centre line of the wedge where the shear stress τ_{xy} is zero Mohr's criterion is satisfied. As the shear stresses increase from zero at the centre line to a maximum at point A, and σ_x and σ_y remain constant, this implies that in this section the stress system is also inadmissable under Mohr's criterion.

In Trollope's model the boundary conditions required for stability at the base of the wedge appear to be somewhat artificial. On a rough horizontal plane an embankment composed of frictionless disks cannot attain stability. To achieve stability in the section from A to the toe of the wedge, it is required that each disk bears against a plane tilted at $6^{\circ}35'$, as shown in Figure 7.5. (See Trollope and Morgan, 1959). The resultant of the forces on the bottom disks is then normal to the tilted base. There are thus no shear couples on any of the disks, whether internal to, or on, the base of the embankment.

In theory it is possible to visualise that if the disks are made sufficiently small the base surface may contain such irregularities that the disks may be restrained in the fashion envisaged in the theoretical model. In such an event it is very likely that the stresses, as calculated by Trollope, will

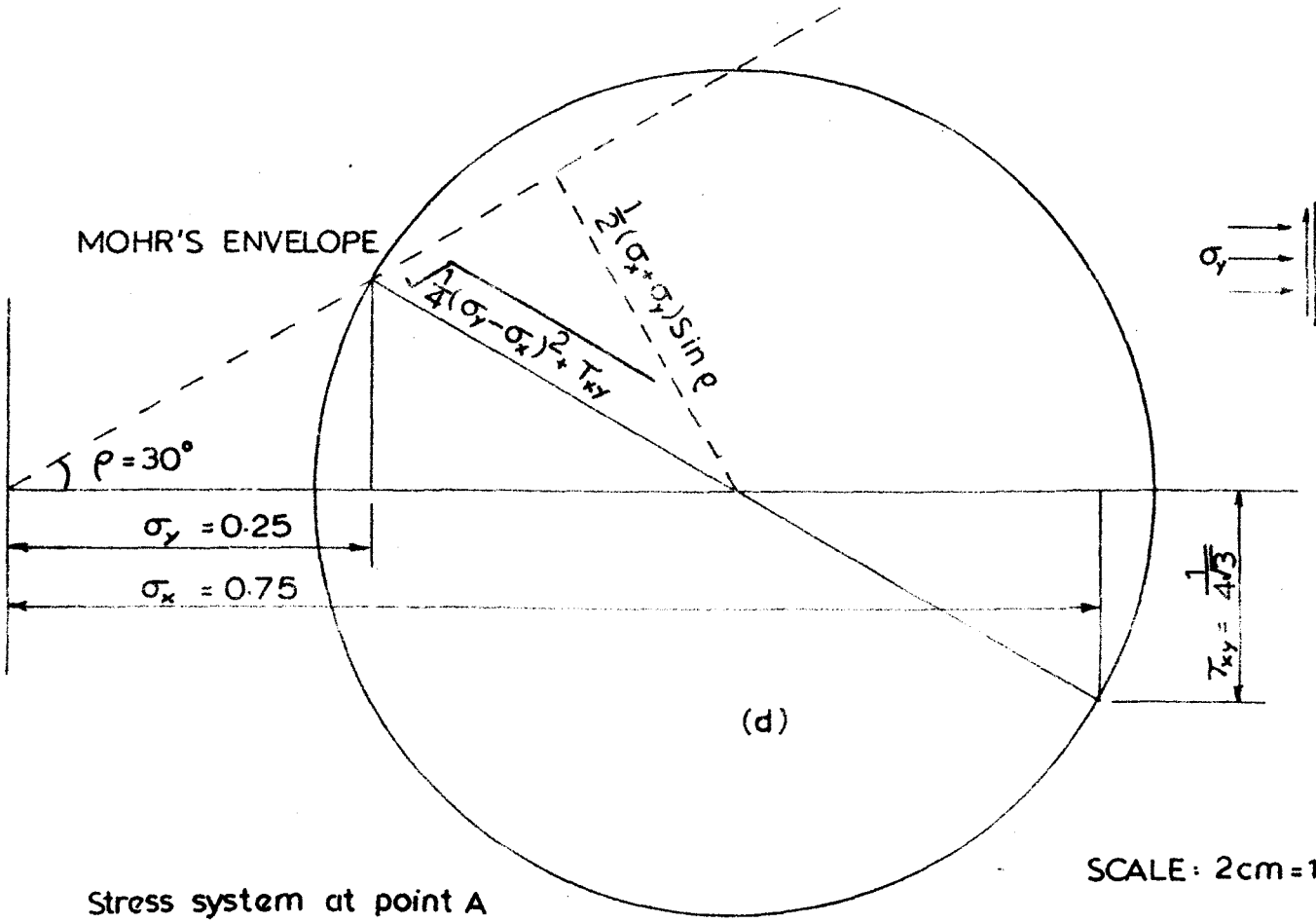

Stress system at point A

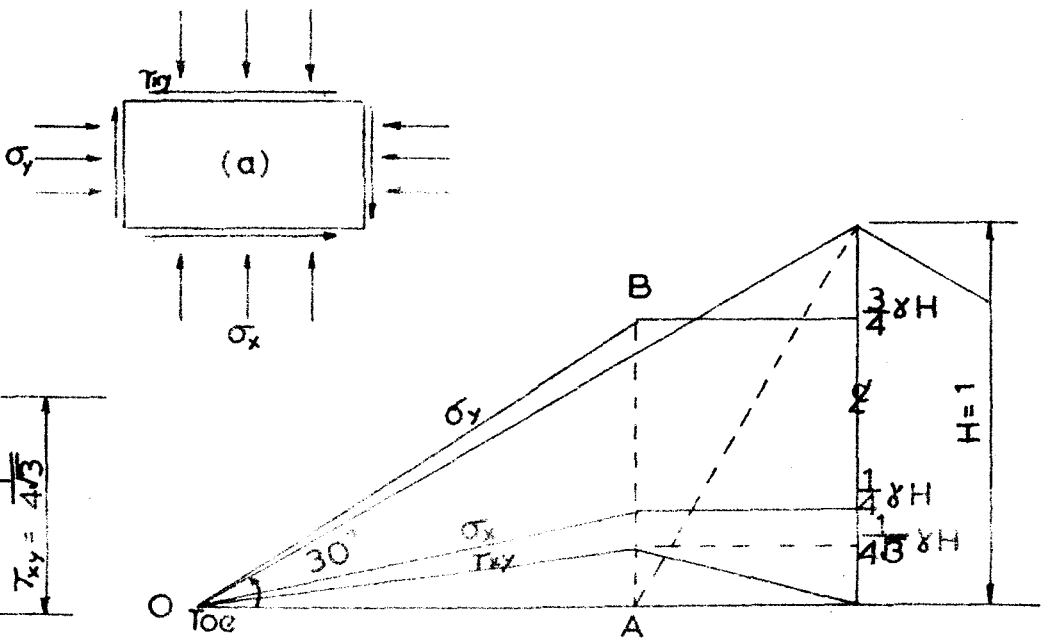

Stress at base of wedge according to Trollope's No-Arching theory.

SCALE: 2cm = 1 stress unit

(b)

(c) Mohr's Hypothesis: $\frac{1}{2}\sqrt{(\sigma_x-\sigma_y)^2+\tau_{xy}^2} \leqslant \frac{1}{2}(\sigma_x+\sigma_y)\sin\rho$

which gives $0.287 > 0.025$ hence inadmissable

MOHR'S RUPTURE HYPOTHESIS AND THE STRESSES AT A POINT IN 30° WEDGE AS CALCULATED BY TROLLOPE.

FIG. 7.4

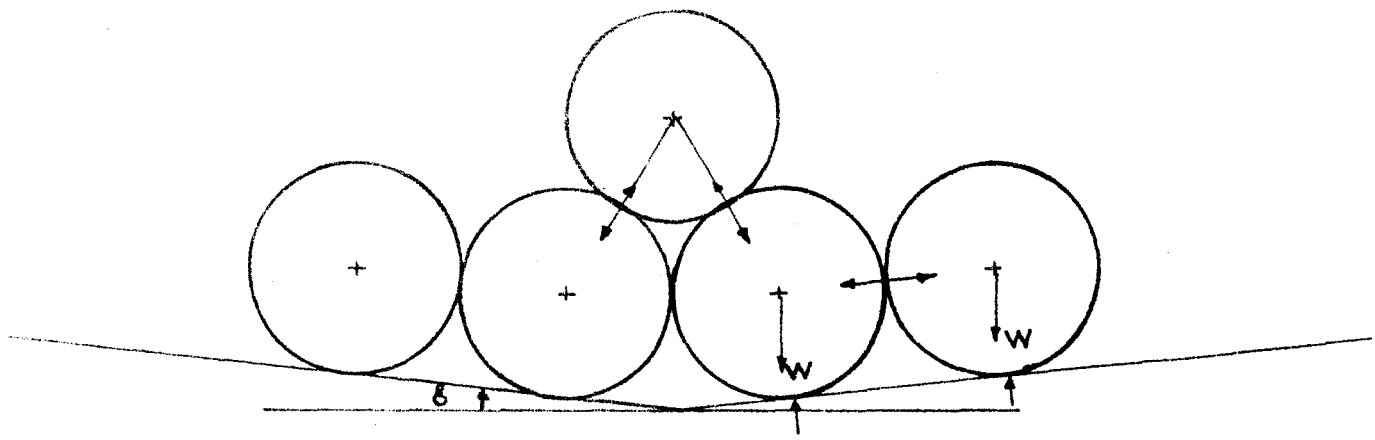

For equilibrium $2w \sin\delta = \frac{W}{\sqrt{3}} \cos(60° + \delta)$

which gives : $\delta = \tan^{-1}\frac{1}{5\sqrt{3}} = 6° 35'$

BASE DEFLECTION REQUIRED FOR STABILITY

FIG. 7.5

be realised because each disk is retained in a geometric pattern, forming a rigid framework in which Mohr's criterion for yield does not apply. (This theoretical model would under normal circumstances not be fully realised due to random arrangement of the disks).

In practice, embankments of normal granular material with irregular grains attain equilibrium on smooth surfaces such as glass. This is due to the frictional shear forces between the glass and the particles, the friction being due to microscopic irregularities on both the macroscopic grains and the glass. These tangential frictional shear forces cause couples on the grains which, due to lever purchase and tangential friction forces between the particles, are transmitted into the mass of particles above as shear stresses. It seems that it is the neglect of these shear couples on the individual grains that has led to the inadmissable stress system in Trollope's model.

Considering the inadmissability of the stress systems under Mohr's criterion a stage further, it may be argued that the friction in a cohesionless material is derived from two causes: the first due to interlocking of the grains and the second due to tangential shear forces at the points of contact between the grains. Internal to the wedge, where the particles can be expected to be more densely packed, the friction coefficient should be higher than that indicated by the natural angle of repose. The wedge might therefore retain "elastic" equilibrium under the stress system as calculated by Trollope. This argument does not, however, appear to be valid, for as the theoretical stress ratios remain constant right to the edge of the slope it is to be expected

that in the immediate neighbourhood of the edge failure should take place.

In Trollope's analysis due to the fact that critical equilibrium is not attained it is not possible to determine theoretically the lines of slip. If, however, it is assumed that the slip lines in the wedge are at $\frac{\frac{\pi}{2} - \rho}{2}$ with respect to the direction of the maximum principal stress, then Trollope's analysis gives a constant direction for the failure lines in the region ABO, Figure 7.3. From the experimental results on the failure of wedges in Section 5, or by simple consideration, it is evident that in wedges with slopes at the natural angle of repose, base failures near the toe of the wedge must lead to failure lines of which one leg lies approximately parallel to the slope - in fact, the outline of a wedge at its natural angle of repose is a failure line. Trollope's theory gives failure lines lying at 45° and 105° to the horizontal. Sokolovski's theory gives corresponding values of 30° and 90°, that is, one leg of the failure does lie parallel to the slope, the other being vertical.

With regard to the practical application of this theory to stability analysis, the fact that Mohr's criterion is not satisfied is no bar to its use as a design method if, by its employment, satisfactory stable designs can be achieved. It is therefore of interest to enquire if Trollope's method would lead to safe designs. In Figure 7.6 the horizontal thrust at any point along the base of the wedge was determined by progressively accumulating the shear stresses, as determined by Trollope's and Sokolovski's method respectively, along the base from the toe to the centre line of the wedge. It is

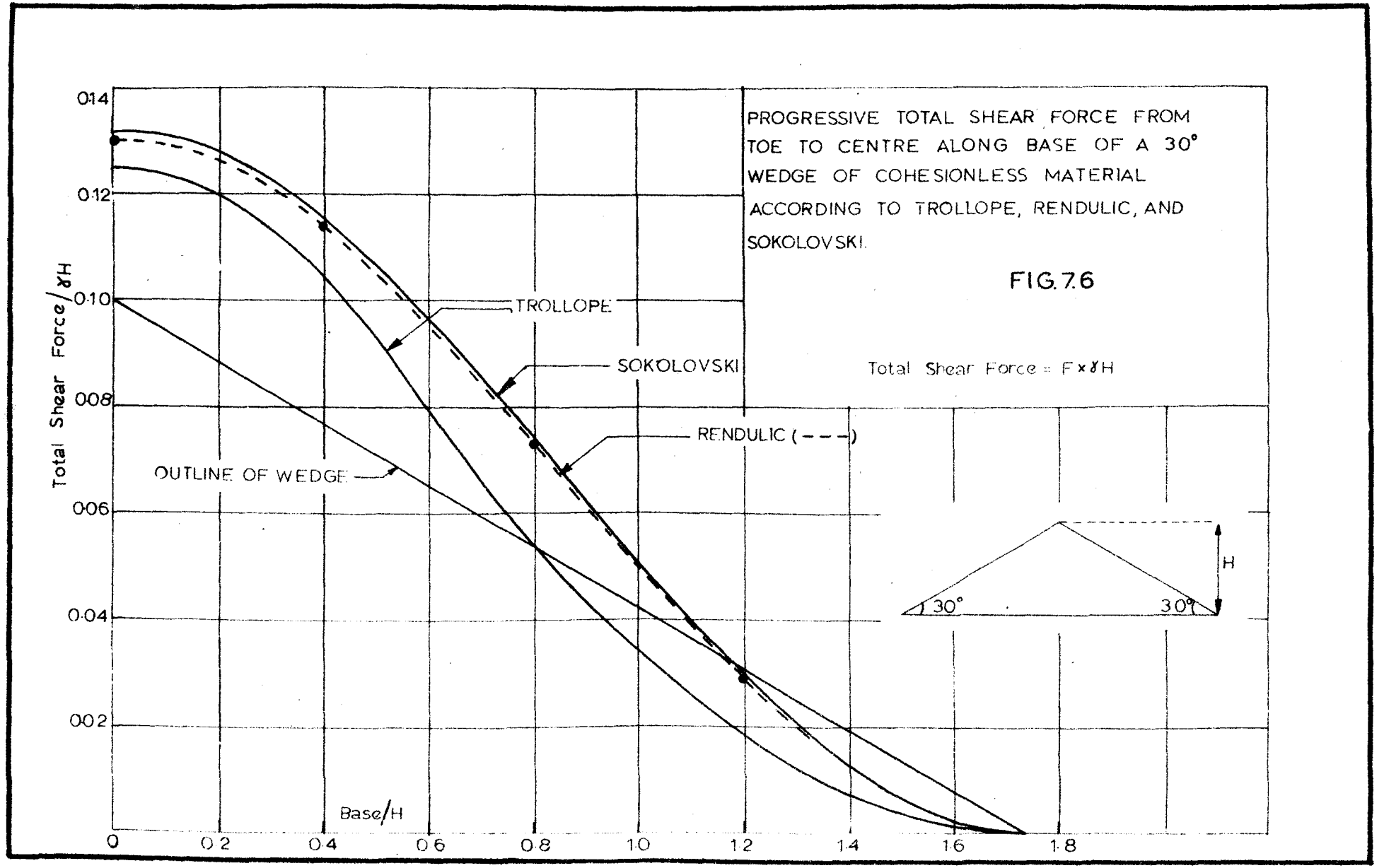
PROGRESSIVE TOTAL SHEAR FORCE FROM TOE TO CENTRE ALONG BASE OF A 30° WEDGE OF COHESIONLESS MATERIAL ACCORDING TO TROLLOPE, RENDULIC, AND SOKOLOVSKI.
FIG. 7.6
Total Shear Force = F × γH
Total Shear Force / γH
0·14
0·12
0·10
0·08
0·06
0·04
0·02
TROLLOPE
SOKOLOVSKI
RENDULIC (- - -)
OUTLINE OF WEDGE
H
30°
30°
Base/H
0
0·2
0·4
0·6
0·8
1·0
1·2
1·4
1·6
1·8

clearly evident that Trollope's method, when compared with Sokolovski's, significantly underestimates the thrust. The difference in thrust is so great that it would in practice be unwise to accept Trollope's values in preference to Sokolovski's.

One observation of practical importance is that the vertical stress distribution in a wedge at rest and in a state of active critical equilibrium appear to be approximately the same. (See Figure 7.3). As experimental data by Trollope and Hummel & Finnan confirm that the vertical normal stresses for wedges at rest are closely given by their method, its use for determining vertical stresses at rest and in a state of critical equilibrium is recommended.

7.5 Rendulic's method

Rendulic presented an approximate method to determine in cohesionless embankments the thrust under active failure conditions for failure of the base layer by sliding.

Referring to Figure 7.7 it can be noted that the failure of the embankment consists of two failure lines, marked AB and AC, enclosing the plastic zone in the embankment, and a third failure line, AD, along the base from the bottom apex of the failure zone to the toe of the embankment.

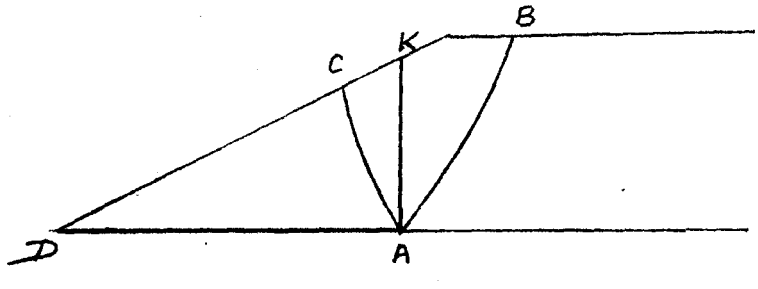

Fig. 7.7

From the theoretical analysis, experimental evidence and observations of failures in the field it is known that the inverted form of wedge failure occurs, that this failure can take place without the adjacent regions of the embankment being in a plastic state.

In the rigorous approach the stresses along the boundary BC are specified and on the assumption that the mass below BC is in a critical state, by applying the differential equations of failure, the failure lines BA and CA are determined. From the values of the critical stresses along BA the total thrust parallel to DA can be determined. (This is according to the general analysis of plastic failure. In the wedge analysis (as was indicated in Section 5) the thrust can be calculated more simply, but here the external shape of the wedge is restricted).

In infinite slopes or finite slopes where the infinite slope condition prevails, as for instance in wedge failures with their bottom apeces in Region A (see Figure 5.9), the failure lines are straight and given by the α_1, β_1, and α_2, β_2 characteristics (equations 5.24, 5.23, 5.25 and 5.26). Rendulic presented a method by means of which these failure lines can be determined. It is based on the requirement that the failure zone ABC, Figure 7.7, is in a state of critical equilibrium. Consequently the thrusts on KA due to the mass on the right must equal the thrust due to the mass on the left of KA. The direction of the thrust is, however, not known initially. In Figure 7.8 assume failure lines AC', AC'' and AC''' at different slopes through A. Taking the failure line AC' the state of critical equilibrium

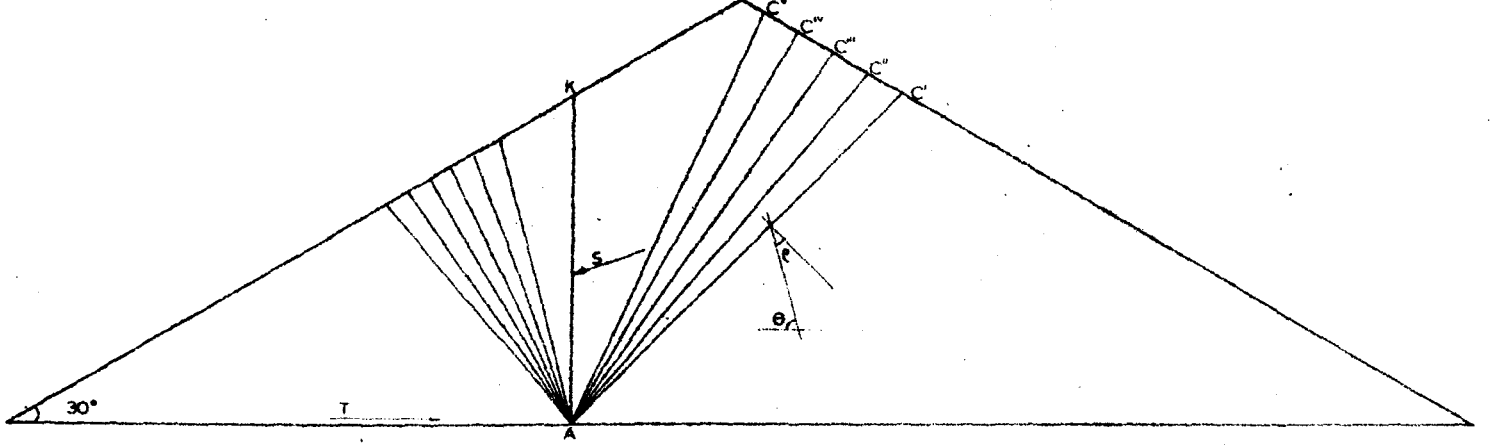

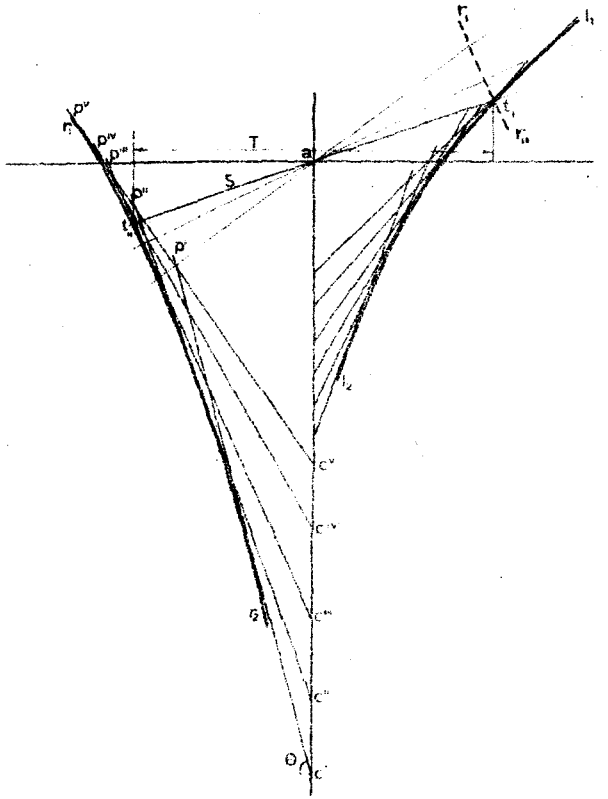

ACTIVE FAILURE THRUST ON SECTION AK IN 30° SYMMETRICAL WEDGE ACCORDING TO RENDULIC

FIG. 78

requires that the thrust P (of unknown magnitude) lies at the angle ρ with respect to the normal on AC'. Hence, the force diagram with W' = mass ABC acting vertically downwards = ac' and the direction of P given as c'p' can be drawn. The force diagram is repeated for failure lines AC" and AC"'. The envelope $r_1 r_2$ can be drawn to the vectors c'p', c"p", etc.

This construction is repeated for the mass to the left of AK, giving the envelope ℓ_1 ℓ_2. A mirror image of $r_1 r_2$ through point α is then constructed, giving curve $r_1 r_n$. Where this curve intersects ℓ_1 ℓ_2 at t_1, the line t_1, t_n gives the thrust S in magnitude and direction, equal and opposite on AK. The horizontal component of S gives the force moving the mass along the base.

Because in the infinite plane condition the critical stresses at the failure lines are proportional to the depth of the failure line below the upper surface of the slope, the location of the thrust S is at 2/3 KA.

Application of this construction to several slopes at infinite slope conditions indicates that it gives the same failure lines and thrusts values as the rigorous solution. The verification for an infinite slope condition, the slope being at 25°, is shown in Figure 7.3.

The simple critical stress conditions prevailing in the infinite slope are not applicable in the failure of wedges where the bottom apeces are in Region B of the wedge (Figure 5.9), or, the outline of the embankment is irregular. In such cases the failure lines are curved and the critical stress distribution

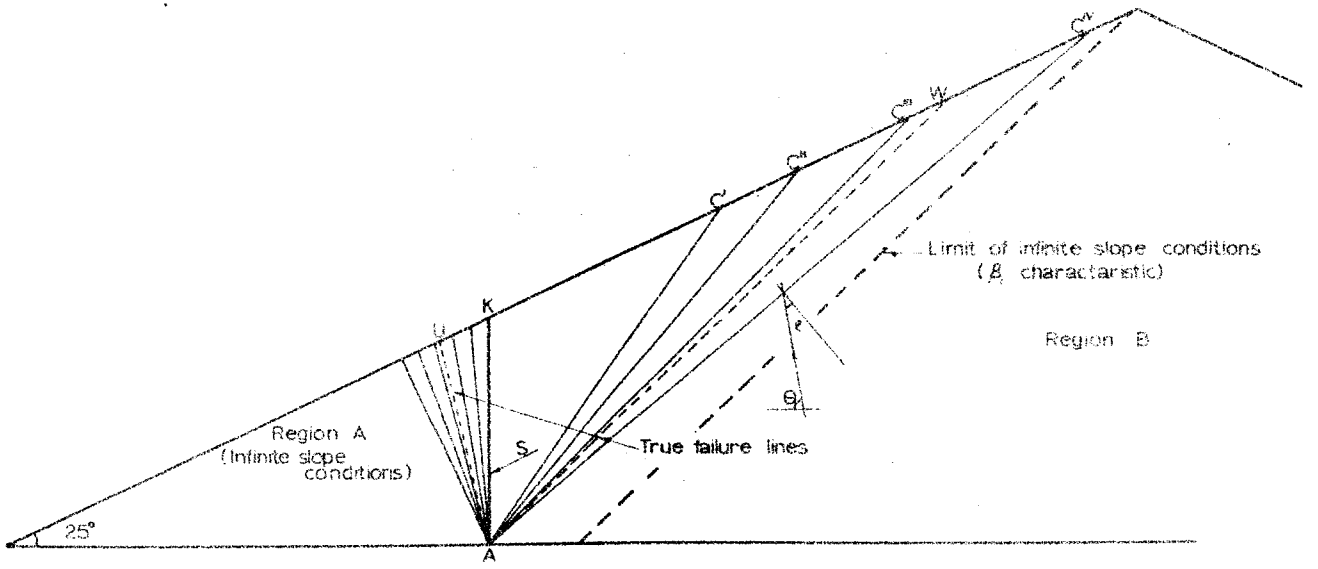

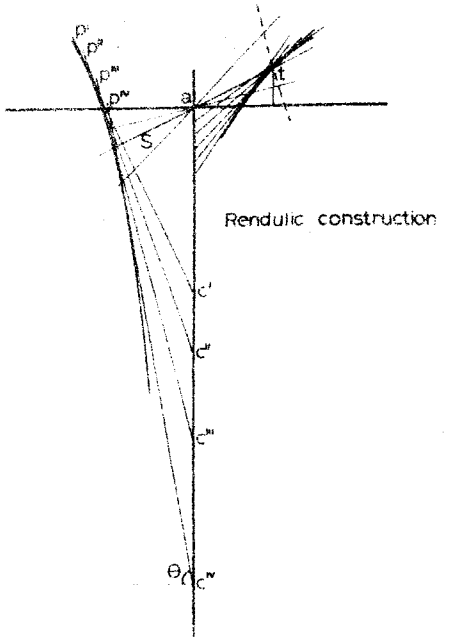

Rendulic construction

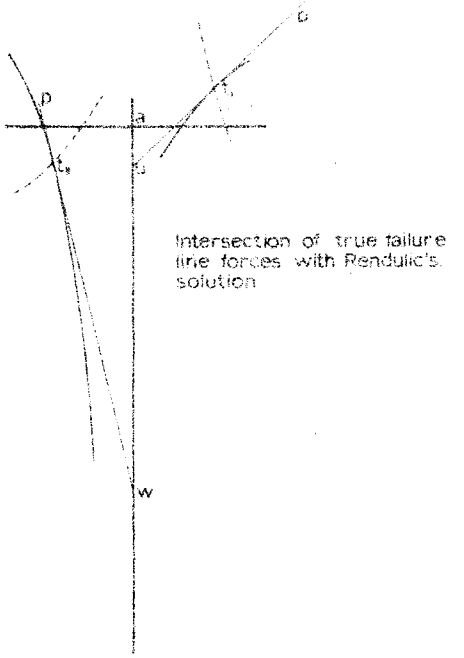

Intersection of true failure line forces with Rendulic's solution

RENDULIC'S SOLUTION
FOR ACTIVE FAILURE UNDER
INFINITE SLOPE CONDITIONS

FIG. 7.9

along a failure line is not simple. In Rendulic's analysis the assumption of straight failure lines through the bottom apex of the failure now leads to errors in the location of the failure lines. Furthermore, the stress distribution on the failure line requires an additional postulation. The usual one is to assume that the stresses on the failure lines are directly given by the distribution of the mass above the failure lines. On this assumption the resisting shear stresses are not everywhere equal to the disturbing shear stresses, although their totals are equal. This leads to the situation in which the thrusts S on AK in magnitude and direction can be determined, but their points of application on AK differ between the right and the lefthand side. Furthermore, if the assumed failure lines do not conform exactly to the true failure lines the thrust S is underestimated.

In order to investigate to what degree Rendulic's solution underestimates the thrust, the horizontal thrusts at different vertical sections along the base of a wedge with 30° slopes and an angle of internal friction = 30° was determined. (An example of one calculation is shown in Figure 7.8). These values are plotted in Figure 7.6 where the thrusts, as determined by Sokolovski's rigorous method and Trollope's method, are also shown.

It is clear that Rendulic's method gives values only insignificantly smaller than those obtained by Sokolovski's method. The maximum absolute difference between the values is found for failures with apeces at the centre line of the base of the wedge. This is to be expected, because here the true failure lines show the greatest curvature and hence the

greatest deviation from the straight lines assumed by Rendulic. (See Figure 5.21). Near the toe of the wedge the values for the two methods are virtually identical which can be explained by noting that the true failure lines near the flank are straight for the greater part of their length.

The maximum curvatures occur in wedges with their slopes at the natural angle of repose (compare Figure 5.21 with 5.22). It can therefore be expected that the thrusts by both methods determined for any other shape of embankment, or, for wedges with slopes less than the angle of repose will show smaller differences than the maximum found for failures of the 30° wedge. In consequence it can be stated that in the active failure of any cohesionless embankment by sliding along the base, Rendulic's method will give values for the thrusts insignificantly smaller than those determined by the rigorous method.

SECTION 8

8. DESCRIPTION OF THE FAILURE OF SACHE'S DAM EAST

8.1 Introduction

At Cullinan, 20 miles east of Pretoria, the Premier (Tvl.) Diamond Mining Company mines a diamondiferous Kimberlite pipe.

Part of the process of diamond extraction requires the crushing of the Kimberlite rock and washing of this crushed material to remove the dust. This is essential as dust derived from Kimberlite is of a clayey nature; in the subsequent liquid gravity separation of the heavy minerals (including the diamonds) if the dust is not removed, the viscosity of the separating liquid is increased, causing the process to operate inefficiently. The plant treats approximately 17,000 tons of material a day, requiring about 3 million gallons of washing water. To recover as much as possible of it for re-use the water, after being used in the process, is treated with hydrated lime to flocculate the clay material to a viscous slurry called slime. The slime is pumped to massive shallow basins called slimes dams (Figure 8.1), in which the flocculated material settles out, leaving a relatively clear supernatent suitable for pumping back to the mine. The slime is discharged along the edge of the slimes dam, the coarser material settling out to form a beach. As the settled slime builds up in the dam, the walls, constructed from the beach material, are raised accordingly.

For about 20 to 30 years after a slimes dam has gone out of commission the settled slime maintains a consistency of weak jelly, below a crust of about 2 - 4 feet. Inspection



Figure 8.1 Slimes dams are shown in the background, with the pond of Sache's Dam West in the foreground.

and reparation of the banks against breaches is therefore required for many years.

The disposal of the 17,000 tons of treated Kimberlite per day (called tailings) is to dumps. In former times these were disposed of separately from the slime.

It was considered that an economic solution to the disposal of both the slime and the tailings could be achieved if a tailings dump to serve as a dam wall was built across a small valley, and the slime pumped into the pond area. For this reason Sache's Dam East was constructed.

8.2 Construction of Sache's Dam East wall

An endless conveyor belt transported the tailings from the mine processing plant to a flinger situated at the top edge of the advancing end of the wall, where the tailings were ejected into the air to fall on the advancing face, the particles rolling and sliding down the face until they came to rest at their natural angle of repose (Figure 8.2). No artificial densification of the material was undertaken, the only densification being due to the settlement of the wall under its own weight.

The tailings dam thus formed is called Sache's Dam East; photographs showing different views of the dam and its surroundings are shown in Figure 8.3. The dam wall has a maximum height of 260 feet above ground level, and a length of approximately 4,000 feet; the sides slope at 34½°, which is the natural angle of repose of the material; the wall is 80 feet wide at the top, giving a maximum base width of approximately 840 feet.

8.3 The slime beach

The tailings material in the wall range in size from +½" to -100 Tylers sieve with the coarse fraction predominating,

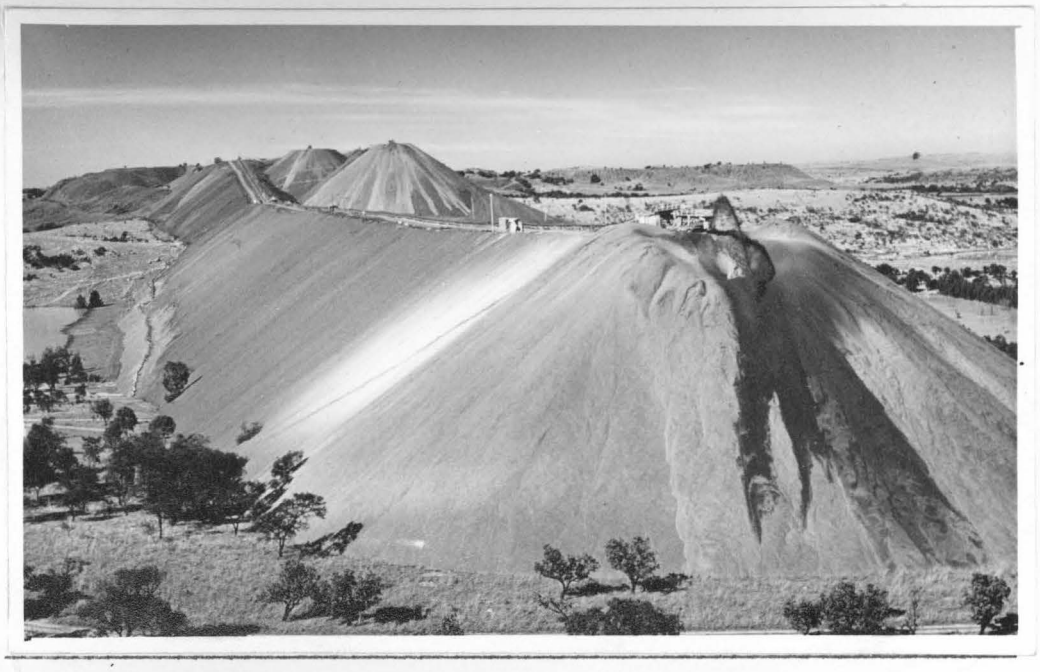



Figure 8.2 Upper photograph shows advancing face of dam with flinger in action. In the background dump No.3 is the extreme right-hand one. Bottom photograph shows close-up of flinger.

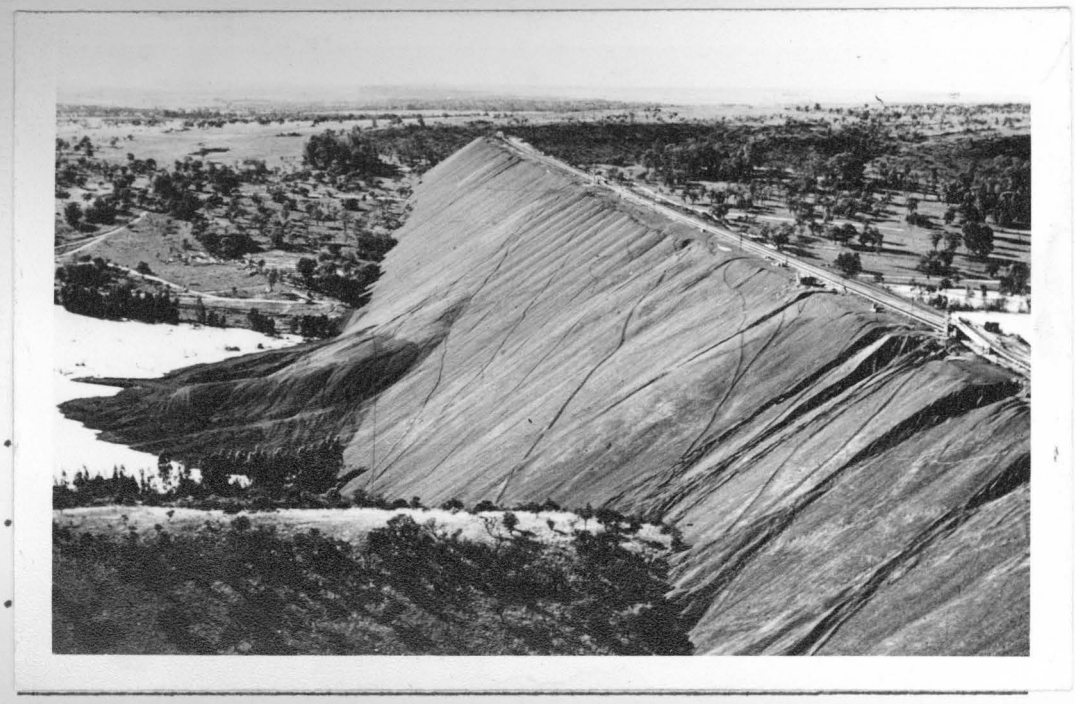



Figure 8.3 Upper photograph shows the downstream flank of the dam, the lower photograph the upstream flank.

making the material very permeable. As the slime can flow through this material, an impervious layer up-stream of the wall was required to contain the ponded slime. A bench cut into the tailings wall about 10 feet or more above the slime pond level carried a 10 inch pipe conveying the slime. At regular intervals along the pipe, 1 inch diameter hoses connected to the pipe discharged the slime at the edge of the wall at water level. The coarse fractions in the slime settled out next to the wall, forming a beach about 100 feet wide, sloping down at about 5° to the water's edge (Figure 8.4).

The beach material was of a very loose consistency, to the degree that it was not possible to walk on it. The beach was rendered more unstable because the 5° slope terminated at the water's edge; below water level the slope increased to that of the natural angle of repose of the material, approximately 30 to 34°.

8.4 Sub-soil conditions

Sache's Dam East was constructed across the pond area of a small dam called Sache's Dam West. This dam has been in existence since 1902, and accumulated sedimentary material to a depth of about 10 to 15 feet. No investigation of this material was made before the wall was constructed across the ponded area.

During the process of construction as the advancing face crossed the pond area of Sache's Dam West, failure of the embankment occurred, confined almost completely to the down-stream side. The subsidence at the wall due to the failure was continually filled in until the wall achieved stability. By that time the failure zone had penetrated

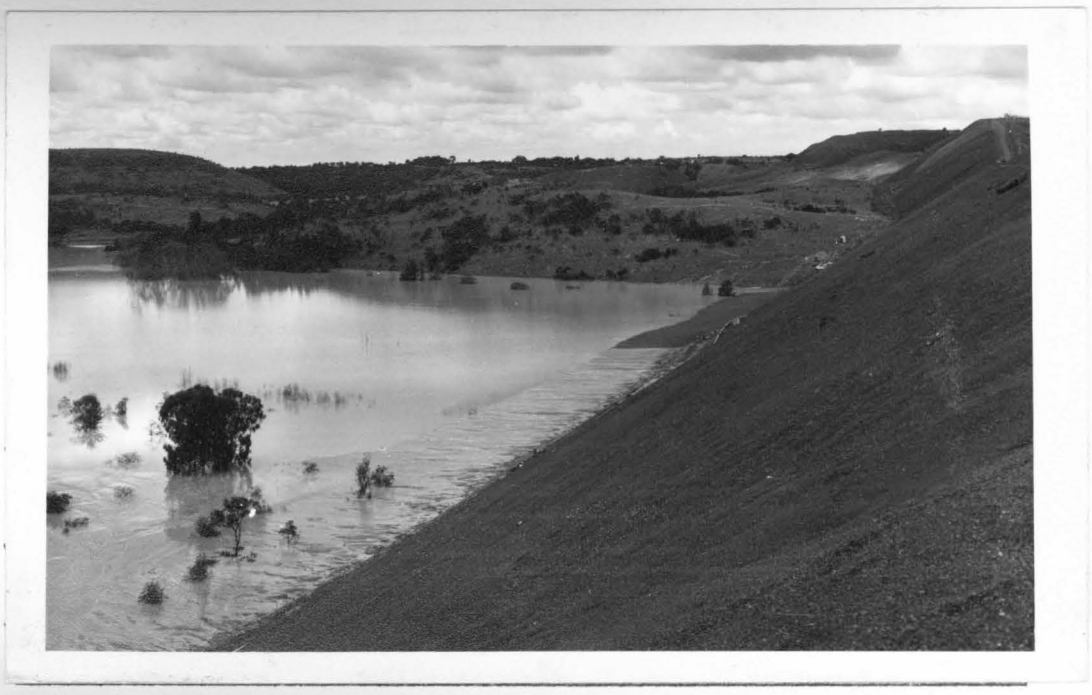

Figure 8.4 The beach. In the foreground it is in the process of being built up.

approximately 400 feet beyond the base limits of the dam wall into the pond of Sache's Dam West (Figure 8.5).

Figure 8.6 shows a plan of Sache's Dam West and the failure area of Sache's Dam East. It will be observed that the failed section lies almost exactly within the pond area. This suggested that the sediments in Sache's Dam had a direct influence on the observed failures.

To obtain information on the sub-soil conditions, exploratory borings were sunk across the lower region of the failure; their locations, all within the pond area of Sache's Dam West, are shown in Figure 8.6. Difficulty was encountered in obtaining undisturbed samples of the soil strata immediately below the tailings. This was due to the loose nature of the tailings, which required driving a bore casing ahead a foot at a time, and cleaning out with an auger. As the upper level of the underlying material was not known to within a foot, in about half the holes the casing intersected the underlying sediments to a depth of 6 inches to 1 foot before this became evident; the soil layers were consequently disturbed by augering out the casing.

The mean profile of the holes exhibited the following essential features:-

1. 20 to 30 feet of tailings.
2. 1 to 2 feet of mixed tailings and slime.
3. A layer of soft slime clay, ranging in thickness from 6 inches to 4 feet.
4. A zone 10 to 15 feet thick of interbedded strata of sands, silts, clays and slime clays of varying thicknesses, with the slime clay layers in the upper part of the zone.



Figure 8.5 Penetration of failure into Sache's Dam West Pond, now dewatered.

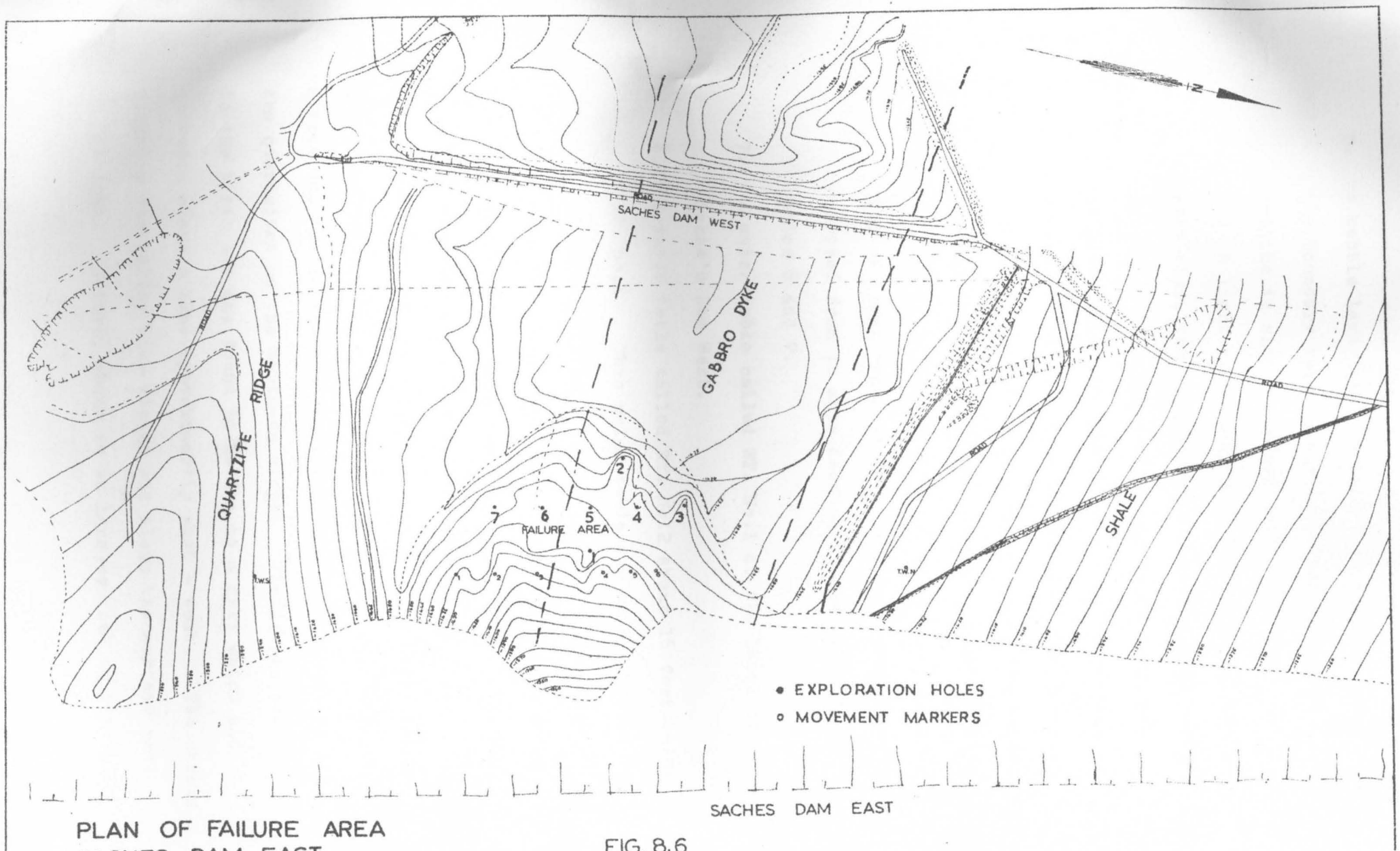

PLAN OF FAILURE AREA
SACHES DAM EAST

FIG. 8.6

8.4(b)

5. A pebble layer about 1 to 2 feet thick forming the boundary between the deposited sediments and the in situ weathered soil.

6. (a) A light brown clay sand with veins of green-gray clay, its consistency increasing with depth from firm to stiff. The soil is derived from in situ decomposed gabbro, the weathering zone extending for more than 80 feet into the gabbro. The weathered gabbro is very pervious, the water visibly draining from the sample. This material was found in holes 1 to 5.

   (b) A light brown stiff silty clay, very impervious, derived from in situ decomposed shale, found in holes 6 and 7.

7. A water table called WT. No.1 at the level of Sache's Dam West.

8. A water table called WT. No.2 about 16 feet below WT. No.1. This water table was only observed after passing through the layer of slime clay, when the upper water table No.1 was lost and the level in the borehole dropped to that of WT. No.2.

The generalised profile is shown in Figure 10.1.

The geology of the valley lies within the Magaliesberg quartzite and shales. The valley lies in an east - west direction, the shales outcropping on the northern slope and the quartzites on the southern slope. The gabbro sampled in the boreholes was found to be due to a dyke which had intruded along a line approximately east - west. The stream draining the valley lies within and along the surface zone of the dyke. Gabbro, which is an igneous rock with a fair

content of plagioclase and pyroxene, weathers very rapidly when exposed to a surface environment; this is probably the reason for the location of the river bed in the gabbro.

A photograph, Figure 8.7, looking east, shows the location of Sache's Dam East in the valley; a sketch of the north-south cross section is given in Figure 8.8. No attempt was made to determine the exact extent of the various strata as it was not considered to be essential to the solution of this problem.

Water table No.2 is an unusual feature and after its existence had been discovered a small experiment was conducted as follows:-

A borehole with casing, the bottom of which penetrated just below the slime clay and the top at level approximately 4 feet above Sache's Dam West water level (WT. No.1) was filled with water. The water drained away quickly, within five minutes, to the level of WT. No.2, showing that the lower strata are very pervious and that there is no connection in nature between the two water tables. The loss of WT. No.1 occurred before the pebble marker was intersected; other clay layers still existed below at the time the water table was lost. From this it was concluded that the clay layers are not continuous, an observation which is of great importance in considering the development of pore water pressure conditions under the embankment of Sache's Dam West.

The experiment was repeated with all the strata cased off down to and including the pebble marker. In holes penetrating the decomposed gabbro, WT. No.2 was quickly established, but in the shale the water table was only

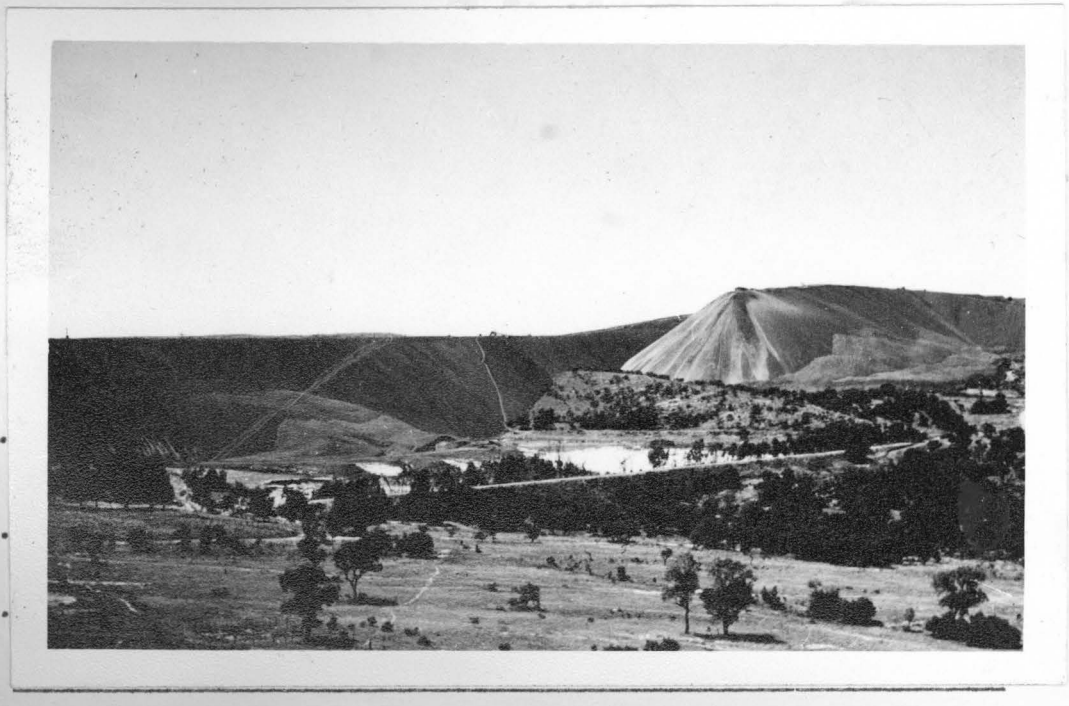

Figure 8.7 Looking east. Sache's Dam West is in the foreground, Sache's Dam East on the left, dump No. 3 on the right. Note the gentle slope of the valley on the north and the quartzite ridge on the south side of Sache's Dam West. The gabbro dyke lies along the trought of the valley.

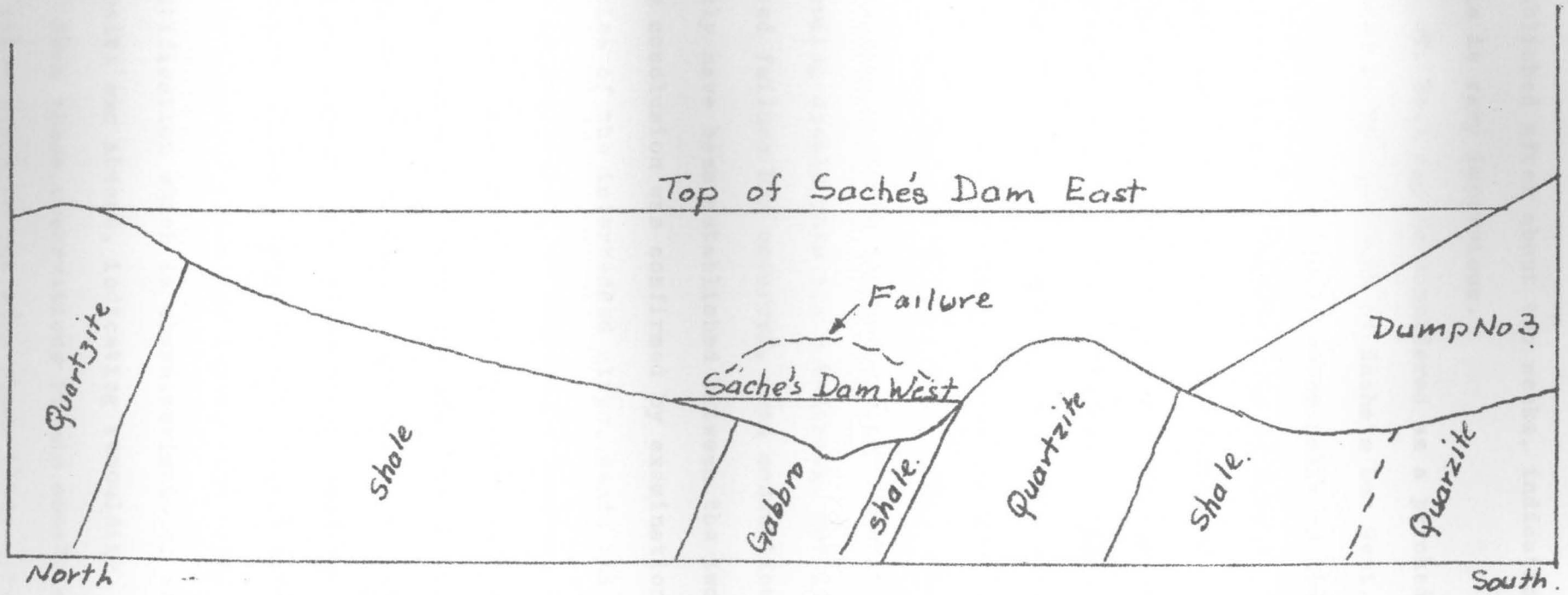

FREE HAND SKETCH of GEOLOGICAL STRATA ON NORTH-SOUTH SECTION AT SACHE'S DAM. (LOOKING EAST)

FIG. 8.8

(8.69)

established after about two weeks, indicating that the shale is very impervious.

WT. No.1 may be considered as a perched water table created by the presence of Sache's Dam West. WT. No.2 is probably the permanent water table in the area, raised above the level it would occupy if Sache's Dam West and Sache's Dam East had not been constructed. The existence of the two water tables appears to be due to the creation of a relatively impervious blanket of silt, clay and slime on the floor of Sache's Dam West. Their occurrence indicates that there was no major rupture of the blanket during the failure of Sache's Dam East. This led to the conclusion that the failure was not consistent with one extending deeply into the sub-strata, for if such a deep-seated failure had occurred, free connection would most likely have been established between the two water tables. This conclusion was confirmed by examination of undisturbed samples of the interbedded clays, sands and gabbro, which gave no indications of failure. However, in the clay slime layer immediately below the tailings there were clear indications of failure; cylinders of the undisturbed slime clay, when left to dry, shrunk skew; on twisting dry or wet samples, rupture took place on well-defined mirror-smooth concoidal surfaces which in nature were slightly inclined to the plane of the slime layer; the usual horizontal stratification which is characteristic of sedimentary deposits was absent, indicating remoulding.

From these observations it was concluded that the failure had taken place in the clay slime layer only.

The water in Sache's Dam West and Sache's Dam East, permeating slowly through the slime layer, is collected by

the large area of sands, silts and the pebble marker underlying the floor of Sache's Dam West. The decomposed gabbro dyke which passes under the wall of Sache's Dam West serves as an aquafir, draining away this water. Below Sache's Dam West the pore pressures in the gabbro are such that the water table (WT. No.2) intersects the ground surface at about 10 feet above the level of the river bed, slowly undermining the wall and reducing its stability. Records show that in 1910 a circular slip failure occurred in this wall in the section overlaying the gabbro. At that time the dam was only a few years old; the gabbro must have been exposed to obtain spoil for the wall, and only a thin layer of clay could have settled out over the pond bottom. It seems now almost certain that the failure was due to connection between the water in Sache's Dam West and the gabbro material raising the pore pressures below Sache's Dam West wall.

The freely draining character of the gabbro, pebble marker and interbedded sands and clay strata could be used to encourage drainage at the down-stream toe of Sache's Dam East; filter drains could with advantage be connected to them to reduce the build-up of pore water pressures. However, if free connection should be established with the water in Sache's Dam East (which would eventually attain a depth of approximately 200 feet) the increased pore pressures could have a significant effect on the stability of Sache's Dam East wall.

8.5 External forms of the failure

The surface indications of the failure of Sache's Dam East are consistent with a sliding type on a weak shallow

base; in Figures 8.9, 8.10 and 8.11 photographs of the failure are shown. The primary failure movement was outwards from the embankment, the subsidence at the wall being continually made good. As the slime clay in the pond of Sache's Dam West was unconsolidated, and very weak, the material virtually flowed into the ponded area on top of the slime clay. With consolidation the shear strength of the slime clay increased, requiring greater depth of tailings material to overcome the sliding resistance of the slime clay layer, leading to the gently curved outline of the failure (Figure 8.9).

When the failure had penetrated beyond the confines of the embankment, a secondary transverse failure in the main failure material took place, also of a sliding type. Evidence of this failure is clearly indicated in the photograph, Figure 8.10, by the formation of ridges at right angles to the main wall (see also Figure 8.11). Inverted wedges of material near the centre of the failure zone subsided, pushing out the sides of the failure zone en bloc, and resulting in the centre being at a lower level than the sides. This subsidence is illustrated in the photographs in Figures 8.10 and 8.12, by noting the outline of the failure zone as exposed by the cutting parallel to the main wall. In the cutting, the planes along which the transverse failure took place are exposed, and are shown by the photographs in Figure 8.13. They occur at intervals of about 3 - 4 feet, and are about ½ inch in thickness. The relative movements between the failing sections ground and pulverised the tailing material, in some instances the material being reduced to a fine powder.

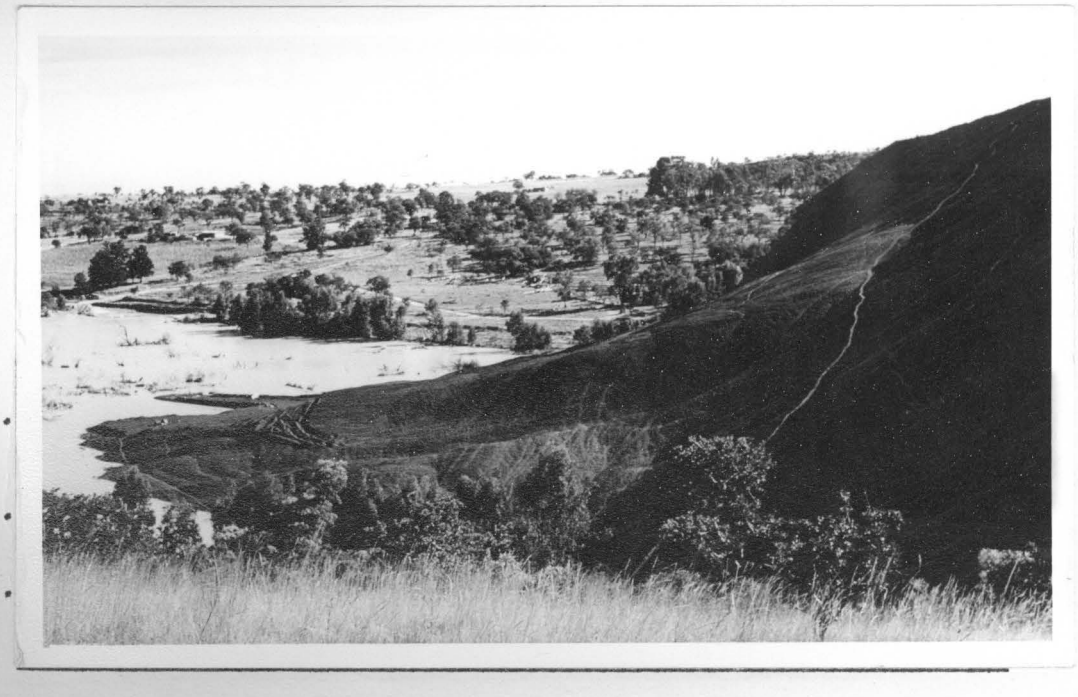

Figure 8.9 Showing the gentle curvature of the failure from the waterline to the flank of Sache's Dam East.





Figure 8.10 Failure of Sache's Dam East. The photographs show the secondary transverse failure lines very clearly. In the upper photograph at the top left-hand side of the failure note the horizontal ridges due to the primary failure. The bottom photograph (taken before Sache's Dam West was emptied) shows the infilling above the failure zone.

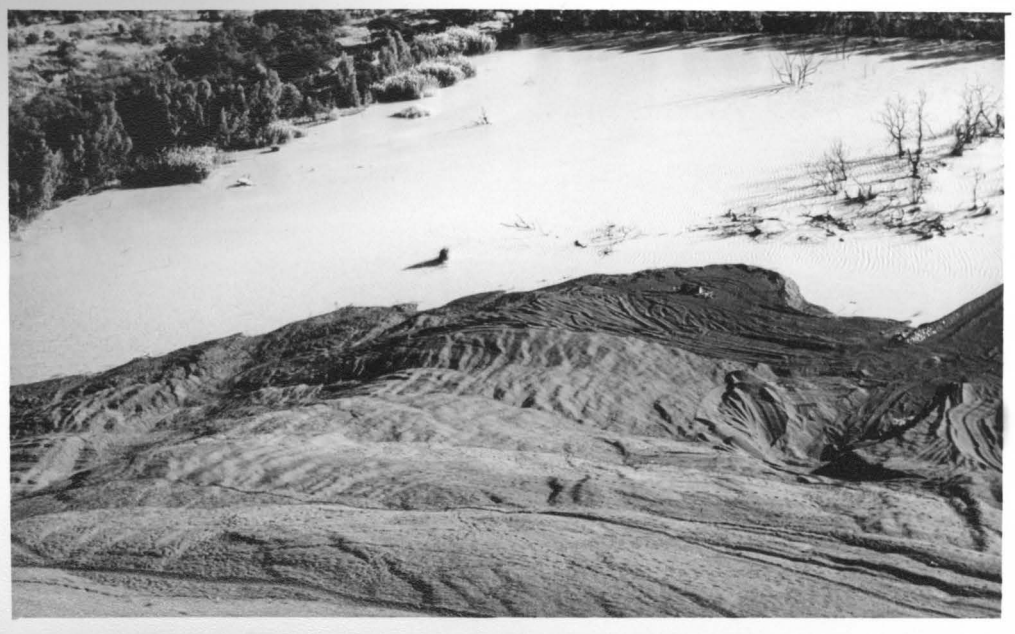

Figure 8.11 Failure of Sache's Dam East from the top of the dam wall, showing the transverse failure lines at right-angles to the wall.

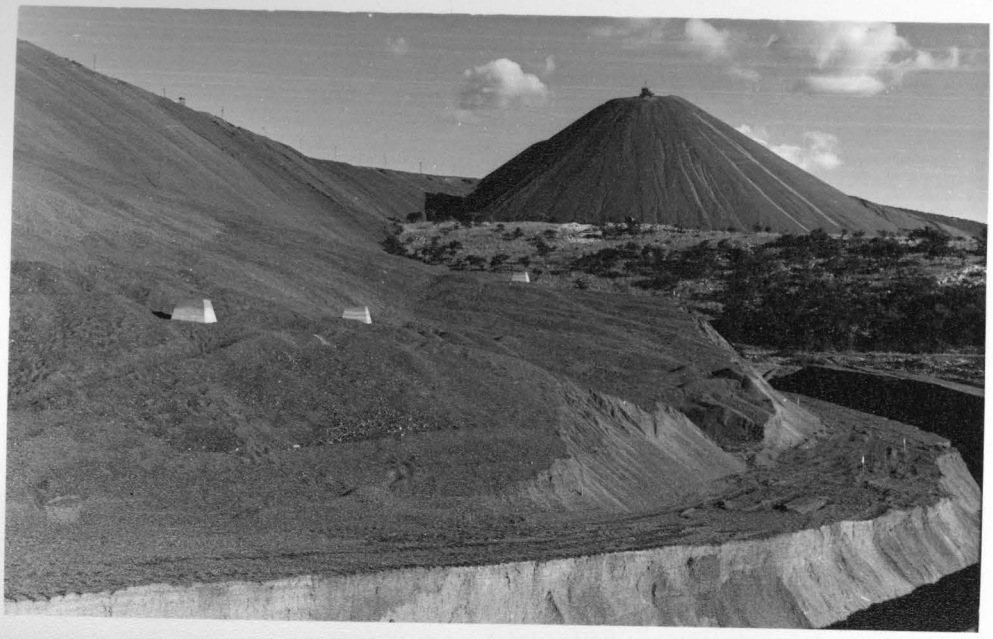

Figure 8.12 Cutting across failure zone - note from the outline of the cutting the subsidence due to the transverse failure near the centre of the failure. Markers to measure horizontal movement of the slide can also be seen.



Looking east. Failure lines near left-hand side of failure on Figure 8.11. Note slope to the right.



Looking east. Failure lines near centre. Note lines crossing.

Figure 8.13 Failure lines exposed in cutting parallel to Sache's Dam East.

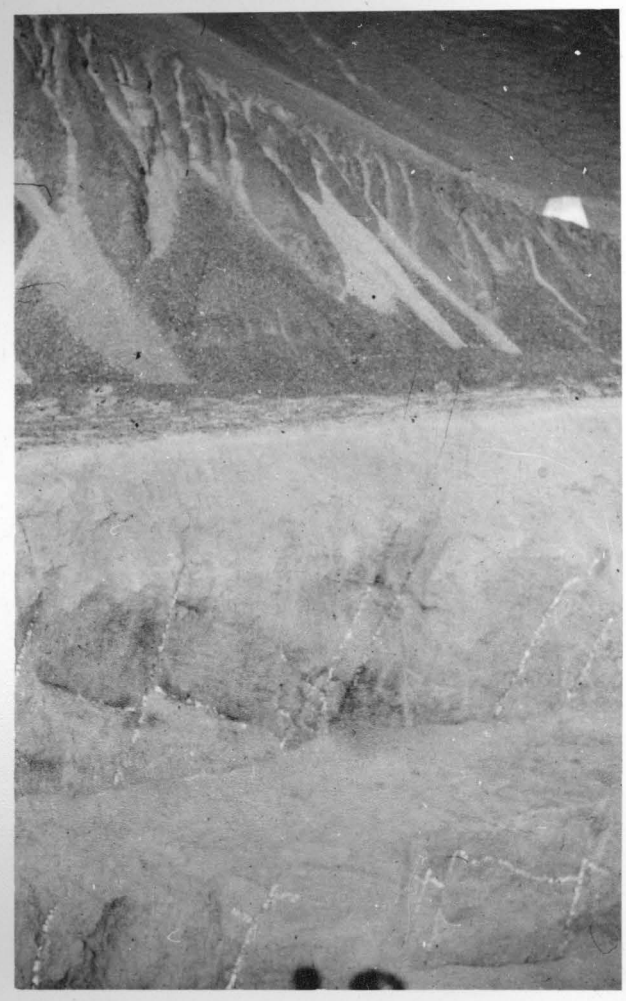



Failure near right-hand side of failure. Note lines sloping to the left.

Figure 8.13 (continued)

Ridges due to the primary failure movement have been almost completely obliterated by the transverse secondary failure. However, remnants of the primary failure ridges are still evident on the main wall in the photograph in Figure 8.10; observe the horizontal ridges on the high left-hand side of the failure zone, and compare these with the ridges formed during the failure of the model wedges in Figures 6.6. and 6.10.

Further evidence of sliding failures are to be found in the dumps at Cullinan. Tailings dump No.3, the extreme right-hand one in Figures 8.2 and 8.7, is about 600 feet above ground level, and was built out from an old tailings disposal dump. Washings of the decomposed material from the surface of the old dumps had spread over the ground surface as layers of clay, thus providing the weak plane necessary for sliding failure. Sliding failure of the new dump took place partly through the old dump material, pushing this material ahead (Figure 8.14). In Figure 8.15 the toe of the slide is shown, up-rooting trees in the path of its movement.

Where the dump crosses a small valley, the main failure took place along the axis of this valley at an angle of approximately 30° with the line of the dump.

Photographs of this failure, from different angles and under different lighting conditions, are shown in Figure 8.16. The characteristic inverted wedge formation of a sliding failure can be noted. The back legs of these failure wedges are shown in Figure 8.17.



Figure 8.14 Failure of dump No.3 showing sliding failure. Note the old dump material (covered in grass) being pushed ahead.



Figure 8.15 Dump No.3. Toe of slide uprooting trees.



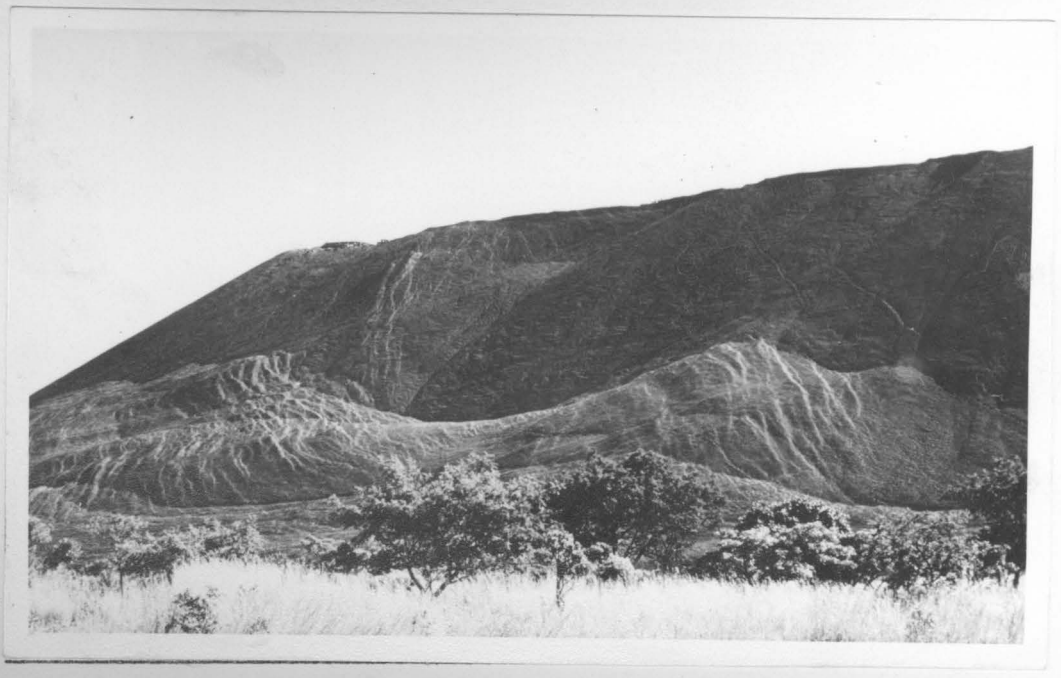

Figure 8.16 Failure of dump No. 3. The subsiding inverted wedge can be clearly seen. Note also that as the wedge subsided it was filled in.



Close-up of failure at front leg of wedge.

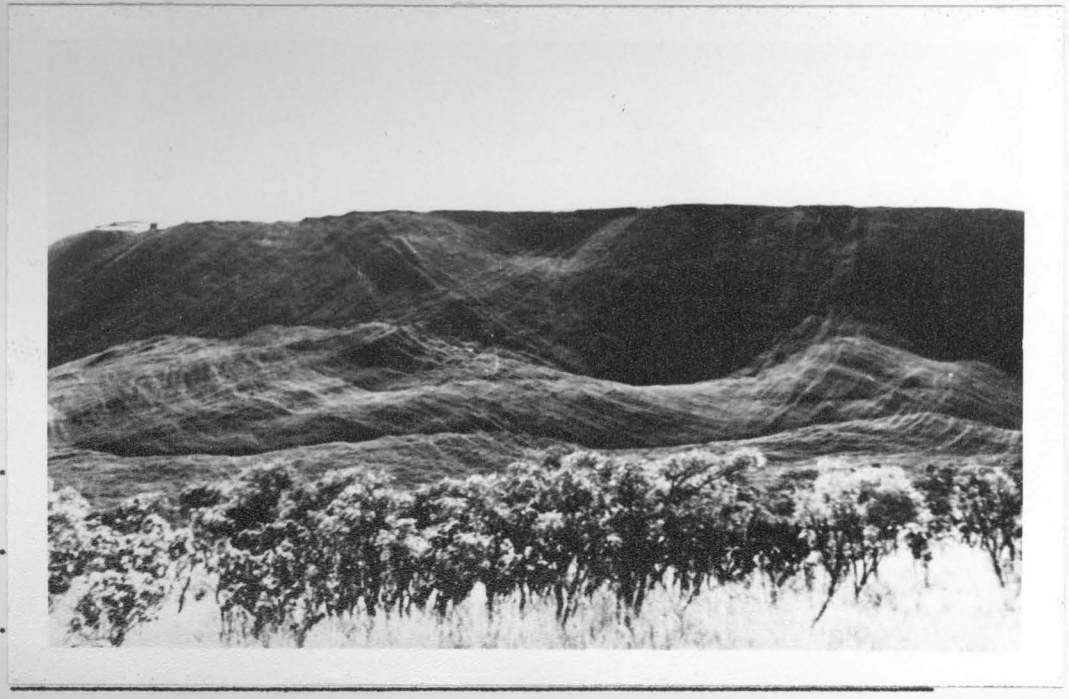

Failure condition at later stage. A new failure wedge is starting, partly through the old one, the two failure lines crossing.

Figure 8.16(continued)





Figure 8.17 Failure of dump No.3. Back leg of failure. Photographs taken from Sache's Dam East wall.

A secondary transverse sliding failure in the material pushed out by the main failure was also observed in the toe of the main failure. Ridges due to the secondary failure are shown in Figure 8.18;* the ridges are curved, indicating that a three-dimensional failure was taking place. The subsidence in the central area can be clearly distinguished. A diagramatic sketch of the main and secondary failure movements in the dump is shown in Figure 8.19.

Sliding failures were also observed on the dumps pushed out by bulldozer during excavation of a trench across the failure zone of Sache's Dam East. The excavated material was pushed onto the layer of slime clay lying on the bottom of Sache's Dam West, and although the dumps were only about 30 feet high, sliding failure took place, indicating the low strength of the unconsolidated slime layer. Photographs of one of these failures are shown in Figure 8.20.

8.7 A passive failure

A passive failure occurred where the toe of the failure of No.3 dump lay against the flank of Sache's Dam East (Figure 8.21). It would appear that this failure was due to the combination of direct pressure and shear forces, the latter being particularly high due to the movement of dump No.3. It was observed that when, due to the nature of the ground surface at the toe, failure movement in dump No.3

---

*Subscript: Normal black and white negatives are insensitive to the blue-gray colour of the dumps and failed to show up the failure clearly. However, it was found that negatives made from Kodak colour slides increase the contrast probably 2 to 3 times. All the best photographs in this section were produced by this method. The writer was made aware of this method only after he had left Cullinan.

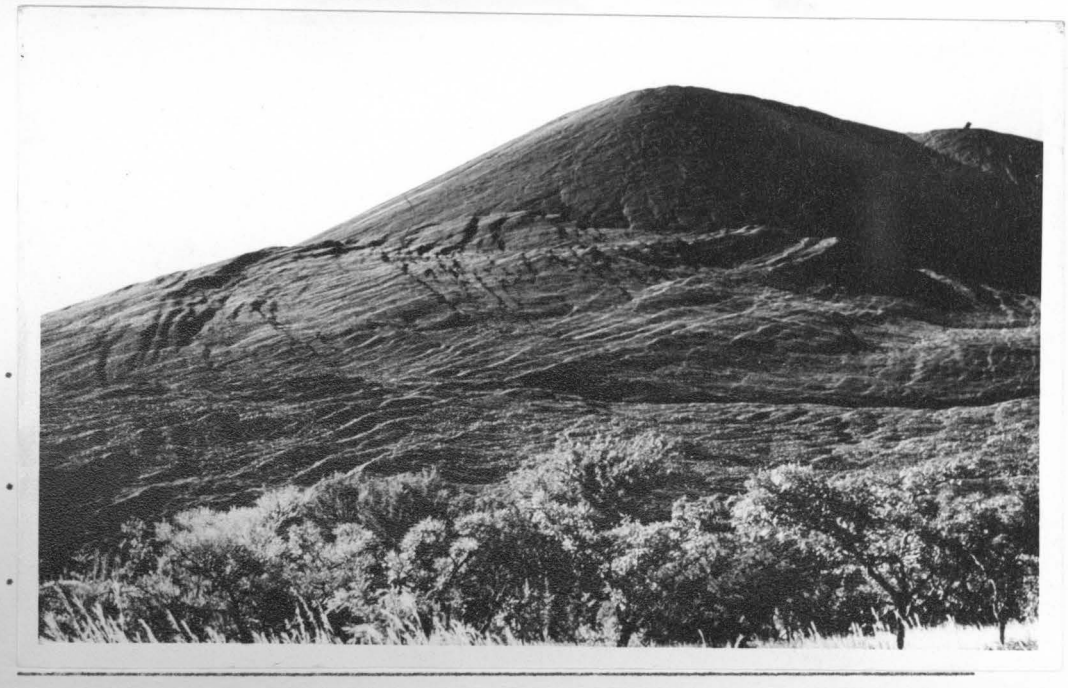

Figure 8.18 Secondary transverse failure in toe of dump No. 3. Note the two sets of curved intersecting failure lines, the zone in between subsiding.

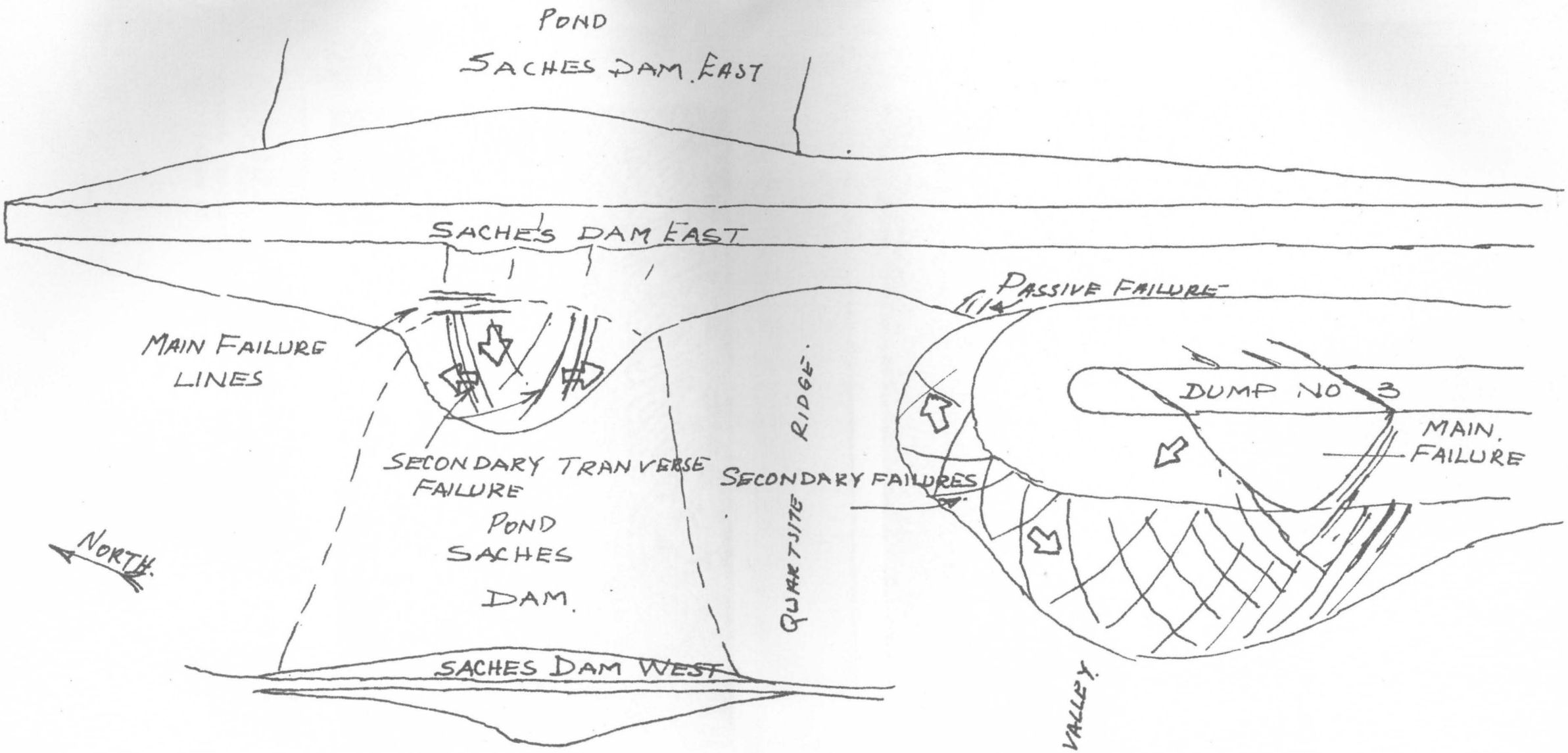

FREE HAND SKETCH OF PLAN OF SACHE'S DAMS AND DUMP NO 3 SHOWING FAILURES

FIG. 8.19

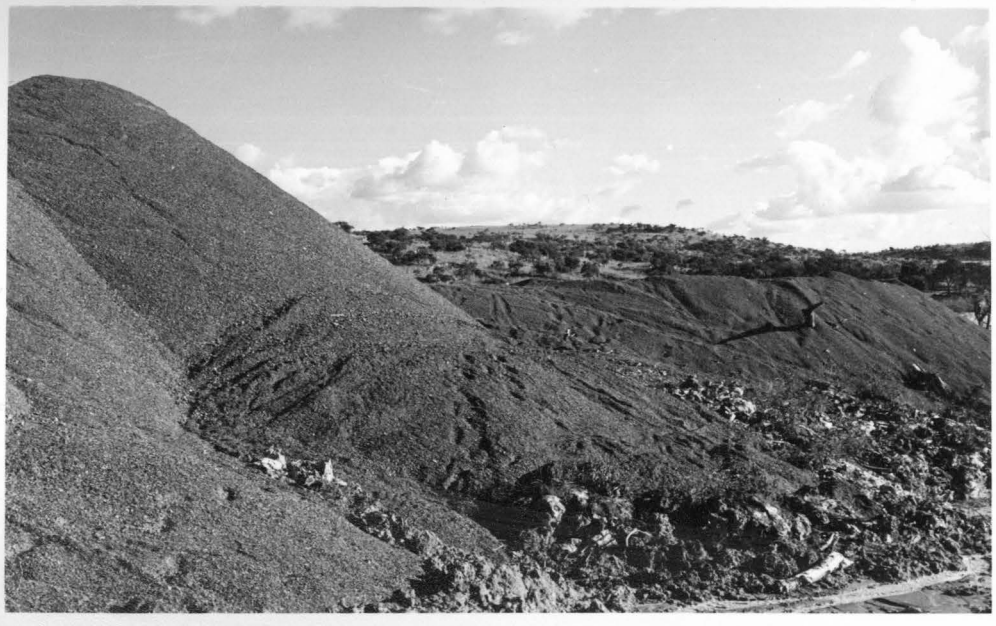



Figure 8.20 Failure of small dump on slime in pond of Sache's Dam West. Upper photograph shows slide taking place. Bottom photograph taken from the top of the small dump, shows the ridges of failure.

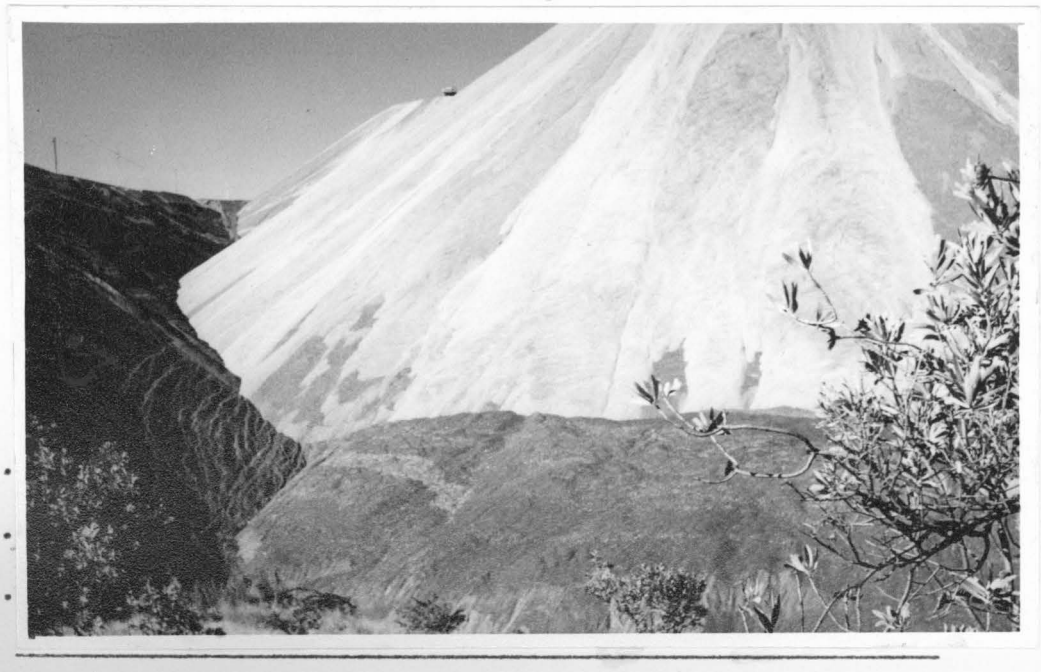

Figure 8.21 Passive failure in flank of Sache's Dam East.

ceased, the passive failure did likewise. Along the slip planes of the passive failure intense pulverisation of the particles took place.

8.8 Discussion and conclusion

Qualitatively the external indications of forms of the failures in Sache's Dam East and the surrounding dumps provide powerful evidence that the failures are of the sliding type, as predicted by the mathematical theory of plasticity for cohesionless soil media. It remains to show quantitatively by analyses such as Rendulic's using the shear strength properties of the materials that these failures are the most likely. In Section 9 the properties of the materials and in Section 10 the stability of the sliding failure in Sache's Dam East will be determined.

The relative softness of the particles compared to normal granular materials is indicated by pulverisation along the lines of slip. As the pulverised material is of a clayey nature it can cause a decrease of strength along this plane once a slip plane develops, leading to a reduction in the stability of the embankment and a tendency for the slip movement to continue along the plane.

It has been postulated that in the failure of soil masses two failure mechanisms can be distinguished - a line failure and a zone failure mechanism. (Jennings & Steffen, 1963, quoting Brinch-Hansen, 1953) Line failures are described as "kinematically possible failures" in which the rupture takes place along a cylindrical surface with the failed zone above still in an elastic state. In zone failures the rupture line is not necessarily circular, but of such a form that plastic deformation in the failed zone is required for this zone to stay in contact with the rupture

line. Plastic deformation takes place internal to the failure region, and slip lines may develop.

The failures in Sache's Dam East , the surrounding dumps and the model fall into the zone failure class. From Figures 8.13 and 6.16 it can be noted that slip lines developed internal to the failure zones. From Figure 8.13 it can be seen that both members of the intersecting set of slip lines developed, but near the sides of the failures only one member developed.

It is doubtful if under normal circumstances both members of the set of intersecting slip lines develop simultaneously. Intuitively it seems that both members could develop simultaneously only if the plastic deformation takes place on a microscale throughout the failure zone, and in such a case it is unlikely that in a completely uniform material the internal slip lines would become visible. An example of such a type of plastic failure can easily be constructed by forming an embankment of cohesionless sand on a thin flexible plate and lifting the plate by its edges. The deformation of the plate causes plastic deformation in the embankment, but no slip lines develop. This condition is approached in the left-hand side of the failure in Figure 6.16, where numerous intersecting failure lines appeared to have formed. More usually failure occurs in blocks, only the outer rupture line or lines of the block developing, but the failure block itself shifting its position as the critical region changes, causing rupture lines to appear next to the previous ones, thus leading to apparent intersection of rupture lines. Sokolovski states that the plastic theory does not predict the actual formation

of rupture lines, but only the potential for their development; furthermore through each element two potential intersecting slip lines pass. This in fact requires microplastic deformation. In practice the particular rupture line which forms depends on the distribution of weak regions in the material, making one plane slightly more favourable to rupture than another, but next to this rupture line the material may be still in a state of elastic rigidity. Once a rupture line develops the remoulding on that line will often have a tendency to reduce the shear resistance and the failure tends to persist along the projection of the line.

Plastic failure, being a propagation phenomenon, must develop from some point and spread out from there. Due to the rigid plastic postulation in the plastic theory, the time effect of propagation cannot be predicted but its effect can sometimes be discerned, as for instance in the model failure in Figure 6.7(c) where the rupture line has not fully developed through the body; in the theoretical plastic rigid material such a partially developed line could not exist, but due to elasticity and the non-uniformity of the material, this appears possible in a real material. Due to the reduction of shear strength where the rupture line forms, the line of rupture might not necessarily conform to the potential slip line as predicted by the theory; if a stability analysis could be done on the actual rupture line as against the theoretically predicted slip line, and if the true strength in the material before reduction due to remoulding could be subscribed on the rupture line, it might be found that this rupture line is not the most critical.

By the time the rupture line forms the critical condition has already been established and one could conclude that the kinematically possible rupture lines are a result of a failure condition instead of a mechanism of failure.

A further point to consider is that no solution by the mathematical theory of plasticity using the modern concepts of effective stress and pore pressure development during failure has yet been attempted. With electronic computors the problem is no longer insoluble, and it would be of interest to see if, when such a solution is eventually achieved, the form of the slip (or rupture line) would not approximate to a circle.

SECTION 9

9. PROPERTIES OF THE MATERIALS IN SACHE'S DAM EAST WALL AND THE FOUNDATIONS

9.1 Introduction

In order to perform the stability analysis of the dam wall the properties of the material out of which the wall was constructed and the soils in the foundations are required.

The material in the wall is the "tailings" or waste of diamondiferous Kimberlite, which had been crushed in order to extract the diamonds. Compared with granular materials normally used in rock-fill dams the tailings are relatively soft, to the degree that it is possible to cut the particles with a knife. It was considered that the particles might shear and crush (i.e.,"collapse") under the shear stresses and consolidation pressures expected in the wall - probably a unique situation in dam building. It was therefore of particular interest to investigate the stresses and physical conditions under which such a collapse of structure of the tailings could take place and the degree of collapse to be expected in the dam wall.

9.2 Some properties of the tailings material

9.2.1 The origin and durability of the individual particles of tailings material

The Kimberlite occurring in this pipe is of the basaltic type and highly basic. (A.L. du Toit 1934). It contains numerous minerals which decompose when exposed to air.

An examination of the old disposal dumps indicate that decomposition of the particles is confined mainly to the surface layers. Internal to the dumps little decomposition

appears to have taken place; the size grading analyses of tailings from the new dumps are statistically indistinguishable from those from the old dumps formed before 1920. Visually there was also no indication of decomposition.

The slime which is derived from the washing of the crushed rock contains a large proportion of - 2 micron material which, on flocculation by lime, settles out as a clay. The settled material has a liquid limit of 90%, a plastic limit of 44% and a linear shrinkage of 13%, making it a very active clay. This was confirmed by a mineralogical analysis of the clay which indicated a fair proportion of the clay mineral Montmorillinite.

A very fine layer of slime clay coats each of the tailings particles which probably influences the frictional properties of the tailings material.

9.2.2 The shape and particle size distribution of the tailings

The shape of the tailings is angular. The size distribution is shown in Figure 9.10. The larger size fraction predominates and the shape of the curve is characteristic of that normally found for crushed rock. The tailings do not contain the bulk of the - 12 Tyler sieve fraction, as a portion of this fraction is treated separately in the plant and disposed with the slime.

9.2.3 The permeability of the tailings

The predominance of the larger sized particles in the size distribution of the tailings has the effect of increasing the void ratio and consequently the permeability. The permeability is of importance in assessing the volume of the water that would flow through the bank should a

rupture occur in the impermeable layer on the upper-stream flank of the dam wall. This aspect is of vital importance to the safety of the dam and special measures had to be taken to prevent the rupture of the impermeable layer and, in the event of such a rupture, to reduce the danger to the stability of the wall from erosion. These measures are treated in detail in Report No. 1 (Marais 1958) and Report No. 3 (Jennings & Marais 1960). In this thesis the stability of the dam wall will be considered on the assumption that rupture does not occur.

9.2.4 Moisture content of tailings

Bank moisture content

To determine the natural bank water content of the particles, a number of samples were taken from different parts of the dam wall. The water contents ranged from 4.3 to 7.8% with a mean of 5.3%. These water contents can only be rough measures of the values in the dam wall as the samples were all taken at depths of less than 3'0" into the dam wall. However, it was noticed in experimental samples that if the water content exceeded the value of about 5.5% the water content at the bottom of the sample increased with a lapse of time indicating a gradual downward movement of the water due to gravity. It was therefore concluded that a water content between 5% and 6% was the most probable one in the bank. This range of water contents was used in all tests at bank moisture content.

Air-dried moisture content

On oven drying the tailings, the particles shattered and apparently changed their chemical composition, but this did not happen if the material was air-dried. Tests were conducted to determine the water content of air-dried tailings.

On cloudy days drying was not very effective, but on sunny days the water content was reduced to values between 1.3 and 1.9%. All tests on air-dried tailings had water contents of this order.

9.2.5 Initial density of tailings

The initial density of the tailings was determined by loose packing of the tailings in a 4-gallon drum. This gave a mean value of approximately 100 lb per cu.ft. dry density. This figure varied little with change of method of placing the tailings in the drum, or the water content of the tailings, and it was concluded that this density was the lowest which applied in the dam.

9.2.6 Maximum density of the tailings

The results of standard compaction tests on the tailings are shown in Figure 9.1; the density is not very sensitive to water content and considerable effort is required to attain a dry density of greater than 110 lb per cu.ft. With the shear failures which have taken place in the dam wall the density of the tailings tended to higher values; it is probable that the average dry density in the wall would be in the region of 105 lb per cu.ft. This value was confirmed by the results of the consolidation tests in Figure 9.26 where it can be noted that under 12 tons per sq. ft. pressure, which is the approximate magnitude of the vertical stress at the bottom of the dam, the dry density did not exceed 110 lb per cu.ft.

9.3 Choice of apparatus for consolidation and shear tests

Because of the large size of the tailings, ranging from +0.116" to -0.371", the normal apparatus for soil tests could not be used. A special giant consolidometer and triaxial

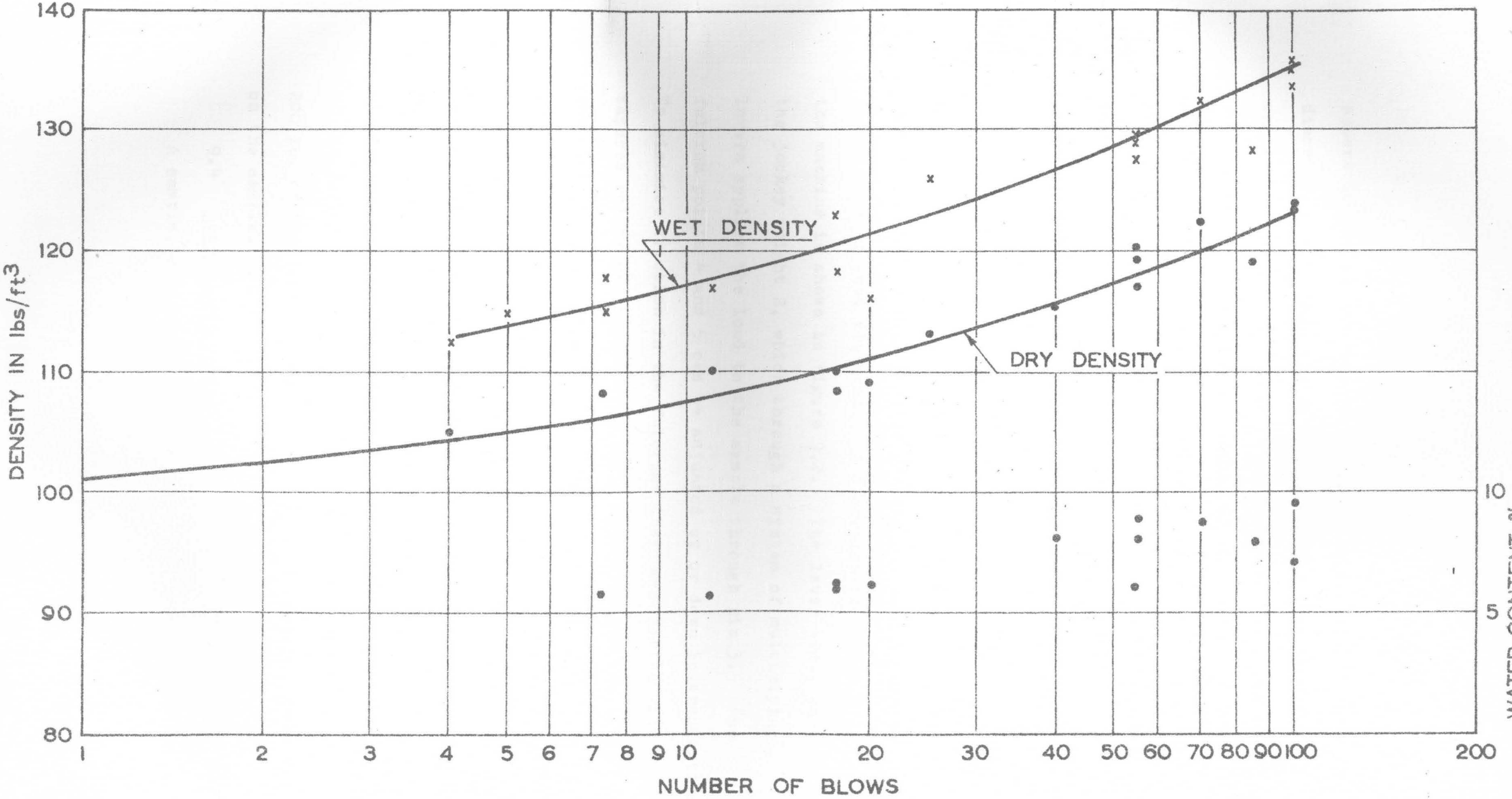

COMPACTION OF TAILINGS BY THE MODIFIED AASHO COMPACTOR

FIG 9.1

9.3(a)

apparatus was constructed for testing samples of 12" diameter. With this sample size the ratio diameter of sample to mean particle size is approximately 12 : 0.2 = 24 : 1, which corresponds approximately to a 2" diameter sample with 1 mm grains. Practical considerations required that both the consolidation and the shear tests be conducted on the same apparatus and consequently a stress control machine was selected. This was also a necessary choice if collapse tests were to be conducted.

The machine consisted essentially of a mechanism for applying the load on the sample through a system of levers and links, and a consolidometer or triaxial cell depending on the type of test required. A diagrammatic sketch of the machine is shown in Figure 9.2. The lever arm 1 carries the jockey weight 2, which through a system of multiplying levers applies the load to the sample through pin 3. The fulcrum points 4 and 5 can be adjusted up or down independently. To minimise friction in the fulcrums they are fitted with tapered roller bearings. The whole apparatus was too large for a single photograph, but an idea of the size of the apparatus can be formed from the photographs in Figure 9.3.

Calibration was carried out with a sensitive hydraulic jack fitted with a pressure gauge which had previously been standardised against a high quality testing machine. Calibration showed that the loads recorded by the position of the jockey weights on the main balance beam were within 200 lb. of the correct weight, i.e., $\pm$ 0.1 ton/sq.ft. pressure on the sample.

9.4 Sample preparation

A sample, sufficient for say six tests, was constituted

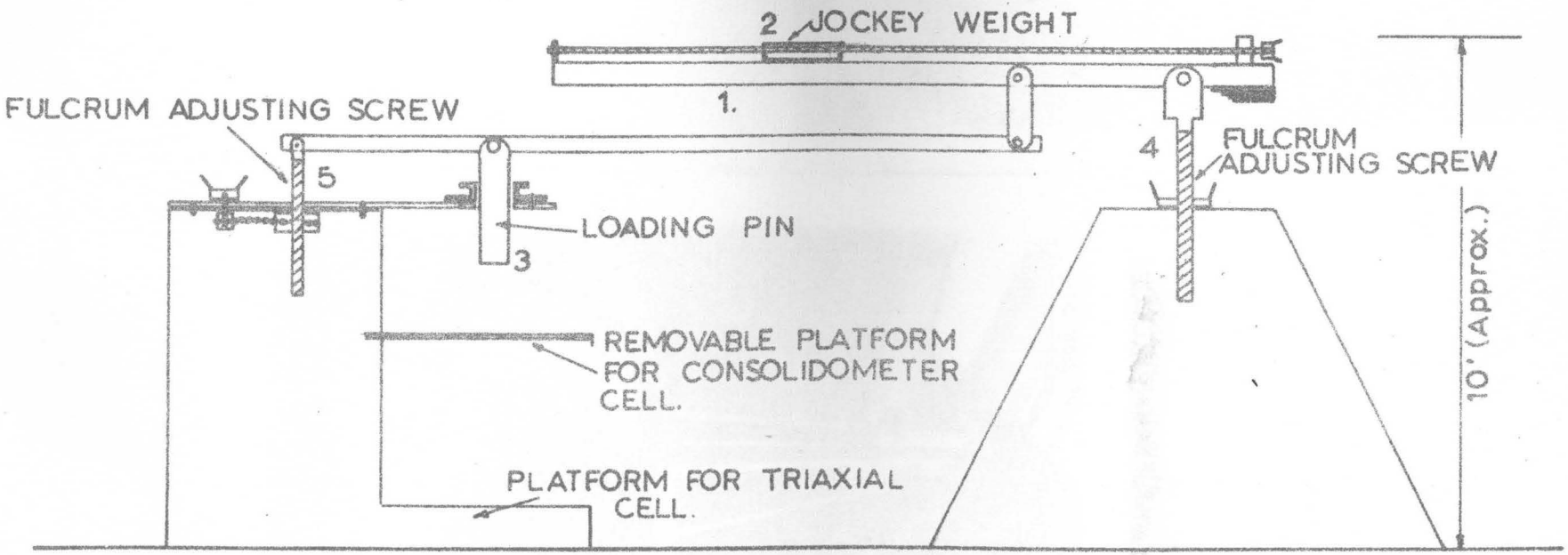

GIANT STRESS CONTROLLED TRIAXIAL – CONSOLIDOMETER

(NOT DRAWN TO SCALE)

FIG.9.2

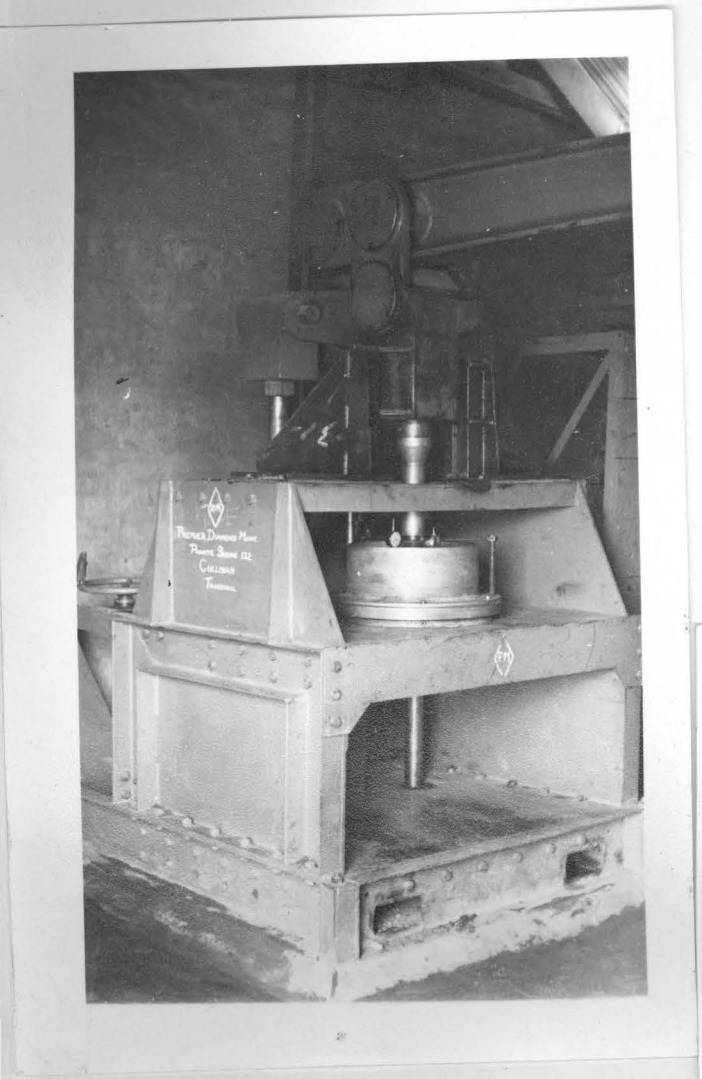

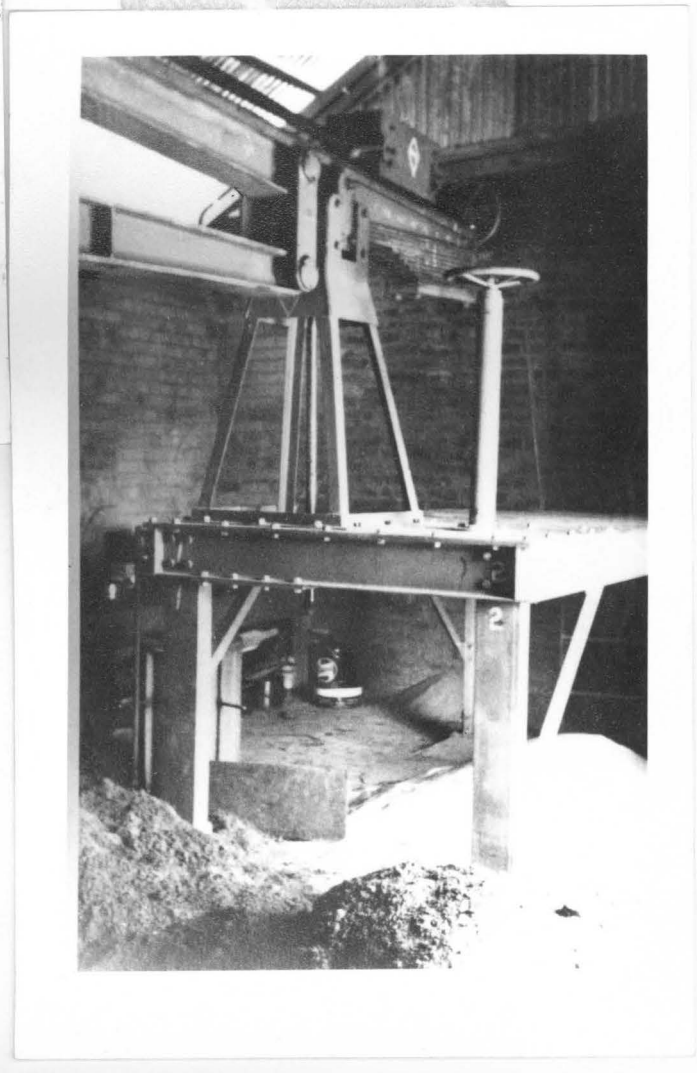

Figure 9.3 Giant stress controlled triaxial-consolidation apparatus.

from sub samples taken from the belt conveying the waste material to the disposal dumps over a period of one hour. The sample was air-dried and riffled into six portions and the water content determined. Knowing the volume of each test sample the weight of tailings was determined to give the test sample volume at a dry density of 100 lb. per cu.ft. In order to make up the sample to this weight exactly and to ensure that the grading analysis was not upset, the sample was riffled and subriffled and these portions added progressively until the required weight was attained. The appropriate amount of water was then added to the sample to bring the water content to the required value.

The test sample material was then divided into eight portions by riffling and these kept in separate closed containers until used. The object of this was to enable the test sample to be formed by adding the portions separately and thus reduce segregation - a constant problem if the sample was formed by adding all the material in one operation.

9.5 Consolidation characteristics

The object of the series of consolidation tests was to investigate:

1. the time rate consolidation and the load consolidation characteristics of tailings at air-dry and natural bank moisture contents respectively;
2. the collapse characteristics of the tailings at the two above-mentioned moisture contents.

9.5.1 Test procedure

Figure 9.4 gives the sequence of operations of putting

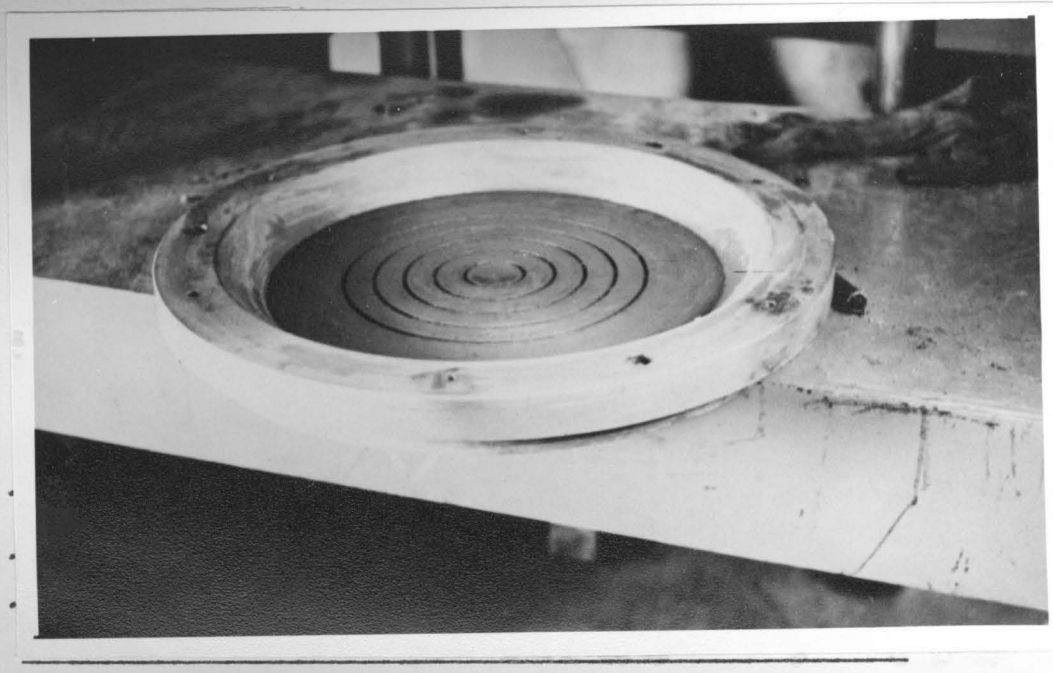

Base plate of consolidometer cell.

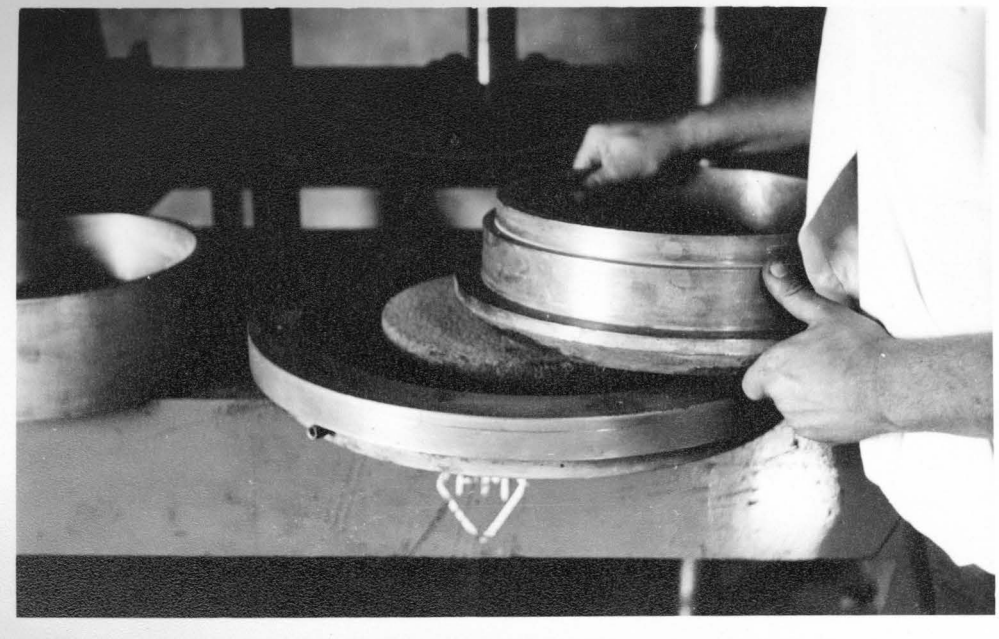

Bottom side plate and bottom drain plate (an Emery wheel with the centre hole filled with lead) placed in position.

Figure 9.4



Loose consolidometer ring slid into position.



Sample placed.

Figure 9.4 (continued)



Sample loaded,



and top side plate, top drain plate and bearing plate placed in position.

Figure 9.4 (continued)

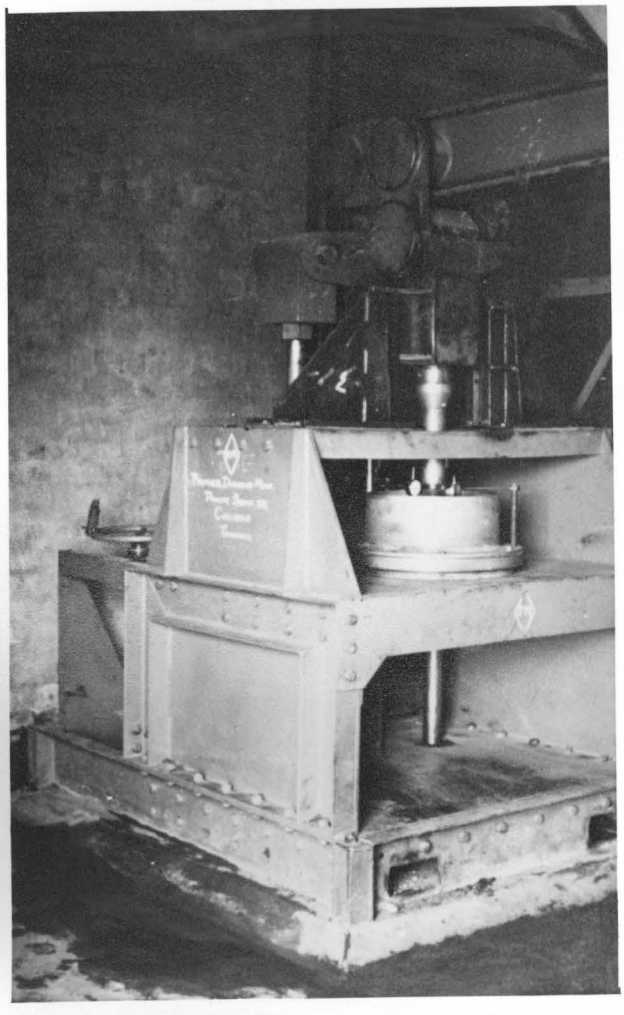

Side plate screwed on to base (to hold water during flooding). Deflection gauges fitted; 2 inch diameter ball-bearing placed on coned recess on top of base plate, and the assembly placed under the loading pin. Loading pin lowered to touch ball-bearing.

Figure 9.4 (continued)

the tailings sample into the consolidometer. After the consolidometer cell is placed in position on the machine the jockey weight is adjusted to the zero position and the loading point lowered on to the sample. The lever arm 1 (Figure 9.2) is raised by lowering the fulcrum 4 or 5. The raised lever arm is then held in position which the weight is moved to the first load. The lever arm is then released and allowed to descend, but without shock. At the same time the fulcrum 4 is lowered to keep the lever arm 1 as level as possible. The procedure for applying the first load is repeated for all subsequent loadings. From the moment the lever arm is released the consolidation of the sample is recorded at approximate equal log (time) increments.

Since the material is very freely draining a minimum time of six hours was allowed for equilibrium to be established. Each succeeding load increment was double the increment preceding, except in the case of the highest loading where a load of 60,000 lb. instead of 80,000 lb. was employed, since it was found that the machine suffered damage under the 80,000 lb. load. The standard load increments were as follows:

Table 9.1

Loading	Load on Machine lbs.	Pressure on sample. Long tons/sq. ft.
Initial load	1,250	0.71
1st Increment	2,500	1.42
2nd Increment	5,000	2.84
3rd Increment	10,000	5.68
4th Increment	20,000	11.36
5th Increment	40,000	22.73
6th Increment	60,000	34.10

9.5.2 The consolidation characteristics and tailings at bank moisture and inundation

In Figures 9.5 and 9.6 the time rate-consolidation curves for each increment of load for the tailings at 6% moisture content and inundation are shown respectively. The load-consolidation curves are shown in Figure 9.8.

9.5.3 The consolidation characteristics of the tailings at air-dried moisture content

In Figure 9.7 the time rate of consolidation curves for each increment of load of the tailings at 1.6% moisture content are shown. The consolidation curves for this test and one conducted at 0.8% moisture content, are shown in Figure 9.8.

9.5.4 Collapse characteristics of the tailings

Tests, to investigate the collapse of the tailings, were performed as follows:
Two samples of air-dried tailings were incrementally loaded to 2.84 and 22.73 tons per sq.ft. respectively. After 6 hours the samples were flooded from the bottom and the additional settlement noted over a further period of 6 hours. In figure 9.9 the load-consolidation curve for the collapse tests at 22.73 tons per sq.ft. is shown. The collapse values recorded for the tests at 2.84 and 22.73 tons per sq.ft. are shown in Figure 9.26.

These tests were repeated for tailings at 6% moisture content. On flooding no perceptible additional settlement was recorded.

9.5.5 Crushing of particles under load

During the consolidation tests clearly audible cracking was heard coming from the samples, particularly immediately after the load had been applied. This observation, together with the compression behaviour of the wet and air-dried

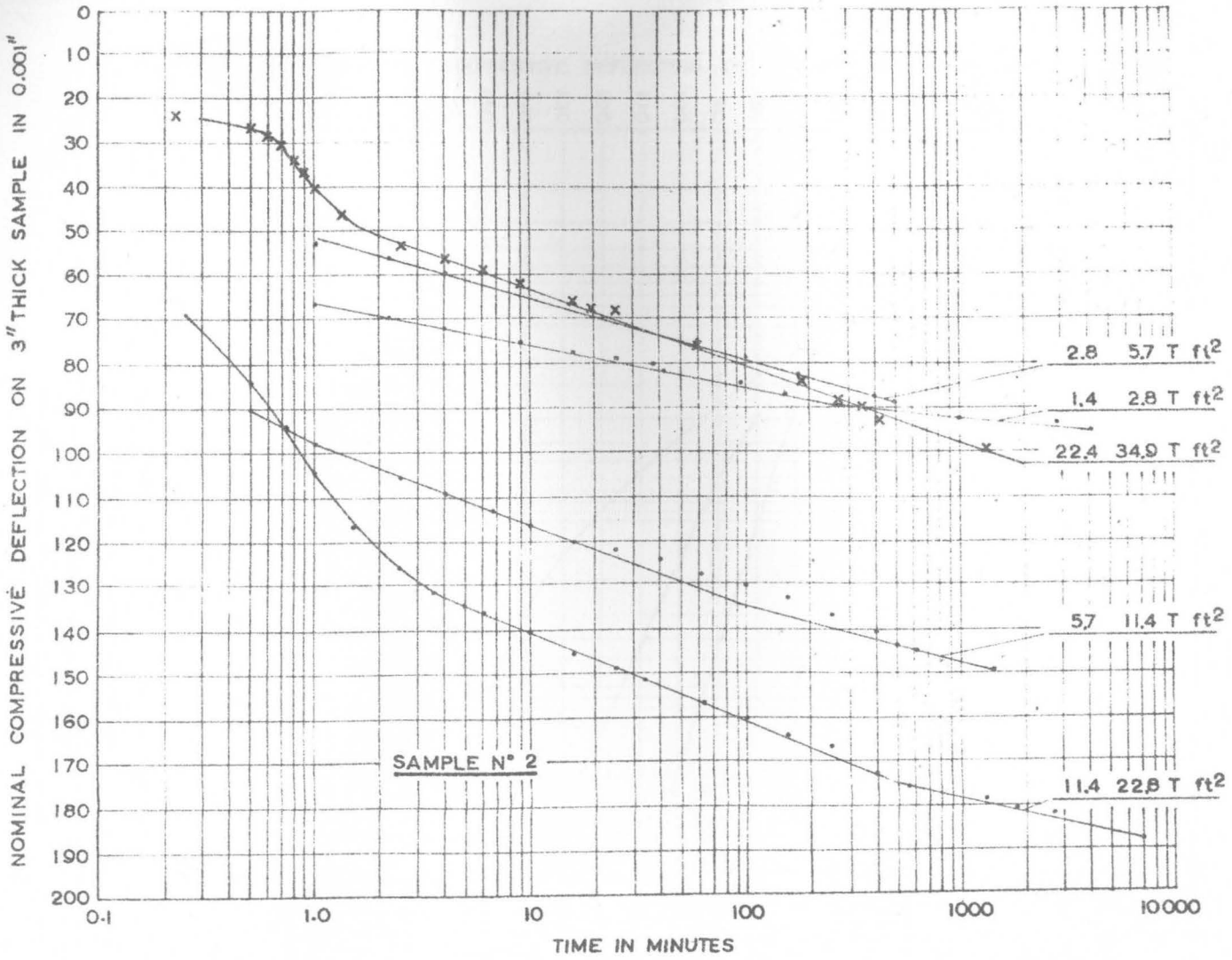

TIME CONSOLIDATION CURVES FOR TAILINGS
IN GIANT CONSOLIDOMETER

SAMPLE SIZE 12"dia. x 3".thick
WATER CONTENT 6 %

FIG.9.5

9.8(a)

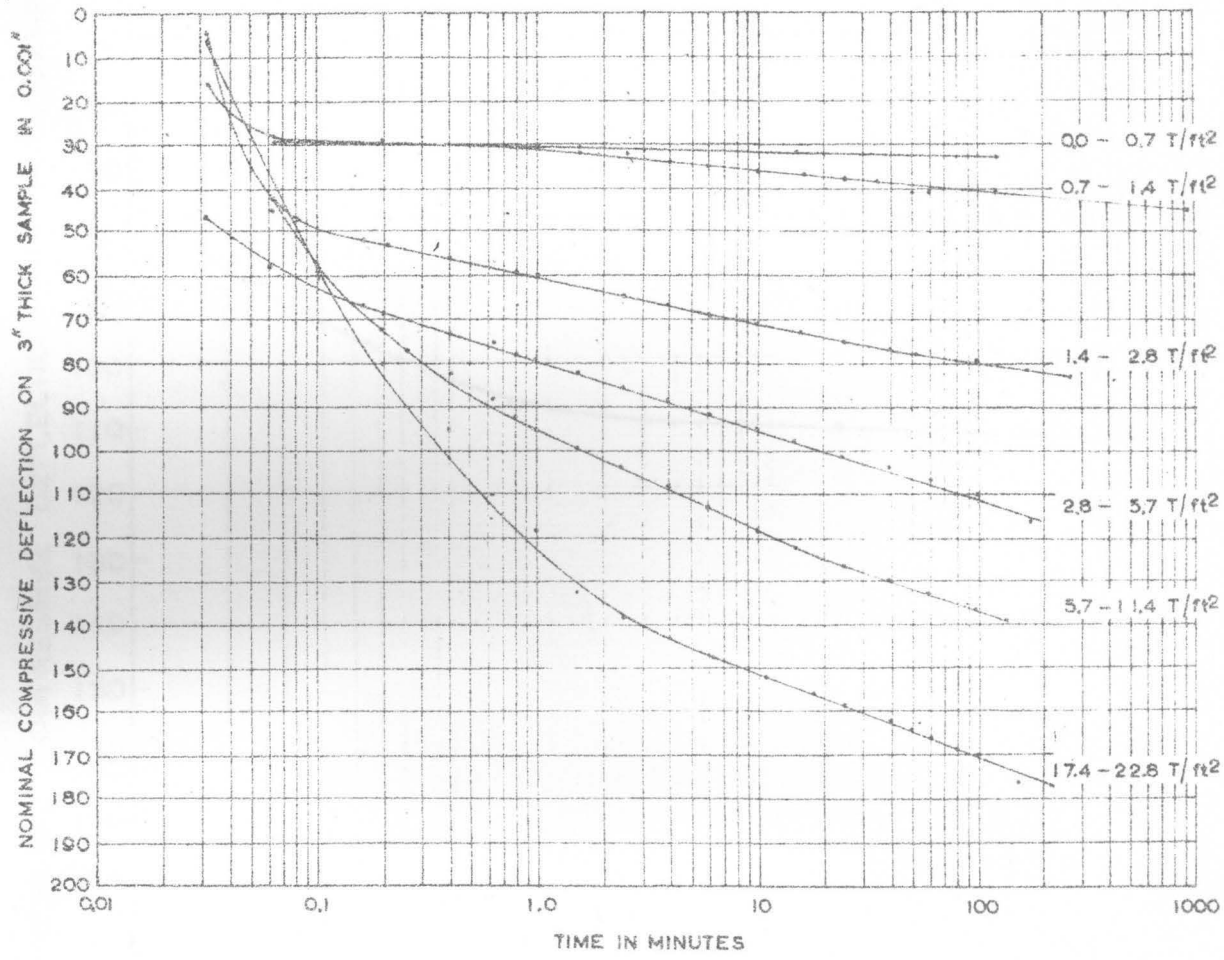

TIME CONSOLIDATION CURVES FOR TAILINGS
IN GIANT CONSOLIDOMETER

SAMPLE SIZE: 12" dia x 3" thick
WATER CONTENT: INUNDATED DURING TEST

FIG. 9.6

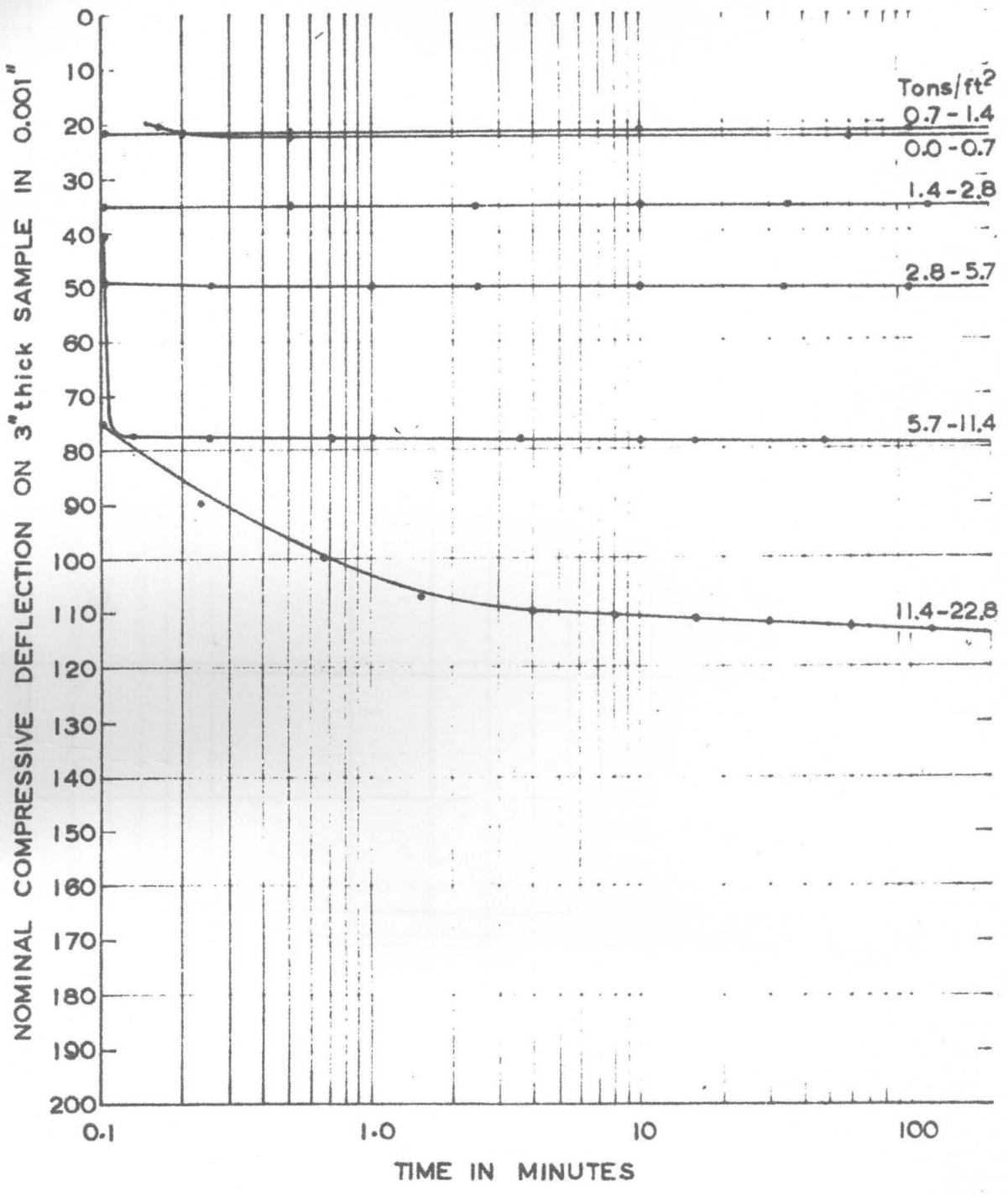

TIME CONSOLIDATION CURVES FOR TAILINGS
IN GIANT CONSOLIDOMETER

SAMPLE SIZE 12" dia x 3" thick
WATER CONTENT AIR DRY 1.6%

FIG. 9.7

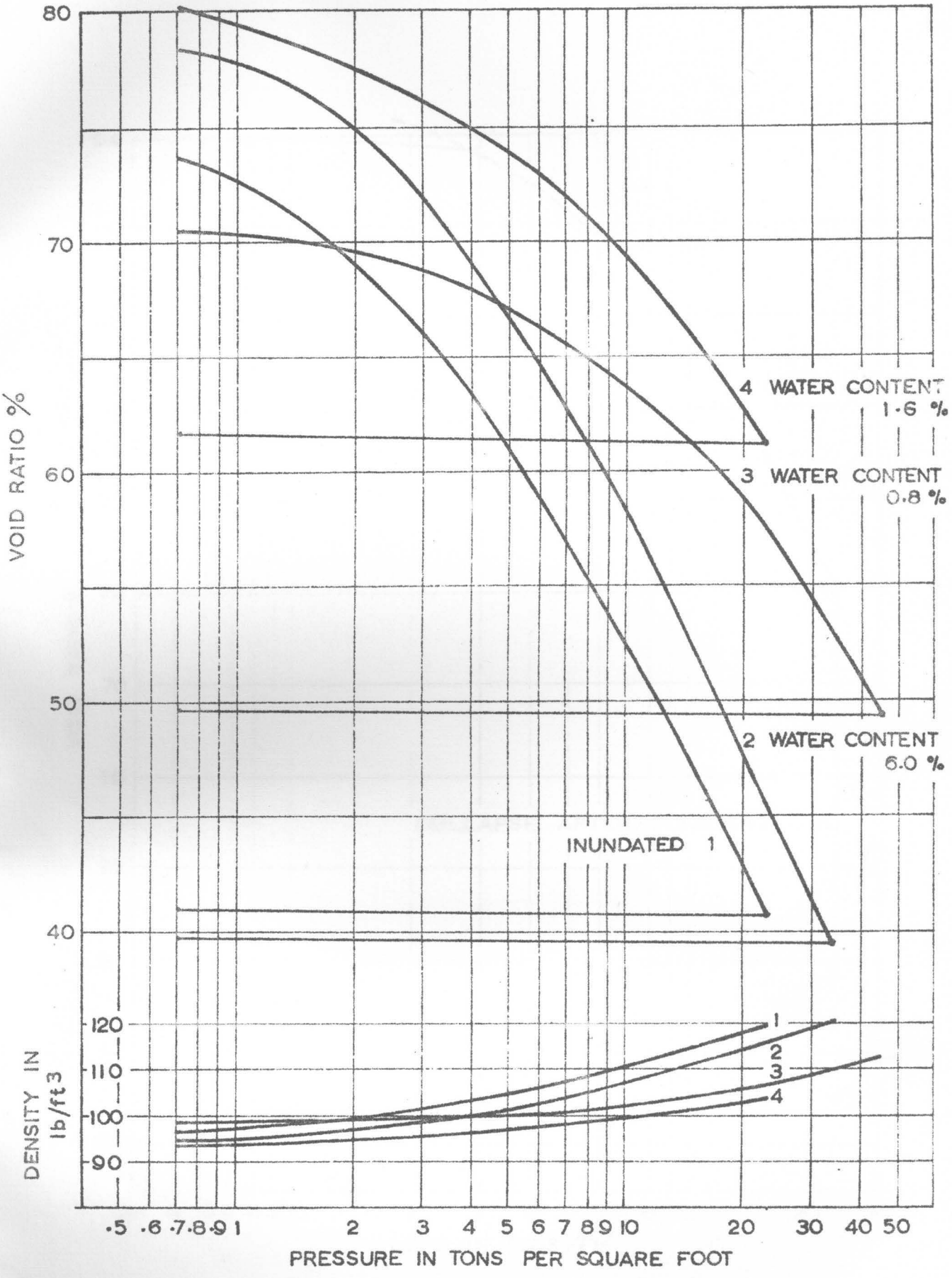

CONSOLIDATION PRESSURE & DENSITY PRESSURE RELATIONSHIP
FOR
AIR DRY & WET TAILINGS IN GIANT CONSOLIDOMETER
SAMPLE SIZE – 12" Dia. x 3" THICK

FIG. 9.8

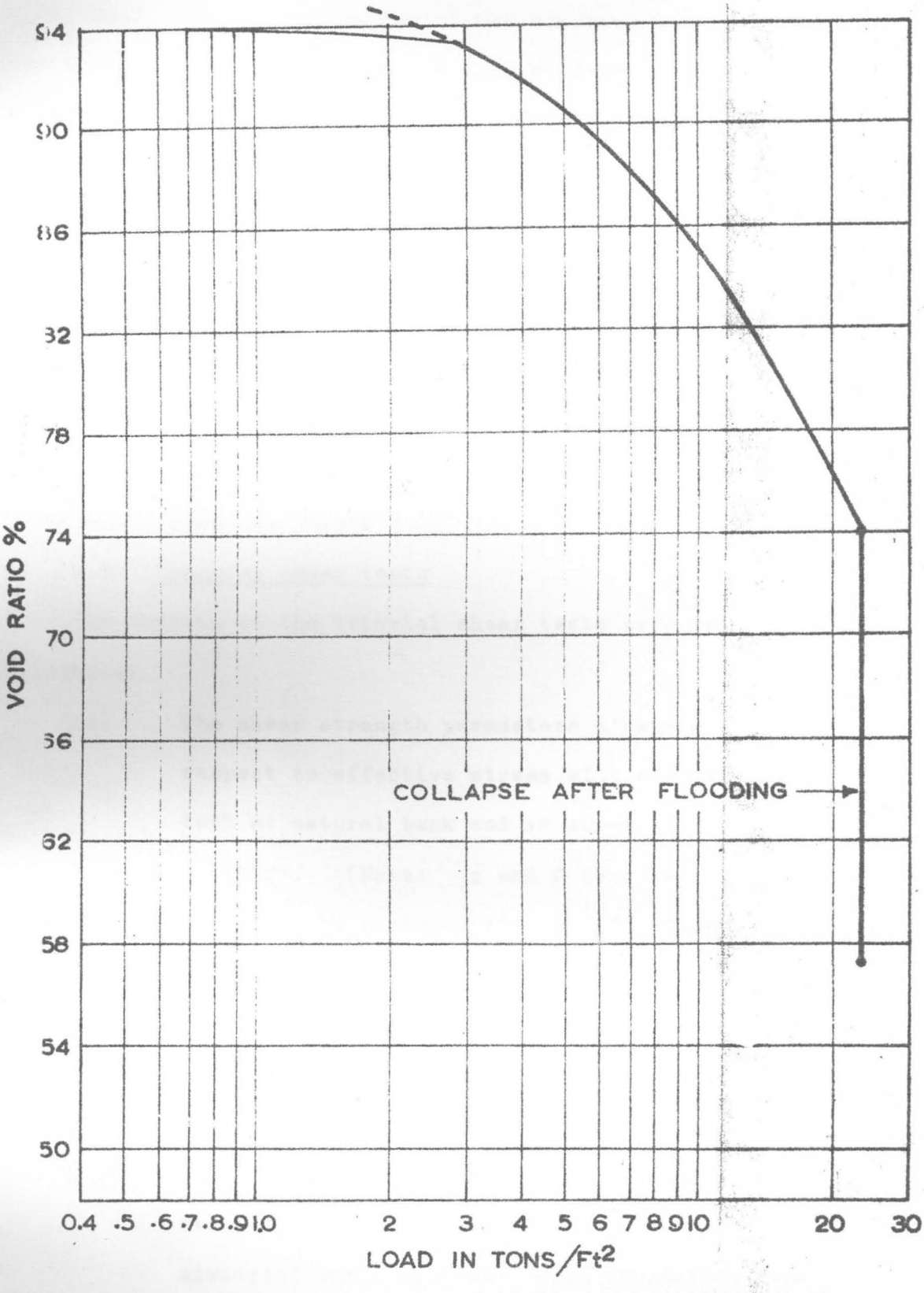

COLLAPSE CHARACTERISTICS OF AIR DRY TAILINGS
IN GIANT CONSOLIDOMETER
WATER CONTENT BEFORE FLOODING 1.1 %

FIG. 9.9

samples, led to the belief that the particles were crushing under load. An investigation of the crushing of the particles during compression was made as follows:
A grading analysis of an air-dried sample sufficient for two tests was made. It was then divided by riffling into two equal samples, and the moisture content of one of the pair raised to about 6%. Consolidation tests to a maximum pressure of 34.10 tons per sq.ft. were then conducted on the two samples. The wet tailings test sample was air-dried and a grading analysis made of each sample. Grading analyses of the pair before and after loading are shown in Figure 9.10.

9.6 Triaxial shear tests

The objects of the triaxial shear tests were to determine:

(i) The shear strength parameters c' and Ø' with respect to effective stress with the tailings both at natural bank and at air-dried water contents. (Note: c and Ø here designate cohesion and angle of internal friction respectively.)

(ii) The load : deflection and load : volume change relationships of the tailings both at the natural bank and air-dried water contents.

(iii) The collapse characteristics and loss of shear strength of the tailings of natural bank and air-dried water contents, when inundated.

9.6.1 Pressure application

The arrangement for application of cell pressures is shown in Figure 9.11. It consists essentially of a

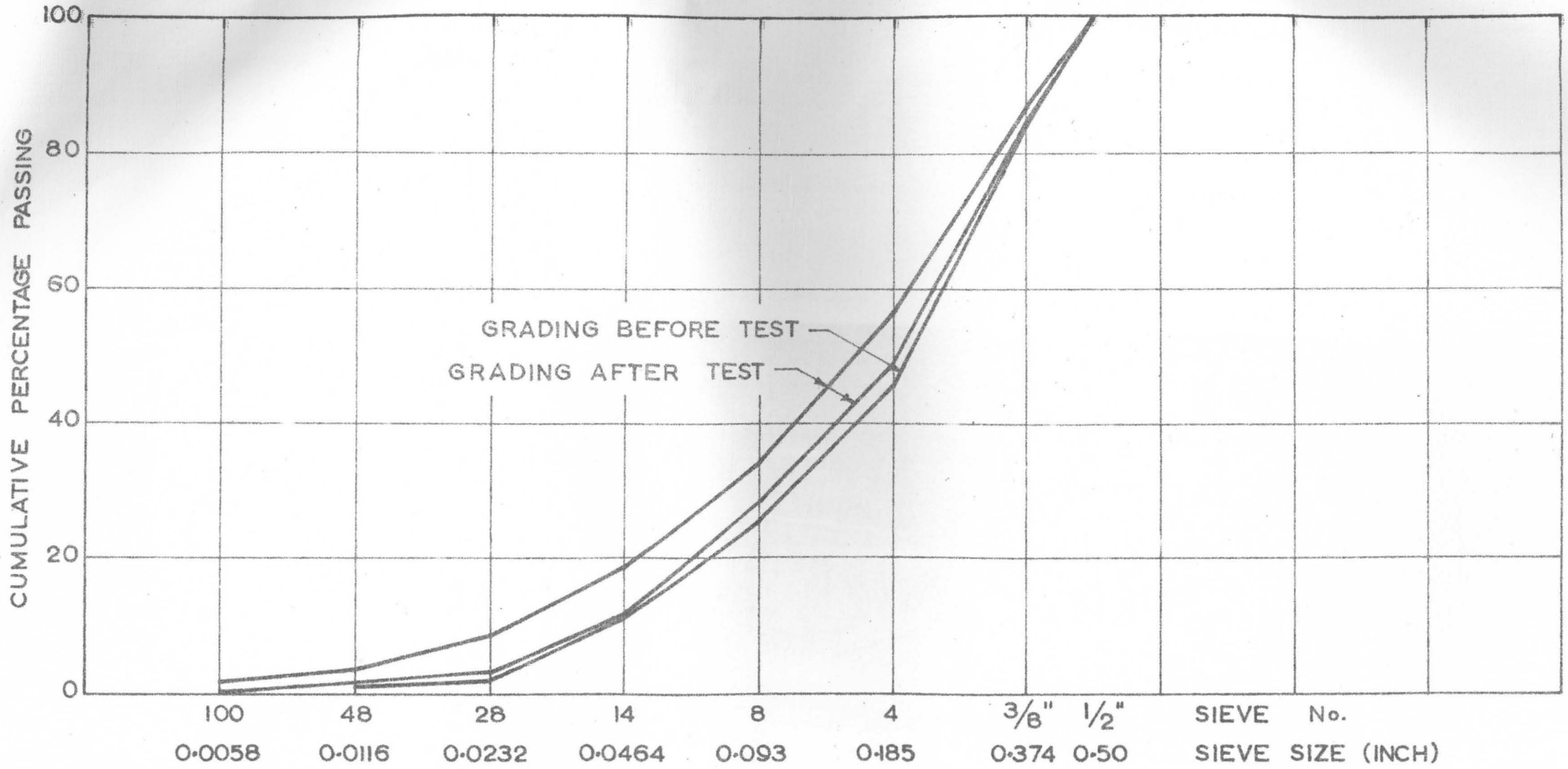

GRADING ANALYSES OF TAILINGS IN GIANT CONSOLIDOMETER BEFORE & AFTER TEST

MAXIMUM CONSOLIDATION STRESS 34·1 TONS/Ft^2 WATER CONTENT 6% & 1%

GRADING BY DRY SIEVE ANALYSIS MATERIAL AIR DRIED BEFORE SIEVING

FIG. 9.10

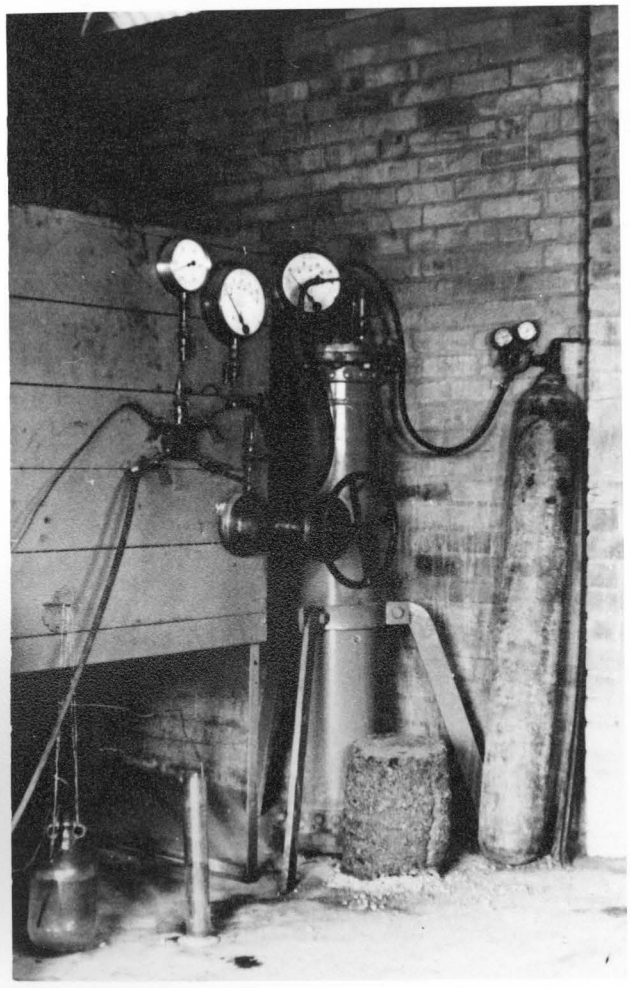

Figure 9.11 Photograph shows compressed air bottle on right to supply air to cylindrical reservoir. Note the star manifold with leads to triaxial cell, hand pressure control and grease pressure seal. The apparatus for measuring volume changes can also be seen below the display board.

cylindrical reservoir, 8 ft. high x 12 in. diameter, which contained water in the lower half and air, under pressure from an air bottle, in the upper half. Water under pressure from the reservoir is connected through a valve to a star manifold which leads (with valves) to the triaxial cell, the pressure gauges, the grease pressure seal at the triaxial cell loading pin, and the hand pressure control cylinder designed to provide positive or negative pressures in the system.

The grease pressure seal is a special feature of the apparatus (Figure 9.11(a)).The hydraulic lead from the star is connected to the bottom of a cylinder containing a free piston with water below and motor-car gearbox grease above the piston. From the top of the cylinder a ¼-in. copper pipe leads to a groove around the internal diameter of the gland through which the triaxial pin operates. After the loading pin is slid into position (Figure 9.12(1)) by closing off all the valves at the star except those leading to the hand control and the grease cylinders, grease is forced into the groove by means of the hand control cylinder. These valves remain open during the subsequent pressure application to the cell, and as the pressure in the gearbox grease equals the cell pressure in the triaxial cell, the groove forms an effective water seal, the grease only welling out past the pin. The seal worked completely satisfactorily for pressures up to 100 lb per sq. in. for periods up to 6 days.

9.6.2 Measurement of volume changes

Volume changes in the sample of tailings, contained between the top and bottom loading plates and the rubber

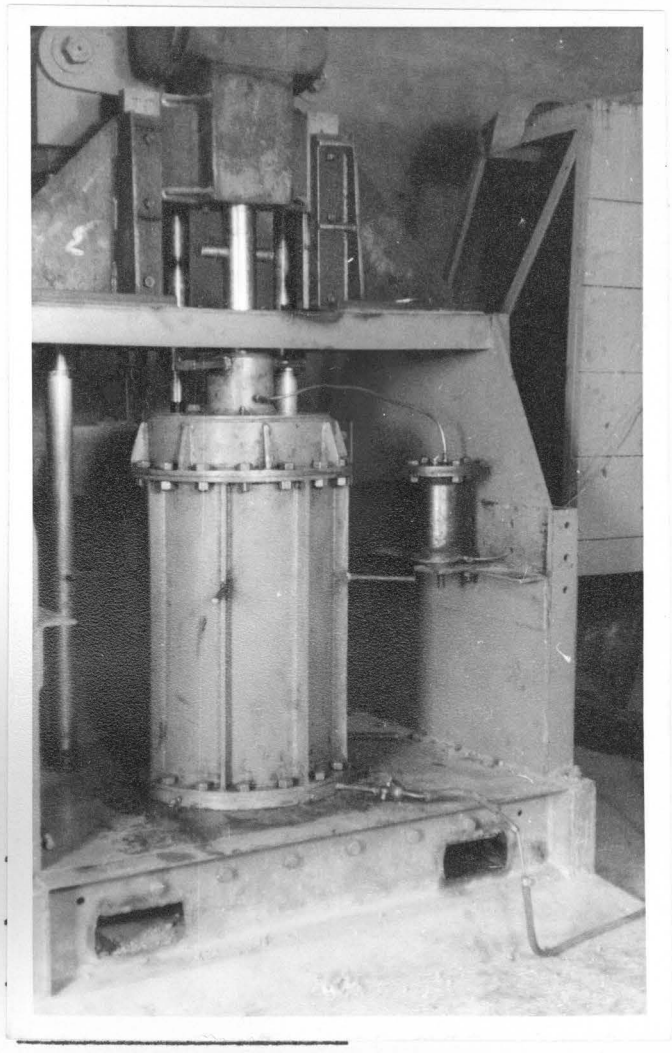

Figure 9.11(a) Photograph of grease pressure seal apparatus. The small cylinder on the right contains a loose piston with grease above and water below. The grease is forced into the groove around the triaxial cell gland.

membrane,were observed by measuring the volume of air expelled from the voids of the tailings. A lead was taken from the bottom loading plate into a 1-gallon glass bottle fitted with a tight rubber stopper. This lead was connected with the air in the upper part of the jar. The jar was filled about three-quarters with water. Another pipe extending to the bottom of the jar, well below the water surface, was also taken through the rubber stopper and carried freely downward below water level in a 1000 c.c. measuring cylinder. Atmospheric pressure in the voids is established when the water levels in the bottle and cylinder are at equal levels. As air is expelled from the voids of the tailings the pressure in the bottle is increased and water flows to the cylinder. By adjusting the level of the cylinder so that the water levels in the cylinder and bottle remain the same, volume changes of the tailings sample may be observed as changes of the volume of water in the cylinder.

9.6.3 Placing of the triaxial sample

In placing the sample, an initial dry density of 100 lb per cu.ft was again employed. The sequence of operations in placing the sample is shown in Figure 9.12:

The rubber membrane is slipped over the bottom bearing place (Figure 9.12(a)) and two ¾-in. diameter rubber rings rolled into position (Figure 9.12(b)). A strap, the ends of which overlap, is screwed tight onto the rubber bands, thus preventing ingress of the cell water, under pressure, into the sample (Figure 9.12(c)). The sample former (Figure 9.12(d)) is fitted on the bottom bearing plate and the rubber membrane folded over the top.

The sample, which had previously been riffled into eight



Figure 12(a) Base plate of triaxial cell.



Figure 12(b) Rubber membrane slipped on to bottom bearing plate and rubber rings rolled on.



Figure 9.12(c) Strap around rubber rings tightened.



Figure 9.12(d) Sample former.

sub-samples, is then placed in the former (Figure 9.12(e)) and the top bearing plate placed in position. The membrane is folded back over the plate (Figure 9.12(f)) and the rubber rings rolled on (Figure 9.12(g)). The top strap is tightened around the rubber rings. A lead from the sample through the bottom bearing plate is connected to the hand pressure control cylinder, and a negative pressure of $\pm$ 2 lb per sq. in applied (Figure 9.12(h)). The valve on the star controlling the lead to the sample is closed, the former removed, and the lead from the top of the sample connected to the bottom (Figure 9.12(i)). The negative pressure holds the sample rigid. The cell cylinder is placed over the sample, the cylinder top fitted and the assembly secured air-tight by tightening the joint bolts (Figure 9.12(j)). The loading pin is slipped into position (Figure 9.12(k)) and the cell moved into position under the load point, which is lowered to touch the loading pin. The grease pressure seal apparatus is fitted (Figure 9.12(l)) and the pressure seal is established by forcing grease into the groove around the loading pin. The cell is now filled with water and connected to the star. A pressure of $\pm$ 2 lb per sq. in is applied to the cell water by means of the hand pressure control cylinder, and the negative pressure inside the sample is released. The volume-measuring apparatus is connected to the bottom of the sample. The valve to the pressure reservoir is opened to the star, which applies the pre-determined pressure to the sample and the grease seal.

Six hours was allowed for the sample to consolidate, and the deviator stress load applied in a manner described in the first paragraph of Section 9.5.1.



Figure 9.12(e) Sample placed in the former.

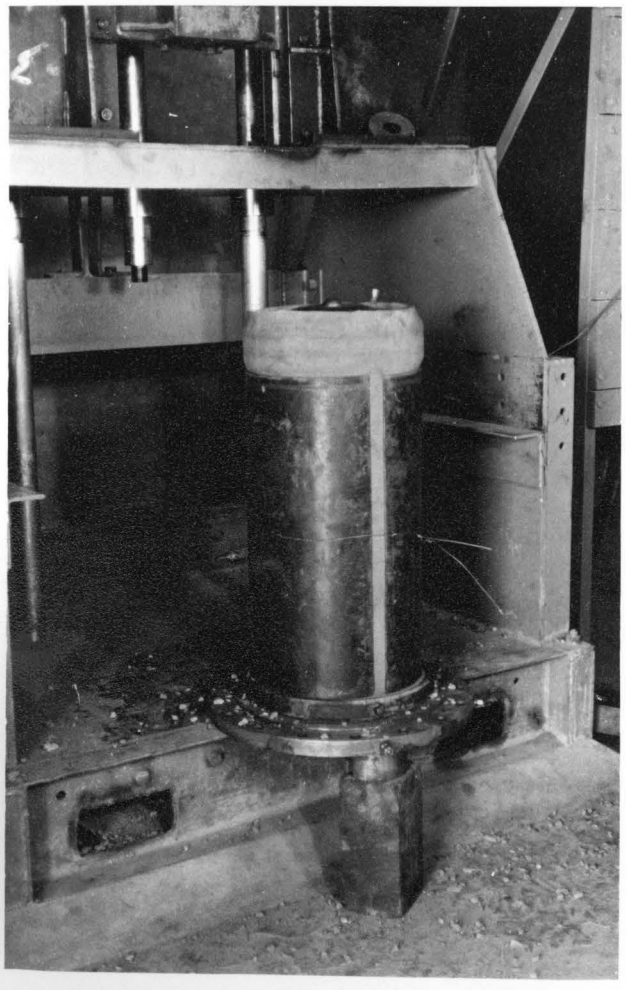

Figure 9.12(f) Rubber membrane folded over the top bearing plate.

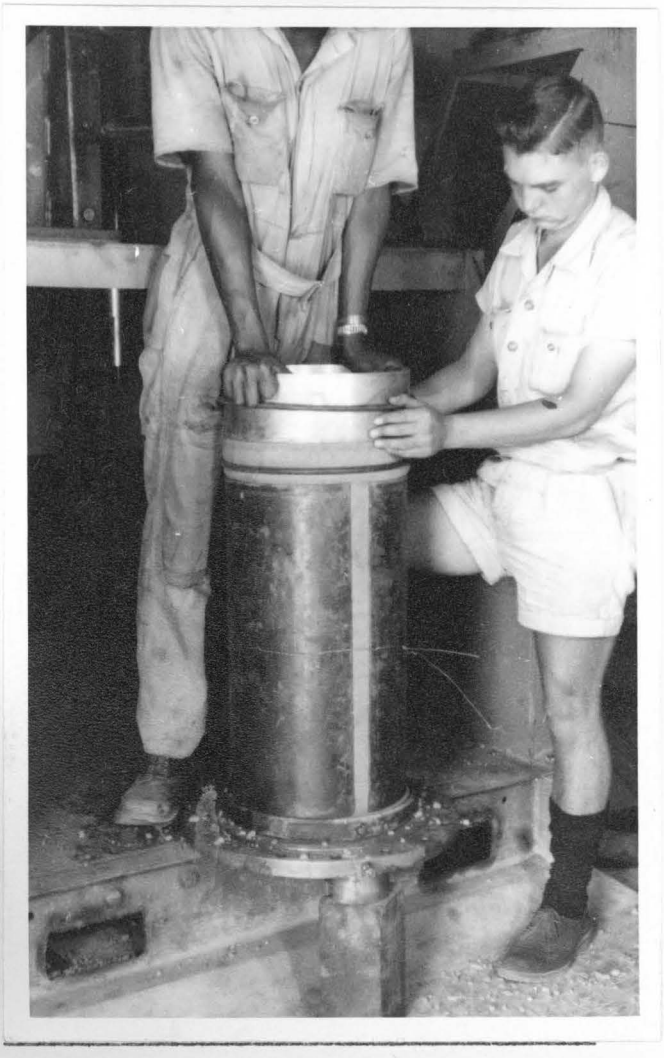

Figure 9.12(g) Rubber rings rolled on.

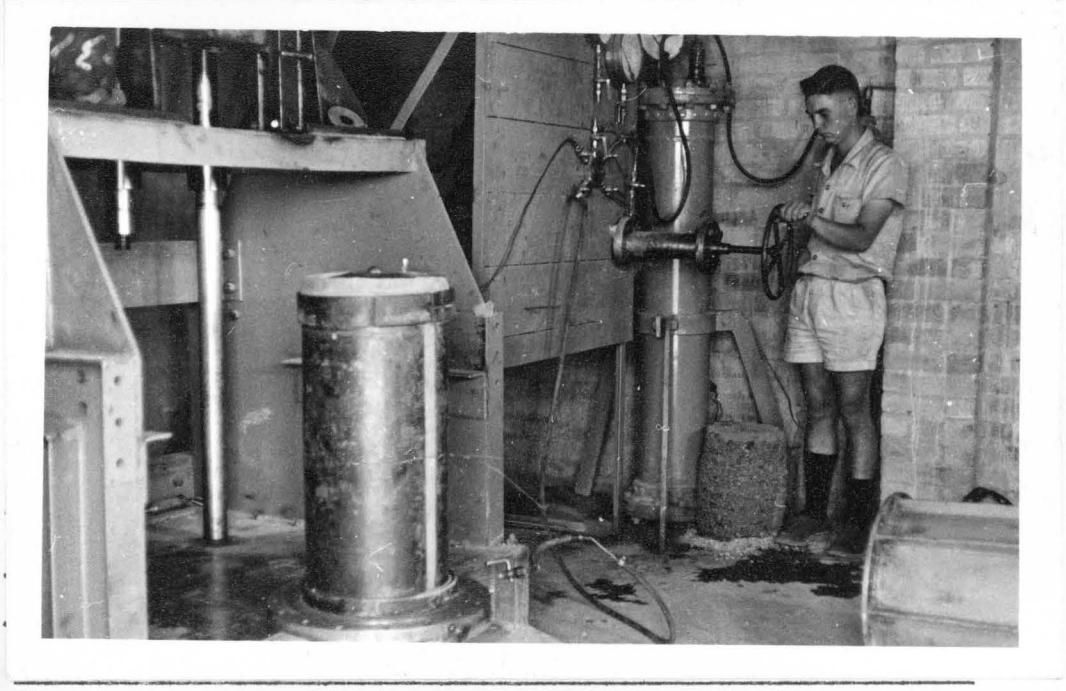

Figure 9.12(h) Top strap tightened, hand pressure control cylinder fitted and negative pressure applied to sample.



Figure 9.12(i) Sample under negative pressure.

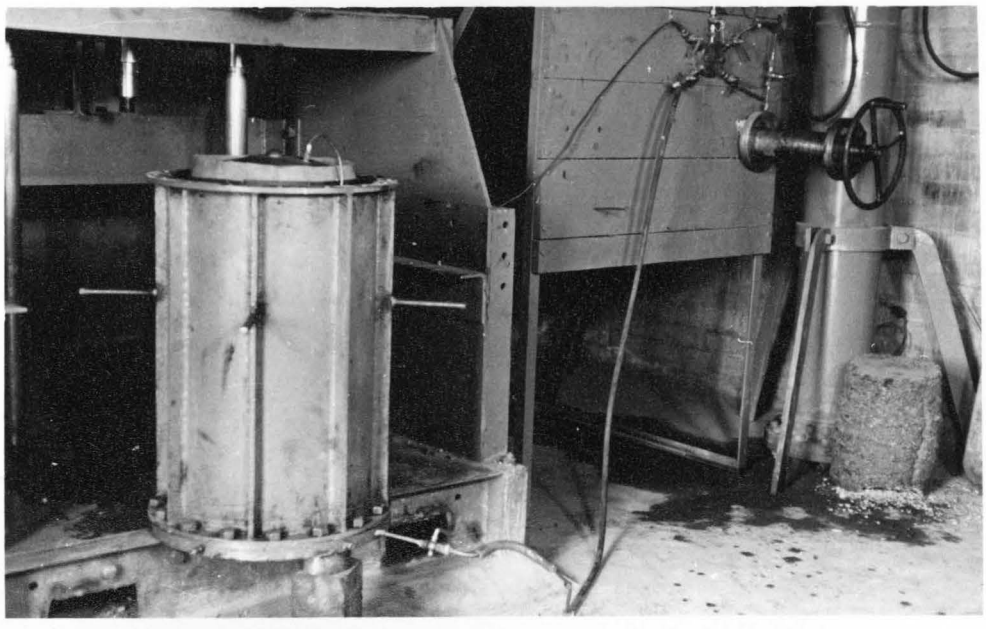

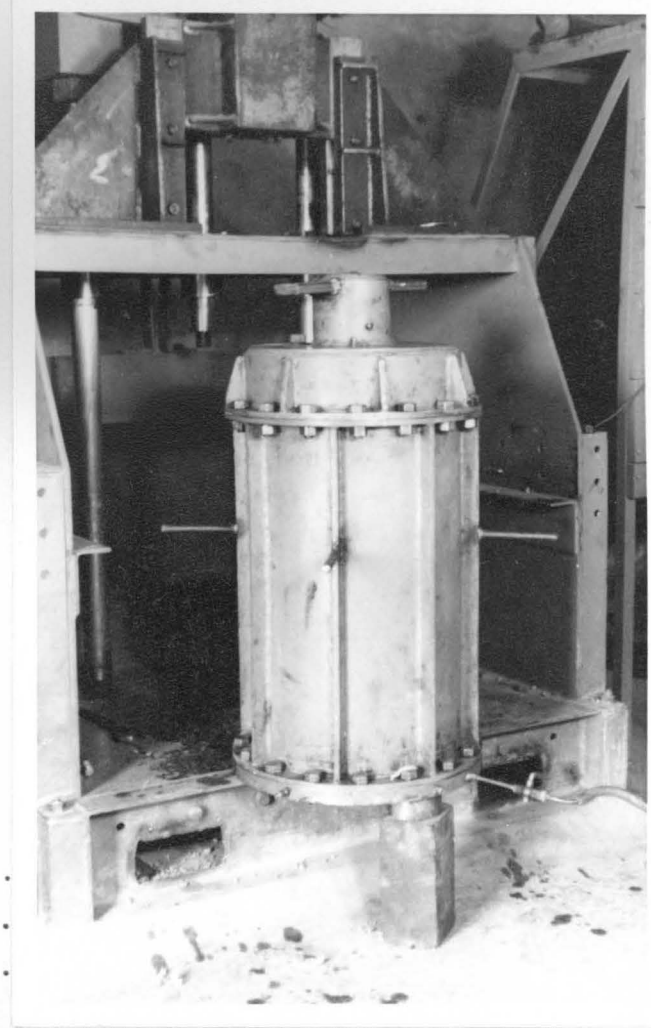

Figure 9.12(j) Cell cylinder placed over sample and cylinder top fitted.



Figure 9.12(k) Triaxial cell pin slipped into position.

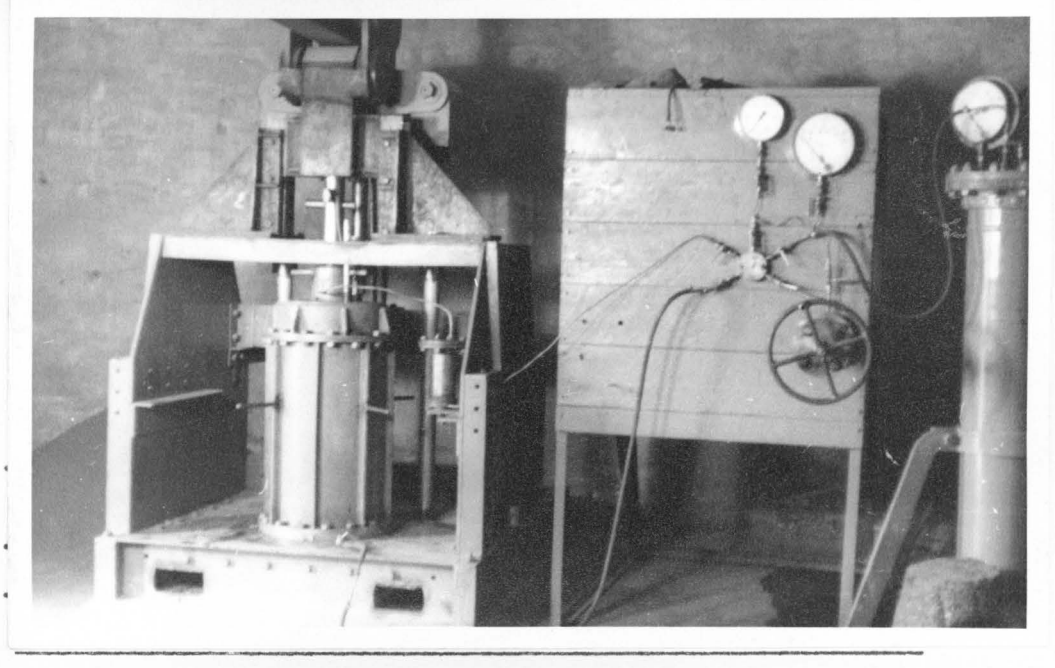

Figure 9.12(l) Pressure seal apparatus fitted and cell moved into position under loading pin. Loading pin lowered to touch the triaxial pin.

Initially trouble was experienced with puncturing of the rubber membrane on the sharp edges of the particles of the tailings. A solution was to use two 1/16 in. thick unvulcanised rubber sheets, glued together only at the edges. The inner membrane was cut but in this it protected the outer membrane.

9.6.4 Load increments

In all triaxial tests the load increments found most satisfactory were:

Consolidation Pressure lb per sq. in.	Deviator Stress $(\sigma_1 - \sigma_3)$ lb per sq. in. on 12" sample	Jockey Load Position lb
100	22.05	2,500
50	22.05	2,500
25	11.02	1,250

9.6.5 Duration of load application

Appreciable creep effects were observed after each application of load and an arbitrary limit of rate of deflection of 0.002 in.min. was set as the indication of equilibrium after the application of a load increment. This gave times per increment varying from about 15 minutes for the lower loads to about 30 minutes for the higher loads. Volume changes were measured at equilibrium at the end of each load application.

9.6.6 Consolidated drained shear tests of tailings at natural bank moisture

The consolidating pressures were 25, 50 and 100 lb per sq. in. respectively, the initial dry densities approximately 100 lb per cu. ft and the moisture contents approximately 6%.

Figures 9.13, 9.14, 9.15 and 9.16 show the axial deflections versus the log of time for each load increment, Figure 9.17 shows the stress-strain curves and volume changes during the test, and Figure 9.18 shows Mohr's envelope of failure.

9.6.7 Consolidated drained shear tests of air-dried tailings

These tests were conducted exactly as for the tests at natural moisture content, except that the water content of the samples ranged from 1.3 to 1.9%. Figures 9.19, 9.20 and 9.21 show the axial deflection versus the log of time for each load increment, Figure 9.22 shows the stress-strain curves and volume changes, and Figure 9.23 shows Mohr's envelope of failure.

9.6.8 Collapse tests

The samples were consolidated under 50 lb per sq.in. and then incrementally loaded until the value of the deviator stresses were approximately one half, or three-quarters, of the estimated failure stresses. This gave two deviator loads of approximately 10,000 and 12,000 lbs which corresponded to deviator stresses of 88.3 lb per sq. in. and 110.5 lb per sq. in. respectively. The samples were then inundated by forcing water at low pressure through the bottom lead until it escaped from the top lead. The additional deflections were recorded at intervals for a period of six hours.

Two series of tests were carried out. The first series was on samples at 6% moisture content and the second series on samples at air-dried moisture content. Figures 9.24 and 9.25 show the axial deflections versus

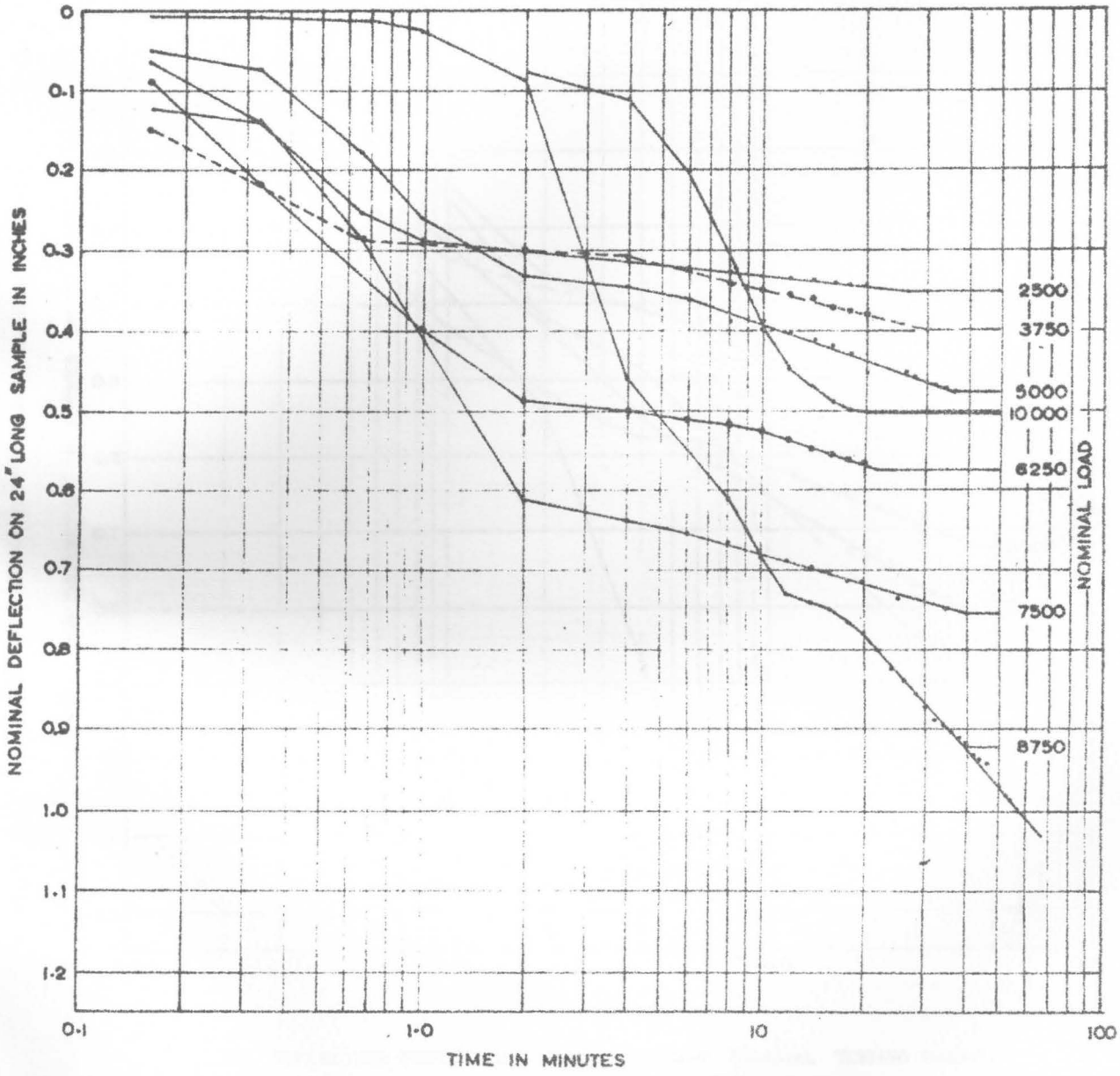

TIME DEFLECTION CURVES FOR TAILINGS IN GIANT TRIAXIAL TESTING MACHINE

TEST : CONSOLIDATED DRAINED STRESS CONTROLLED CONSOLIDATING & LATERAL STRESS : 25 psi

WATER CONTENT : 6 % INITIAL DRY DENSITY : 100 lbs/Ft^3 SAMPLEESIZE : 12" dia x 24" LONG

FIG.9.13

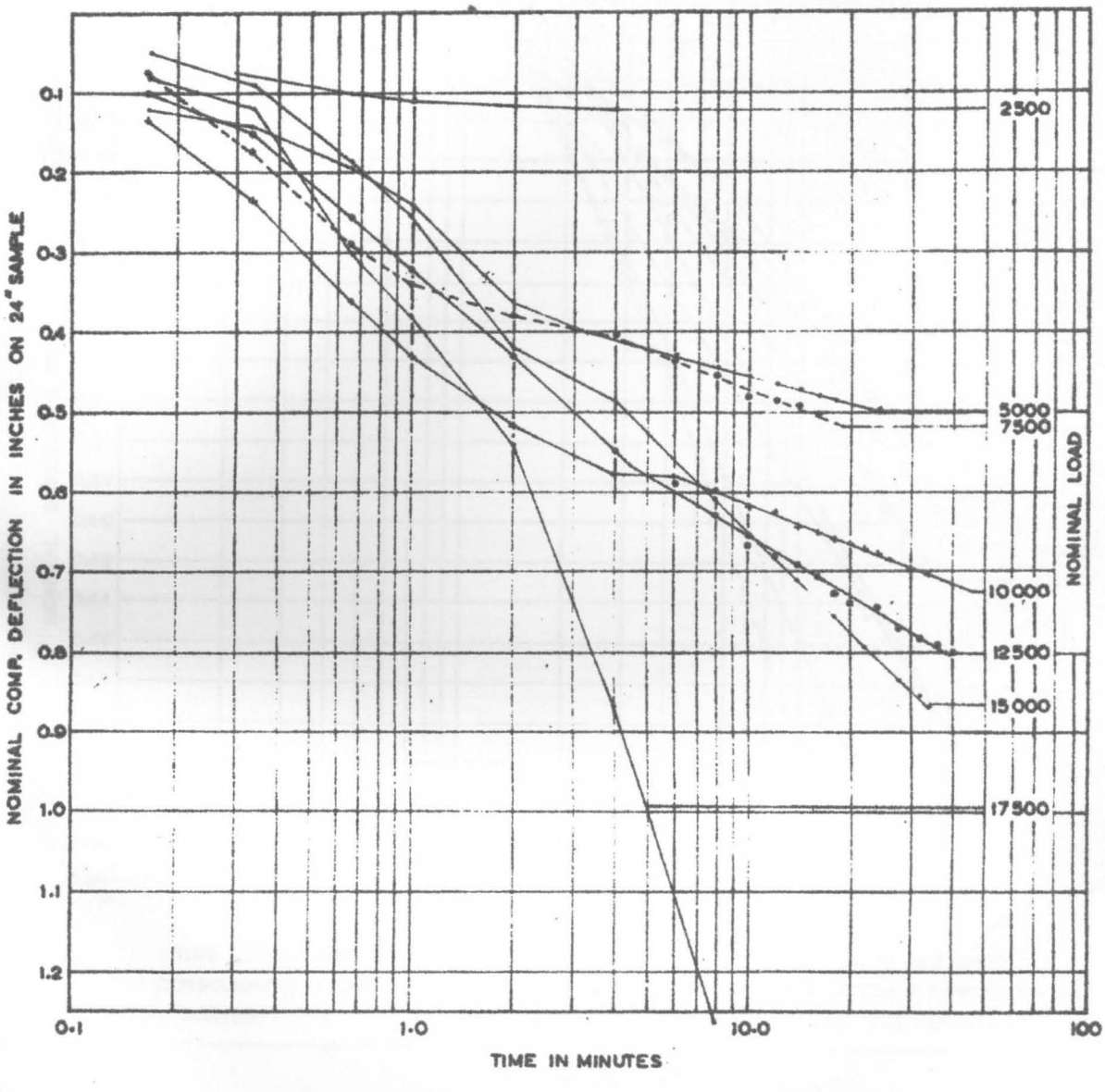

TIME DEFLECTION CURVES FOR TAILINGS IN GIANT TRIAXIAL TESTING MACHINE

TEST: CONSOLIDATED DRAINED STRESS CONTROLLED CONSOLIDATING & LATERAL STRESS 50 psi

WATER CONTENT 6 % INITIAL DENSITY (DRY) 100 lbs/ft^3 SAMPLE SIZE 12 dia x 24 LONG

FIG.9.14

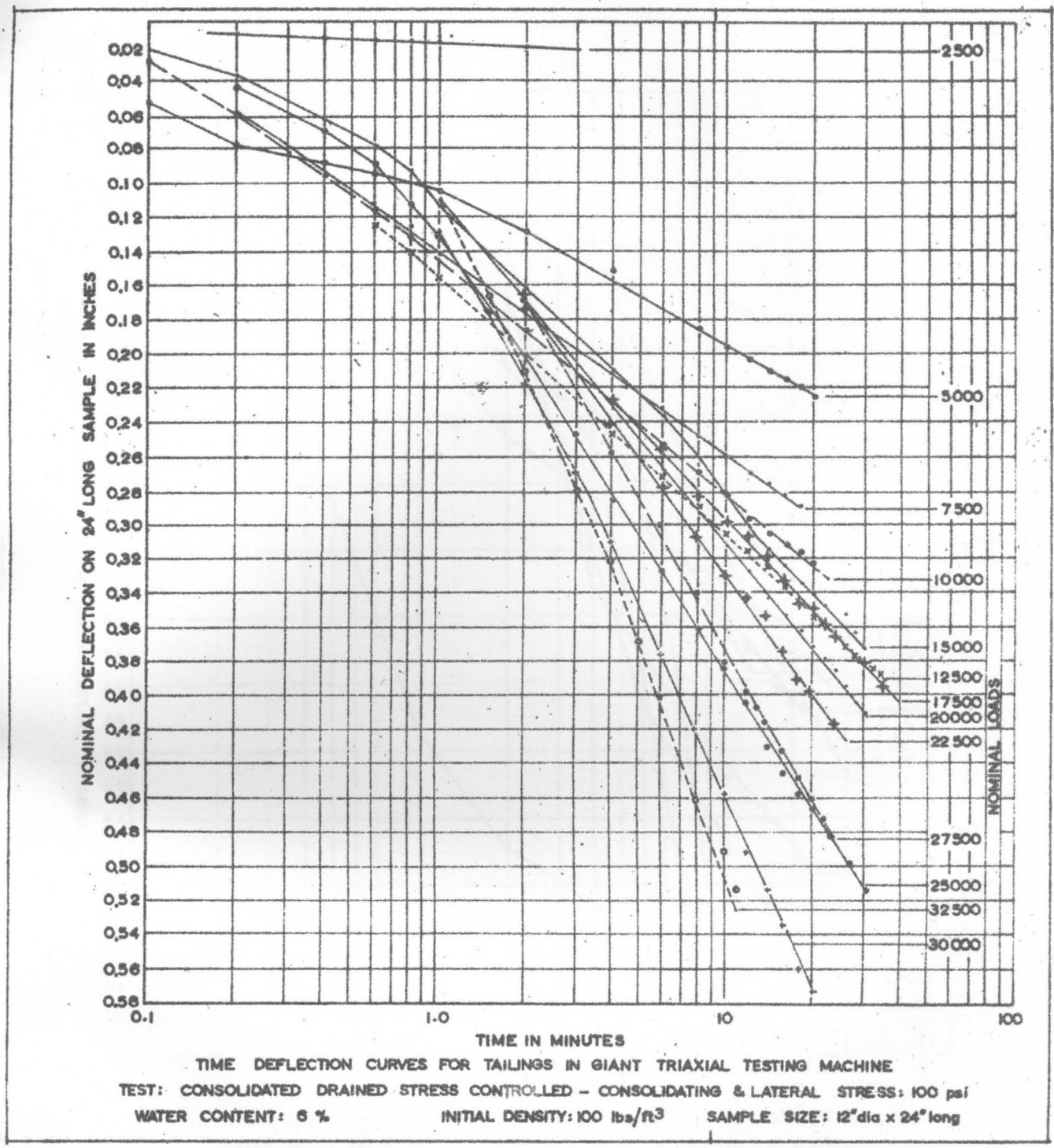

TIME DEFLECTION CURVES FOR TAILINGS IN GIANT TRIAXIAL TESTING MACHINE

TEST: CONSOLIDATED DRAINED STRESS CONTROLLED – CONSOLIDATING & LATERAL STRESS: 100 psi

WATER CONTENT: 6 % INITIAL DENSITY: 100 lbs/ft^3 SAMPLE SIZE: 12"dia x 24" long

FIG. 9.15

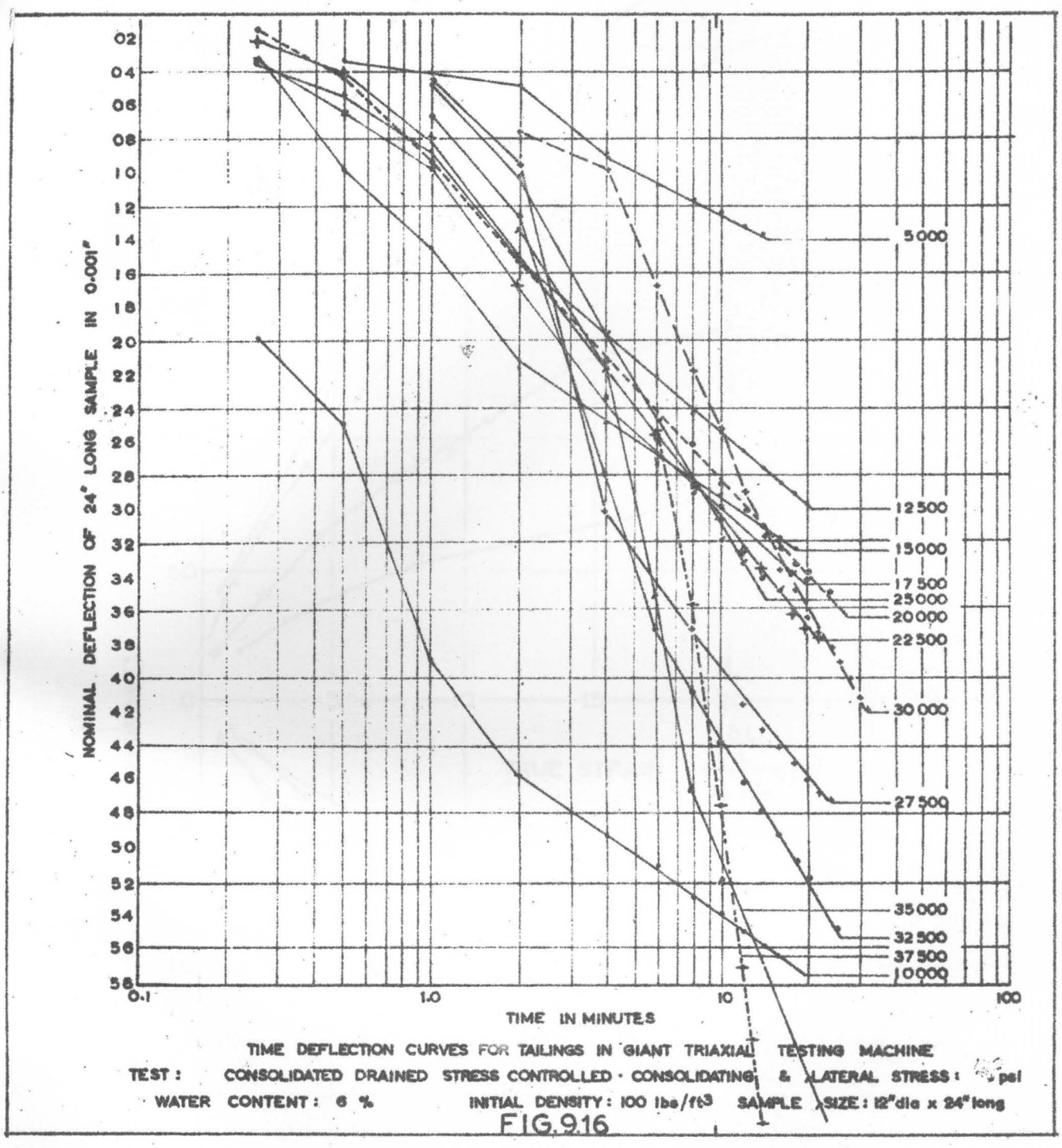

TIME DEFLECTION CURVES FOR TAILINGS IN GIANT TRIAXIAL TESTING MACHINE

TEST : CONSOLIDATED DRAINED STRESS CONTROLLED · CONSOLIDATING & LATERAL STRESS : psi

WATER CONTENT : 6 % INITIAL DENSITY : 100 lbs/ft^3 SAMPLE SIZE : 12"dia x 24" long

FIG.9.16

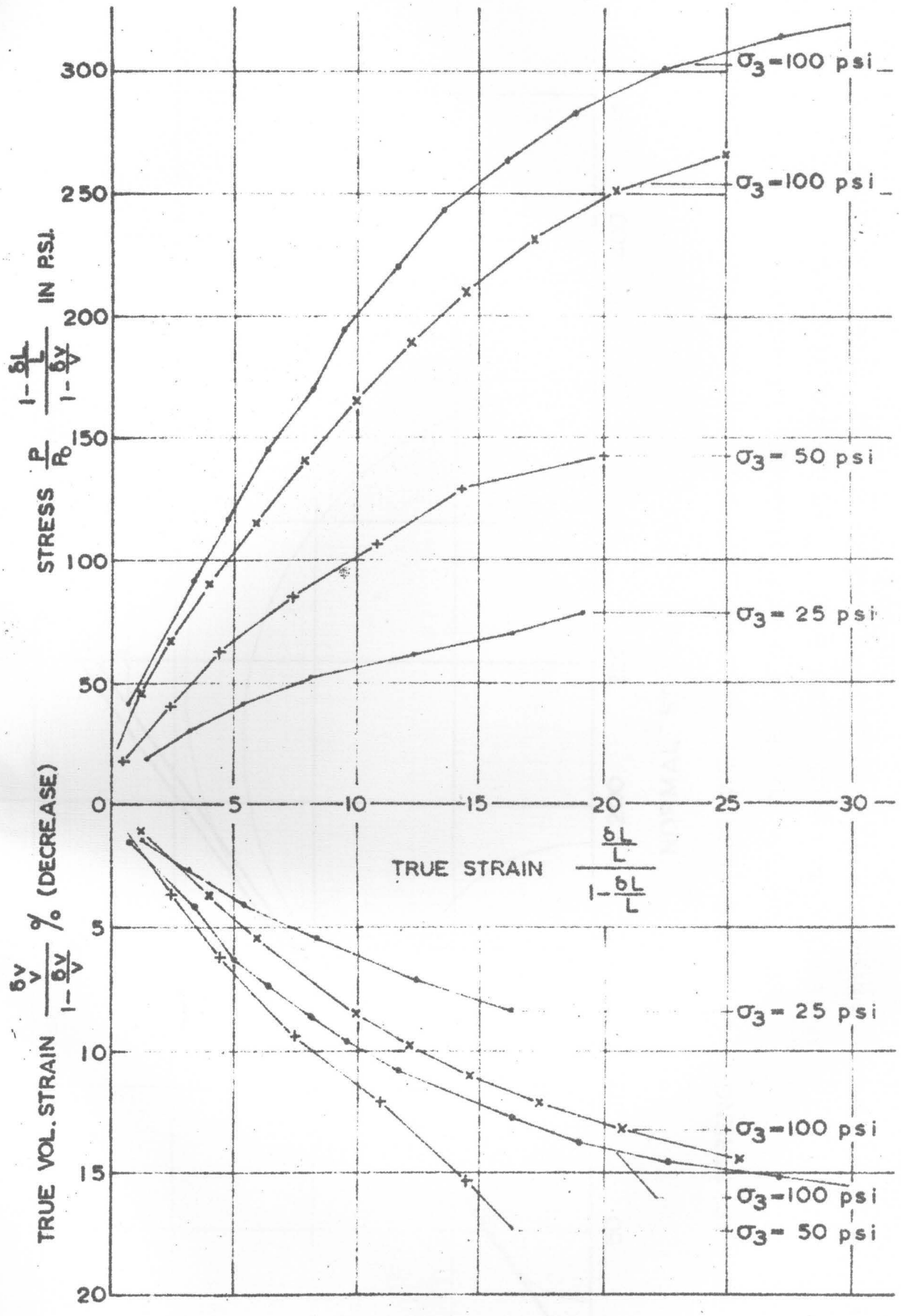

STRESS AND VOLUMETRIC STRAIN vs STRAIN RELATIONSHIPS
FOR TAILINGS IN GIANT TRIAXIAL TESTING MACHINE
TEST: CONSOLIDATED DRAINED STRESS CONTROLLED
WATER CONTENT: 6.0% INITIAL DRY DENSITY: 100 lbs/ft3

FIG. 9.17

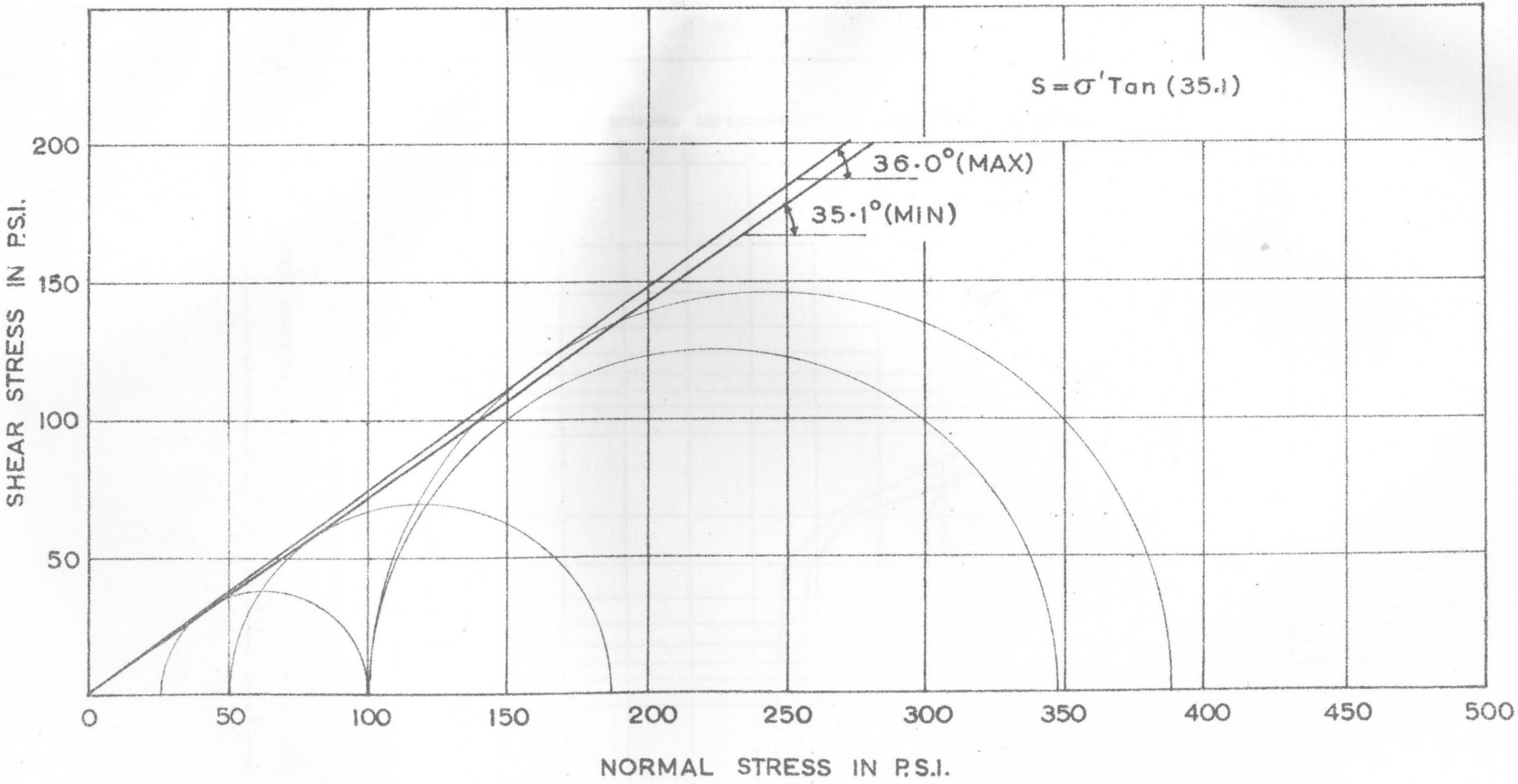

MOHRS STRENGTH ENVELOPE FOR WET TAILINGS IN GIANT TRIAXIAL TESTING MACHINE

TEST: STRESS CONTROLLED CONSOLIDATED DRAINED

MATERIAL: TAILINGS FROM BELT WATER CONTENT 6%

INITIAL DRY DENSITY 100 Lbs/Ft^3 SAMPLE SIZE 12"Dia x 24" LONG

FIG 9.18

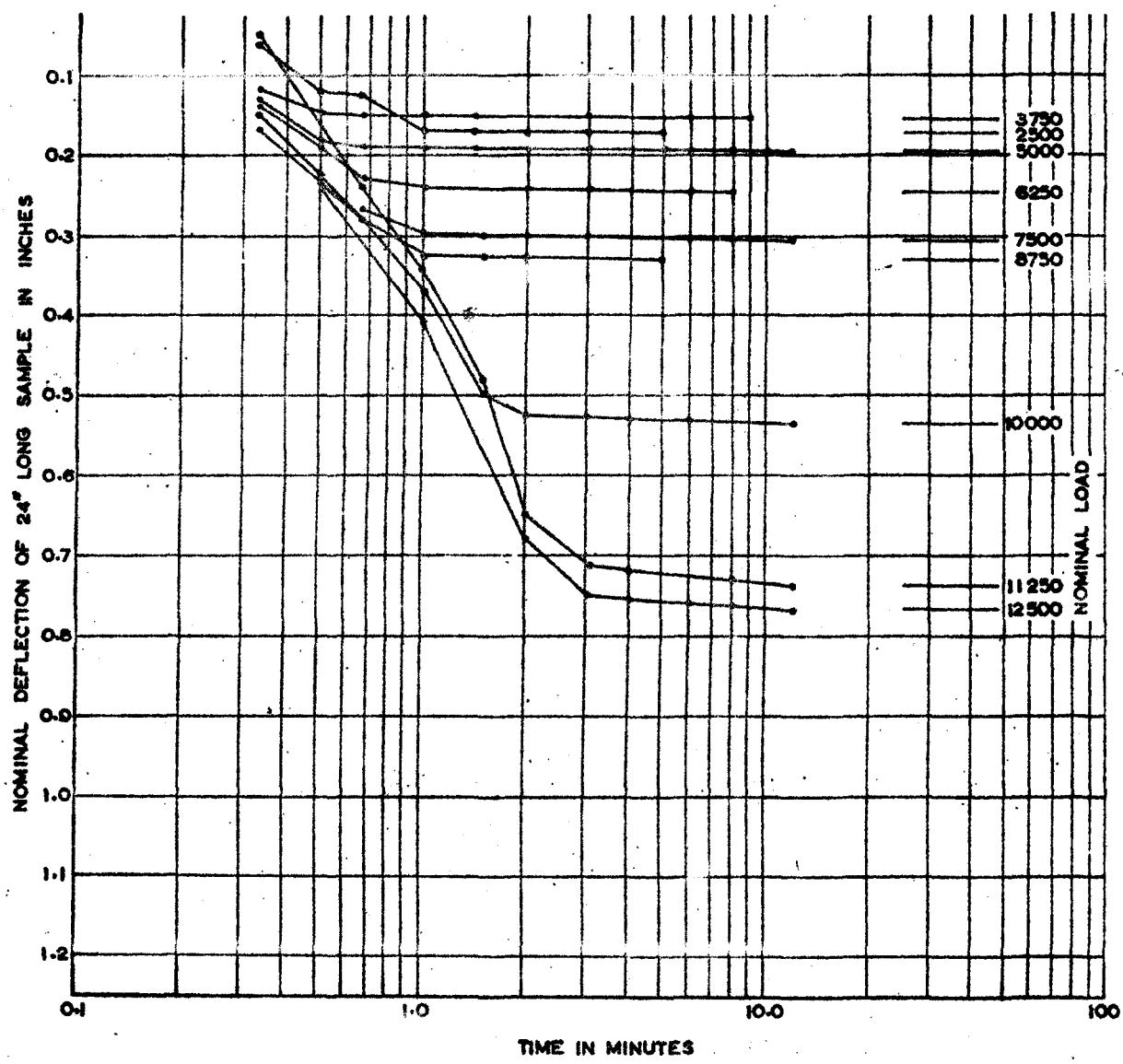

TIME DEFLECTION CURVES FOR TAILINGS IN GIANT TRIAXIAL TESTING MACHINE

TEST: CONSOLIDATED DRAINED, STRESS CONTROLLED

CONSOLIDATING & LATERAL STRESS: 25 psi

INITIAL DRY DENSITY 100 lbs ft^3

WATER CONTENT: 1·3 %

SAMPLE SIZE: 12" dia x 24" long

FIG. 9.19

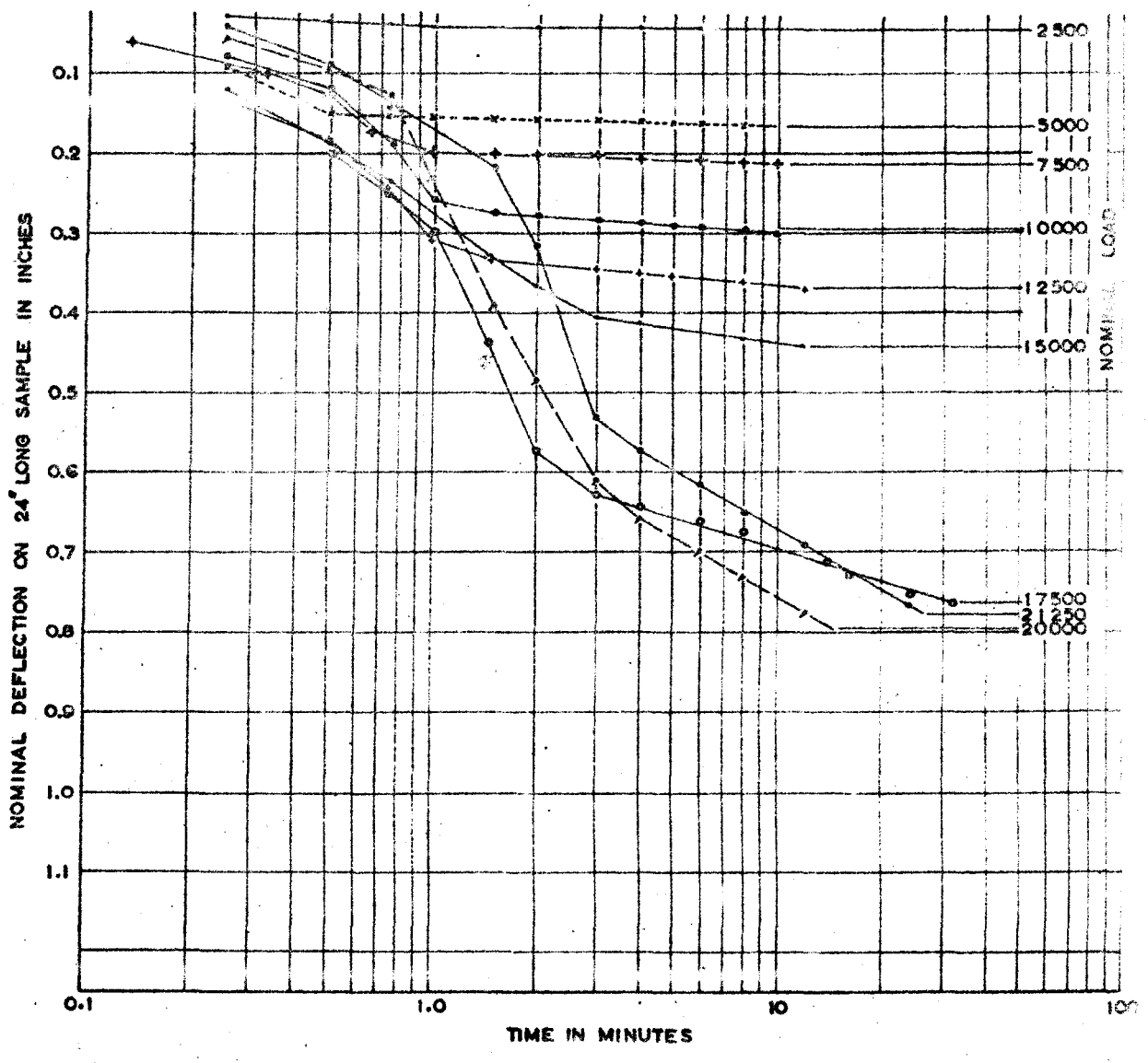

TIME DEFLECTION CURVES FOR TAILINGS IN GIANT TRIAXIAL TESTING MACHINE

TEST: CONSOLIDATED DRAINED STRESS CONTROLLED CONSOLIDATING & LATERAL STRSS: 50 psi

WATER CONTENT: 1.4 % INITIAL DENSITY: 100 lbs/ft^3 SAMPLE SIZE: 12"dia x 24"long

FIG. 9.20

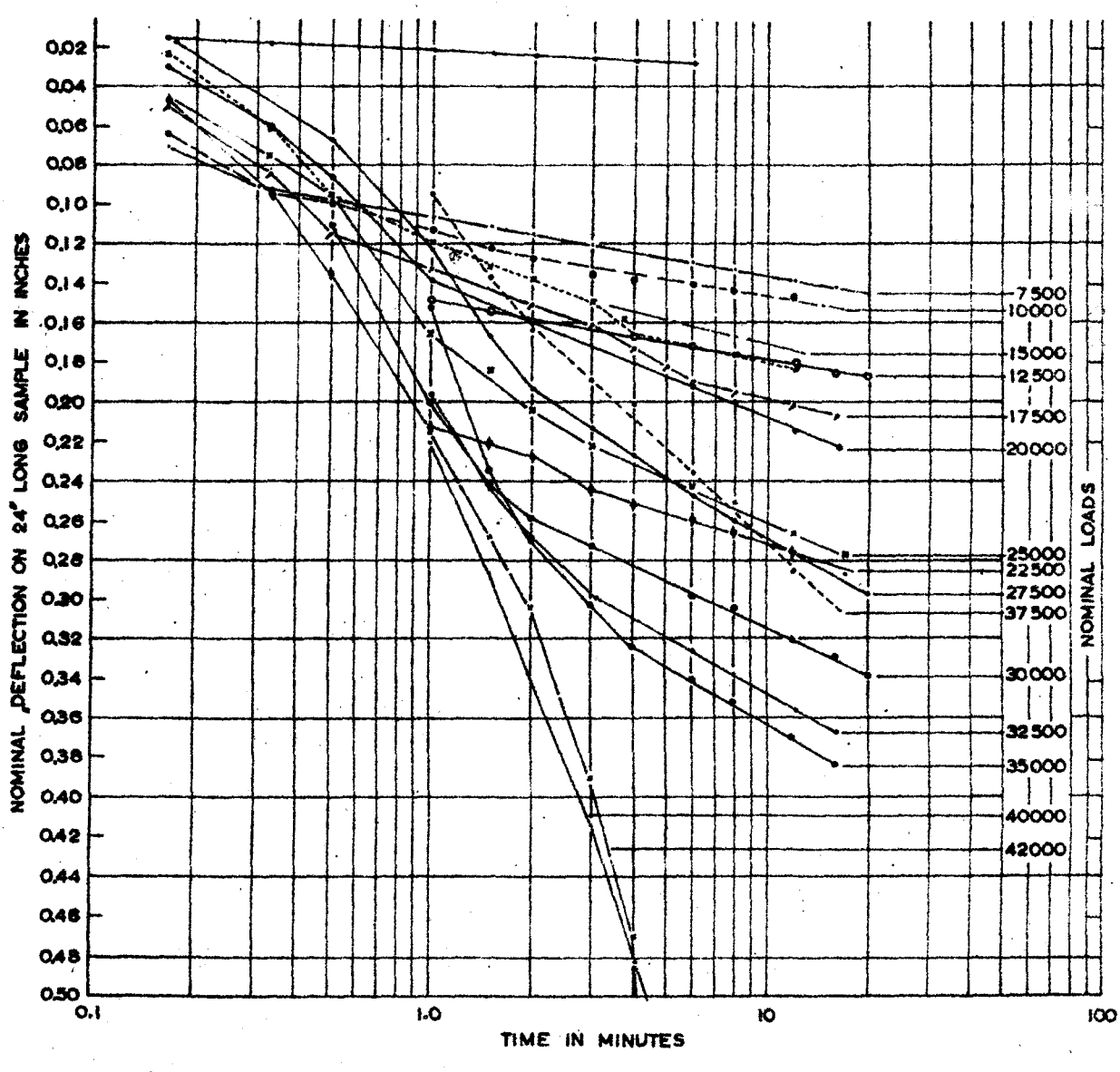

TIME DEFLECTION CURVES FOR TAILINGS IN GIANT TRIAXIAL TESTING MACHINE

TEST: CONSOLIDATED DRAINED STRESS CONTROLLED – CONSOLIDATING & LATERAL STRESS: 100 psi

WATER CONTENT: 1.9 % INITIAL DENSITY: 100 lbs/ft^3 SAMPLE SIZE: 12"dia x 24" long

FIG.9.21

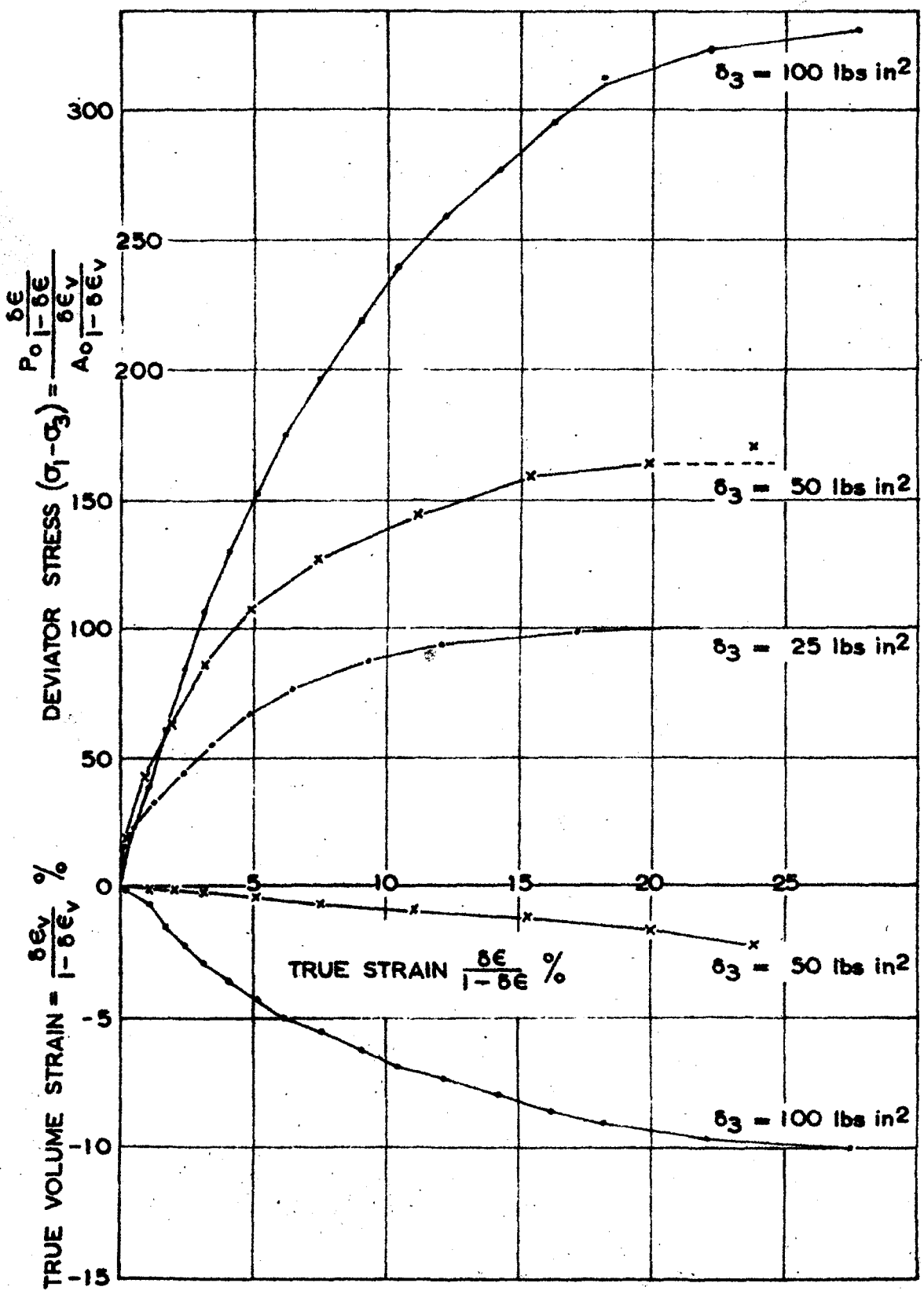

TRIAXIAL STRESS-STRAIN & VOLUMETRIC STRAIN RELATIONSHIPS
FOR
AIR DRIED TAILINGS IN GIANT TRIAXIAL TESTING MACHINE

SAMPLE SIZE: 12"dia x 24"long INITIAL DRY DENSITY: 100 lbs/ft^3
TEST: CONSOLIDATED DRAINED STRESS CONTROLLED

FIG.9.22

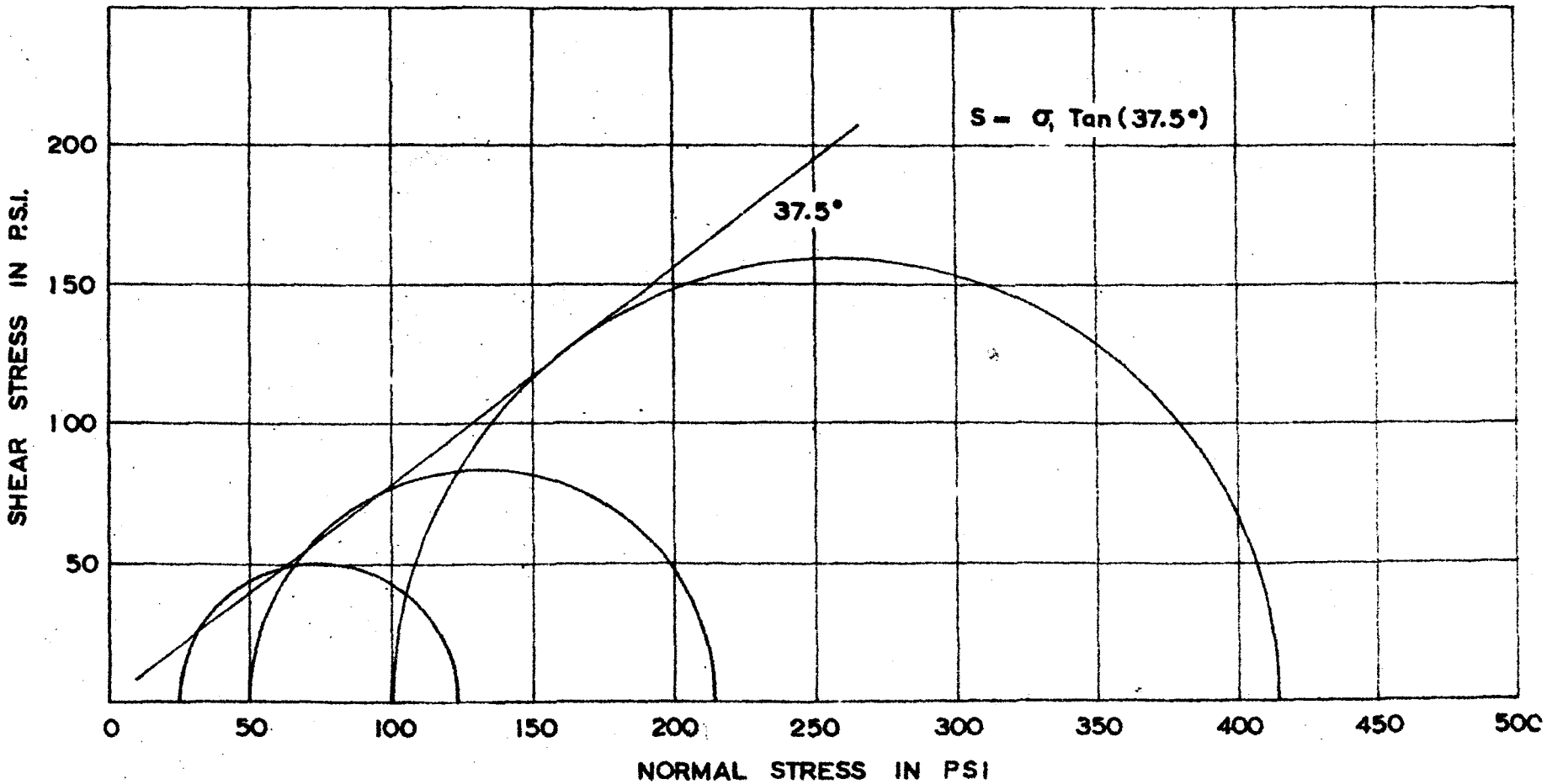

MOHRS STRENGTH ENVELOPE FOR AIR TAILINGS IN GIANT TRIAXIAL TESTING MACHINE

TEST : STRESS CONTROLLED CONSOLIDATED DRAINED

MATERIAL: TAILINGS FROM BELT WATER CONTENT: 1.6 % INITIAL DENSITY: 100 lbs/ft^3

FIG.9.23

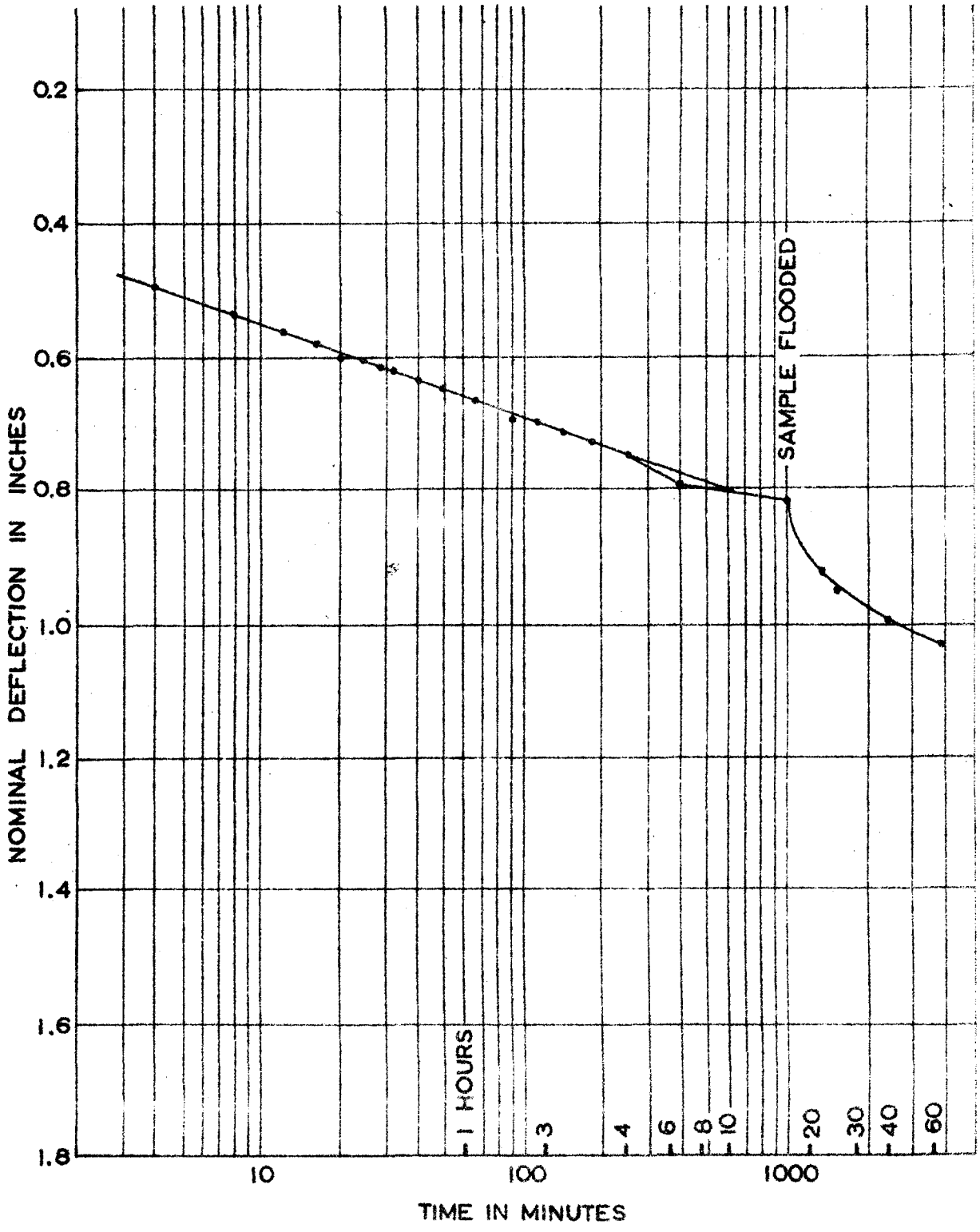

COLLAPSE CHARACTERISTCS OF TAILINGS IN GIANT TRIAXIAL TEST

TIME DEFLECTION CURVE

WATER CONTENT BEFORE FLOODING: 5% LATERAL PRESSURE: 50 psi

LOAD INCREMENT 7500 – 10000 lbs

TEST : CONSOLIDATED DRAINED STRESS CONTROLLED

INITIAL DRY DENSITY 100 lbs/ft^3

INITIAL SAMPLE SIZE : 12" dia. x 24" long

FIG.9.24

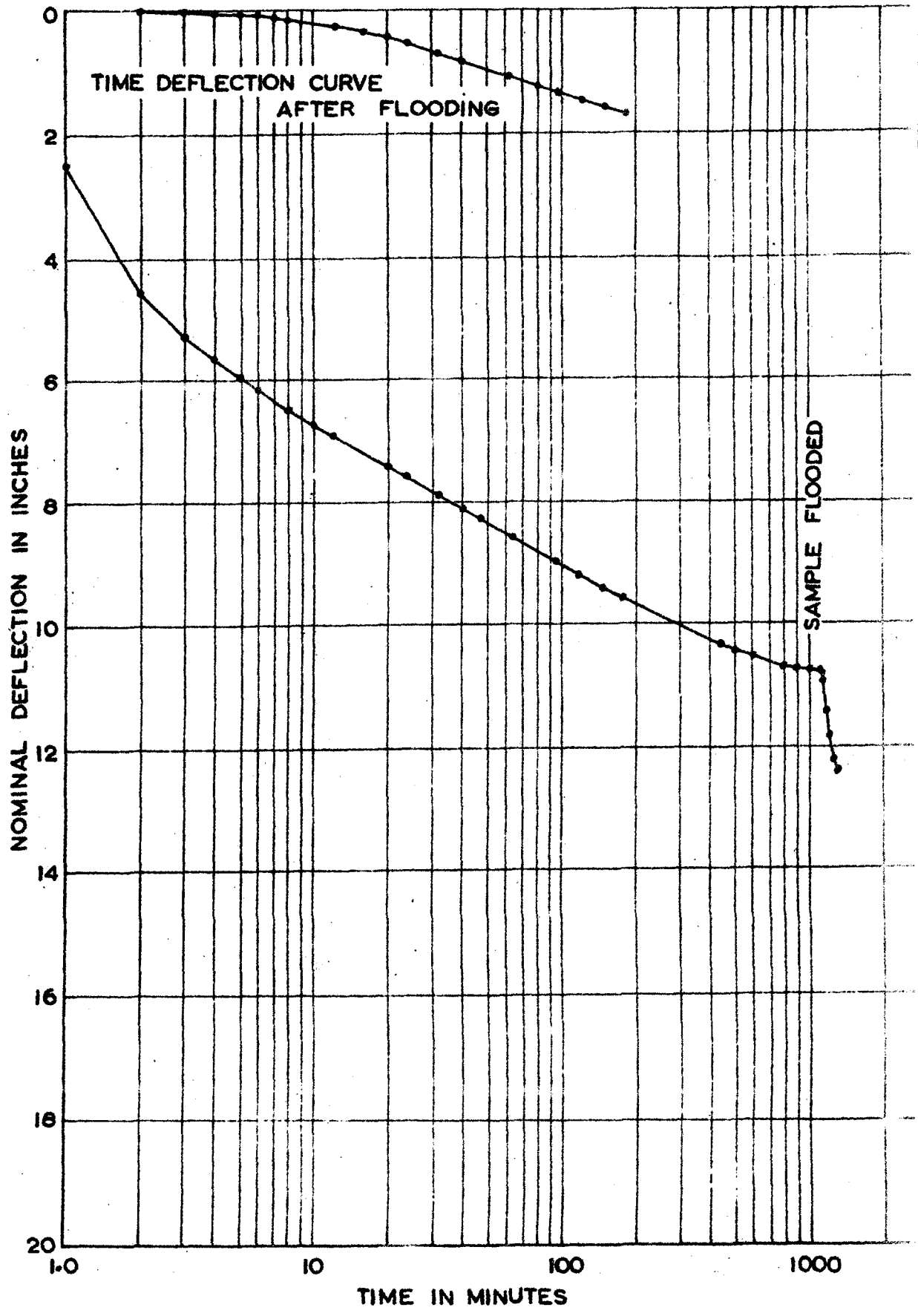

COLLAPSE CHARACTERISTICS OF TAILINGS IN GIANT TRIAXIAL TEST

TIME DEFLECTION CURVE

WATER CONTENT BEFORE FLOODING: 5% LATERAL PRESSURE: 50 psi

LOAD INCREMENT 10000–12500 lbs STRESS INCREMENT 88–111 lbs/in

TEST : CONSOLIDATED DRAINED STRESS CONTROLLED

INITIAL DRY DENSITY 100 lbs/ft^3

FIG.9.25

time from the moment of inundation for the samples at 5% moisture content.

Collapse tests for tailings at air-dried moisture content could not be completed because of the excessive deflections (which took place at great speed) and the bulging of the samples.

9.7 Discussion of Results of consolidation and shear tests

9.7.1 Consolidation results

(1) Particle strength and consolidation: From the consolidation time curves of the air-dry and 6% moisture content tailing samples, the compression deflection is linear with respect to the logarithm of time. The compression is not a primary consolidation process as the material is freely draining. It appears to be analagous to the secondary consolidation in clays, for, in both materials the compression deflection is linear to the logarithm of time.

In clays the secondary consolidation is considered to be due to rearrangement of the clay particles; in the tailings material the low strength of the individual particles (as indicated by the crushing of the particles under load (Figure 9.9)) will cause progressive crushing of the particles at the points of contact resulting in a progressive stress re-distribution until an equilibrium condition is attained in which the point stresses are all at or below some critical stress related to the crushing strength of the material. This process would also lead to a degree of rearrangement of the particles.

It is clear from both th- onsolidation time and load consolidation curves that the tailing at 5 - 6% moisture content is more compressible than the air-dry tailings. This indicates (from the hypothesis that point crushing of the particles is the principal cause of consolidation)

that there is a loss of strength of the particles on wetting. The collapse tests on the air-dry tailings confirm this.

(2) Quantitative collapse estimation: Instead of performing collapse tests as described in Section 9.6.8 the more standard procedure could have been followed whereby consolidation curves for the air-dried tailings and the inundated tailings are plotted on the same graph and one of the curves adjusted up or down to coincide near the top of the curve. (In this case the curves are made coincident at 0.71 tons per sq. ft (see Figure 9.26). The difference between the two curves gives a useful measure of the collapse on inundation to be expected at any pressure. The results of the direct collapse tests are superimposed on this graph and show good agreement with the normal method of estimating collapse.

The collapse test of the tailings at bank moisture content indicates that no measurable collapse will take place on inundation.

9.7.2 Discussion of shear tests

Deformation and failure: The shear tests on all samples showed large deformations, giving true strains of the order of 25 - 30% at plastic failure. The failures were all of the bulging type without exhibiting slip planes. (Figure 9.27).

Time deformation, or creep effects: The creep, which is given by the axial deflection with time after the application of each load increment, is linearly related to the logarithm of time (Figures 9.13 - 9.16, and 9.19 - 9.21). (The discontinuities in the creep curves are due to machine operation and coincided with adjustments made to the fulcrum of the upper loading beam in order to keep it from coming to

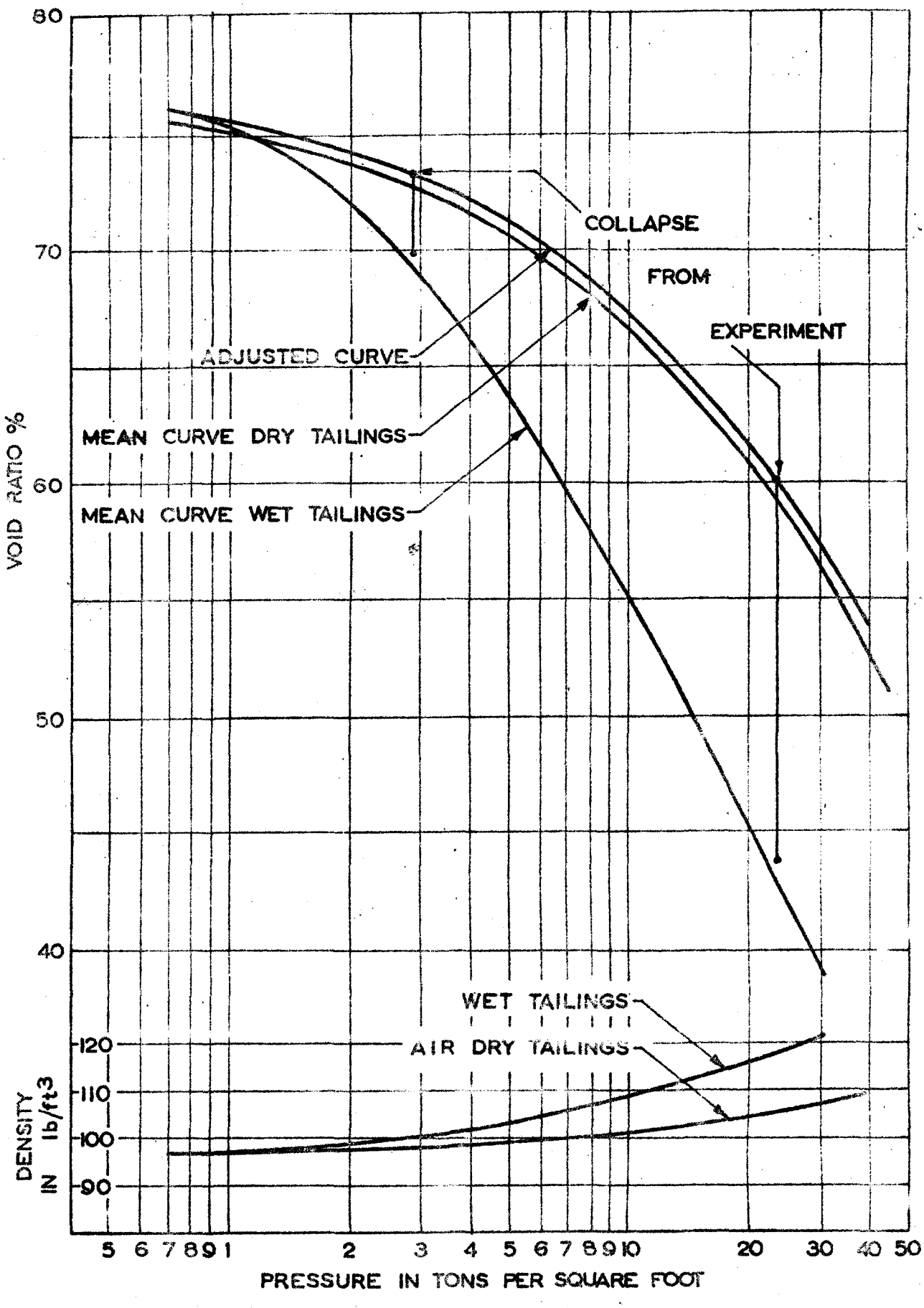

MEAN & ADJUSTED CONSOLIDATION PRESSURE CURVES FOR AIR DRY & WET TAILINGS SHOWING COLLAPSE CHARACTERISTICS

SAMPLE SIZE – 12 Dia. x 3" THICK

FIG.9.26

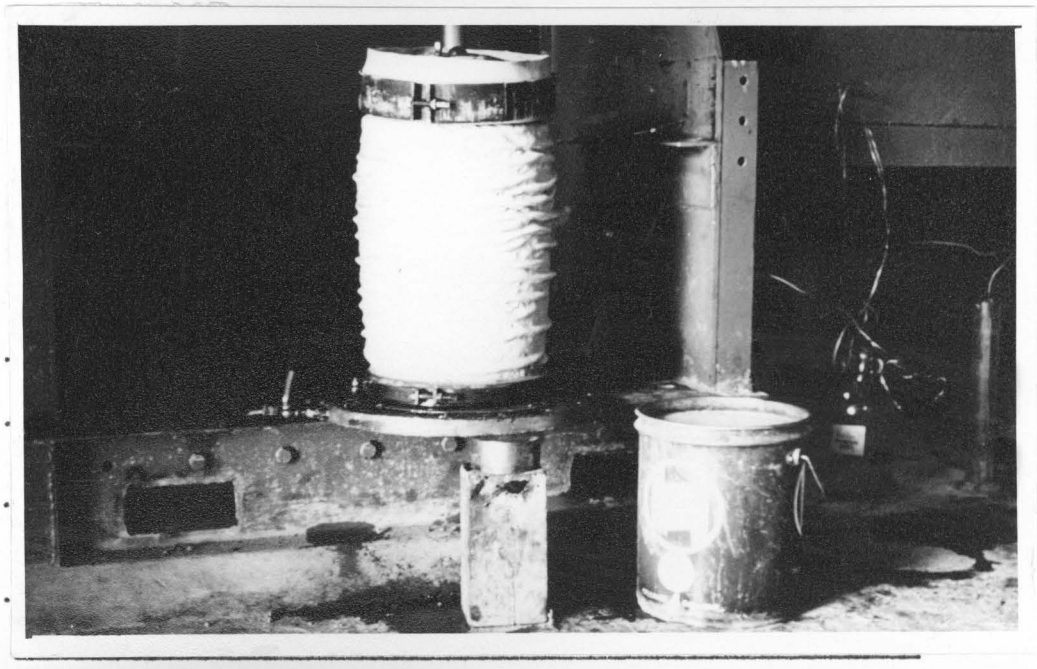

Figure 9.27 Triaxial sample after failure.

rest on the bottom stop). The creep curves are similar to those found in the consolidation tests and their cause can similarly be ascribed to rearrangement of the particles due to crushing at the points of contact.

The rate of creep for the tailings at 6% moisture content is much higher than for the air-dry tailings, which again indicates a loss of strength in the tailings particles on wetting. An interesting feature is that up to a particular stress the slopes of the creep curves on the semi log plot are linearly related to the deviator stress; with higher stresses the creep rate increases sharply. This, for the shear test with σ_3 = 100 lb per sq. in., is illustrated in Figure 9.28.

Volume changes and shear strength: The real volumetric strains in all the shear tests were linearly related to the deviator stresses, the volume strain for the tailings at 6% moisture content being significantly higher than for the air-dried tailings (Figure 9.29). From Figure 9.29 it is clear that continuous densification took place during the shear tests.

In Figure 9.30 the triaxial stress-strain curves for the tailings at the two moisture contents are superimposed. For the pairs of curves the difference between the strains at the same deviator stress shows the collapse potential of the air-dry tailings on inundation. The peak deviator stress for the air-dry tailings is also higher than for tailings at 6% moisture content, indicating a loss of shear strength. This is confirmed by comparing the Mohr's strength envelopes (Figures 9.23 and 9.18) which show a reduction in the angle of internal friction from 37.5° to 35.5°.

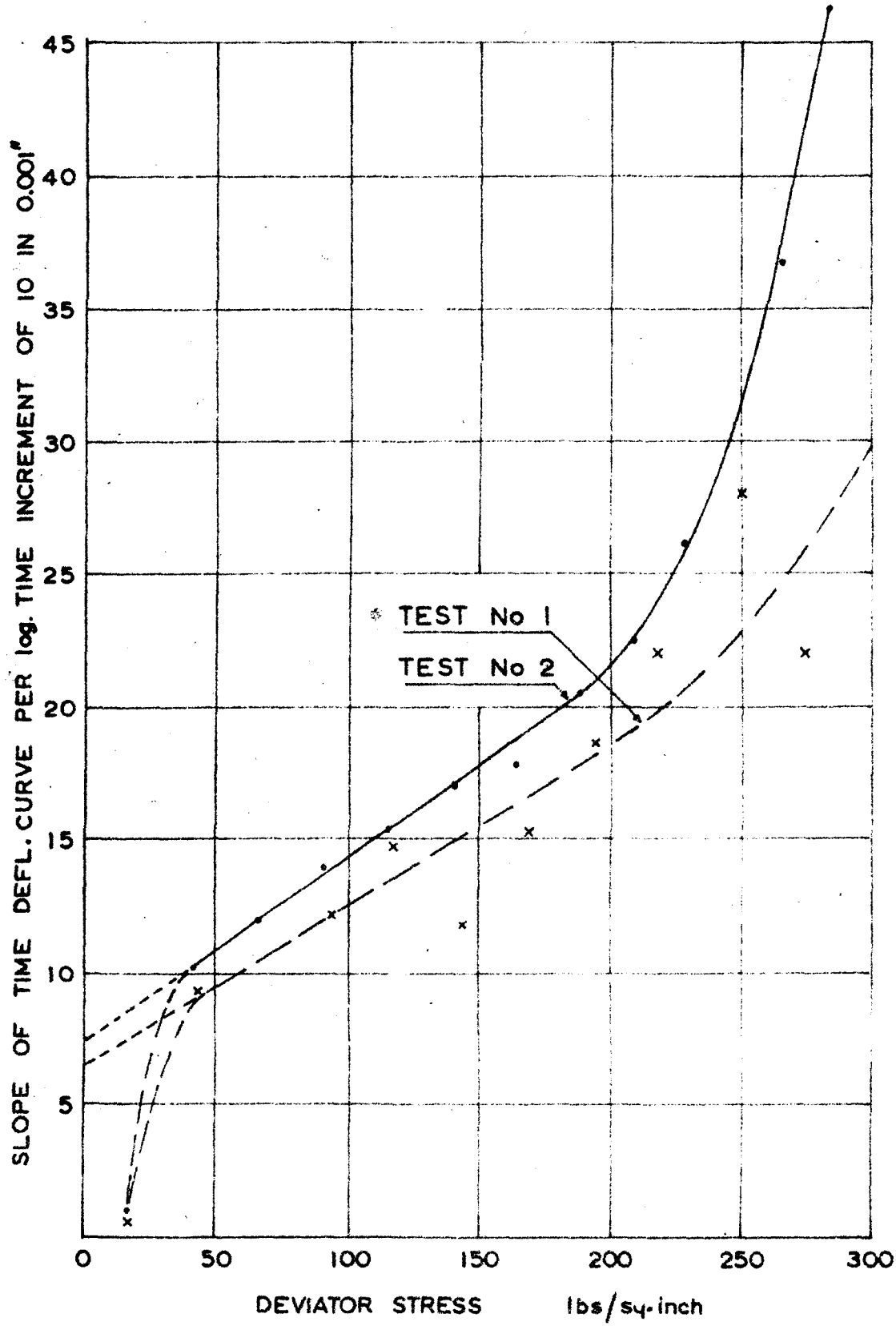

RELATIONSHIP BETWEEN DEVIATOR STRESS AND CREEP DEFLECTION/Log_{10} TIME INCREMENT IN GIANT TRIAXIAL TESTING MACHINE

TEST: CONSOLIDATED DRAINED STRESS CONTROLLED

LATERAL PRESSURE: 100 psi WATER CONTENT = 6%

MATERIAL: TAILINGS FROM BELT SAMPLE SIZE: 12 dia x 24 long

FIG. 9.28

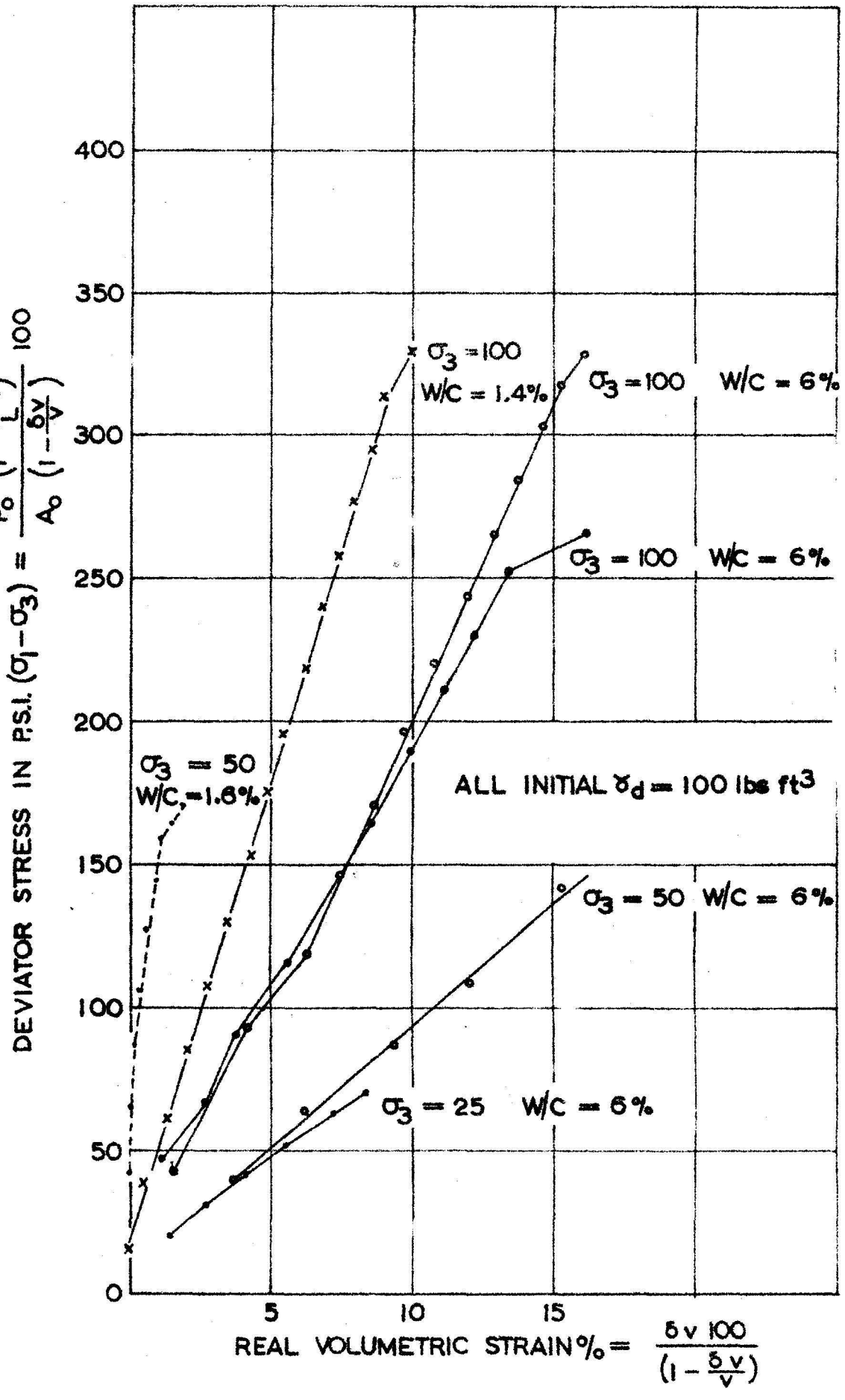

RELATIONSHIP BETWEEN DEVIATOR STRESS AND REAL VOLUMETRIC STRAIN

TRIAXIAL TEST: CONSOLIDATED DRAINED ON 12"dia x 24" long SAMP
SOIL : TAILINGS FROM BELT

FIG 9.29

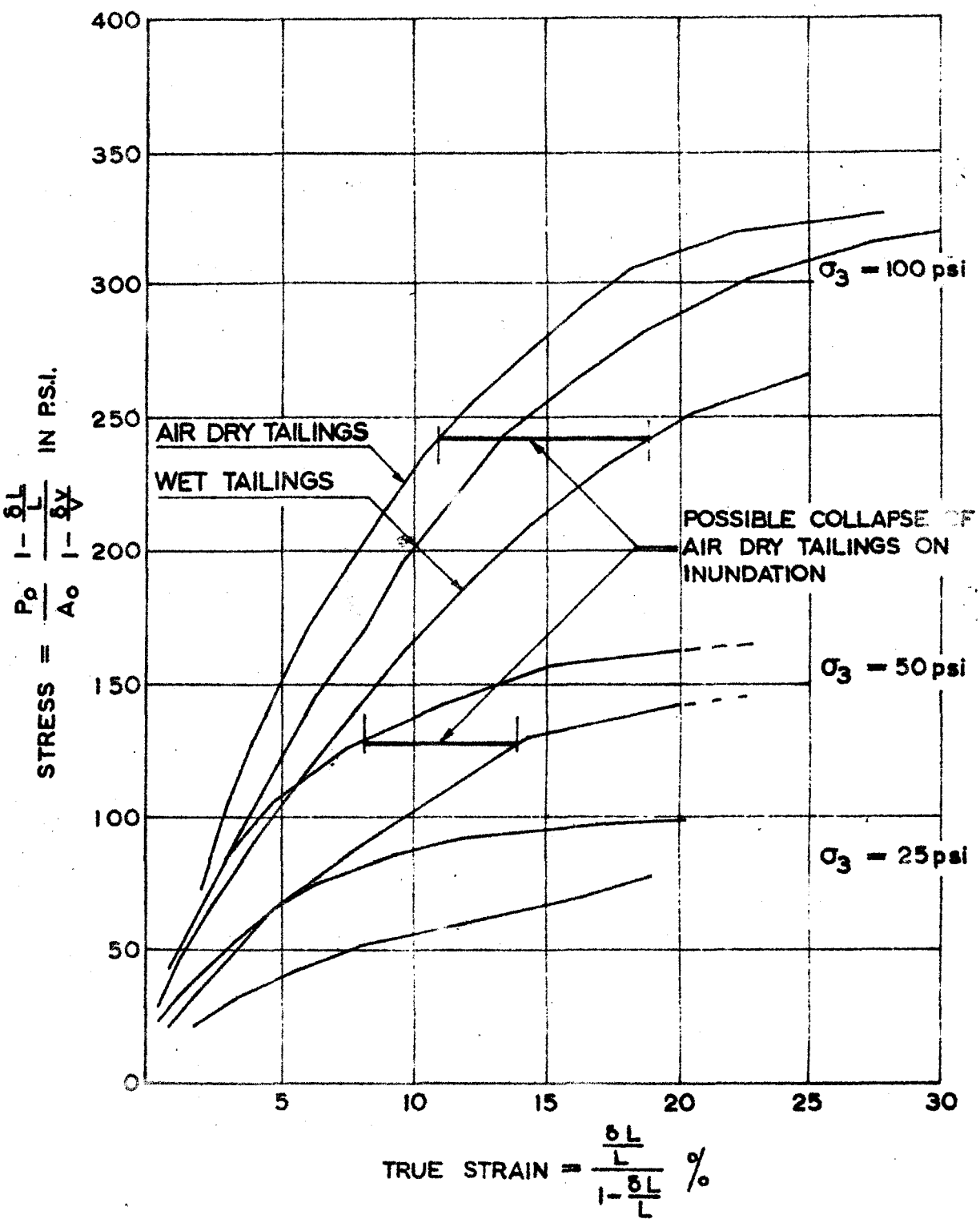

STRESS-STRAIN CURVES FOR AIR DRY & WET TAILINGS
IN GIANT TRIAXIAL TESTING MACHINE
INDICATING REGIONS OF COLLAPSE

WATER CONTENT WET TAILINGS 6 % AIR DRY TAILINGS 0.9–1.6 %
INITIAL DRY DENSITY 100 lbs/ft^3
TEST: CONSOLIDATED DRAINED STRESS CONTROLLED

FIG. 9.30

Collapse potential: The collapse tests on the tailings at natural bank moisture content (Figures 9.24 and 9.25) indicated that no sudden loss of strength occurred, though the rate of deformation increased. However, it should be noted that the deformations are plotted against the logarithm of time giving an exaggerated impression of the rate of deformation. If the additional deflections are plotted against log (time) taking zero time as the time of inundation, as shown at the top of Figure 9.25, then the slow rate of this deformation is appreciated.

It is possible that the accelerated rate of deformation is due to the slight decrease in σ_3 on flooding of the 24 inches high sample.

9.8 Conclusions

The behaviour of the tailings material under stress is dominated by the crushing strength of the particles. The crushing of the particles takes place at the high stress concentrations at the points of contact between the particles, and due to particle reorientation leads to progressive stress redistribution and equalisation, creep effects and densification of the mass.

The crushing strength of the particles is dependent on the moisture content, being much higher at air-dry than at natural bank moisture content. For moisture contents of 5% and above, the behaviour of the mass is as if the material is inundated.

The behaviour of the air-dry tailings material is approximately that of normal granular material of high crushing strength, the creep effects being significantly smaller and the densification less than for material at

natural bank moisture content. However, as the stress increases, the air-dry tailings exhibit these effects to an increasing degree, but always to a lesser degree than for tailings at natural bank moisture content. Due to the reduction of the particle strength, inundation of air-dry tailings under load exhibits large collapse characteristics.

The behaviour of the tailings material in the dam wall at natural bank moisture content (5 - 6%) can be expected to be as follows:-

Under consolidation and shear stresses, deformations due to creep strains can be expected. These will continue at a steadily diminishing rate for fairly long periods of time after the bank is formed, and lead to stress re-distribution within the embankment. On inundation of the embankment, small additional strains may occur but no significant loss of strength or collapse of structure is expected. Crushing of the particles will take place, and it is feasible that where failure planes develop in the embankment the grinding of the particles on these planes may cause pulverisation and clay formation, resulting in possible loss of shear strength.

There appears to be a significant similarity between the consolidation characteristics of the tailings material at 5-6% moisture content and the secondary consolidation in clays. This suggests that a closer investigation of the deformation characteristics of the former may shed light on the secondary consolidation characteristics of the latter.

9.9 Strength and consolidation properties of the sub-soil materials

9.9.1 Strata

The sub-soil can be divided into three distinctive strata of materials:-

(i) the slime clay layer;

(ii) the interbedded silts, clays and sands deposited in Sache's Dam West, and the pre-Sache's Dam West valley sediments;

(iii) the decomposed gabbro and shale material.

9.9.2 The slime clay layer

The slime clay layer is the critical sub-soil material; its strength and consolidation properties are therefore considered in detail.

Consistency limits:

Liquid Limit	90%
Plastic Limit	43.6%
Plastic Index	46.4%
Linear Shrinkage	12.9%
Specific Gravity	2.64

These values indicate that the slime clay material is probably a very active clay.

Shear strength:

If little or no drainage occurs during failure, the strength of the clay in the slime layer is estimated from the results of unconsolidated undrained triaxial shear tests, the S_{uu} tests. The consolidation pressure on the clay layer varies from practically zero at the toe to approximately 10 tons per sq. ft near the centre of the dam wall. This would result in a considerable difference in the shear strength of the clay near the toe and near the centre of the dam wall,

and require sampling along the whole line of the critical cross-section if a reasonable estimate of the shear strength of the layer is to be made. Due to the difficulty of driving a casing through the tailings material it was not practical to sink exploration holes along the whole line of the critical cross section. Hence, the strength of the clay layer as reflected in the S_{uu} tests could not be obtained. The only alternative was to obtain samples near the toe, and for a number of these apply artificial consolidation pressures ranging over the pressures expected in nature, and to perform triaxial shear tests on these in undrained conditions with pore pressure measurements, the S_{csu} test. The results of these tests are reported as follows:-

(i) In Figure 9.31 the stress-strain and pore pressure strain curves.

(ii) In Figure 9.32 the Mohr's envelope of the consolidated undrained and effective inter-granular stress values as obtained from the S_{csu} test. The following strength parameters were found:-

Total stress:

$C = 0$ psi $\quad \phi = 12^{\circ}$

Effective stress:

$C' = 1$ psi $\quad \phi' = 18^{\circ}$

It is apparent from Figure 9.31 that the pore pressure development during shear was practically equal to the deviator $(\sigma_1 - \sigma_3)$ stress and the failure took place due to the reduction of the effective σ_3 stress rather than due to an increase in the σ_1 stress. This effect for one test is illustrated in Figure 9.33. The applicability of these

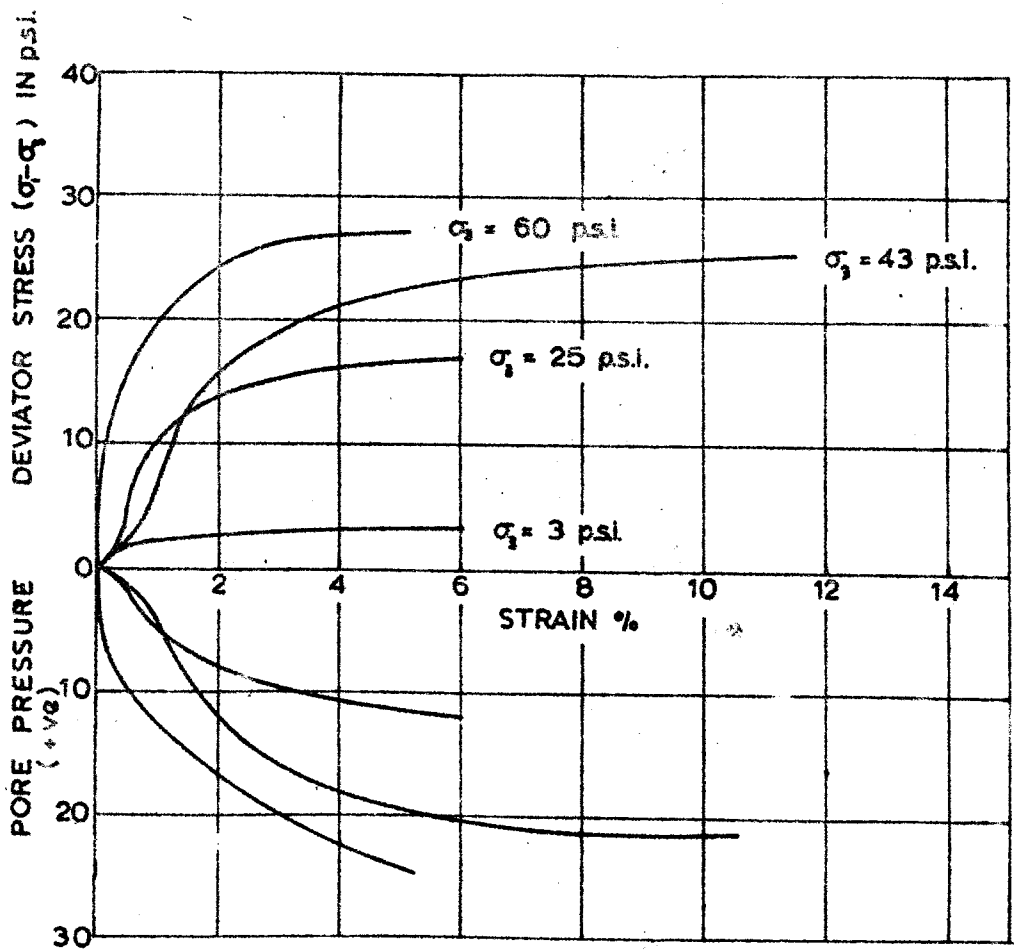

SHEAR TEST RESULTS.

TEST := S_{csu} with p.p. measurements
SOIL := Slime clay
SPEED OF TESTING := 0·00074"/min

FIG 9. 31

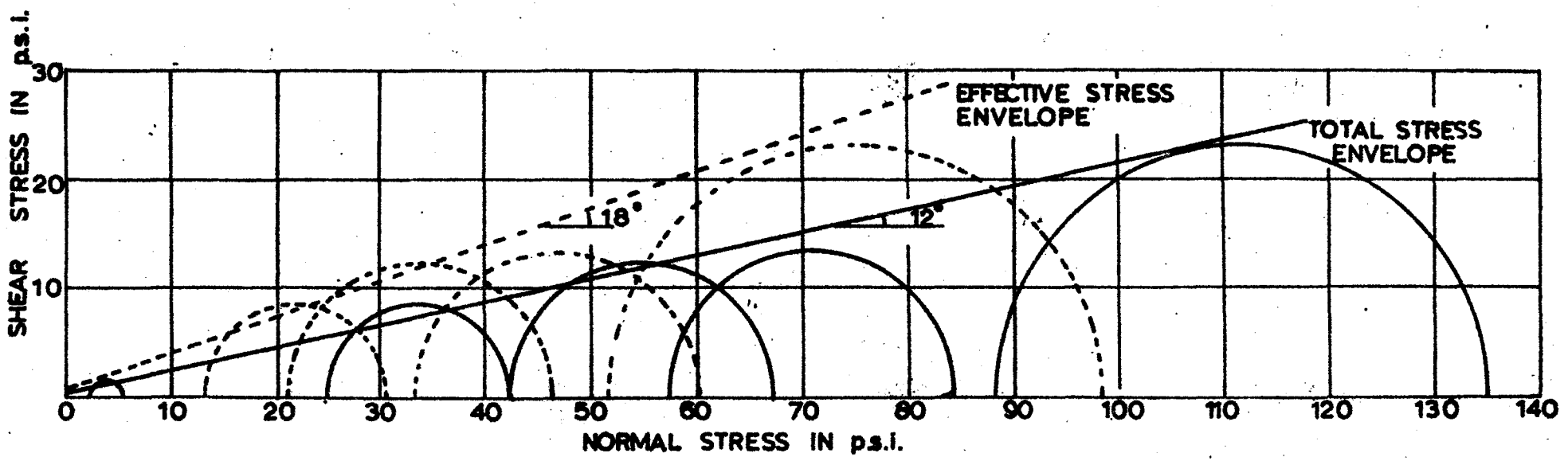

MOHR'S ENVELOPE

TEST := S_{csu} with p.p. measurements

SOIL := Slime clay

SPEED OF TESTING := 0·00074"/min

SHEAR CONSTANTS := c = 0 p.s.i. ϕ = 12°
c' = 1 p.s.i. ϕ' = 18°

FIG. 9.32

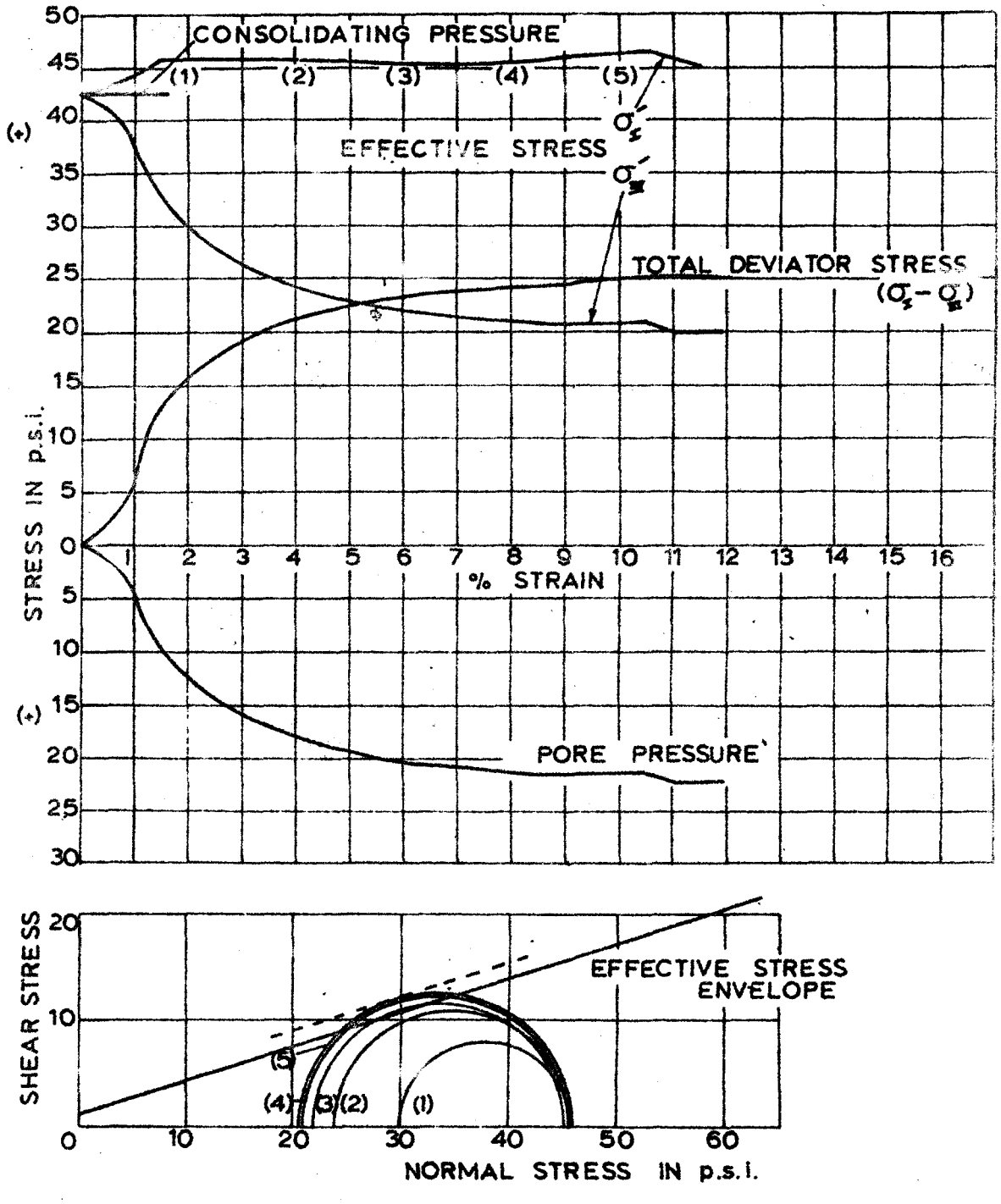

EFFECTIVE STRESS STATE NEAR AND AT FAILURE IN A NORMALLY CONSOLIDATED CLAY.

FIG.9.33

strength parameters to the stability analysis of Sache's Dam East is discussed in Section 9.

Consolidation strength:

The results of the consolidation tests on the slime clay material are shown in Figures 9.34 and 9.35. An examination of these results indicates that the load consolidation curves give the pre-consolidation overburden pressure of the right order and the time consolidation curves indicate that the slime material is of medium-to-low permeability.

9.9.3 Interbedded material

The interbedded material is extremely variable, and it was not possible to distinguish the valley sediments from the dam material. Not one of the exploration holes showed the same sequence of deposition, and it was in consequence impossible to determine mean strength parameters for this material. As all the evidence of failure indicated that no failure took place in this material, it is not of importance to the stability analysis of the dam. In designing the new flank, the slime layer was to be removed, and the interbedded material would then become of prime importance. For the purposesof design, the strength parameters for the weakest layer were selected, $C = 3$ psi, $\phi = 10^{\circ}$. The use of these values probably led to a conservative design of the flank. This aspect however falls outside the scope of this thesis, and reference must be made to Jennings and Marais (1959) for a detailed evaluation.

9.9.4 Shale

The shale underlying a section of the interbedded material is of a very stiff consistency, and it is most unlikely that any form of failure, sliding or circular slip, could pass through it.

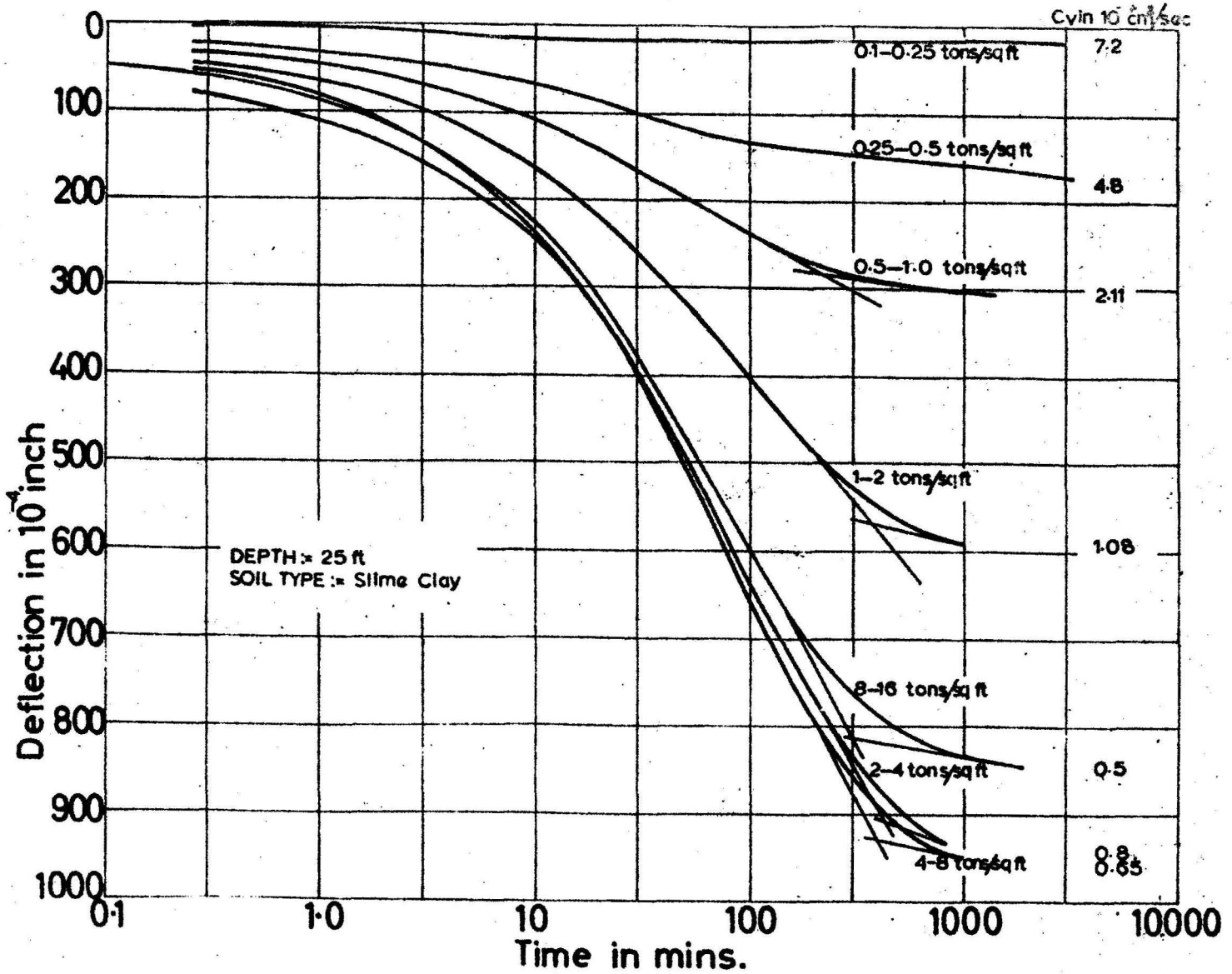

CONSOLIDATION-TIME CURVES FOR SLIME CLAY.

FIG 9.34

9.22(a)

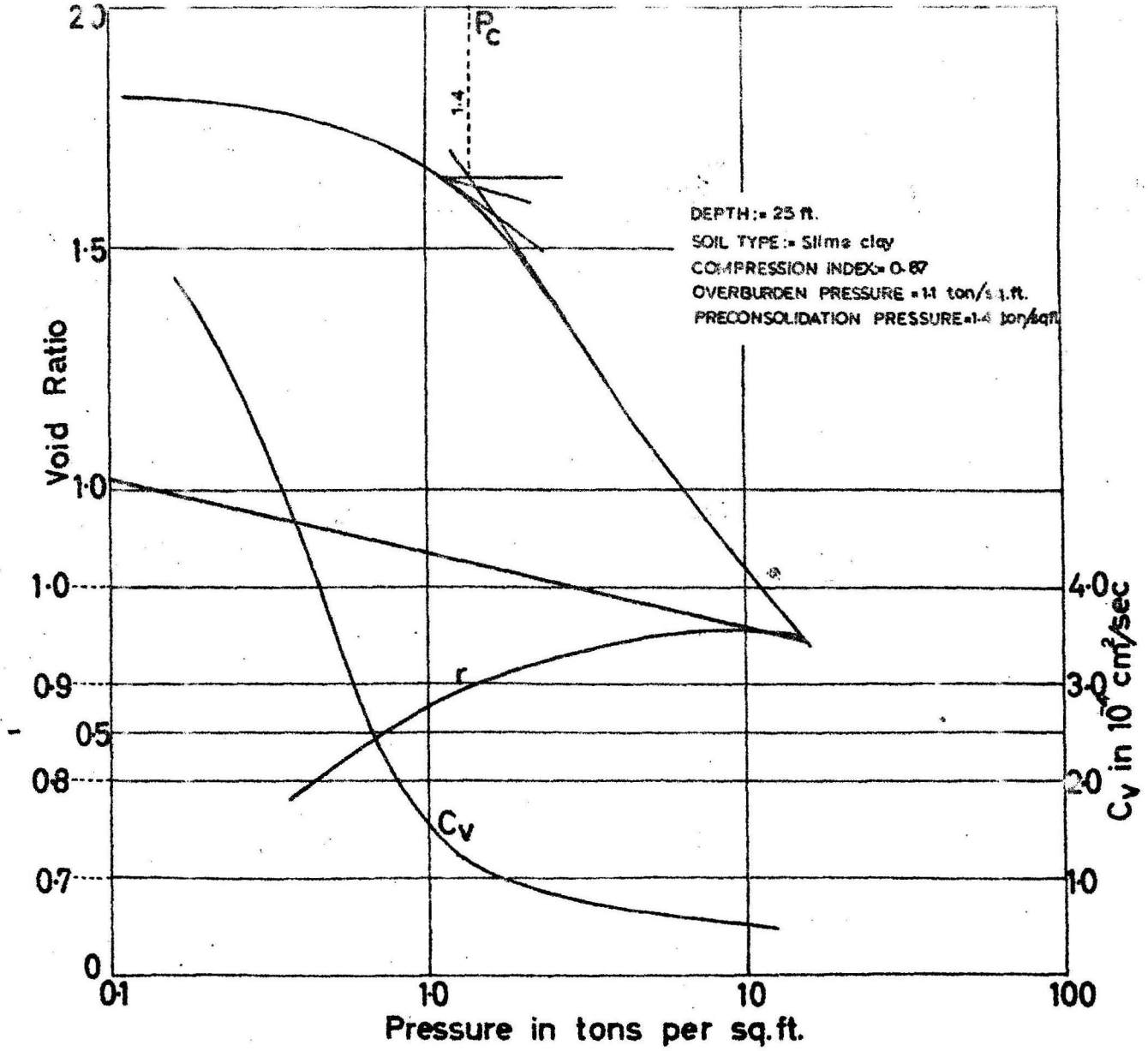

FIG. CONSOLIDATION-LOAD CURVES FOR SLIME CLAY.

FIG 9.3.5

9.9.5 Gabbro

Consistency limits:

Liquid Limit	41.3%
Plastic Limit	32%
Plastic Index	9.3%
Linear Shrinkage	1%
Specific Gravity	2.86
$<60\ \mu$	100%

The material is extremely fine-grain, and the Consistency Limits show it to be relatively inert.

Shear strength:

The decomposed gabbro material is very pervious and the pore water drained out after the sampling operation and prior to the tests in the laboratory. The first attempts to restore the condition of full saturation which existed in nature by restoring the pore water in the laboratory were not successful, and air voids remained in the soil even after several days of sweeping the voids with a stream of air-free water. This introduced doubts as to the validity of the pore pressure measurements in these tests, and the apparatus was modified to limit the volume changes of the sample during shearing to zero by keeping the pressure inside the sample at zero and varying the σ_3 stress (constant volume tests). Subsequently it was found that full saturation could be restored in the sample by raising the confining pressure and the pressure inside the sample to approximately 100 lb per sq. in. By establishing a differential of about 2 lb per sq. in between the two pressures, the confining pressure being higher, the sample was kept from falling apart. The normal S_{csu} test with pore pressure measurement was then carried out. In Figure 9.36 the stress-strain and the pore pressure strain curves are shown, and in Figure 9.37 the

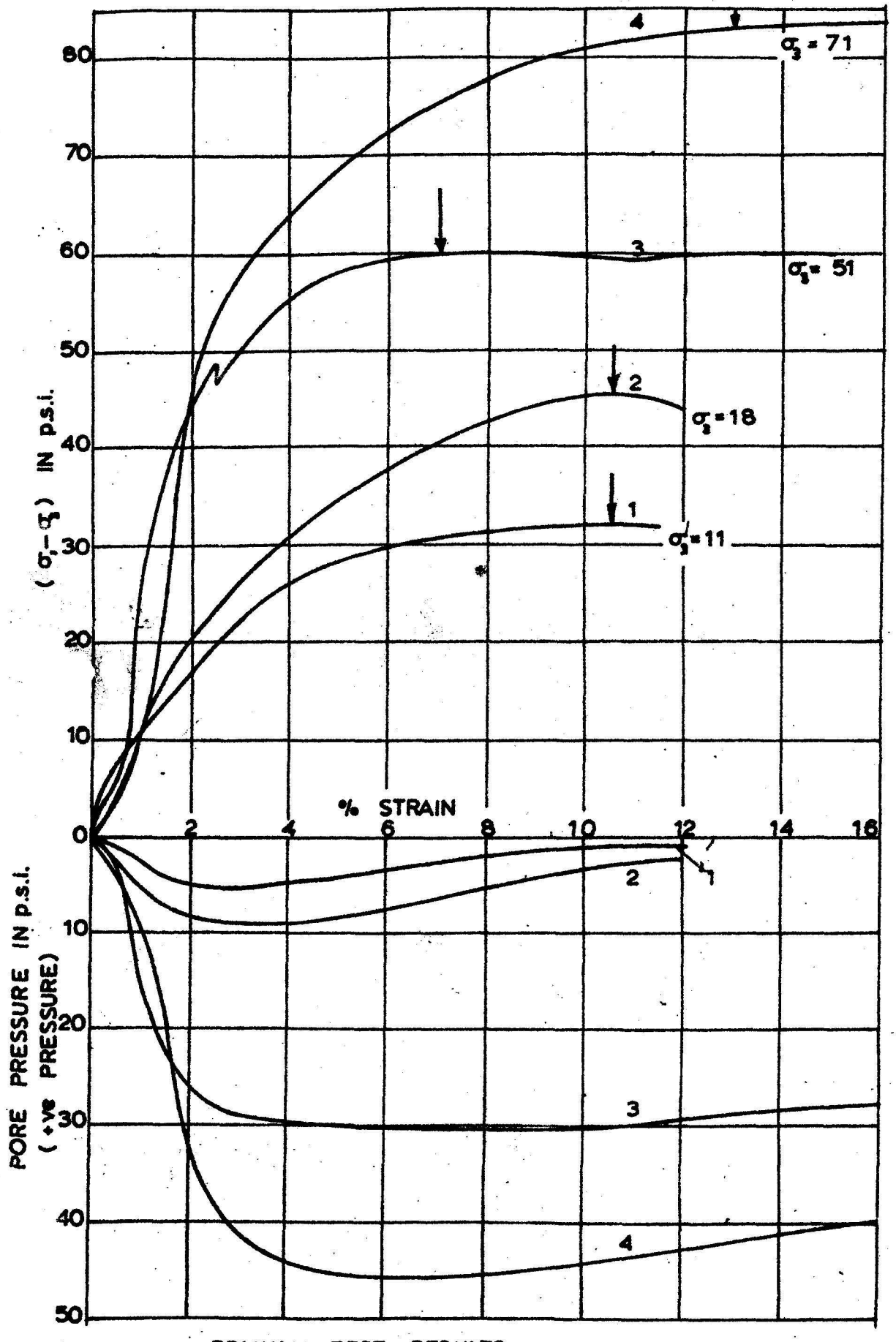

TRIAXIAL TEST RESULTS

SOIL :- Decomposed Gabbro, a clayey sand.

LOCATION :- Sache's Dam East, Hole No. 3, Depth 50ft.

TEST :- S_{CSU} with p.p. measurement.

FIG. 9.36

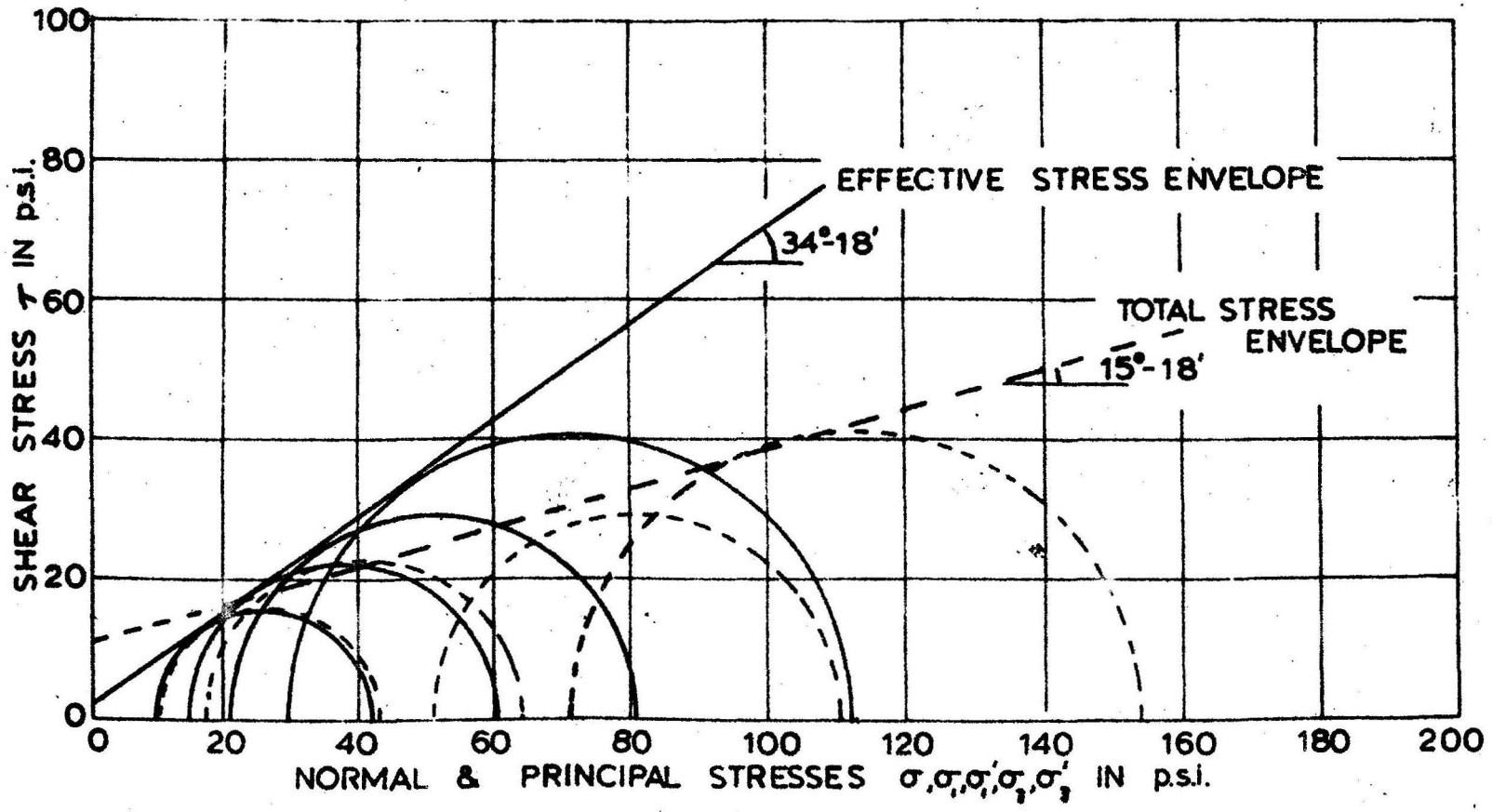

MOHR'S ENVELOPE

TEST := S_{csu} with p.p. measurement

LOCATION:= Saches Dam East, Hole No. 3, Depth 50 ft.

SOIL TYPE := Decomposed Gabbro, a clayey sand.

DIRIVED STRENGTH PARAMETERS := c = 11 p.s.i. ϕ = 15°-18'

c' = 2 p.s.i. ϕ' = 34°-18'

FIG. 9.37

Mohr's envelopes for the total and the effective stresses respectively are shown.

The constant volume and the S_{csu} tests gave effective stress envelopes which were practically identical, indicating that these two forms of testing are equivalent. If this is true for all soils it is a point worth noting, as the constant volume tests are considerably easier than the S_{csu} tests. The pore pressure changes during the later stage of each test (Figure 9.36) indicate that the material expanded slightly causing a reduction in the pore pressures developed during the earlier stage of the test. This had the effect of causing the critical effective stress circle on the Mohr diagram to remain in contact with the envelope over a considerable range of pressure, indicating that the failure point is not necessarily given by the peak point stress. For one test this effect is illustrated in Figure 9.38. It was also found that the maximum pore pressures that developed during each test were linearly related to the consolidation pressures (Figure 9.39).

The strength parameters for the gabbro material were as follows:-

Total stress:

$C = 10 - 50$ psi $\quad \phi = 14 - 16^{\circ}$

Effective stress:

$C' = 4 - 8$ psi $\quad \phi' = 28 - 34^{\circ}$

This material is so much stronger than the slime clay that sliding failure through it is not possible. A number of trial circular slip failure analyses also indicated that the factor of safety against this form of failure was so high that they were unlikely. In consequence for the critical stability analysis of the failure of Sache's Dam East this material is unimportant.

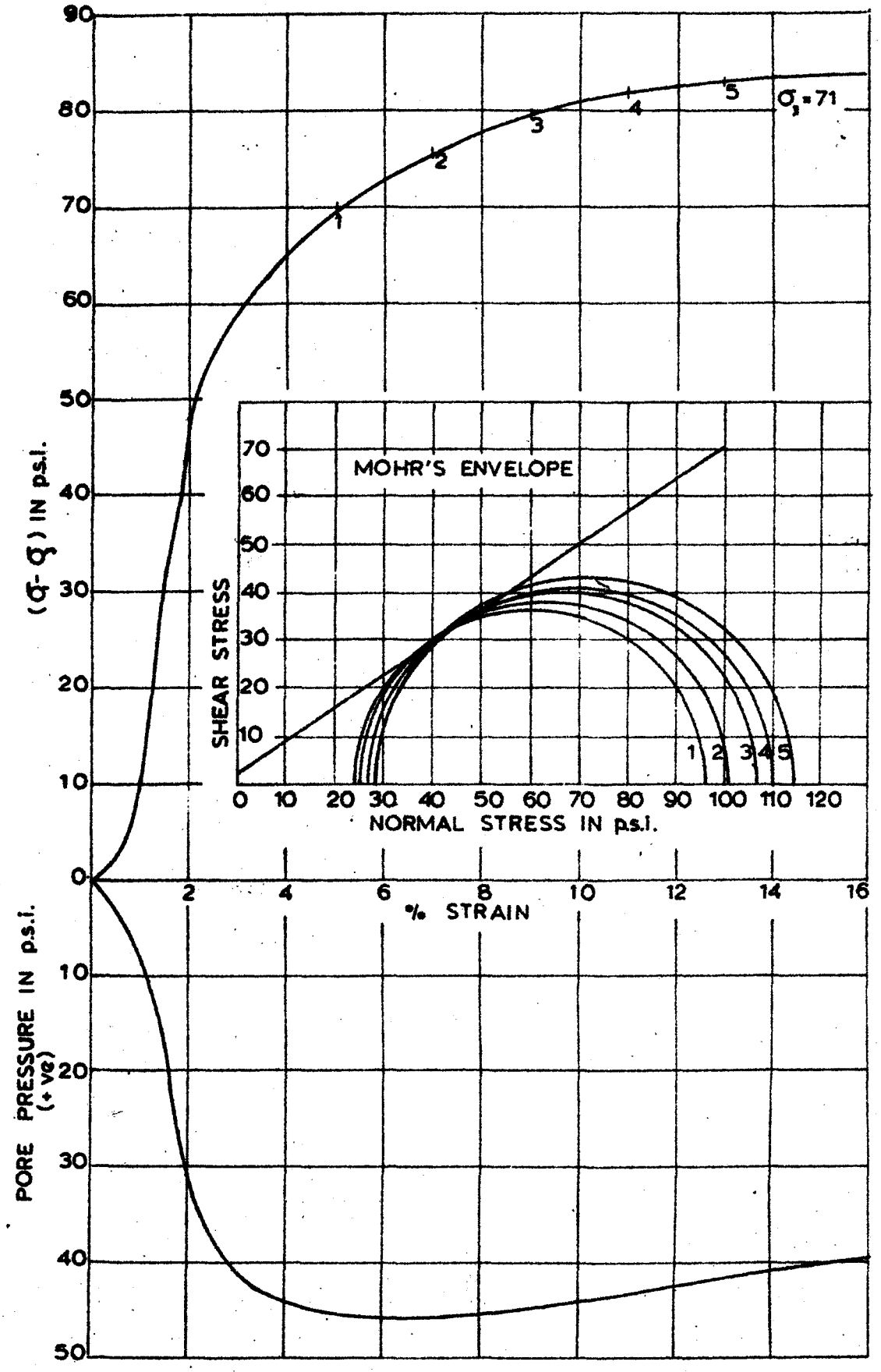

EFFECTIVE STRESS STATE NEAR & AT FAILURE IN A OVER CONSOLIDATED CLAYEY SAND.

FIG. 9.38

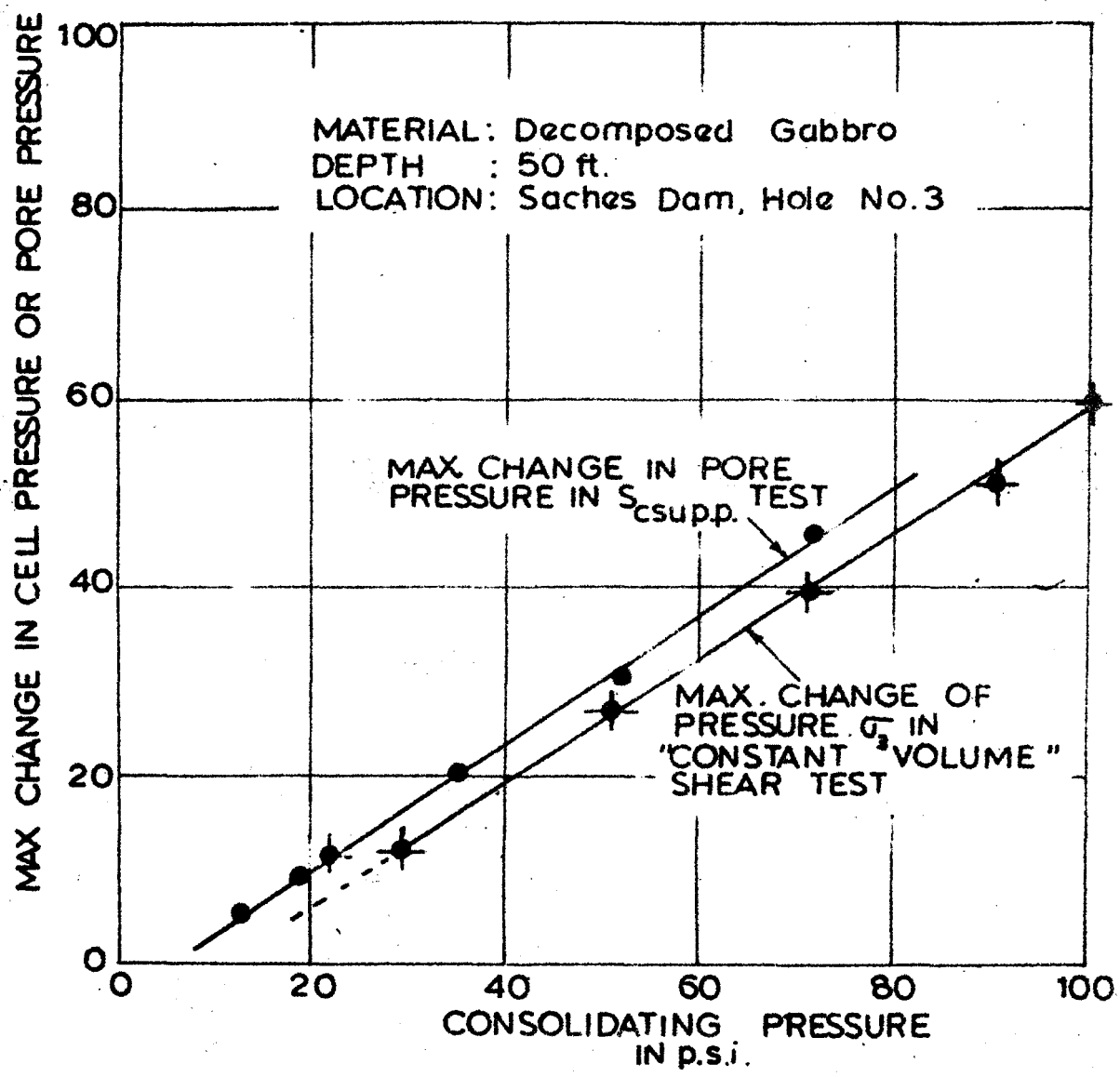

RELATIONSHIP BETWEEN CONSOLIDATING PRESSURE & MAXIMUM CHANGE IN PORE PRESSURE OR LATERAL PRESSURE IN CELL DURING SERIES OF UNDRAINED SHEAR TESTS.

FIG. 9.39

S E C T I O N 1 0

10. STABILITY ANALYSIS OF SACHE'S DAM EAST

10.1 Introduction

In Section 8, from the external evidence of failure, it was concluded that the mode of failure of Sache's Dam East wall was of a sliding type. In Section 9, shear strength and consolidation characteristics of the critical strata in the foundation and the embankment material were experimentally determined. In this Section the intention is to analyse the stability of the embankment based on a sliding mode of failure, making use of experimentally derived strength parameters of the material. Such an analysis is essential for two reasons: firstly, it is a fact that the embankment has failed, and hence the analysis should verify this, otherwise there is reason to believe that either the mode of failure and/or the strength parameters of the soils are not correct. Secondly, if the analysis confirms that the mode of failure can reasonably be accepted as being the correct one, then this information can be used in designing a stable flank.

10.2 An examination of the shear strength parameters

The experimental shear strength parameters as obtained in the triaxial tests are determined under standard conditions of consolidation and drainage. It is necessary to examine how appropriate these values are to the failure of the dam, and in what manner the stress history and drainage conditions of the critical strata under the embankment could cause deviations from the experimentally determined values. This is particularly pertinent in the case of the strength parameters for the slime clay, as the length of the

shear plane in this material is up to 700 ft and a small change in the value of the shear strength leads to a disproportionate change in the stability of the embankment.

The failure of Sache's Dam East has this unusual feature - that as subsidence at the wall occurred it was continually made good. The failure therefore grew until stability was achieved, and the speed of the slide movement was governed to a degree by the amount of material being deposited in the region of subsidence.

The long period of time that elapsed before the failure achieved stability makes it necessary to consider two stability situations: (i) that during the period in which the failure took place, and (ii) the present stability of the dam:-

(i) At any point in the clay layer during the period of failure the following events were taking place simultaneously:- The clay was consolidating under the temporal load, increasing its strength and requiring a higher build-up of material in the zone of subsidence to generate the force necessary to overcome the increasing shear resistance of the clay layer. The rate of build-up and consequently the final outline of the failure depended on:-

(1) the speed of deposition

(2) the increase in the shear strength of the clay layer.

The shear strength depended in turn on the length of the failure line in the clay and the gain in the shear strength with time due to consolidation.

The combination of these two factors led to a gradually decreasing speed of failure until the shear resistance of

the clay layer equalled the disturbing active failure force at the embankment, and failure movement ceased. It also led, as illustrated in Section 8, to the gently increasing slope in the outline of the failure zone.

Consolidation of the clay layer was taking place under conditions of plastic shear, a condition not reproduced in the normal consolidated sheared undrained S_{csu} test. Being continually in a partially consolidated state (in contrast to the over-consolidated state) shear strain would develop positive pore pressures in addition to those due to the superimposed load.

The temporal pore pressures in each clay unit would be dependent upon the rate of increase in the overburden pressure due to the growth of the failure zone dimensions, and the rate of pore pressure dissipation. The latter depends on the thickness of the clay layer and its permeability. There is no data available on the rate of growth of the failure zone, and it is therefore not possible to calculate the degree of consolidation (and hence the shear strength development) up to the time the failure movement ceased. If, however, at the time the failure movement ceased the clay was unconsolidated, the lapse of time since then would allow the consolidation to proceed to completion and "freeze" the failure in its present form to a higher factor of safety. This situation is the most likely, for from the consolidation tests on the clay it appears that in a 5 ft thick layer (which is the estimated mean thickness of the slime clay layer under the dam)(see Figure 10.1) the drainage at the top and bottom surfaces would require 2 - 3 months to give 90% consolidation.

The depth of the tailings at the toe of the failure would be governed to a great extent by the unconsolidated, undrained shear strength of the clay as deposited on the floor of Sache's Dam West. As the movement of the failure slowed down, there was increasing opportunity for some consolidation to take place underneath the toe, thus increasing the shear strength of the clay to a value greater than that required to achieve stability in the toe. Consequently at any time after failure movement was initiated, the factor of safety at this section would be greater than unity, this value continually increasing during the period of failure movement. Applying this argument to all the sections of the failure zone, it can be expected that by the time the failure movement ceased, the critical zone for the failure would be in the region near the back leg of the subsidence furthest away from the toe and all other sections would have factors of safety equal to or greater than unity.
(ii) Once the failure movement ceased, the residual pore pressures due to the overburden and the shear stresses would in time be dissipated, raising the factor of safety. The increase in the factor of safety would be dependent on the amount of excess pore pressure existing at the time of cessation of movement.

After the pore pressures in the clay layer had been completely dissipated, if due to some cause shear failure should commence, and assuming such a failure to take place in undrained conditions (which is most likely due to slow pore pressure dissipation in the clay layer), then because of the previous development of shear pore pressures, the pore pressure development in the new failure would probably

be less than that in a slime clay layer which had not been subjected to a previous shear strain history. If this argument is correct, then it can be expected that the $\emptyset$ in the clay material under the dam will show a larger value than that given by the S_{csu} test.

The S_{csu} triaxial shear tests were performed on samples of the clay layer consolidated under about 30 ft of tailings (consolidation pressure approximately 3,500 lb per sq. ft), and have suffered shear deformation. But for the series of tests the consolidation pressures ranged from 3,500 - 14,000 lb per sq. ft. Under the higher pressures the historical effects of the shear strain on the pore preasure development would be diminished, and it is therefore likely that the value of $\emptyset$ obtained from this series of S_{csu} tests would approximate to that obtained from a clay layer not subject to previous shear deformation.

From the above considerations the following conclusions are postulated as to the applicability of the S_{csu} test parameter to the analysis of the dam failure:-

(1) At any point in the clay layer during failure, due to the partially consolidated state, the equivalent value of $\emptyset$ would probably be less than that given by the S_{csu} test.

(2) After failure had ceased and sufficient time had elapsed for total pore pressure dissipation, due to the effects of the previous shear deformation history the pore pressure development in a new failure would probably be less than that given by the S_{csu} test, resulting in the equivalent value of $\emptyset$ greater than that given by the test. For the moment no estimate can be made of this equivalent value.

(3) The drainage conditions in the clay layer are such that the factors of safety for sections of the failure zone should indicate a maximum near the toe, decreasing to a minimum value near the back leg of the failure. This should be true both during the period of, and in the present state of, the failure.

In the absence of samples from all sections of the clay layer along the plane of failure, it is not possible to obtain the true strength parameters for the stability analysis of the failure in its present state, i.e., after all pore pressures have dissipated. It is however possible to form an idea of the stability by performing the analysis using the value of $\emptyset$ equal to 12° for the clay as obtained from the S_{csu} tests. If values of $\emptyset$ smaller than 12° are required to give a minimum factor of safety equal to unity, this would indicate that pore pressure dissipation was not complete at the time failure movement ceased. If values of $\emptyset$ greater than 12° are required, then this would indicate that pore pressures had developed (now dissipated) due to the shear deformation. In each analysis the value of $\emptyset$ can be assumed constant, although this is only approximately true as the actual value at any point of the failure line would depend on the pore pressure development due to the previous shear strain, and the degree of pore pressure dissipation that had taken place by that time.

10.3 Stability analysis

10.3.1 Selected shear strength parameters

The following values for the shear strength parameters for the critical clay slime layer and the tailings material were selected:-

Slime clay layer: $\phi = 9^\circ \ 10^\circ \ 12^\circ$

$C = 0$ lb per sq. ft

It is assumed that the failure takes place in undrained conditions.

Tailings material: $\phi' = 34^\circ$

$C' = 0$ lb per sq. ft

Due to the high permeability and unsaturated condition, failure through this material is assumed to take place in drained conditions. The density, γ , of the tailings material at bank moisture content is taken at 110 lb per cubic foot.

10.3.2 Failure cross-section

The general vertical profile of the strata in the failure region is shown in Figure 10.1. In Figure 10.2 the critical cross-section of the dam on the line drawn in Figure 10.3 is shown. It should be noted that the slope of the ground surface is approximately 2° towards the down-stream side. The cross-section is divided into sections numbered to facilitate numerical integration of the required force functions.

10.3.3 Method of analysis

The disturbing forces at any point along the slime layer are due to:-

(1) Active failure in the tailings; this force was determined by two methods - that due to Rendulic and that due to Trollope, assuming $\phi = 34^\circ$.

(2) The component of weight of the tailings material down the 2° slope, determined by accumulating this component from the toe inwards to point x as follows:-

$$\text{Slope component} = \int_{\text{toe}}^{x} \gamma \, h \tan(2^\circ) \, ds$$

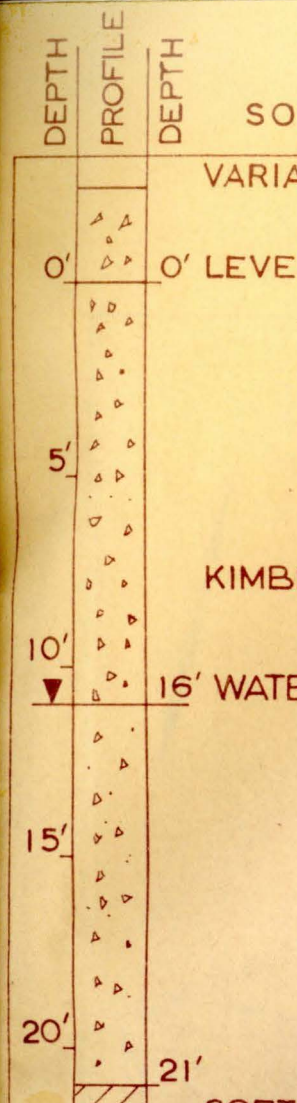

SOIL DESCRIPTION	SHEAR DATA		CONSOLIDATION DATA	
VARIABLE SURFACE LEVEL 0' LEVEL SACHES DAM WEST R.L.:1450 KIMBERLITE TAILINGS $-\frac{3}{4}$" MESH 16' WATER TABLE No. 2	$\phi' = 34°$ $C' = 0$ $\gamma \simeq 110$ lbs ft^3 $W \simeq 6$ %		$C_c = 0.34$ $e_o \simeq 0.65$ $C_v = ?$	
	FOR TRI. CONSOL. UNDER LOW W/Cs, LARGE COLLAPSE OCCURS WHEN WETTING UNDER SHEAR. SMALL ADDITIONAL MOVEMENTS OCCUR ON INUND. OF TAILINGS (5% W/C) UNDER SHEAR		C_v CANNOT BE DETERMINED AS CONSOLIDATION IS CHIEFLY SECONDARY. WHEN CONSOLIDATING UNDER LOW WATER CONTENTS ($\simeq$1%) LARGE COLLAPSE OCCURS ON INUNDATION	
21' SOFT BLUE GRAY SLIME SHOWING SIGNS OF HORIZONTAL SHEAR MOVEMENT 25'	$\phi = 12°$ $\phi_{min} = 10°$? $C = 0$ psi		$C_c = 0.9$ $e_o = 1.85$ $2H = 4$ ft. $C_v = 1.0 \times 10^{-4}$ cm^2/sec NORMALLY CONSOLIDATED	
VALLEY AND DAM SEDIMENTS OF SOFT CLAYS AND SILTS INTERBEDDED WITH LOOSE SANDS SEDIMENTS VERY VARIABLE AND LENTICULAR NO LAYERS OF THICKNESS GREATER THAN 2 FEET	$\phi = 10°$ $C = 3$ psi		$C_c = 0.45$ $C_v = 8 \times 10^{-4}$ cm^2 sec $e_o = 1.4$ NORMALLY CONSOLIDATED $2H = 2$ ft	
40' PEBBLE MARKER SUB ANGULAR QUARTZITE 42'	$\phi' = 30°$ $C' = 1$ psi $\phi = 15°$ $C = 12$ psi	NOT TESTED	$C_c = 0.24$ $C_v = 140 \times 10^{-4}$ $e_o = 1.0$ SLIGHTLY OVER – CONSOLIDATED $H = 40$ ft ESTIM.	NOT TESTED
			NOTE: IN SELECTING THE ABOVE DESIGN VALUES THE LOWEST TEST VALUES WHERE TAKEN. THE VALLEY AND DAM ARE VERY VARIABLE	

SUMMARISED SOIL TEST DATA USED IN STABILITY ANALYSIS OF SACHES DAM EAST WALL

FIG.10.1

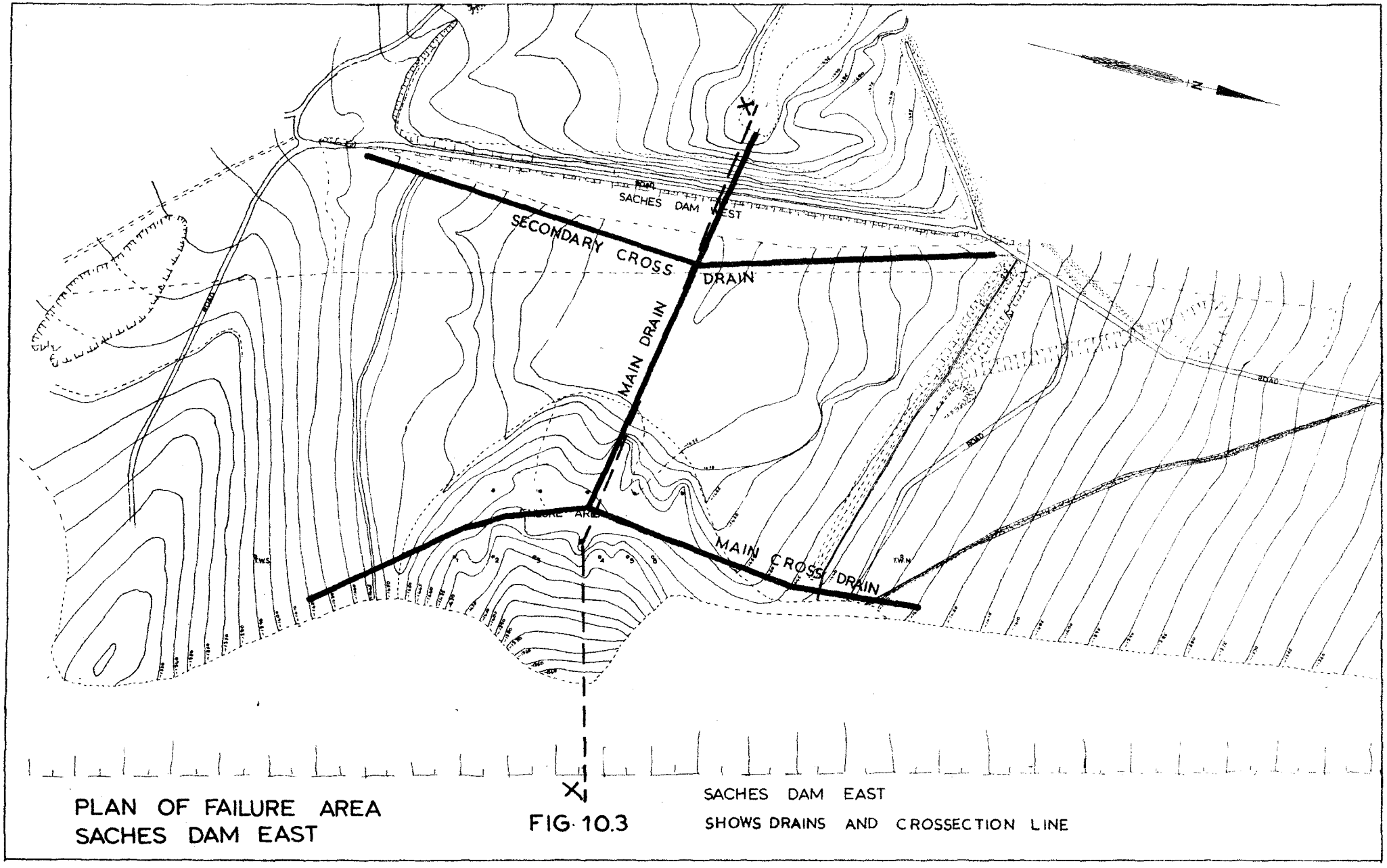

PLAN OF FAILURE AREA
SACHES DAM EAST

FIG. 10.3

SACHES DAM EAST
SHOWS DRAINS AND CROSSECTION LINE

Where γ = density of tailings

h = height of tailings above increment ds

ds = increment of length failure line, s, in the clay layer.

The resisting shear force at any point in the clay layer was determined as follows:-

Trollope's method was followed (see Section 7.3) for determining the vertical consolidation stress, P, assuming no arching conditions, and the resisting total shear forces in the clay layer found by accumulating the shear stresses from the toe inwards for the values of $\phi = 9^{\circ}$, 10° and 12°. Quantitatively shear resistance from the toe to point x, say, is given by:-

$$\text{Shear resistance} = \int_{\text{toe}}^{x} P \tan \phi \, ds$$

The factor of safety was determined from:-

$$FS = \frac{\text{Disturbing forces}}{\text{Resisting forces}}$$

The result of the analysis is given in Figure 10.4.

10.4 Discussion

10.4.1 Change in the value of ϕ

The stability analysis with $\phi = 12^{\circ}$ gives the minimum stability of the embankment as 1.30. This value is so much larger than unity that it can be concluded that up to the time of cessation of failure movement the clay was still in a partially unconsolidated state, which as we have seen would lead to an equivalent value of ϕ less than 12°. If a value for $\phi = 9^{\circ}$ is taken, it can be noted that from

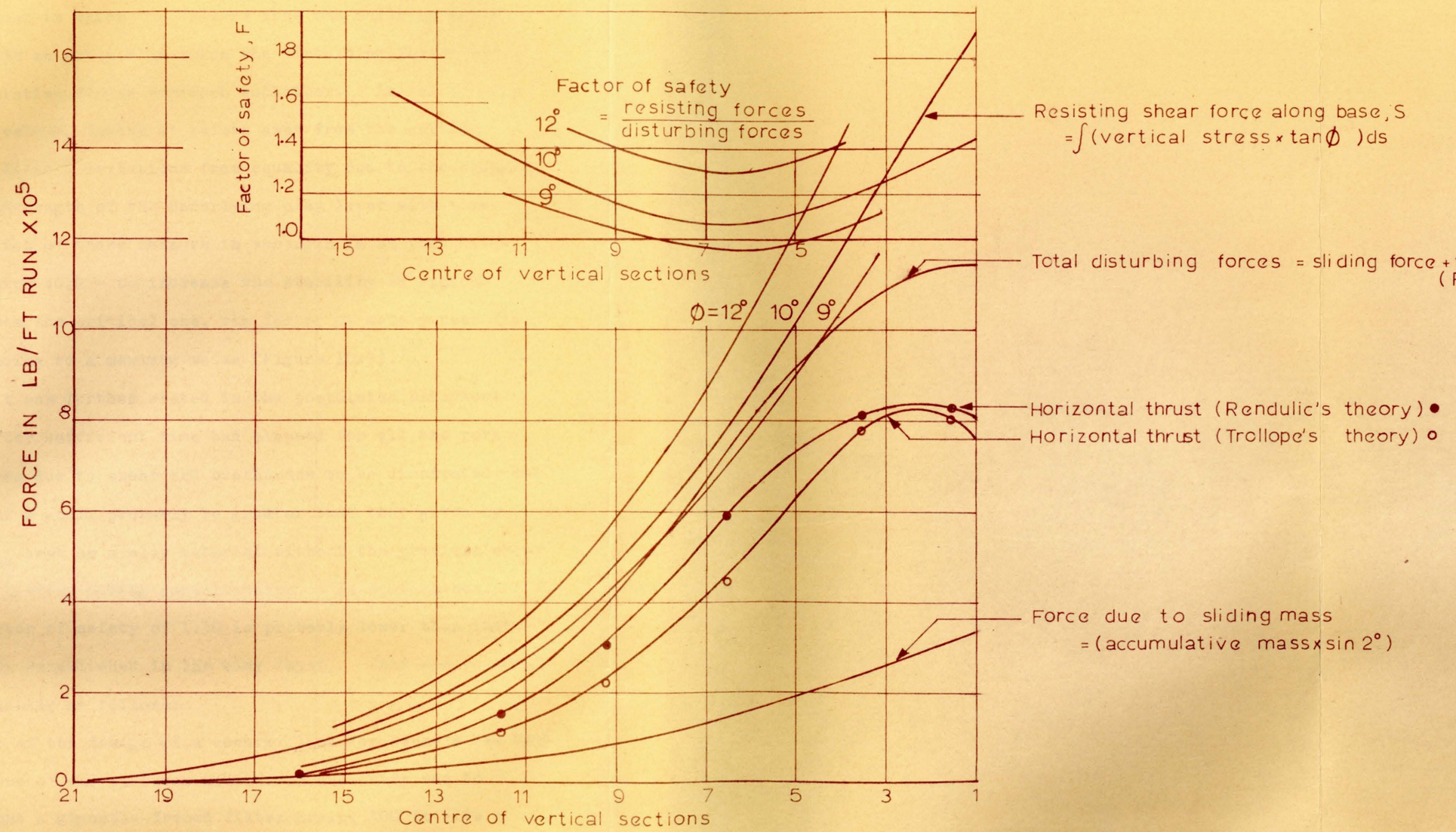

STABILITY ANALYSIS OF SACHE'S DAM EAST WALL AGAINST SLIDING ALONG BASE

FIG. 10.4

section 4 to section 9 (Figures 10.2 and 10.4), the factor of safety is approximately equal to unity. Such a state of stability does not appear to be unreasonable because the manner in which the failure zone was built up would result in an outline in which the disturbing forces and the resisting forces approach eachother. As the failure zone develops, forces at points away from the critical zone will show deviations from equality due to the changes of the strength of the underlying clay layer with time. The effect of these changes in strength is as postulated in Section 10.2 - to increase the stability in regions away from the critical one, the factor of safety near the toe tending to a maximum value (Figure 10.4).

It was further stated in the postulated behaviour that after sufficient time had elapsed for all the pore pressures due to shear and overburden to be dissipated, the value of $\emptyset$ would probably be greater than that given by the S_{csu} test on a clay material without the previous shear strain history during consolidation. In consequence, the factor of safety of 1.30 is probably lower than that actually established in the clay layer. This was verified unexpectedly as follows:

As part of the design of a secure flank for Sache's Dam East wall, one of the measures considered necessary was to construct a gigantic french filter drain, 100 ft wide x 40 ft high, on the downstream side of the wall. The object of the drain was to prevent erosion of the toe of the new flank should rupture occur through the upstream impervious beach, the drain to collect and drain away the water. For maximum effectiveness, the drain had to be

sited as closely as possible to the present downstream flank of Sache's Dam East, and one section was sited through the toe of the failure zone (Figure 10.3 shows the location of the drain, and Figures 8.5 and 8.12 show photographs of the trench being excavated).

At the time an analysis was made to determine the factor of safety of the dam should the trench be excavated across the failure zone. This analysis gave that the factor of safety would be about 1.1. It was considered that this low factor of safety would be allowable for the short period after the trench was excavated and before the drain was constructed.

After the trench was excavated, movement in the failure zone took place. No visible failure lines developed, but measurements on concrete markers placed across the failure zone (Figure 8.12) indicated that movement did take place. On the top of Sache's Dam East very slight movement, more in the nature of strain adjustment, was observed - a crack about 2 - 3 inches wide opened up parallel to the line of the crest of the dam about 10 feet from the downstream top edge.

An analysis in terms of Rendulic's theory now indicates that the previous analysis was too optimistic, and that for $\phi = 12^{\circ}$ the factor of safety is reduced to approximately 0.85 (see Figure 10.7). If the stability was in fact 0.85, the failure movement should have been much more extensive, and it can therefore be concluded that the value of ϕ was greater than 12°. If a value of $\phi = 14^{\circ}$ is taken, the minimum factor of safety is increased to

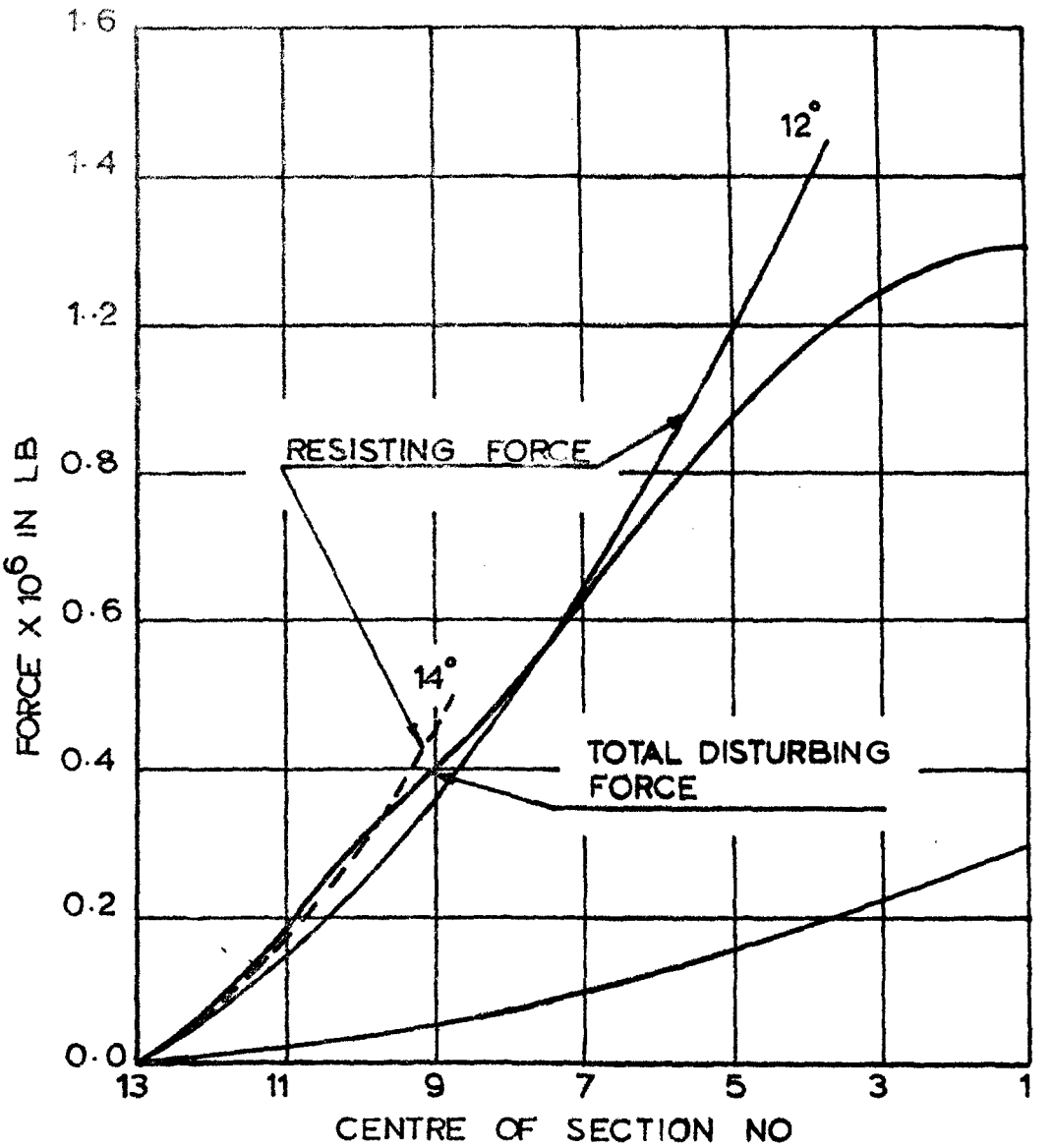

FORCES IN SACHE'S DAM EAST AFTER DRAIN WAS CUT

FIG. 10. 7

approximately equal to one, and the slight movements that were observed can reasonably be expected. It can also be concluded that previous pore pressure development due to shear strain had raised the equivalent S_{csu} value for $\emptyset$ to above 12°, to approximately 14°.

To conclude, during failure movement the consolidation of the critical slime layer was incomplete, leading to an equivalent value of $\emptyset$ less than that given by the S_{csu} tests. After failure movement had ceased, the dissipation of the pore pressure increased the stability of the dam. This increase was greater than that predicted from the S_{csu} test because of the dissipation of the pore pressure due to previous shear strain movement.

10.4.2 Choice of method to determine active forces in the embankment

A comparison of the active failure forces as determined by Trollope's and Rendulic's methods (Figure 10.3) shows that the former gives appreciably lower values than the latter. This of course constitutes no proof that Trollop's method is in error, but it does warn that in the present state of knowledge, for safe design Rendulic's method is to be preferred.

REFERENCES

CASE, J., (1948) 'The Strength of Materials', 3rd Edn. Edward Arnold & Co., London.

COLLATZ, L., (1960) 'The Numerical Treatment of Differential Equations', 3rd Edn. Springer-Verlag, Berlin.

COURANT, R. and FRIEDRICHS, K.O., (1956) 'Supersonic Flow and Shock Waves', 1st Edn. Interscience Publishers Inc., New York.

CRANDALL, S.H., (1956) 'Engineering Analysis', 1st Edn. McGraw-Hill Book Co., Inc., New York.

FORSYTHE, G.E. and WASOW, W.R., (1960) 'Finite-Difference Methods for Partial Differential Equations', 1st Edn. John Wiley & Sons Inc., New York.

HARTREE, D.R., (1958) 'Numerical Analysis', 2nd Edn. Oxford University Press.

HILL, R., (1960) 'The Mathematical Theory of Plasticity', 1st Edn. Oxford University Press.

HVORSLEV, M.J., (1937) 'Uber die Festigkeitseigenschaften gestorter bindiger Boden'. Danmarks Naturvidenskabelige Samfund, Copenhagen.

HUMMEL, F.H. and FINNAN, E.J., (1920) 'The Distribution of Pressure on Surfaces supporting a Mass of Granular Material'. Proc. Inst. Civ. Eng. Vol. CCXXII, Pt.2.

JENNINGS, J.E. and KIRCHMANN, P.F., (1961) 'Critical Strain Energy of Distortion in Soil at Limited Yield'. Boston Society of Civil Engineers.

JENNINGS, J.E. and MARAIS, G. van R., (1959) 'Report No. 3: Failure of Sache's Dam East'. Premier (Tvl.) Diamond Mining Co. Ltd. (restricted circulation).

MARAIS, G. van R., (1958) 'Report No. 1: Failure of Sache's Dam East'. Premier (Tvl.) Diamond Mining Co. Ltd. (restricted circulation).

MARAIS, G. van R., (1958) 'Report No. 2: Ibid.'

RALSTON, A. and WILF, H.S., (1962) 'Mathematical Methods for Digital Computers', 1st Edn. John Wiley & Sons, Inc., New York.

RENDULIC, L., (1938) 'Der Erddruck im Strassenbau und Bruckenbau'. Forschungsarb. Strassenwesen, Bd.10, Volk u. Reich Verlag, Berlin.

SOKOLOVSKI, V.V., (1960) 'Statics of Soil Media'. (English Translation from Russian 2nd Edn.). Butterworth Scientific Publications, London.

SOUTHWELL, R.V. and ALLEN, D.N. de G., (1950) Phil. Trans. Roy. Soc. A 242 quoted from Hill (1960) above.

TERZAGHI, K., (1943) 'Theoretical Soil Mechanics', 1st Edn. Chapman & Hall, London.

TROLLOPE, D.H., (1957) 'The Systematic Arching Theory applied to the Stability Analysis of Embankments'. 4th Inter. Conf. Soil Mech. Found. Eng., London. Butterworth Scientific Publications.

TROLLOPE, D.H. and MORGAN, J.R., (1959) 'Stress Systems within Simple Slopes of Granular Materials'. Trans. Inst. Eng. Australia (Civil Engineering Section).

APPENDIX I

NUMERICAL SOLUTION OF THE SET OF DIFFERENTIAL EQUATIONS GOVERNING THE CRITICAL STRESSES IN SYMMETRICAL WEDGES OF COHESIONLESS MATERIALS UNDER ACTIVE FAILURE CONDITIONS.

The following program is written in UMAC (University of Miami Algebraic Compiler) mathematical code for an I.C.T.1500 computer of 20 KC capacity. This code is very similar to FORTRAN and a reader familiar with the latter will have no trouble in following the former.

The program has made use of the SDE (Scientific Data Editing) version which requires a minimum of 3 tape decks.

The annotations next to the code instructions are descriptive only and do not form part of the program.

The inversion or change of independent variable from θ to ψ in the differential equations is based on the following relationships:

$$\frac{d\theta}{d\psi} = \frac{1}{\frac{d\psi}{d\theta}}$$

$$\frac{ds}{d\psi} = \frac{ds}{d\theta} \cdot \frac{d\theta}{d\psi}$$

SOURCE PROGRAM

TAPE321	Notes
FIX ALL,I,J,N	
READ,P,MU,CØNV	ρ, μ, and conversion constant to change radians to degrees.
DIMENSIØN,A(4),B(4),C(4),Q(3),Y(3),R(3),K(3)	
FUNCTIØN,SIN:LBG,CØS:LBH,MØD:LBE,ATAN:LBI,EXP:LBD	
READ ARRAY,A,B,C,Q	Constants required in Runge-Kutta-Gill step by step method (See Romanelli).
READ,V2	
6 READ ARRAY,Y	Initial values for θ, ψ and S.
H=V2	Convert to initial step length after previous calculation.
D1=.5*Y(3)+.14	Determine value of θ at which inversion of equations takes place.
IF (100.-Y(1)) 10,200,20	Last set of initial values for array Y is 100.,0.,0., if Y(1)=100. then program completed.
10 STØP 0001	
20 THETA=Y(1)	Store θ, ψ and S.
EPSI=Y(2)	
S=Y(3)	
AREAS=0.0	Initialise summation of areas for determining radius arms of failure lines.
AREAD=0.0	
STØRT=0.0	

```
   SUM=EPSI+MU
   DIFR=EPSI-MU
   STLS=CØSF(SUM)/SINF(SUM)
   STLD=CØSF(DIFR)/SINF(DIFR)
   SINP=SINF(P)
   CØSP=CØSF(P)
   CØSP2=CØSP*CØSP
```

Condense various functions occurring in differential equations.

```
   JUMP TØ 2000
```

Calculate stress components in wedge.

```
   PRINT AND LABEL,THETA,EPSI,S,VCOMP,HCOMP,SHEAR
   NNN=0
   N3=0
   NN=0
   NKK=0
   NKKK=0
```

Initialise various constants.

```
30 DØ 100 J=1,4,1
   IF (NN) 40,50,80
```

If NN=0 normal equations i.e. θ independent. If NN>0 inverted equations with independent variable ψ.

```
40 STØP 0002
50 JUMP TØ 1000
```

Calculate various functions in equations.

```
   K(1)=H
   K(2)=H*(U/V-1.0)
   K(3)=H*W/X
   GØ TØ 90
```

Independent variable θ

```
 80 JUMP TØ 1000                    Calculate various functions
                                    in equations.
    K(1)=H
    K(2)=H*V/(U-V)                  Independent variable ψ .
    K(3)=K(2)*W/X
 90 DØ 100 I=1,3,1
    R(I)=A(J)*(K(I)-B(J)*Q(I)       Runge-Kutta-Gill step by step
                                    calculation of either ψ and S
    Y(I)=Y(I)+R(I)                  or Θ and S.
    Q(I)=Q(I)+3.0*R(I)-C(J)*K(I)
    IF (NN) 110,120,130             NN=0  normal equations
                                    NN>0  inverted equations
110 STØP 0003
120 THETA=Y(1)
    EPSI=Y(2)                       Normal equations
    S=Y(3)
    GØ TØ 100
130 THETA=Y(2)
    EPSI=Y(1)                       Inverted equations
    S=Y(3)
100 CØNTINUE
    JUMP TØ 2000                    Calculate stresses
```

```
      PRINT,THETA,EPSI,S,VCØMP,HCØMP,SHEAR,(SINF(THETA)/CØSF(THETA))
                                                  X Coordinate in wedge
      THETD=CØNV*THETA                    Convert θ in radians to
                                          degrees.
      PRINT,(K(1)/H),(K(2)/H),(K(3)/H),THETD      Print slopes
                                                  dθ/dθ , dψ/dθ , ds/dθ , θ
                                          or      dθ/dψ , dψ/dψ , ds/dψ , θ
      SUM=EPSI+MU
      DIFR=EPSI-MU
      DIFT=THETA-STØRT
      IF (0.5-MØDF(EPSI)) 4000,3000,3000  | If |EPSI|>.5 do not
                                          | calculate the longer
                                          | radius arm.
3000  LS=CØSF(SUM)/SINF(SUM)
      AREAS=(STLS+LS)*.5*DIFT+AREAS
      RADS=EXPF(AREAS)
      STLS=LS
      PRINT,RADS
4000  LD=CØSF(DIFR)/SINF(DIFR)            Calculate and print radius arms.
      AREAD=(STLD+LD)*.5*DIFT+AREAD
      RADD=EXPF(AREAD)
      STLD=LD
      STØRT=THETA
      PRINT,RADD
      X=P+2.*THETA
```

```
    IF (NKKK) 101,102,5
```

If NKKK=0 continue.
>0 final step has been completed. Calculate slope of wedge etc. and start new solution.

```
101 STØP 0005

  5 E=ATANF(SINP*CØSF(X)/(SINP*SINF(X)-1.0))
```

Calculate slope of wedge and

```
    SLØPE=E*CØNV
```

convert to degrees.

```
    CHEKS=CØSF(THETA+P)/CØSF(P)
```

Calculate check of S on α_2 characteristic.

```
    PRINT AND LABEL,E,SLØPE,CHEKS

    CHANGE PAGE

    DØ 105 J=1,3,1

105 Q(J)=0.0
```

Change Q(J) back to zero for new calculation

```
    GØ TØ 6

102 IF (DI-MØDF(EPSI)) 150,150,170
```

Test |EPSI|>DI
True. Continue calculation using normal equations.

```
170 GØ TØ 30

150 IF (NNN)  300, 310, 320
```

False. Then first use NNN=0.

```
300 STØP 0005
```

now

```
310 H=-H*.1
```

step length is reduced

```
    Y(1)=EPSI

    Y(2)=THETA
```

equations are to be used in inverted form θ dependent.

```
    NN=1
```

to ensure this set NN=1

```
    Q(1)=0.0

    Q(2)=0.0
```

because equations are inverted start off with Q(J)=0.

```
    Q(3)=0.0
```

To ensure that these steps are not repeated in next cycle set

```
    NNN=1
```

NNN=1 and steps missed out from

```
    IF (NKKK) 101,102,5
```

If NKKK=0 continue.
>0 final step has been completed. Calculate slope of wedge etc. and start new solution.

```
101 STØP 0005

  5 E=ATANF(SINP*CØSF(X)/(SINP*SINF(X)-1.0))
```

Calculate slope of wedge and

```
    SLØPE=E*CØNV
```

convert to degrees.

```
    CHEKS=CØSF(THETA+P)/CØSF(P)
```

Calculate check of S on α_2 characteristic.

```
    PRINT AND LABEL,E,SLØPE,CHEKS

    CHANGE PAGE

    DØ 105 J=1,3,1

105 Q(J)=0.0
```

Change Q(J) back to zero for new calculation

```
    GØ TØ 6

102 IF (DI-MØDF(EPSI)) 150,150,170
```

Test $|EPSI| > DI$
True. Continue calculation

```
170 GØ TØ 30
```

using normal equations.

```
150 IF (NNN)  300, 310, 320
```

False. Then first use NNN=0.

```
300 STØP 0005
```

now

```
310 H=-H*.1
```

step length is reduced

```
    Y(1)=EPSI

    Y(2)=THETA
```

equations are to be used in inverted form θ dependent.

```
    NN=1
```

to ensure this set NN=1

```
    Q(1)=0.0

    Q(2)=0.0
```

because equations are inverted start off with Q(J)=0.

```
    Q(3)=0.0
```

To ensure that these steps are not repeated in next cycle set

```
    NNN=1
```

NNN=1 and steps missed out from 150 in next cycle.

```
    GØ TØ 30

320 IF (.521-MØDF(EPSI)) 321,321, 30    Step length now in terms of ψ
                                        Maximum value of ψ =.52354...
                                        As ψ approaches near this value
                                        violent changes in θ and S
                                        occur.
                                        Hence if EPSI≯.521
321 IF (N3) 322,323,330

322 STØP 0007

323 H=H*.1                              reduce step length once again
                                        and
    N3=1                                set N3=1 to miss out reduction
                                        in next cycle.
    NK=MØDF((MU+EPSI)/H)                Now calculate in terms of this
                                        new step length the whole
                                        number of steps remaining.
330 NKK=NKK+1                           Set tally on this number

    IF (NK-NKK) 325,30,30               if exceeded

325 H=-MØDF(MU+EPSI)                    determine final step length
                                                  and
    NKKK=1                              set NKKK=1 to ensure final
                                        calculation cycle is not
                                        repeated.
    GØ TØ 30

1000 U=CØSF(THETA)-SINP*CØSF(EPSI*2.0-THETA)-S*CØSP2

    X=CØSF(2.0*EPSI)-SINP

    W=-SINF(2.*EPSI+THETA)+S*SINK(2.*EPSI)

    V=2.0*S*SINP*X

    JUMP BACK

2000 CØST=S/CØSF(THETA)

    EPTH=2.0*(EPSI+THETA)

    FRACT=SINP*CØSF(EPTH)

    VCØMP=CØST+CØST*FRACT               Vertical normal stress
```

```
    HCØMP=CØST-CØST*FRACT          Horizontal normal stress
    SHEAR=CØST*SINP*SINF(EPTH)     Shear stress
    JUMP BACK
200 END
```

```
DATA23
.52359878 .52359878 57.295780 ,    β, μ, conversion constant
                                   from radians to degrees
0.5 .29289322 1.7071068 .16666667 , Array A  )
                                             ) Constants for
2.0 1.0 1.0 2.0 ,                    "   B   )
                                             ) the Runge-Gutta-
0.5 .29289322 1.7071068 .5 ,         "   C   )
                                             ) Gill method.
0.0 0.0 0.0 ,                        "   Q   )
0.87266463E-2 ,                    V2 = step length, δθ in
                                   radians (0.5°)
0.0 0.0 .66666667 ,                θ₀ , ψ₀ , S₀  (Array Y)
0.0 0.0 0.66 ,                       "
0.0 0.0 0.65 ,                       "
0.0 0.0 0.64 ,                       "
     etc.
0.0 0.0 0.53 ,                       "
100.0 0.0 0.0 ,                    Ending card
E/D                                End of data
```

APPENDIX 2

SOLUTIONS FOR THE ACTIVE CRITICAL STATE IN SYMMETRICAL WEDGES OF COHESIONLESS MATERIAL FOR AN ANGLE OF INTERNAL FRICTION OF 30°

The solutions are listed for the wedge slopes ξ = 0, 5, 10, 15, 20, 25 and 30°. Solutions cannot be obtained directly for these slopes as the initial values for the function, S, leading to the solutions for the specified slopes are unknown. Solutions for the slopes ξ were obtained for a number of initial values of S ranging from 0.66666667 to 0.527, and the initial values of S leading to the specified slopes were found by a Lagrangian 4th Order Interpolation*. The initial values for S thus obtained led to slopes ξ very near the specified ones, the maximum deviation being 2.48 seconds of arc. The specified slopes and the computed slopes found from the interpolated initial values of S are listed below:-

Specified Slope	Computed Slope			Difference
0°	(-) 0°	0'	0.52"	-0.52"
5°	5°	00'	1.15"	+1.15"
10°	10°	00'	2.48"	+2.48"
15°	14°	59'	57.60"	-2.40"
20°	19°	59'	59.92"	-0.08"
25°	25°	0'	0.38"	+0.38"
30°	29°	59'	59.51"	-0.49"

* See Whittaker & Robinson's "The Calculus of Observations", Blackie & Son, 4th Edn., 1962, page 29. For a solution on an electronic computer the form (B) is required; when the interpolated point is near a known point, form (A) frequently leads to an overflow in the computer and its use is therefore not advised.

For each specified slope $\mathcal{E}$, on the first page the functions ψ (Epsi), S, and the first differentials $\frac{dS}{d\theta}$ and $\frac{d\psi}{d\theta}$ are listed against θ (Theta) in degrees and radians. On the second page the stresses along the base of a wedge of unit height (x = 1) (i.e., the vertical component of normal stress (σ_x), the horizontal component of normal stress (σ_y), the shear component (τ_{xy})), the positional point along the base, Y, and the length of the radius arms r_1 and r_2 of the two intersecting failure lines for r_o = 1 on the x axis, are all listed against Theta (θ) in degrees. (See Figure below).

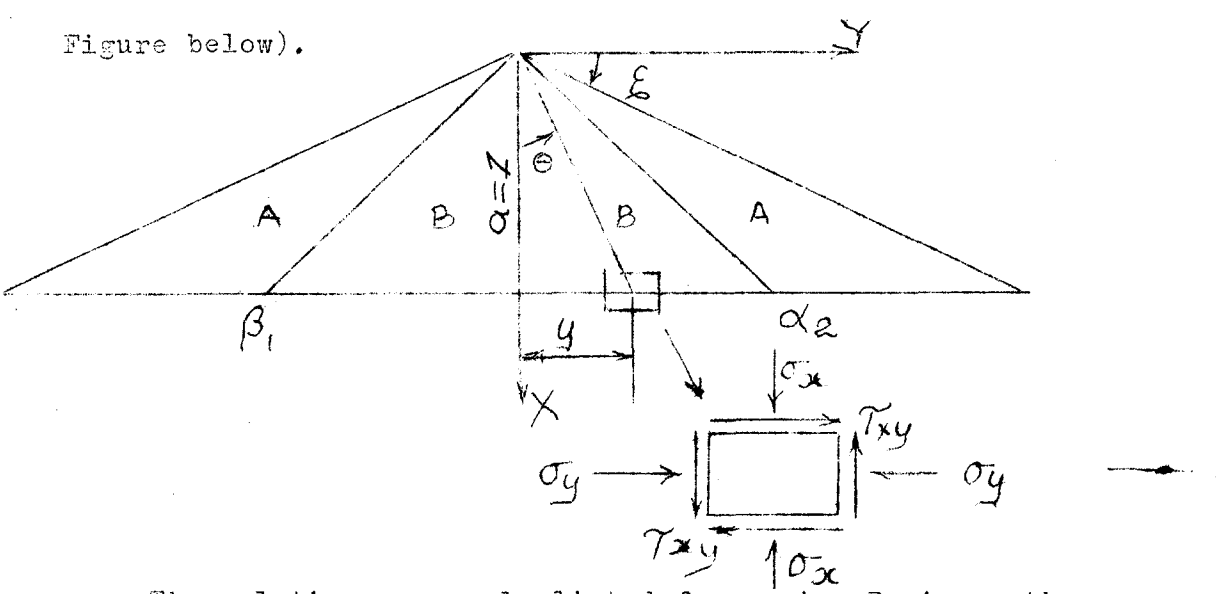

The solutions are only listed for region B, i.e., the region bounded by the α_2 characteristic through the apex of the wedge separating the infinite slope region from the solution below the apex. In region A all the stresses are linear functions, being zero at the toe and a maximum at the α_2 characteristic. For each slope the values for the stresses for the point of intersection of the α_2 characteristic with the base are listed in the last line of the second page.

The density of the material in the wedge is assumed to be equal to one, and the height of the wedge is also equal to

one. Solution of the stresses along the base for wedges with height, h, and density, γ , requires merely the multiplication of the listed stress values by γh. Similarly, radius arm values for r_o = a can be found by multiplying r_1, r_2 by a.

SLOPE (ε) = 0°

θ° (+)	θ^R (+)	ψ (-)	S (+)	$\frac{d\psi}{d\theta}$ (-)	$\frac{dS}{d\theta}$ (-)
0.0000000	0.00000	0.000000	0.666667	0.000000	0.000000
1.0000000	0.01745	0.017453	0.666565	1.000000	0.011635
2.0000000	0.03491	0.034907	0.666261	1.000000	0.023266
3.0000000	0.05236	0.052360	0.665753	1.000000	0.034891
4.0000000	0.06981	0.069813	0.665043	1.000000	0.046504
5.0000000	0.08727	0.087266	0.664130	1.000000	0.058104
5.9999998	0.10472	0.104720	0.663015	1.000000	0.069686
6.9999990	0.12217	0.122173	0.661697	1.000000	0.081246
7.9999983	0.13963	0.139626	0.660179	1.000000	0.092782
8.9999976	0.15708	0.157080	0.658459	1.000000	0.104290
9.9999969	0.17453	0.174533	0.656539	1.000000	0.115766
10.999996	0.19199	0.191986	0.654418	1.000000	0.127206
11.999996	0.20944	0.209439	0.652098	1.000000	0.138608
12.999995	0.22689	0.226893	0.649580	1.000000	0.149968
13.999994	0.24435	0.244346	0.646864	1.000000	0.161281
14.999993	0.26180	0.261799	0.643951	1.000000	0.172546
15.999993	0.27925	0.279253	0.640841	1.000000	0.183759
16.999992	0.29671	0.296706	0.637537	1.000001	0.194915
17.999991	0.31416	0.314159	0.634038	1.000001	0.206012
18.999991	0.33161	0.331612	0.630346	1.000001	0.217046
19.999990	0.34907	0.349066	0.626462	1.000001	0.228014
20.999989	0.36652	0.366519	0.622387	1.000001	0.238913
21.999988	0.38397	0.383972	0.618123	1.000001	0.249739
22.999988	0.40143	0.401426	0.613670	1.000002	0.260489
23.999987	0.41888	0.418879	0.609030	1.000003	0.271160
24.999986	0.43633	0.436332	0.604205	1.000004	0.281748
25.999986	0.45379	0.453785	0.599196	1.000006	0.293352
26.999985	0.47124	0.471239	0.594004	1.000002	0.302669
27.999983	0.48869	0.488692	0.588632	0.999999	0.312979
28.999989	0.50615	0.506145	0.583080	0.999999	0.323206
29.994989	0.52351	0.523511	0.577379	0.999880	0.333399
29.999942	0.52360	0.523599	0.577349	54.693000	35.599900

SLOPE (ϵ) = 0°

THETA (+)	VERT. COMP. (+)	HORIZ. COMP. (+)	SHEAR	Y (+)	FAILURE LINES RADIUS 1 (+)	FAILURE LINES RADIUS 2 (+)
0.0000	1.000000	0.333333	0.000000	0.000000	1.0000	1.0000
1.0000	1.000000	0.333333	0.000000	0.017455	1.0313	0.9708
2.0000	1.000000	0.333333	0.000000	0.034920	1.0650	0.9435
3.0000	1.000000	0.333333	0.000000	0.052408	1.1014	0.9180
4.0000	1.000000	0.333333	0.000000	0.069927	1.1406	0.8941
5.0000	1.000000	0.333333	0.000000	0.087489	1.1831	0.8717
6.0000	1.000000	0.333333	0.000000	0.105104	1.2293	0.8506
7.0000	1.000000	0.333333	0.000000	0.122785	1.2797	0.8308
8.0000	1.000000	0.333333	0.000000	0.140541	1.3348	0.8121
9.0000	1.000000	0.333333	0.000000	0.158384	1.3952	0.7945
10.0000	1.000000	0.333333	0.000000	0.176327	1.4619	0.7779
11.0000	1.000000	0.333333	0.000000	0.194380	1.5358	0.7621
12.0000	1.000000	0.333333	0.000000	0.212556	0.6181	0.7472
13.0000	1.000000	0.333333	0.000000	0.230868	1.7102	0.7331
14.0000	1.000000	0.333333	0.000000	0.249328	1.8141	0.7198
15.0000	1.000000	0.333333	0.000000	0.267949	1.9320	0.7071
16.0000	1.000000	0.333333	0.000000	0.286745	2.0670	0.6951
17.0000	1.000000	0.333333	0.000000	0.305731	2.2229	0.6837
18.0000	L.000000	0.333333	0.000000	0.324920	2.4052	0.6728
19.0000	1.000000	0.333333	0.000000	0.344327	2.6208	0.6625
20.0000	1.000000	0.333333	0.000000	0.363970	2.8799	0.6527
21.0000	1.000000	0.333333	0.000000	0.383864	3.1970	0.6434
22.0000	1.000000	0.333333	0.000000	0.404026	3.5937	0.6345
23.0000	1.000000	0.333333	0.000000	0.424475	4.1044	0.6261
24.0000	1.000000	0.333333	0.000000	0.445228	4.7860	0.6180
25.0000	1.000000	0.333333	0.000000	0.466307	5.7415	0.6104
26.0000	1.000000	0.333333	0.000000	0.487732	7.1769	0.6031
27.0000	1.000000	0.333333	0.000000	0.509525	9.5755	0.5962
28.0000	1.000000	0.333333	0.000000	0.531709	14.3743	0.5896
29.0000	1.000000	0.333333	0.000000	0.554309	-	0.5833
29.9950	0.999998	0.333333	0.000000	0.577234	-	0.5774
29.9999	0.999997	0.333332	0.000000	0.577349	-	0.5773

SLOPE (ϵ) = 5°

θ° (+)	θ^{R} (+)	ψ (-)	S (+)	$\frac{d\psi}{d\theta}$ (-)	$\frac{dS}{d\theta}$ (-)
0.0000000	0.00000	0.000000	0.635731	0.000000	0.000000
1.0000000	0.01745	0.016179	0.635632	0.926990	0.011332
2.0000000	0.03491	0.032358	0.635335	0.926940	0.022661
3.0000000	0.05236	0.048535	0.634841	0.926857	0.033984
4.0000000	0.06981	0.064711	0.634149	0.926740	0.045299
5.0000000	0.08727	0.080884	0.633260	0.926590	0.056602
5.9999998	0.10472	0.097055	0.632173	0.926407	0.067892
6.9999990	0.12717	0.113222	0.630890	0.926190	0.079165
7.9999983	0.13963	0.129385	0.629410	0.925940	0.090419
8.9999976	0.15708	0.145543	0.627734	0.925657	0.101651
9.9999969	0.17453	0.161696	0.625862	0.925342	0.112859
10.9999996	0.19199	0.177844	0.623795	0.924993	0.124040
11.9999996	0.20944	0.193984	0.621532	0.924613	0.135193
12.9999995	0.22689	0.210118	0.619076	0.924201	0.146315
13.9999994	0.24435	0.226245	0.616425	0.923759	0.157403
14.9999993	0.26180	0.242364	0.613581	0.923287	0.168458
15.9999993	0.27925	0.258474	0.610545	0.922787	0.179476
16.9999992	0.29671	0.274575	0.607317	0.922260	0.190458
17.9999991	0.31416	0.290666	0.603897	0.921710	0.201401
18.9999991	0.33161	0.306748	0.600287	0.921139	0.212307
19.9999990	0.34907	0.322820	0.596486	0.920551	0.223176
20.9999989	0.36652	0.338882	0.592497	0.919953	0.234009
21.9999988	0.38397	0.354932	0.588318	0.919353	0.244810
22.9999988	0.40143	0.370973	0.583951	0.918760	0.255581
23.9999987	0.41888	0.387003	0.579397	0.918190	0.266331
24.9999986	0.43633	0.403024	0.574655	0.917662	0.277069
25.9999986	0.45379	0.419036	0.569725	0.917207	0.287812
26.9999985	0.47124	0.435041	0.564608	0.916869	0.298583
27.9999984	0.48869	0.451042	0.559303	0.916719	0.309422
28.990828	0.50599	0.466896	0.553858	0.916860	0.320289
30.026628	0.52406	0.483476	0.547963	0.917590	0.331945
31.006633	0.54117	0.499184	0.542187	0.919390	0.343578
31.983398	0.55822	0.514892	0.356220	0.924440	0.357069
32.516113	0.56751	0.523531	0.532847	0.945590	0.375905
32.519459	0.56757	0.523599	0.532816	0.759300	6.400000

SLOPE (β) = 5°

THETA (+)	VERT. COMP.(+)	HORIZ. COMP.(+)	SHEAR (+)	Y (+)	FAILURE LINES RADIUS 1 (+)	RADIUS 2 (+)
0.0000	0.953596	0.317865	0.000000	0.000000	1.0000	1.0000
1.0000	0.953592	0.317865	0.000810	0.017455	1.0313	0.9708
2.0000	0.953580	0.317865	0.001620	0.034921	1.0648	0.9434
3.0000	0.953559	0.317865	0.002431	0.052408	1.1009	0.9177
4.0000	0.953530	0.317865	0.003243	0.069927	1.1396	0.8936
5.0000	0.953492	0.317865	0.004057	0.087489	1.1815	0.8709
6.0000	0.953446	0.317865	0.004872	0.105104	1.2268	0.8495
7.0000	0.953391	0.317865	0.005689	0.122785	1.2759	0.8294
8.0000	0.953327	0.317865	0.006509	0.140541	1.3293	0.8104
9.0000	0.953254	0.317864	0.007331	0.158384	1.3876	0.7924
10.0000	0.953171	0.317863	0.008157	0.176327	1.4515	0.7754
11.0000	0.953078	0.317862	0.008986	0.194380	1.5218	0.7593
12.0000	0.952975	0.317861	0.009819	0.212556	1.5993	0.7440
13.0000	0.952861	0.317859	0.010656	0.230868	1.6854	0.7295
14.0000	0.952736	0.317856	0.011497	0.249328	1.7814	0.7157
15.0000	0.952599	0.317853	0.012343	0.267949	1.8890	0.7026
16.0000	0.952450	0.317849	0.013194	0.286745	2.0105	0.6902
17.0000	0.953388	0.317844	0.014050	0.305731	2.1485	0.6784
18.0000	0.952112	0.317838	0.014912	0.324920	2.3068	0.6671
19.0000	0.951921	0.317830	0.015779	0.344327	2.4898	0.6564
20.0000	0.951714	0.317821	0.016652	0.363970	2.7037	0.6462
21.0000	0.951490	0.317810	0.017531	0.383864	2.9568	0.6364
22.0000	0.951247	0.317796	0.018416	0.404026	3.2608	0.6271
23.0000	0.950984	0.317779	0.019307	0.424475	3.6321	0.6183
24.0000	0.950699	0.317759	0.020203	0.445338	4.0953	0.6098
25.0000	0.950389	0.317734	0.021104	0.466307	4.6884	0.6017
26.0000	0.950051	0.317704	0.022009	0.487732	5.4733	0.5940
27.0000	0.949682	0.317667	0.022917	0.509525	6.5581	0.5867
28.0000	0.949276	0.317633	0.023827	0.531709	8.1496	0.5796
28.9908	0.948832	0.317567	0.024726	0.554100	10.6634	0.5730
30.0266	0.948313	0.317494	0.025660	0.577970	15.5439	0.5664
31.0066	0.947752	0.317402	0.026527	0.601018	26.6938	0.5604
31.9834	0.947091	0.317278	0.027354	0.624467	-	0.5547
32.5161	0.946635	0.317174	0.027757	0.637466	-	0.5517
32.5195	0.946616	0.31716	0.027750	0.637548	-	0.5517

SLOPE (ϵ) = 10°

θ° (+)	θ^{R} (+)	ψ (-)	S (+)	$\frac{d\psi}{d\theta}$ (-)	$\frac{dS}{d\theta}$ (-)
0.0000000	0.00000	0.000000	0.609053	0.000000	0.000000
1.0000000	0.01745	0.014997	0.608953	0.858080	0.011486
2.0000000	0.03491	0.029952	0.608652	0.858004	0.022970
3.0000000	0.05236	0.044926	0.608151	0.857876	0.034451
4.0000000	0.06981	0.059898	0.607449	0.857697	0.045927
5.0000000	0.08727	0.074865	0.606548	0.857467	0.057397
5.9999998	0.10472	0.089829	0.605446	0.857188	0.068859
6.9999990	0.12217	0.104786	0.604144	0.856860	0.080312
7.9999983	0.13963	0.119738	0.602642	0.856482	0.091755
8.9999976	0.15708	0.134683	0.600941	0.856058	0.103186
9.9999969	0.17453	0.149620	0.599041	0.855587	0.114605
10.9999996	0.19199	0.164548	0.596941	0.855072	0.126011
11.9999996	0.20944	0.179467	0.594642	0.854514	0.137403
12.9999995	0.22689	0.194376	0.592145	0.853916	0.148782
13.9999994	0.24435	0.209275	0.589449	0.853280	0.160147
14.9999993	0.26180	0.224161	0.586555	0.852611	0.171499
15.9999993	0.27925	0.239036	0.583462	0.851912	0.182840
16.9999992	0.29671	0.253898	0.580172	0.851189	0.194170
17.9999991	0.31416	0.268748	0.576685	0.850448	0.205492
18.9999991	0.33161	0.283585	0.572999	0.849699	0.216809
19.9999990	0.34907	0.298408	0.569117	0.848949	0.228126
20.9999989	0.36652	0.313219	0.565036	0.848213	0.239449
21.9999988	0.38397	0.328016	0.560758	0.847505	0.250783
22.9999988	0.40143	0.342802	0.556282	0.846846	0.262140
23.9999987	0.41888	0.357577	0.551608	0.846260	0.273530
24.9999986	0.43633	0.372343	0.546734	0.845780	0.284970
25.9999986	0.45379	0.387101	0.541660	0.845448	0.296481
26.9999985	0.47124	0.401856	0.536384	0.845320	0.308092
27.9999984	0.48869	0.416610	0.530905	0.845475	0.319839
28.9999983	0.50615	0.431370	0.525219	0.846020	0.331778
29.9999983	0.52360	0.446145	0.519322	0.847118	0.343991
31.002371	0.54109	0.460980	0.513194	0.849000	0.356626
32.001850	0.55854	0.475815	0.506859	0.852130	0.369853
32.996593	0.57590	0.490650	0.500316	0.857300	0.384072
33.983322	0.59312	0.505486	0.493566	0.866580	0.400342
35.009640	0.61103	0.521194	0.486191	0.895170	0.427540
35.158925	0.61364	0.523550	0.485061	0.929860	0.448914
35.161397	0.61368	0.523599	0.485036	8.071400	5.200000

SHEAR (ξ) = 10°

FAILURE LINES

THETA (+)	VERT. COMP. (+)	HORIZ. COMP. (+)	SHEAR (+)	Y (+)	RADIUS 1 (+)	RADIUS 2 (+)
0.0000	0.913579	0.304526	0.000000	0.000000	1.0000	1.0000
1.0000	0.913564	0.304526	0.001508	0.017455	1.0312	0.9707
2.0000	0.913519	0.304526	0.003017	0.034921	1.0646	0.9432
3.0000	0.913444	0.304526	0.004527	0.052408	1.1004	0.9174
4.0000	0.913339	0.304526	0.006038	0.069927	1.1387	0.8931
5.0000	0.913203	0.304526	0.007550	0.087489	1.1800	0.8701
6.0000	0.913036	0.304525	0.009064	0.105104	1.2244	0.8485
7.0000	0.912838	0.304525	0.010581	0.122785	1.2724	0.8280
8.0000	0.912607	0.304523	0.012100	0.140541	1.3243	0.8087
9.0000	0.912343	0.304521	0.013622	0.158384	1.3807	0.7904
10.0000	0.912045	0.304518	0.015148	0.176327	1.4422	0.7730
11.0000	0.911713	0.304515	0.016677	0.194380	1.5093	0.7565
12.0000	0.911433	0.304509	0.018210	0.212556	1.5828	0.7409
13.0000	0.910938	0.304503	0.019747	0.230868	1.6638	0.7260
14.0000	0.910494	0.304494	0.021288	0.249328	1.7532	0.7118
15.0000	0.910009	0.304483	0.022834	0.267949	1.8525	0.6984
16.0000	0.909482	0.304469	0.024384	0.286745	1.9633	0.6855
17.0000	0.908911	0.304452	0.025939	0.305731	2.0876	0.6733
18.0000	0.908294	0.304431	0.027498	0.324920	2.2279	0.6616
19.0000	0.907627	0.304405	0.029061	0.344327	2.3873	0.6505
20.0000	0.906909	0.304373	0.030628	0.363970	2.5700	0.6399
21.0000	0.906136	0.304336	0.032198	0.383864	2.7810	0.6297
22.0000	0.905304	0.304290	0.033771	0.404026	3.0273	0.6200
23.0000	0.904410	0.304236	0.035346	0.424475	3.3181	0.6108
24.0000	0.903448	0.304171	0.036922	0.445228	3.6660	0.6019
25.0000	0.902414	0.304094	0.038496	0.466307	4.0891	0.5934
26.0000	0.901302	0.304002	0.040068	0.487732	4.6133	0.5853
27.0000	0.900104	0.303892	0.041634	0.509525	5.2782	0.5776
28.0000	0.898811	0.303762	0.043192	0.531709	6.1463	0.5702
29.0000	0.897415	0.303607	0.044736	0.554309	7.3227	0.5630
30.0000	0.895902	0.303421	0.046260	0.577350	8.998	0.5562
31.0024	0.894252	0.303197	0.047761	0.600917	11.5572	0.5287
32.0019	0.892453	0.302925	0.049217	0.624914	15.8776	0.5435
32.9966	0.890479	0.302593	0.050608	0.64932	24.5246	0.5375
33.9833	0.888288	0.302176	0.051897	0.674085	-	0.5319
35.0096	0.885620	0.301578	0.053042	0.700458	-	0.5263
35.1589	0.885155	0.301455	0.053162	0.704349	-	0.5255
35.1614	0.885137	0.301448	0.053157	0.704414	-	0.5255

SLOPE (ε) = 15°

θ° (+)	θ^R (+)	ψ (-)	S (+)	$\frac{d\psi}{d\theta}$ (-)	$\frac{dS}{d\theta}$ (-)
0.0000000	0.00000	0.000000	0.585439	0.000000	0.000000
1.0000000	0.01745	0.013821	0.585335	0.791848	0.011988
2.0000000	0.03491	0.027640	0.585021	0.791750	0.023976
3.0000000	0.05236	0.041458	0.584498	0.791588	0.035963
4.0000000	0.06981	0.055272	0.583765	0.791361	0.047948
5.0000000	0.08727	0.069081	0.582824	0.791071	0.059932
5.9999998	0.10472	0.082885	0.581673	0.790717	0.071914
6.9999990	0.12217	0.096682	0.580314	0.790303	0.083893
7.9999983	0.13963	0.110471	0.578745	0.789827	0.095871
8.9999976	0.15708	0.124252	0.576967	0.789293	0.107847
9.9999969	0.17453	0.138022	0.574980	0.788703	0.119822
10.999996	0.19199	0.151782	0.572785	0.788058	0.131796
11.999996	0.20944	0.165531	0.570380	0.787363	0.143771
12.999995	0.22689	0.179266	0.567766	0.786620	0.155746
13.999994	0.24435	0.192988	0.564943	0.785834	0.167725
14.999993	0.26180	0.206697	0.561911	0.785010	0.179710
15.999993	0.27925	0.220390	0.558670	0.784154	0.191702
16.999992	0.29671	0.234069	0.555220	0.783273	0.203705
17.999991	0.31416	0.247732	0.551560	0.782377	0.215724
18.999991	0.33161	0.261379	0.547689	0.781474	0.227762
19.999990	0.34907	0.275010	0.543609	0.780579	0.239827
20.999989	0.36652	0.288626	0.539318	0.779706	0.251924
21.999988	0.38397	0.302227	0.534815	0.778873	0.264062
22.999988	0.40143	0.315814	0.530100	0.778102	0.276252
23.999987	0.41888	0.329389	0.525172	0.777420	0.288505
24.999986	0.43633	0.342952	0.520029	0.776860	0.300837
25.999986	0.45379	0.356507	0.514670	0.776464	0.313266
26.999985	0.47124	0.370057	0.509093	0.776281	0.325814
27.999984	0.48869	0.383606	0.503296	0.776378	0.338510
28.999983	0.50615	0.397160	0.497276	0.776837	0.351389
29.999983	0.52360	0.410725	0.491029	0.777767	0.364499
30.999982	0.54105	0.424312	0.484551	0.779315	0.377901
31.999981	0.55851	0.437933	0.477836	0.781683	0.391683
33.021253	0.57633	0.451895	0.470725	0.785230	0.406268
33.973654	0.59295	0.464985	0.463855	0.790020	0.420530
34.981906	0.61055	0.478948	0.456315	0.797350	0.436637
35.978863	0.62795	0.492910	0.448567	0.808330	0.454220
37.019223	0.64611	0.507746	0.440129	0.827750	0.476192
37.999508	0.66322	0.522232	0.431725	0.881980	0.513600
38.083566	0.66468	0.523541	0.430963	0.918560	0.533605
38.086556	0.66474	0.523599	0.430930	17.100000	8.999900

SLOPE (α) = 15°

FAILURE LINES

THETA. (+)	VERT. COMP. (+)	HORIZ. COMP. (+)	SHEAR (+)	Y(+)	RADIUS 1 (+)	RADIUS 2 (+)
0.0000	0.878159	0.292720	0.000000	0.000000	1.0000	1.0000
1.0000	0.878128	0.292720	0.002127	0.017455	1.0312	0.9707
2.0000	0.878035	0.292720	0.004253	0.034921	1.0644	0.9431
3.0000	0.877880	0.292719	0.006381	0.052408	1.0999	0.9171
4.0000	0.877663	0.292719	0.008508	0.069927	1.1379	0.8926
5.0000	0.877382	0.292719	0.010637	0.087489	1.1785	0.8694
6.0000	0.877037	0.292718	0.012767	0.105104	1.2222	0.8475
7.0000	0.876628	0.292716	0.014897	0.122785	1.2691	0.8267
8.0000	0.876152	0.292713	0.017030	0.140541	1.3197	0.8070
9.0000	0.875610	0.292709	0.019163	0.158384	1.3744	0.7884
10.0000	0.874998	0.292703	0.021298	0.176327	1.4336	0.7707
11.0000	0.874315	0.292695	0.023434	0.194380	1.4978	0.7538
12.0000	0.973560	0.292685	0.025571	0.212556	1.5679	0.7378
13.0000	0.872730	0.292671	0.027710	0.230868	1.6444	0.7225
14.0000	0.871823	0.292654	0.029850	0.249328	1.7283	0.7080
15.0000	0.870836	0.292631	0.031990	0.267949	1.8206	0.6841
16.0000	0.869765	0.292604	0.034131	0.286745	1.9225	0.6809
17.0000	0.868608	0.292569	0.036271	0.305731	2.0356	0.6683
18.0000	0.867361	0.292527	0.038411	0.324920	2.1617	0.6563
19.0000	0.866019	0.292476	0.040549	0.344327	2.3030	0.6447
20.0000	0.846578	0.292415	0.042684	0.363970	2.4623	0.6337
21.0000	0.863033	0.292342	0.044816	0.383864	2.6430	0.6232
22.0000	0.861379	0.292254	0.046942	0.404026	2.8493	0.6131
23.0000	0.859609	0.292150	0.049061	0.424475	3.0871	0.6034
24.0000	0.857716	0.292028	0.051171	0.445228	3.3633	0.5942
25.0000	0.855694	0.291883	0.053269	0.466307	3.6877	0.5853
26.0000	0.853532	0.291713	0.055353	0.487732	4.0733	0.5768
27.0000	0.851223	0.291514	0.057418	0.509525	4.5380	0.5687
28.0000	0.848755	0.291281	0.059461	0.531709	5.1073	0.5609
29.0000	0.846117	0.291008	0.061476	0.554309	5.8188	0.5534
30.0000	0.843294	0.290689	0.063456	0.577350	6.7294	0.5462
31.0000	0.840271	0.290316	0.065394	0.600860	7.9307	0.5393
32.0000	0.837029	0.289878	0.067280	0.624869	9.5777	0.5326
33.0312	0.833468	0.289353	0.069140	0.649935	12.0142	0.5262
33.9737	0.829895	0.288778	0.070798	0.673840	15.5131	0.5203
34.9819	0.825811	0.288057	0.072450	0.699737	21.8510	0.5144
35.9789	0.821419	0.287202	0.073947	0.725979	34.8548	0.5088
37.0192	0.816374	0.286106	0.075301	0.754080	-	0.5033
37.9995	0.810977	0.284749	0.076221	0.781272	-	0.4982
38.0836	0.810451	0.284597	0.076257	0.783637	-	0.4978
38.0866	0.810422	0.284586	0.076251	0.783721	-	0.4978

SLOPE (ξ) = 20°

θ° (+)	θ^{R} (+)	ψ (-)	S (+)	$\frac{d\psi}{d\theta}$ (-)	$\frac{dS}{d\theta}$ (-)
0.0000000	0.00000	0.000000	0.564083	0.000000	0.000000
1.0000000	0.01745	0.012692	0.563971	0.727168	0.012776
2.0000000	0.03491	0.025382	0.563637	0.727042	0.025552
3.0000000	0.05236	0.038070	0.563079	0.726833	0.038329
4.0000000	0.06981	0.050753	0.562299	0.726541	0.051108
5.0000000	0.08727	0.063431	0.561295	0.726167	0.063890
5.9999998	0.10472	0.076101	0.560068	0.725712	0.076674
6.9999990	0.12217	0.088762	0.558619	0.725177	0.089463
7.9999983	0.13963	0.101414	0.556946	0.724563	0.102256
8.9999976	0.15708	0.114054	0.555049	0.723872	0.115056
9.9999969	0.17453	0.126681	0.552929	0.723107	0.127864
10.999996	0.19199	0.139295	0.550586	0.722269	0.140680
11.999996	0.20944	0.151893	0.548019	0.721363	0.153509
12.999995	0.22689	0.164475	0.545227	0.720391	0.166350
13.999994	0.24435	0.177039	0.542212	0.719359	0.179208
14.999993	0.26180	0.189585	0.538972	0.718271	0.192085
15.999993	0.27925	0.202111	0.535507	0.717133	0.204985
16.999992	0.29671	0.214617	0.531816	0.715952	0.217912
17.999991	0.31416	0.227102	0.527900	0.714738	0.230870
18.999991	0.33161	0.239566	0.523757	0.713499	0.243864
19.999990	0.34907	0.252008	0.519387	0.712249	0.256902
20.999989	0.36652	0.264428	0.514789	0.711000	0.269989
21.999988	0.38397	0.276827	0.509962	0.709769	0.283135
22.999988	0.40143	0.289204	0.504906	0.708577	0.296347
23.999987	0.41888	0.301561	0.499618	0.707446	0.309638
24.999986	0.43633	0.313899	0.494097	0.706404	0.323018
25.999986	0.45379	0.326220	0.488342	0.705485	0.336503
26.999985	0.47124	0.338526	0.482350	0.704731	0.350108
27.999984	0.48869	0.350821	0.476120	0.704189	0.363854
28.999983	0.50615	0.363108	0.469648	0.703920	0.377764
29.999983	0.52360	0.375394	0.462932	0.703999	0.391863
30.999982	0.54105	0.387685	0.455968	0.704517	0.406186
31.999981	0.55851	0.399989	0.448752	0.705591	0.420774
32.999981	0.57596	0.412318	0.441279	0.707370	0.435676
33.999980	0.59341	0.424686	0.433542	0.710050	0.450958
34.983386	0.61058	0.436903	0.425670	0.713800	0.466432
36.030207	0.62885	0.449993	0.416993	0.719420	0.483534
36.998602	0.64575	0.462210	0.408682	0.726630	0.500098
38.023704	0.66364	0.475300	0.399570	0.737230	0.518706
39.031459	0.68123	0.488390	0.390274	0.752150	0.538604
40.015320	0.69840	0.501480	0.380841	0.774110	0.560706
41.025469	0.71603	0.515443	0.370712	0.815180	0.590384
41.577934	0.72567	0.523558	0.364882	0.918180	0.640194
41.580028	0.72571	0.523599	0.364855	15.444000	6.799900

SLOPE (ϵ) = 20°

THETA (+)	VERT. COMP.(+)	HORIZ. COMP.(+)	SHEAR	Y (+)	FAILURE LINES RADIUS 1 (+)	FAILURE LINES RADIUS 2 (+)
0.0000	0.846124	0.282041	0.000000	0.000000	1.0000	1.0000
1.0000	1.846073	0.282041	0.002686	0.017455	1.0312	0.9706
2.0000	0.845919	0.282041	0.005371	0.034921	1.0643	0.9430
3.0000	0.845663	0.282041	0.008056	0.052408	1.0995	0.9168
4.0000	0.845303	0.282041	0.010741	0.069927	1.1371	0.8921
5.0000	0.844839	0.282040	0.013425	0.087489	1.1772	0.8686
6.0000	0.844269	0.282038	0.016108	0.105104	1.2201	0.8465
7.0000	0.843593	0.282035	0.018790	0.122785	1.2660	0.8254
8.0000	0.842808	0.282030	0.021471	0.140541	1.3153	0.8054
9.0000	0.841912	0.282024	0.024149	0.158384	1.3684	0.7864
10.0000	0.840904	0.282014	0.026826	0.176327	1.4255	0.7683
11.0000	0.839781	0.282001	0.029500	0.194380	1.4872	0.7511
12.0000	0.838539	0.281984	0.032170	0.212556	1.5541	0.7347
13.0000	0.837176	0.281962	0.034837	0.230868	1.6266	0.7191
14.0000	0.835689	0.281933	0.037498	0.249328	1.7056	0.7042
15.0000	0.834072	0.281897	0.040155	0.267949	1.7917	0.6899
16.0000	0.832322	0.281852	0.042804	0.286745	1.8862	0.6763
17.0000	0.830435	0.281797	0.045446	0.305731	1.9899	0.6633
18.0000	0.828404	0.281730	0.048079	0.324920	2.1043	0.6509
19.0000	0.826225	0.281648	0.050700	0.344327	2.2309	0.6390
20.0000	0.823890	0.281551	0.053310	0.363970	2.3718	0.6275
21.0000	0.821394	0.281424	0.055904	0.383864	2.5291	0.6166
22.0000	0.818728	0.281296	0.058481	0.404026	2.7058	0.6061
23.0000	0.815885	0.281134	0.061039	0.424475	2.9054	0.5961
24.0000	0.812856	0.280943	0.063574	0.445228	3.1322	0.5864
25.0000	0.809632	0.280719	0.066083	0.466307	3.3918	0.5772
26.0000	0.806201	0.280459	0.068561	0.487732	3.6912	0.5683
27.0000	0.802552	0.280156	0.071004	0.509525	4.0397	0.5597
28.0000	0.798673	0.279805	0.073407	0.531709	4.4492	0.5515
29.0000	0.794549	0.279399	0.075764	0.075764	4.9361	0.5436
30.0000	0.790167	0.278929	0.078067	0.577350	5.5225	0.5360
31.0000	0.785507	0.278388	0.080310	0.600860	6.2400	0.5287
32.0000	0.780553	0.277765	0.082482	0.624869	7.1340	0.5217
33.0000	0.775283	0.277047	0.084573	0.649407	8.2731	0.5150
34.0000	0.769673	0.276220	0.086569	0.674508	9.7644	0.5085
34.9834	0.763799	0.275284	0.088426	0.699775	11.7449	0.5023
36.0302	0.757125	0.274134	0.090267	0.727348	14.7519	0.4960
36.9986	0.750528	0.272903	0.091824	0.753516	18.9548	0.4904
38.0237	0.743057	0.271393	0.093287	0.781952	29.2965	0.4847
39.0315	0.735166	0.269659	0.094500	0.810694	40.1954	0.4794
40.0153	0.726862	0.267667	0.095409	0.839555	-	0.4743
41.0255	0.717575	0.265201	0.095943	0.870067	-	0.4693
41.5779	0.712007	0.263543	0.095923	0.887153	-	0.4667
41.5800	0.711979	0.263532	0.095917	0.887218	-	0.4667

SLOPE (ϵ) = 25°

θ° (+)	θ^{R} (+)	ψ (-)	S (+)	$\frac{d\psi}{d\theta}$ (-)	$\frac{dS}{d\theta}$ (-)
0.0000000	0.00000	0.000000	0.544457	0.000000	0.000000
1.0000000	0.01745	0.011577	0.544336	0.663250	0.013812
2.0000000	0.03491	0.023151	0.543975	0.663077	0.027625
3.0000000	0.05236	0.034722	0.543372	0.662790	0.041441
4.0000000	0.06981	0.046286	0.542538	0.662389	0.055262
5.0000000	0.08727	0.057843	0.541443	0.661874	0.069089
5.9999998	0.10472	0.069389	0.540116	0.661245	0.082923
6.9999990	0.12217	0.080924	0.538548	0.660503	0.096767
7.9999983	0.13963	0.092445	0.536739	0.659649	0.110622
8.9999976	0.15708	0.103949	0.534687	0.658685	0.124491
9.9999969	0.17453	0.115436	0.532393	0.657610	0.138375
10.999996	0.19199	0.126904	0.529857	0.656428	0.152278
11.999996	0.20944	0.138349	0.527077	0.655140	0.166203
12.999995	0.22689	0.149772	0.524055	0.653747	0.180151
13.999994	0.24435	0.161169	0.520789	0.652253	0.194127
14.999993	0.26180	0.172539	0.517278	0.650662	0.208134
15.999993	0.27925	0.183881	0.513523	0.648976	0.222177
16.999992	0.29671	0.195192	0.509523	0.647201	0.236260
17.999991	0.31416	0.206472	0.505276	0.645343	0.250388
18.999991	0.33161	0.217718	0.500782	0.643406	0.264567
19.999990	0.34907	0.228930	0.496041	0.641401	0.278802
20.999989	0.36652	0.240107	0.491050	0.639335	0.293101
21.999988	0.38397	0.251247	0.485809	0.637219	0.307472
22.999988	0.40143	0.262350	0.480317	0.635067	0.321922
23.999987	0.41888	0.273415	0.474571	0.632893	0.336460
24.999986	0.43633	0.284442	0.468571	0.630717	0.351098
25.999986	0.45379	0.295431	0.462315	0.628558	0.365845
26.999985	0.47124	0.30638	0.455800	0.626443	0.380716
27.999984	0.48869	0.317299	0.449025	0.624402	0.395722
28.999983	0.50615	0.328179	0.441986	0.622472	0.410880
29.999983	0.52360	0.339028	0.434682	0.620696	0.426207
30.999982	0.54105	0.349847	0.427108	0.619128	0.441721
31.999981	0.55851	0.360641	0.419261	0.617829	0.457444
32.999981	0.57596	0.371415	0.411139	0.616877	0.473400
33.999980	0.59341	0.382176	0.402735	0.616368	0.489616
34.999979	0.61086	0.392933	0.394046	0.616418	0.506125
35.999978	0.62832	0.403697	0.385066	0.617174	0.522962
36.999978	0.64577	0.414482	0.375789	0.618821	0.540171
37.967655	0.66266	0.424954	0.366523	0.621470	0.557220
39.010138	0.68086	0.436298	0.356214	0.625840	0.576110
40.987173	0.71536	0.458115	0.335692	0.640270	0.613776
41.993531	0.73293	0.469459	0.324734	0.652160	0.634177
42.978645	0.75012	0.480804	0.313651	0.668380	0.655289
44.008414	0.76809	0.493021	0.301663	0.692730	0.679145
44.995417	0.78532	0.505238	0.289746	0.728530	0.705055
45.985020	0.80259	0.518328	0.277293	0.797600	0.739837
46.346958	0.80891	0.523564	0.272545	0.915680	0.780849
46.348770	0.80894	0.523599	0.272518	15.879000	4.599900

SLOPE (β) = 25°

FAILURE LINES.

THETA (+)	VERT. COMP.(+)	HORIZ. COMP.(+)	SHEAR	Y (+)	RADIUS 1 (+)	RADIUS 2 (+)
0.0000	0.816685	0.272228	0.000000	0.000000	1.0000	1.0000
1.0000	0.816610	0.272228	0.003199	0.017455	1.0311	0.9706
2.0000	0.816384	0.272228	0.006398	0.034921	1.0641	0.9428
3.0000	0.816007	0.272228	0.009595	0.052408	1.0991	0.9165
4.0000	0.815478	0.272227	0.012790	0.069927	1.1363	0.8916
5.0000	0.814796	0.272226	0.015983	0.087489	1.1758	0.8679
6.0000	0.813960	0.272223	0.019172	0.105104	1.2180	0.8454
7.0000	0.812966	0.272219	0.022356	0.122785	1.2630	0.8241
8.0000	0.811814	0.272212	0.025535	0.140541	1.3111	0.8038
9.0000	0.810501	0.272203	0.028708	0.15838	1.3626	0.7844
10.0000	0.809023	0.272189	0.031874	0.176327	1.4178	0.7660
11.0000	0.807378	0.272170	0.035031	0.194380	1.4772	0.7484
12.0000	0.805560	0.272145	0.038178	0.212556	1.5412	0.7317
13.0000	0.803567	0.272112	0.041314	0.230868	1.6100	0.7156
14.0000	0.801393	0.272071	0.044438	0.249328	1.6846	0.7003
15.0000	0.799034	0.272018	0.047548	0.267949	1.7653	0.6857
16.0000	0.796483	0.271953	0.050641	0.286745	1.8531	0.6717
17.0000	0.793734	0.271874	0.053716	0.305731	1.9487	0.6583
18.0000	0.790781	0.271777	0.056771	0.324920	2.0531	0.6454
19.0000	0.787616	0.271660	0.059802	0.344327	2.1675	0.6331
20.0000	0.784231	0.271520	0.062808	0.363970	2.2932	0.6213
21.0000	0.780618	0.271353	0.065785	0.383864	2.4318	0.6099
22.0000	0.776767	0.271157	0.068729	0.404026	2.5852	0.5990
23.0000	0.772668	0.270926	0.071627	0.424475	2.7558	0.5885
24.0000	0.768310	0.270656	0.074504	0.445228	2.9461	0.5785
25.0000	0.763681	0.270342	0.077327	0.466307	3.1594	0.5688
26.0000	0.758768	0.269977	0.080098	0.487732	3.3999	0.5595
27.0000	0.753558	0.269556	0.082813	0.509525	3.6724	0.5505
28.0000	0.748035	0.269069	0.085465	0.531709	3.9831	0.5419
29.0000	0.742183	0.268510	0.088047	0.554309	4.3397	0.5336
30.0000	0.735985	0.267869	0.090551	0.577350	4.7522	0.5256
31.0000	0.729421	0.267135	0.092968	0.600860	5.2332	0.5179
32.0000	0.722472	0.266296	0.095288	0.624869	5.7994	0.5105
33.0000	0.715114	0.265339	0.097499	0.649407	6.4732	0.5033
34.0000	0.707324	0.264249	0.099590	0.674508	7.2848	0.4964
35.0000	0.699075	0.263008	0.101546	0.700207	8.2762	0.4897
36.0000	0.690339	0.261598	0.103352	0.726542	9.5076	0.4833
37.0000	0.681083	0.259995	0.104991	0.753553	11.0675	0.4770
37.9677	0.671600	0.258239	0.106398	0.780377	13.0156	0.4712
39.0101	0.660765	0.256089	0.107695	0.810077	15.8238	0.4652
39.9647	0.650241	0.253855	0.108657	0.838050	19.3817	0.4599
40.9872	0.638280	0.251141	0.109420	0.868894	24.9082	0.4543
41.9935	0.625759	0.248098	0.109862	0.900200	33.4253	0.4491
42.9786	0.612722	0.244708	0.109957	0.931818	47.7158	0.4442
44.0084	0.598187	0.240653	0.109638	0.965973	78.1876	0.4392
44.9954	0.583286	0.236175	0.108849	0.999840	-	0.4346
45.9850	0.567219	0.230923	0.107428	1.034989	-	0.4302
46.3470	0.560956	0.228697	0.106644	1.048159	-	0.4286
46.3488	0.560920	0.228682	0.106637	1.048225	-	0.4286

SLOPE (ϵ) = 30°

θ° (+)	θ^R (+)	ψ (-)	S (+)	$\frac{d\psi}{d\theta}$ (-)	$\frac{dS}{d\theta}$ (-)
0.0000000	0.00000	0.000000	0.526287	0.000000	0.000000
1.0000000	0.01745	0.010470	0.526155	0.599812	0.015068
2.0000000	0.03491	0.020936	0.525761	0.599564	0.030138
3.0000000	0.05236	0.031397	0.525103	0.599149	0.045213
4.0000000	0.06981	0.041850	0.524183	0.598567	0.060296
5.0000000	0.08727	0.052290	0.522998	0.597819	0.075389
5.9999998	0.10472	0.062717	0.521551	0.596904	0.090495
6.9999990	0.12217	0.073125	0.519840	0.595820	0.105617
7.9999983	0.13963	0.083514	0.517864	0.594567	0.120758
8.9999976	0.15708	0.093879	0.515624	0.593144	0.135921
9.9999969	0.17453	0.104207	0.513119	0.591550	0.151110
10.999996	0.19199	0.114527	0.510349	0.589785	0.166327
11.999996	0.20944	0.124804	0.507313	0.587846	0.181577
12.999995	0.22689	0.135045	0.504011	0.585732	0.196865
13.999994	0.24435	0.145248	0.500441	0.583442	0.212194
14.999993	0.26180	0.155410	0.496604	0.580975	0.227569
15.999993	0.27925	0.165527	0.492497	0.578329	0.242995
16.999992	0.29671	0.175597	0.488121	0.575503	0.258479
17.999991	0.31416	0.185615	0.483474	0.572495	0.274025
18.999991	0.33161	0.195579	0.479556	0.569303	0.289641
19.999990	0.34907	0.205486	0.473364	0.565928	0.305333
20.999989	0.36652	0.215333	0.467897	0.562366	0.321109
21.999988	0.38397	0.255116	0.462154	0.558618	0.336976
22.999988	0.40143	0.234831	0.456134	0.554682	0.352945
23.999987	0.41888	0.244476	0.449834	0.550558	0.369023
24.999986	0.43633	0.354048	0.443252	0.546245	0.385221
25.999986	0.45379	0.263543	0.436386	0.541742	0.401549
26.999985	0.47124	0.272957	0.429234	0.537051	0.418020
27.999984	0.48869	0.282288	0.421794	0.532172	0.434646
28.999983	0.50615	0.291533	0.414061	0.527106	0.451439
29.999983	0.52360	0.300687	0.406034	0.521855	0.468414
30.999982	0.54105	0.309748	0.397709	0.516421	0.485585
31.999981	0.55851	0.318712	0.389083	0.510809	0.502969
32.999981	0.57596	0.327577	0.380151	0.505021	0.520582
33.999980	0.59341	0.336340	0.370910	0.499064	0.538441
34.999979	0.61086	0.344997	0.361355	0.492943	0.556565
35.999978	0.62832	0.353545	0.351481	0.486667	0.574974
36.999978	0.64577	0.361983	0.341283	0.480243	0.593687
37.999977	0.66322	0.370308	0.330755	0.473682	0.612726
38.999976	0.68068	0.378517	0.319892	0.466996	0.632111
39.999976	0.69813	0.386608	0.308688	0.460198	0.651866
40.999975	0.71558	0.394580	0.297136	0.453304	0.672013
41.999974	0.73304	0.402431	0.285228	0.446329	0.692574
42.953275	0.74968	0.409801	0.273539	0.439600	0.712570
43.985484	0.76769	0.417655	0.260503	0.432300	0.734710
45.035469	0.78602	0.425509	0.246829	0.424850	0.757750
45.984494	0.80258	0.432490	0.234102	0.418120	0.779060
46.949028	0.81942	0.439472	0.220801	0.411300	0.801200
48.053523	0.83869	0.447326	0.205107	0.403560	0.827180
49.053282	0.85614	0.454307	0.190464	0.396640	0.851280
49.942487	0.87166	0.460415	0.177083	0.390590	0.873210
50.975743	0.88969	0.467397	0.161102	0.383690	0.899280
52.027676	0.90805	0.474378	0.144342	0.376850	0.926480
52.963806	0.92439	0.480487	0.129003	0.370940	0.951260
54.051929	0.94338	0.487468	0.110659	0.364320	0.980740
55.020202	0.96028	0.493576	0.093859	0.358670	1.007590
56.003645	0.97745	0.499685	0.076326	0.535210	1.035450
57.002242	0.99488	0.505794	0.058028	0.347980	1.064360
58.015730	1.01257	0.511902	0.038938	0.343390	1.094330
59.042757	1.03049	0.518011	0.019046	0.343660	1.125480
59.941166	1.04617	0.523509	0.001186	0.811300	1.153200
59.946667	1.04627	0.523599	0.001075	1595.8000	1.070400

SLOPE (β) = 30°

THETA (+)	VERT. COMP.(+)	HORIZ. COMP.(+)	SHEAR (+)	Y (+)	FAILURE LINES RADIUS 1 (+)	FAILURE LINES RADIUS 2 (+)
0.0000	0.789430	0.263143	0.000000	0.000000	1.0000	1.0000
1.0000	0.789328	0.263143	0.003675	0.017455	1.0311	0.9706
2.0000	0.789019	0.263143	0.007348	0.034921	1.0639	0.9427
3.0000	0.788505	0.263143	0.011019	0.052408	1.0987	0.9162
4.0000	0.787783	0.263142	0.014686	0.069927	1.1355	0.8911
5.0000	0.786852	0.263140	0.018347	0.087489	1.1745	0.8672
6.0000	0.785711	0.263137	0.022002	0.105104	1.2160	0.8444
7.0000	0.784356	0.263131	0.025647	0.122785	1.2601	0.8228
8.0000	0.782785	0.263122	0.029283	0.140541	1.3070	0.8021
9.0000	0.780995	0.263108	0.032906	0.158384	1.3571	0.7824
10.0000	0.778981	0.263089	0.036516	0.176327	1.4105	0.7636
11.0000	0.776739	0.263064	0.040110	0.194380	1.4676	0.7457
12.0000	0.774264	0.263030	0.043687	0.212556	1.5288	0.7285
13.0000	0.771551	0.262986	0.047243	0.230868	1.5944	0.7121
14.0000	0.768594	0.262929	0.050777	0.249328	1.6649	0.6964
15.0000	0.765386	0.262858	0.054285	0.267949	1.7408	0.6813
16.0000	0.761919	0.262770	0.057765	0.286745	1.8226	0.6669
17.0000	0.758186	0.262662	0.061214	0.305731	1.9111	0.6531
18.0000	0.754179	0.262531	0.064629	0.324920	2.0068	0.6398
19.0000	0.749887	0.262373	0.068004	0.344327	2.1107	0.6270
20.0000	0.745301	0.262185	0.071337	0.363970	2.2236	0.6148
21.0000	0.740410	0.261961	0.074623	0.383864	2.3468	0.6030
22.0000	0.735201	0.261698	0.077857	0.404026	2.4814	0.5917
23.0000	0.729662	0.261389	0.081033	0.424475	2.6288	0.5808
24.0000	0.723780	0.261028	0.084146	0.445228	2.7909	0.5703
25.0000	0.717540	0.260609	0.087189	0.466307	2.9695	0.5602
26.0000	0.710925	0.260123	0.090155	0.487732	3.1669	0.5504
27.0000	0.703918	0.259563	0.093036	0.509525	3.3859	0.5410
28.0000	0.696502	0.258920	0.095825	0.531709	3.6297	0.5319
29.0000	0.688656	0.258182	0.098510	0.554309	3.9022	0.5232
30.0000	0.680358	0.257338	0.101084	0.577350	4.2078	0.5147
31.0000	0.671587	0.256375	0.103534	0.600860	4.5522	0.5065
32.0000	0.662318	0.255279	0.105847	0.624869	4.9420	0.4987
33.0000	0.652524	0.254033	0.108012	0.649407	5.3854	0.4910
34.0000	0.642176	0.252620	0.110013	0.674508	5.8925	0.4836
35.0000	0.631245	0.251020	0.111834	0.700207	6.4757	0.4765
36.0000	0.619697	0.249211	0.113457	0.726542	7.1505	0.4696
37.0000	0.607496	0.247167	0.114865	0.753553	7.9368	0.4628
38.0000	0.594606	0.244862	0.116034	0.781285	8.8594	0.4563
39.0000	0.580985	0.242264	0.116943	0.809783	9.9508	0.4500
40.0000	0.566588	0.239339	0.117567	0.829099	11.2530	0.4439
41.0000	0.551368	0.236049	0.117877	0.869286	12.8218	0.4380
42.0000	0.535274	0.232351	0.117845	0.900403	14.7320	0.4322
42.9533	0.519066	0.228402	0.117464	0.930992	16.9635	0.4269
43.9855	0.500502	0.223605	0.116631	0.965199	19.9745	0.4213
45.0355	0.480465	0.218105	0.115290	1.001239	23.8929	0.4158
45.9845	0.461286	0.212531	0.113609	1.034970	28.4529	0.4109
46.9490	0.440684	0.206212	0.111402	1.070458	34.4675	0.4061
48.0535	0.415621	0.198071	0.108197	1.112701	43.8203	0.4007
49.0533	0.391484	0.189769	0.104612	1.152531	55.6809	0.3960
49.9425	0.368773	0.181553	0.100826	1.189327	70.3721	0.3919
50.9757	0.340809	0.170910	0.095653	1.233829	95.1976	0.3873
52.0277	0.310470	0.158722	0.089454	1.281217	134.8998	0.3827
52.9638	0.281762	0.146593	0.083068	1.325302	192.2479	0.3787
54.0519	0.246208	0.130790	0.074516	1.379009	310.8356	0.3742
55.0202	0.212434	0.115006	0.065787	1.429220	518.8634	0.3703
56.0036	0.175900	0.097112	0.055737	1.482765	983.3803	0.3664
57.0022	0.136308	0.076794	0.044191	1.539997	-	0.3625
58.0157	0.093329	0.053693	0.030955	1.601313	-	0.3587
59.0428	0.046636	0.027415	0.015823	1.667096	-	0.3549
59.9412	0.002960	0.001773	0.001024	1.727951	-	0.3517
59.9467	0.002685	0.001608	0.000928	1.728334	-	0.3516

A C K N O W L E D G M E N T S

Acknowledgements are made to:

Mr. H. Hodgson, Manager, Premier (Tvl.) Diamond Mining Co. Ltd., for permission to use the results of the experimental investigations at Cullinan in this thesis. Also Mr. Richardson, the Chief Mechanical Engineer, and Mr. Shanks, the Plant Supervisor, for their assistance. The writer remembers with pleasure his stay on this Mine, and the goodwill and co-operation extended to him by the staff.

Professor J.E. Jennings, who was the Consulting Engineer for this investigation and is the Supervisor for this thesis. For his patience and encouragement over the long period of time it took to complete the thesis, the writer is very grateful.

The African Housing Board, Lusaka, Zambia. The theoretical part of this thesis was completed while the writer was employed by the African Housing Board of the Republic of Zambia. To the Board the writer is greatly indebted for, although the investigation lay outside the research interests of the Board, every possible facility and help was given. Mr. L.J. Vincent, Manager of the Board, without whose interest and encouragement during periods of despondency, this thesis would probably not have been completed.

The Government of Zambia, for permission to use the electronic computer. It is not possible to appreciate

the value of this facility until one has struggled for nine months to solve differential equations manually.

The electronic computer staff - to this ever-cheerful and hard-working group, ready to help at any time, day or night, an "overflow" of thanks.

The International Computer and Tabulators (S.A.) Ltd. for giving, free of charge, a course on mathematical programming to the writer.

The South African Council for Scientific and Industrial Research for awarding a grant to enable the writer to attend the Master of Science Course at the University of the Witwatersrand.

Special thanks to: Mrs. Olive Burns and Mrs. Joan Ryan, for all they did to help; Andrew Jennings, for checking some of the mathematical derivations; and Mrs. Patricia Thomson for her excellent typing.